Université Pierre et Marie Curie

ED-515 : Complexité du vivant

*Observatoire Océanologique de Banyuls-sur-Mer/ Laboratoire d'océanographie microbienne*

# Influence de la lumière et de l'horloge circadienne sur la gestion de la carence en fer chez *Ostreococcus sp.*

Par Hugo Botebol

Thèse de doctorat de Biologie

Dirigée par François-Yves Bouget et Stéphane Blain

Présentée et soutenue publiquement le 11 décembre 2014

Devant un jury composé de :

| | | |
|---|---|---|
| Christel Hassler | Professeur Université de Genève | Rapporteur |
| Jean-François Briat | Directeur de recherche CNRS | Rapporteur |
| Antoine Sciandra | Directeur de recherche CNRS | Président |
| Frédéric Gaymard | Directeur de recherche INRA | Examinateur |
| François-Yves Bouget | Directeur de recherche CNRS | Directeur de thèse |
| Stéphane Blain | Professeur UPMC | Co-directeur de thèse |

*A tous ceux qui m'ont soutenu et supporté,*
*Merci*

# Remerciements

Je tiens tout d'abord à remercier les membres de mon jury pour avoir accepté de participer à la soutenance de cette thèse en commençant par Monsieur Antoine Sciandra pour avoir accepté de présider le jury.
Je remercie vivement Madame Christel Hassler et Monsieur Jean-François Briat, pour avoir consacré du temps à la lecture de ce document en tant que rapporteurs de ce travail.
Je remercie vivement les membres de mon comité de thèse qui ont pris le temps de suivre mon travail et de me conseiller.

Je tiens à grandement remercier mes deux directeurs de thèse Messieurs François-Yves Bouget et Stéphane Blain, pour leur temps, leur patience et leur soutien tout au long de cette thèse. Un merci tout particulier à François-Yves grâce à qui j'ai appris à développer mes idées, à poser des hypothèses et à gérer un projet scientifique. Je le remercie aussi pour son investissement dans la direction de ma thèse et pour la confiance et la liberté qu'il m'a laissée dans la prise de décisions concernant mon travail de thèse.

Je remercie chaque personne qui a contribué de près ou de loin à la réalisation de ma thèse. Merci à tous mes collaborateurs dont les compétences variés et complémentaires m'ont apporté une vraie expertise tout au long de mon travail.

Un grand merci aux ingénieurs de l'équipe, pour leur grande aide dans leurs domaines d'expertise. Merci à Coco, « BiomolMan », Merci Valérie, « BiochemGirl », Merci à Fifi, « BricolGuy », Merci à Rémy, « The Director ». Merci à vous pour cette super ambiance de travail, grâce à vous ces « trois » années de laboratoire ont été très, très décalées.

Merci à Audrey pour toutes ces heures passées à fondre pour quelques litres d'AQUIL, Saint-Graal sans Fer, et pour m'avoir initié aux joies de la salle blanche et des rinçages à l'acide.

Un grand merci à tous les membres de l'équipe « Mitochondrie, métaux et stress oxydatif », merci pour votre accueil, toujours chaleureux, merci Arthur, Rachel, Romain, Mélanie, Christel, Françoise, Jean Michel. Un grand merci à Emmanuel Lesuisse, « Mister Iron Fifty-Five » et à son complice tchèque Robert Sütak, sans qui tout ceci aurait été moins drôle

Je tiens à remercier mon encadrante de Master à Marseille, Brigitte Meunier-Gontero, pour son soutien, sa gentillesse et ses conseils. Merci d'avoir cru en mes compétences. Merci à Malika pour sa gentillesse et grâce à qui j'ai trouvé ce sujet de thèse.

Un grand merci à toute ma famille, qui m'a supporté, dans les deux sens du terme, pendant la rédaction. Merci d'avoir cru en moi. Un merci tout particulier à Claudine, Mikhaël, Martial, Nicky et Pablo pour leurs critiques constructives. Merci Romain, d'avoir supporté la présence d'un squatteur de canapé pendant 3 semaines chaque année, sans le jeter dehors. Merci pour ces restos et ces soirées à Paris.

Enfin un grand merci à Aurel, Schoff, Ceri, (The Crew), Barto, Tatiana, Remy, Marine, Matthieu, Carlos, Amandine, et j'en passe et des meilleurs . . . Bref, merci à vous les amis !

# Table des matières

# I. Introduction Générale

# 1 Le fer : rôle et répartition dans l'océan

Le fer est un élément essentiel aux êtres vivants du fait de son implication dans de nombreux processus d'oxydo-réduction. Alors que le fer est l'élément le plus abondant du noyau terrestre, il n'est présent qu'à l'état de trace dans l'environnement marin et est de ce fait limitant pour la productivité des écosystèmes océaniques. Ce paradoxe est dû à un changement écologique majeur, qui s'est déroulé il y a 3.6 millions d'années (MA). Le fer était alors un élément abondant, essentiel au métabolisme des protistes qui peuplaient alors les zones anoxiques de l'océan primitif. L'émergence de la photosynthèse 1 MA plus tard a été à l'origine d'une production de dioxygène considérable, rendant l'océan oxique. Dans ces conditions oxydantes, la forme oxydée du fer, $Fe^{3+}$, qui est la moins soluble a massivement précipité, devenant rare et limitante pour les êtres vivants. Ainsi au cours de l'évolution, la vie dans l'océan est devenue dépendante du fer alors que cet élément y est très peu bio-disponible (Falkowski, 2006).

## 1. Sources et Répartition du Fer dans l'océan

De nombreux processus comme l'érosion des côtes (Elrod, 2004; Blain *et al.*, 2008; Sarthou *et al.*, 2008), le ruissellement des fleuves (Guieu and Martin, 2002) et les sources hydrothermales (Bennett *et al.*, 2008; Boyle *et al.*, 2005; Saito *et al.*, 2013; Tagliabue *et al.*, 2014) apportent du fer dans l'océan. Les poussières transportées par les vents en provenance des grands déserts sont une composante majoritaire des apports atmosphériques en fer à l'océan ouvert (Mahowald *et al.*, 2008; Boyd and Ellwood, 2010). On estime que ces poussières contribuent pour 14 à $35x10^9$ kg du fer exporté vers les océans chaque année (Jickells *et al.*, 2005). Le fer provient aussi de manière sporadique, des cendres et les poussières engendrées par les éruptions volcaniques (Hoffmann *et al.*, 2012). Ces particules peuvent mettre plusieurs mois voire des années à retomber dans les océans. Les poussières atmosphériques riches en fer (Fe) peuvent aussi se concentrer dans la neige et la glace des calottes glaciaires (iceberg, banquise) qui fertilisent les océans polaires lors des fontes annuelles (Lannuzel *et al.*, 2008; Lannuzel *et al.*, 2010). Enfin les déjections des grands animaux marins (Lavery *et al.*, 2010) et du zooplancton (Arístegui *et al.*, 2014) représentent une source de fer ponctuelle

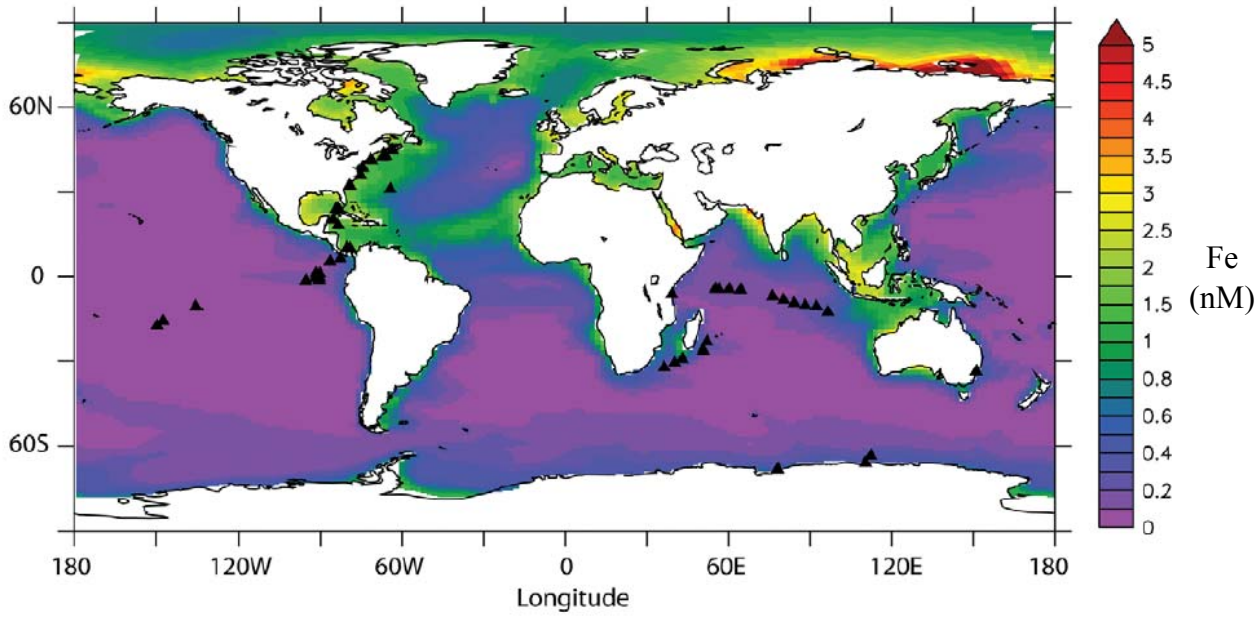


*Figure 1: Carte annuelle de la concentration en fer dissous à la surface des océans (0-100m) à partir de NEMO-PISCES (Toulza et al., 2012)*

Même si le fer est un élément abondant dans la croûte terrestre, et que les nombreux processus mentionnés ci-dessus contribuent à l'exporter vers l'océan, ses propriétés physico-chimiques en font un élément rare à la surface des océans (Figure 1).

On distingue principalement trois formes de fer, en fonction de la porosité des filtres sur lesquels il est collecté : le fer particulaire (PFe > 0.45µm), le fer colloïdal (entre 0.02 et 0.45µm) et le fer soluble (SFe < 0.02µm). La partie dissoute (DFe < 0.4µm) comprend le fer colloïdal et le fer soluble. Le fer océanique est majoritairement présent sous forme particulaire, mais des études de fractionnement ont montré que les microorganismes privilégiaient l'utilisation du fer dissout (Nodwell and Price, 2001; Wu *et al.*, 2001). Les concentrations en DFe sont particulièrement faibles dans les océans ouverts, de l'ordre de 20pM à 1nM (Johnson *et al.*, 1997; Bruland *et al.*, 2001; de Baar and de Jong, 2001), ce qui n'est pas suffisant pour permettre la croissance du phytoplancton (Morel and Price, 2003). Il existe une forte compétition pour la ressource en fer entre les microorganismes (Tortell *et al.*, 1999; Kirchman, 1994; Thingstad, 2000).

En raison de la forte teneur en dioxygène, la forme oxydée du fer ($Fe^{3+}$) est prédominante dans l'océan. Cependant cette forme du fer est très peu soluble à pH 8 avec des concentrations de l'ordre de 0.01nM dans l'eau de mer (Liu and Millero, 2002), ce qui conduit à la formation de colloïdes et de précipités insolubles qui sont difficilement utilisables par les

microorganismes. Le $Fe^{2+}$ peut à nouveau être produit au cours de la réduction photochimique du $Fe^{3+}$ dans les eaux oxygénées à la surface des océans. La forte concentration en matière organique dissoute favorise la photo-réduction du $Fe^{3+}$ en $Fe^{2+}$, ce qui explique des concentrations en $Fe^{2+}$ plus importantes dans les eaux côtières. Dans les eaux froides la lente ré-oxydation du $Fe^{2+}$ en $Fe^{3+}$ est à l'origine de concentrations en $Fe^{2+}$ plus élevées (Moffett, 2001). La plupart des éléments nutritifs sont recyclés régénérés sur l'ensemble de la colonne d'eau, mais le Fe3+ précipite et s'adsorbe sur les particules qui sédimentent, diminuant rapidement le pool de fer en surface. L'effet combinée de cette exportation et des processus de reminéralisation conduit à une augmentation de la concentration en fer avec la profondeur (Figure 2) (Butler, 1998). En surface, la consommation du fer par les organismes phototrophes peut conduire à une limitation de la production primaire (Hudson and Morel, 1990; Sunda and Huntsman, 1995; Sunda and Huntsman, 1997).

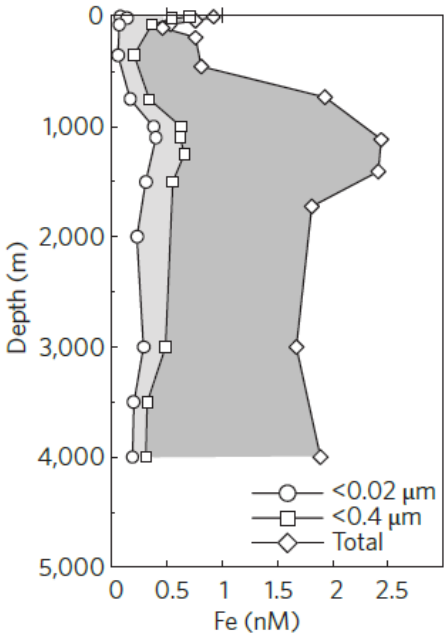


*Figure 2: Concentrations en fer soluble (<0.02µm), fer dissout (<0.04µm) et fer total dans la colonne d'eau en fonction de la profondeur, d'après Boyd & Ellwood, 2010*

## 2. Rôle biologique

Le fer est un élément important pour tous les êtres vivants, qui est impliqué dans de nombreux processus biochimiques. Il existe sous deux formes au sein de la cellule : réduit ($Fe^{2+}$) et oxydé ($Fe^{3+}$). Sa capacité à facilement perdre ou gagner un électron et son potentiel d'oxydoréduction élevé en font un élément de choix pour de nombreuses réactions

biochimiques (Beinert *et al.*, 1997).Un tiers des enzymes connues sont dépendantes d'ions métalliques comme le fer, qui interviennent dans les réactions d'oxydo-réduction et participent à la formation et au maintien des structures tertiaires de ces protéines. Le fer est présent sous forme de co-facteur, héme ou centre Fe-S, dans les protéines et permet de contrôler leur potentiel rédox (-300mV/+700mV) en fonction de l'état de spin et la géométrie des atomes de fer. Cette caractéristique qui permet le transfert d'électrons est particulièrement importante au niveau des chaînes respiratoire et photosynthétique.

Le fer est impliqué dans de nombreux processus biologiques tels que la photosynthèse, la réduction d'azote (Rueter and Ades., 1987), la respiration, la production d'hydrogène, la méthanogénèse (Zhang *et al.*, 2005), le cycle de l'acide citrique (Somerville *et al.*, 1999; Oexle *et al.*, 1999) ou encore la régulation de l'expression des génomes, la biosynthèse et la réparation de l'ADN (McHugh *et al.*, 2003; Lukianova and David, 2005; Thompson *et al.*, 2011). C'est aussi un élément essentiel dans la détoxification des radicaux libres (Andrews, Robinson, & Rodriguez-Quiñones, 2003; Mittler, 2002). Ainsi, au cours de l'évolution, le fer est devenu indispensable pour tous les organismes vivants à part quelques exceptions, comme *Borrelia burgdorferi,* la bactérie responsable de la maladie de Lyme (Posey and Gherardini, 2000).

### *a) Les chaines de transfert des électrons*

Les chaines de transfert des électrons sont les principales utilisatrices du fer intracellulaire, on retrouve une quarantaine d'atomes de fer impliqués dans la respiration (Cramer and Knaff, 1991), et on estime que 90% du fer intracellulaire est présent au niveau de la chaîne respiratoire chez les bactéries (*E.coli*, (Tortell *et al.*, 1999)).

Le fer se concentre au niveau des chaînes de transports des électrons car c'est un élément indispensable à son fonctionnement. Chez les organismes photosynthétiques, la chaîne de transfert associée à la photosynthèse fonctionne grâce au transit d'électrons à travers différents complexes protéiques. Le flux d'électron s'effectue à partir d'une molécule donneuse ($H_2O$-> ½ $O_2$ + $2H^+$ + $2e^-$) jusqu'à l'accepteur final (2 $NADP^+$ + $2H^+$ + $2e^-$ -> 2 NADPH) et passe par une série de complexes transmembranaires d'origine lipidiques (plastoquinone) ou protéiques (cytochromes). Ces complexes sont appelés transporteurs d'électrons car ils assurent le transfert des électrons entre les différents composants de la chaîne photosynthétique. On peut regrouper les transporteurs d'électrons en plusieurs catégories, en fonction du groupe prosthétique qu'ils contiennent. Les flavoprotéines

contiennent une flavine adénine di-nucléotide (FAD) et les plastoquinones sont des molécules organiques pouvant être réduites, ces deux groupes ne nécessitent pas d'atomes métalliques pour transporter des électrons. Les protéines FeS ont un centre fer-souffre composé de deux (2Fe-2S), trois (3Fe-4S) ou quatre (4Fe-4S) atomes de fer associés avec des anions sulfure $S^{2-}$ (Centre Fe-S) et les cytochromes contiennent des hèmes, un noyau porphyrique ayant incorporé un atome de fer, ces groupes prosthétiques sont les plus anciens et les plus répandus, ce sont les principaux médiateurs dans les réactions d'oxydo-réduction. Les groupes prosthétiques sont les véritables acteurs du transfert d'électron le long de la chaîne photosynthétique.

### *b) L'appareil photosynthétique*

Le photosystème 2 (PSII) contient un atome de fer non hémique (Fe2+) et 3 hèmes, il est capable d'oxyder une molécule d'$H_2O$ en $O_2$ afin de réduire les plastoquinones (PQ) aux sites *Qa* et *Qb* en di-hydro plastoquinones ($PQH_2$) à l'aide d'énergie lumineuse, leur transférant à chacune 2 électrons (Müh *et al.*, 2012). Les $PQH_2$ transportent ces électrons jusqu'au cytochrome b6/f, contenant un centre 2Fe-2S et 3 hèmes, où elles sont ré-oxydées en PQ. Les électrons sont transférés aux plastocyanines (contenant du cuivre) ou au cytochrome $c_{553}$ composé d'un hème. Le photosystème 1 (PSI), contenant 12 atomes de fer (3 centres 4Fe-4S, $F_X$, $F_A$, $F_B$), récupère ces électrons et les transmet à la ferrédoxine à l'aide d'énergie lumineuse. La ferrédoxine a un centre 2Fe-2S, elle donne ces électrons à la Ferrédoxine-$NADP^+$ Réductase (FNR) qui réduit le $NADP^+$ en NADPH.

Cependant, du fait de ces propriétés redox, le fer est un atome très réactif qui peut interagir facilement avec les espèces réactives de l'oxygène (ROS). Ces ROS sont produites au niveau des chaînes de transfert des électrons lorsque le système est soumis à un stress fort et qu'une partie des électrons s'échappe de la chaîne de transfert. La présence de fer libre à proximité des chaînes de transfert peut conduire à la formation de radicaux hydroxyles ($OH^-$), qui sont capables d'endommager les molécules organiques avec lesquels ils réagissent.

## 2 Les différents systèmes d'incorporation du fer

### 1. Les réductases ferriques :

Il existe 3 types de familles de réductases ferriques : les NADPH oxydases (NOX) et les NADH-cytochrome $b_5$ réductases (NADH-CBR), qui contiennent un flavocytochrome, et les cytochromes $b_{561}$ qui contiennent deux hèmes et utilisent comme donneur d'électron

l'ascorbate (Blaby-Haas and Merchant, 2012). Ces enzymes réduisent le $Fe^{3+}$, insoluble (oxydé) ou en interaction avec un chélateur, en $Fe^{2+}$. Cette forme du fer est plus soluble et facilement importée dans la cellule à l'aide de perméases à cations bivalents. C'est chez la levure *S.cerevisiae* que l'implication d'une NOX dans la réduction du fer ferrique a été mise en évidence pour la première fois. Au sein de la famille NOX, on trouve chez la levure un variant, Fre3p, facilitant l'incorporation du fer lié à un sidérophore (Yun *et al.*, 2001). Lorsqu' *A.thaliana* est carencée en fer, c'est une réductase de type NOX (FRO2) qui est induite au niveau des racines (Robinson *et al.*, 1999). Cependant les réductases de la famille NOX n'interviennent pas seulement dans le transport du fer, certains homologues des NOX, appelés respiratory burst oxidase homolog (RBOH), sont aussi impliqués dans la production de superoxide ($O_2^-$), à des fins de protection (Katsuyama, 2012) ou de signalisation (Torres and Dangl, 2005). On a détecté les NADH-CBR au niveau des racines de la tomate et de la citrouille et mis en évidence que leur activité réductase ferrique est induite lors d'une carence en fer (Sparla *et al.*, 1997; Bagnaresi *et al.*, 1997; Yi and Guerinot, 1996; Xoconostle-Cázares *et al.*, 2000). Il existe de nombreux isoformes solubles ou membranaires des NADH-CBR et, chez les plantes, il semblerait que ces homologues soient plus impliqués dans la mobilisation du fer intracellulaire et intercellulaire que dans la réduction du fer extracellulaire. Le dernier type de réductase ferrique, le cytochrome $b_{561}$, est le domaine principal du duodénal cytochrome b (DcytB). Il a été découvert chez une souris présentant un taux d'absorption du fer très élevé et il existe des protéines contenant ce domaine chez tous les eucaryotes.

Chez la microalgue verte *Chlamydomonas reinhardtii*, on trouve quatre gènes qui pourraient coder des réductases ferriques impliquées dans l'absorption du fer. Seul l'un d'entre eux *FRE1* est fortement induit par la carence en fer. FRE1 une enzyme de type NOX. Chez les diatomées, on retrouve ces 3 familles de réductases ferriques. Chez *Thalassiosira pseudonana,* l'expression de *FRE1* (NADH-CBR) et *FRE2* (NOX) est induite en réponse à la carence en fer (Kustka *et al.*, 2007). De même chez *Phaeodactylum tricornutum*, l'expression des réductases *FRE1* et *FRE2* (NOX) (Kustka *et al.*, 2007), ainsi que de deux réductases de type *DcytB* appartenant à la famille des cytochromes b561(Allen *et al.*, 2008), est induite lors d'une carence en fer. Cependant les séquences protéiques de FRE2 (*T.pseudonana*) et FRE1 (*P.tricornutum*) sont plus proches de la famille RBOH, ces réductases ferriques seraient donc plutôt impliquées dans la détoxification ou la signalisation. Chez *T.oceanica* on retrouve une réductase ferrique FRE, appartenant à la famille NOX, induite en absence de fer (Lommer *et al.*, 2012).

### 2. Import dépendant des ferroxydases

On a identifié chez *S.cerevisiae*, une ferroxydase à cuivre (Fet3p) appartenant à la famille des Multi Copper Oxydase (MCO) capable d'oxyder le $Fe^{2+}$en $Fe^{3+}$avant de le transférer à une perméase spécifique du $Fe^{3+}$ (FTR : Fe TRansporteur) (Blaby-Haas and Merchant, 2012). La majorité des métaux de transition naturellement abondants ont un état d'oxydation +2, l'état d'oxydation +3 est une propriété spécifique du fer dont se servent les organismes pour l'absorber préférentiellement. Les oxydases à plusieurs ions cuivre de type Fet3p sont composées de trois domaines protéiques, deux contenant un ion cuivre et un contenant un cluster de deux cuivre, chez la levure. Chez *C.reinhardtii*, la protéine FOX (Ferrous OXydase) est constituée de six domaines : 5 contenant un ion cuivre et un contenant 2 ions cuivre. Il est nécessaire au sein de ces ferroxydases que le domaine contenant deux ions cuivre soit suffisamment proche d'un autre domaine contenant un ion cuivre pour former un cluster à trois atomes de cuivre. Les MCO oxydent le fer en acceptant les électrons au niveau d'un domaine contenant un seul cuivre avant de les transmettre au cluster de trois cuivres. Ce cluster fixe une molécule de dioxygène qui sera réduite en deux molécules d'eau après le transfert de quatre électrons (Bento *et al.*, 2005) (i.e. oxydation de 4 $Fe^{2+}$). Les perméases de type FTR sont composées de 7 domaines transmembranaires et d'une boucle extracellulaire contenant un motif EPTD qui récupérerait le $Fe^{3+}$ oxydé par une MCO. Sur les hélices transmembranaires 1 et 4, il y a un motif REXXE qui permettrait le transport du $Fe^{3+}$ à travers la membrane (Terzulli and Kosman, 2010) (Figure 3). Sans MCO, les perméases de la famille FTR ne peuvent transporter le $Fe^{3+}$. Il faut que ces deux protéines soient co-maturées pour permettre l'insertion du complexe MCO-FTR dans la membrane plasmique. Ce système d'absorption spécifique du fer nécessitant du cuivre a été découvert chez les levures mais il est aussi présent chez *C.reinhardtii* (Fontaine *et al.*, 2002)*, T.pseudonana* (Maldonado *et al.*, 2006) et *T.oceanica* (Peers *et al.*, 2005).

### 3. Les perméases à cations bivalents (non spécifiques)

Ces perméases ne transportent que des ions métalliques ayant un état d'oxydation +2. Il en existe deux grandes familles qui sont présentes dans la plupart des règnes du vivant (Blaby-Haas and Merchant, 2012): ZIP (Zinc/Iron Perméases) et NRAMP (Natural Resistance-Associated Macrophage Protein) (Figure 3). Ces perméases peuvent aussi bien être localisées sur la membrane plasmique qu'au niveau des organelles.

La famille ZIP regroupe les protéines responsables de l'incorporation du zinc (ZRT : Zinc Regulated Transporter) ou du fer (IRT : Iron Regulated Transporter). Les membres de la famille ZIP sont composés de huit segments transmembranaires (TM) et d'une région centrale riche en résidus histidine, située entre les TMs III et IV et qui dépasse dans le cytoplasme. La famille ZIP est subdivisée en 4 sous familles sur des bases phylogénétiques, mais sans relation avec leur localisation cellulaire ou les ions métalliques transportés préférentiellement. Le transport passif des métaux au travers des protéines de la famille ZIP serait dû aux gradients de concentration en ions métalliques. Le transporteur IRT1, présent au niveau de la membrane des racines d'*A.thaliana*, est fortement exprimé lors d'une carence en fer (Vert and Grotz, 2002). De même IRT2 est fortement induit mais on le trouve dans les vésicules intracellulaires où il est sans doute impliqué dans la compartimentation du fer (Vert *et al.*, 2009). Chez *C.reinhardtii* il existe 13 membres de la famille ZIP, mais seulement *Irt1* et *Irt2* sont régulés en fonction du fer disponible (Reinhardt *et al.*, 2006). *Irt2* est induit lorsque la concentration en fer est faible alors que *Irt1* est fortement induit lorsque le fer devient limitant, que le taux de croissance diminue et que la chlorose apparait (Blaby-Haas and Merchant, 2012). L'expression de ces deux gènes varie aussi en fonction des concentrations en zinc et en cuivre : *Irt1* est induit en carence de zinc et *Irt2* lors d'une carence en cuivre (Blaby-Haas and Merchant, 2012). L'induction d'*Irt2* pourrai servir soit à pourvoir le cytochrome c6 en fer (remplaçant les plastocyanines en absence de cuivre), soit à compenser la baisse d'incorporation du fer lorsque le système de ferroxydase (MCO) est privé de cuivre.

La famille de perméase NRAMP regroupe des protéines composées de 10 à 11 segments transmembranaires, permettant principalement l'import de fer et/ou de manganèse. Chez les eucaryotes, il existe deux sous-familles NRAMP : NRAMP I et NRAMP II. Les perméases appartenant à la sous-famille NRAMP I, situées au niveau des compartiments intracellulaires (Picard *et al.*, 2000), transportent les métaux de façon active à l'aide d'un système d'antiport de protons (Goswami *et al.*, 2001) qui transfère les ions métalliques contre le gradient de proton. Ceci permet de transporter les métaux vers les organelles, gérant ainsi l'homéostasie du fer. Les perméases de la sous-famille NRAMP II permettent de transporter en symport métaux et protons (Gunshin *et al.*, 1997). Les membres de cette sous-famille sont situés à la membrane plasmique et participent à l'assimilation des métaux. Chez *A.thaliana*, NRAMP1 appartenant à la sous-famille NRAMP II, est induit par la carence en fer dans les racines mais pas dans les feuilles. On retrouve des transporteurs de la famille NRAMP chez la plupart des

algues dont le génome a été séquencé, *O.tauri* inclus, à l'exception de *P.tricornutum* (Kustka *et al.*, 2007).

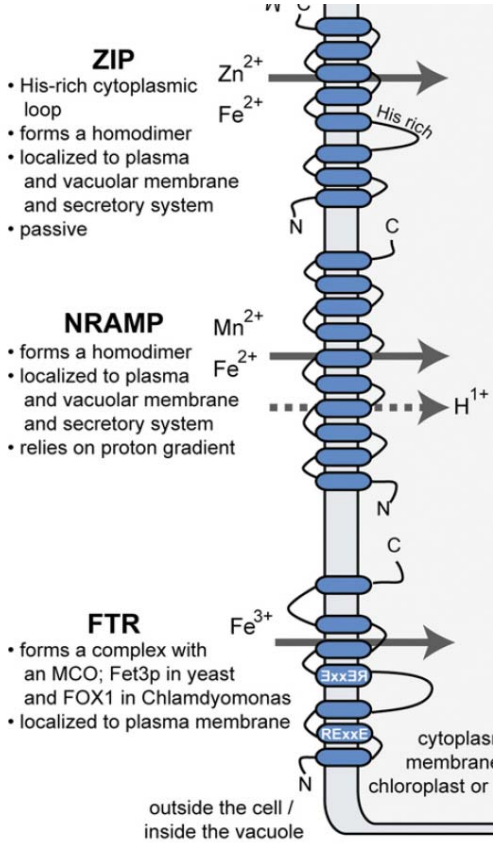


*Figure 3: Représentation schématique des perméases à fer (Blaby-Haas and Merchant, 2012)*

### 4. Les pseudo-sidérophores phytoplanctoniques

Certaines diatomées, dont le genre *Pseudo-nitzschia*, produisent des composés organiques apparentés aux sidérophores, comme l'acide domoïque qui est toxique pour les oiseaux et les mammifères. Ce type de composé permet de capturer le fer et le cuivre (Rue and Bruland, 2001) avec une efficacité accrue comparée aux autres systèmes d'incorporation. De plus, d'autres espèces, comme *Phaeocystis antartica* et *Proboscia inermis* sont capables de récupérer du fer en interaction avec des molécules organiques bactériennes tel que l'aerobactine, l'enterobactine et la desferrioxamine b (Strzepek *et al.*, 2011).

# 3 Stratégies du phytoplancton pour gérer la carence en fer

Dans les écosystèmes océaniques, les microorganismes phytoplanctoniques font fréquemment face à un problème récurrent de carence en fer. Plusieurs processus d'acclimatation et/ou d'adaptation dédiés à la survie dans des environnements pauvres en fer ou fertilisés de façon épisodiques, ont été mis en évidences

## 1. Optimiser l'incorporation

Chez les diatomées *P.tricornutum* et *T.oceanica*, les systèmes de réductase ferrique et les transporteurs de type ZIP sont induits en carence en fer (Allen *et al.*, 2008). De nombreux systèmes d'incorporation du fer sont induits lors d'une carence mais les membranes cytoplasmiques ne peuvent dépasser un nombre fini de protéines membranaires par unité de surface membranaire. Ainsi *T.pseudonana* (3.5µm) importe le fer à une vitesse par unité de surface équivalente à celle de microalgues de plus grande taille comme *Prorocentrum minimum* (12µm) (Sunda and Huntsman, 1997), mais elle a un taux de croissance et un ratio Fer/Carbone plus élevé. La capacité d'incorporation maximale est donc fonction de la surface cellulaire disponible notamment par rapport au volume. Cependant, Hudson & Morel (1990) montrent aussi que l'incorporation du fer est limité par la faible concentration en fer libre (Fe') dans le milieu : ce n'est pas seulement l'affinité et/ou l'efficacité des systèmes d'incorporation qui limitent l'assimilation du fer mais aussi sa disponibilité à proximité de la membrane.

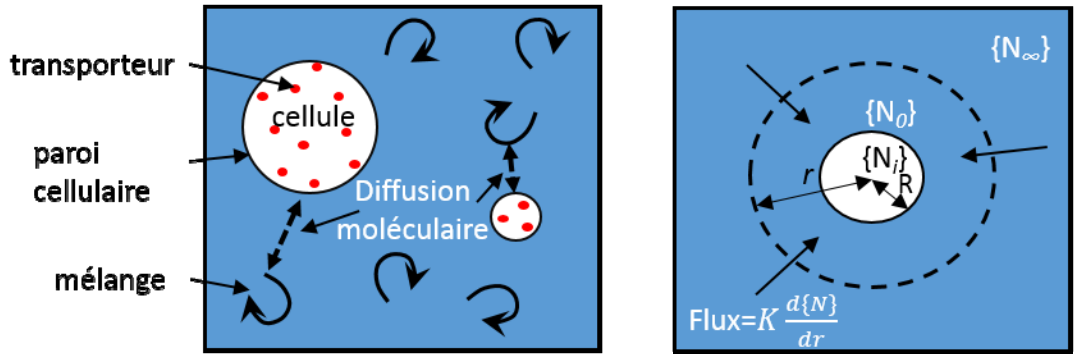


*Figure 4: Représentation schématique de l'import de nutriment dans un microorganisme marin et du gradient de concentration en nutriment {N} qui amène par diffusion des nutriments à proximité de la cellule. D'après Williams & Follows, 2011*

Les modèles de Pasciak & Gavis (1974, 1975) utilisés jusqu'à maintenant pour décrire le phénomène de diffusion du fer en direction de la cellule ne tiennent pas compte de la forme de la cellule, et considèrent que les cellules immobiles, évoluent dans un environnement sans turbulences (Figure 4). Armstrong (2008) intègre ces variables et met en évidence que les paramètres limitant l'incorporation du fer sont différents pour les petites et les grandes cellules. Pour les petites cellules c'est le nombre de perméases disponibles qui est limitant alors que pour les grandes cellules c'est la diffusion du fer vers la membrane cellulaire qui limite l'incorporation. Ainsi, les espèces ayant une taille réduite et celles capables de réduire leur taille ont un avantage non négligeable, elles ont plus d'unité de surface membranaire par unité de volume cellulaire que les cellules ayant une taille plus élevée. De fait elles peuvent plus facilement absorber le fer nécessaire à leur survie (Sunda and Huntsman, 1997; Sunda and Huntsman, 1995). Chez les diatomées *P.tricornutum* et *T.oceanica,* plusieurs protéines sont fortement induites lors d'une carence en fer, ISIP1, ISIP2 et ISIP3 (Iron Starvation Induceed Protein). Leur rôle n'est pas encore clairement déterminé mais ces trois protéines seraient membranaires et participeraient à la captation du fer extracellulaire (Lommer *et al.*, 2012; Allen *et al.*, 2008).

## 2. Une utilisation parcimonieuse du fer

Dans des milieux limités en fer, certaines espèces du phytoplancton sont capables de restreindre leurs besoins en fer en modifiant leur appareil photosynthétique et plus globalement leur métabolisme.

### *a) Modifications de l'appareil photosynthétique*

#### (1) La chaîne de transfert des électrons

Chez les diatomées *T.pseudonana* et *P.tricornutum*, les cyanobactéries marines (*Synechococcus, Prochlorococcus*) et les diazotrophes comme *Crocospaera watsonii*, les protéines impliquées dans la photosynthèse (Figure 5) (Yruela, 2013; Raven *et al.*, 1999), et notamment dans le transfert d'électron, sont remaniées lors d'une carence en fer (Morrissey and Bowler, 2012). Les protéines du photosystème II (PSII) ne contenant que 3 atomes de fer, sont préservées alors que celles du cytochrome b6/f (six atomes de fer) et du photosystème I (PSI) (12 atomes de fer) sont fortement réprimées (Allen *et al.*, 2008; Lommer *et al.*, 2012;

Moseley *et al.*, 2002). Ainsi le ratio PSII : PSI augmente fortement lors d'un manque de fer, permettant une utilisation plus parcimonieuse du fer. D'ailleurs, Strzepek (2004) montre que *Thalassiosira oceanica* s'est adaptée à la carence en fer en augmentant son ratio PSII:PSI (≈10) de manière constitutive alors que ce ratio n'excède pas 2 chez les diatomées côtières et est souvent proche de 1.

Dans les mêmes conditions, on observe un remplacement du cytochrome c6 contenant un hème, par une plastocyanine contenant un ion cuivre pour transférer les électrons du cyt b6/f au PSI (Lommer *et al.*, 2012), quand le cyt c6 n'est pas absent du génome comme chez O.tauri (Morrissey and Bowler, 2012).

Le dernier partenaire de la chaine de transfert des électrons, la ferrédoxine, contient un centre [2Fe-2S]. Elle aussi est réprimée en absence de fer et remplacée par la flavodoxine (Allen *et al.*, 2008; Lommer *et al.*, 2012; La Roche *et al.*, 1996), une protéine contenant une molécule de 5-phosphate riboflavine. Grâce aux propriétés oxydo-réductrices de cette molécule, les flavodoxines peuvent transférer les électrons du PSI à la FNR (Fd-$NADP^+$ réductase) afin de

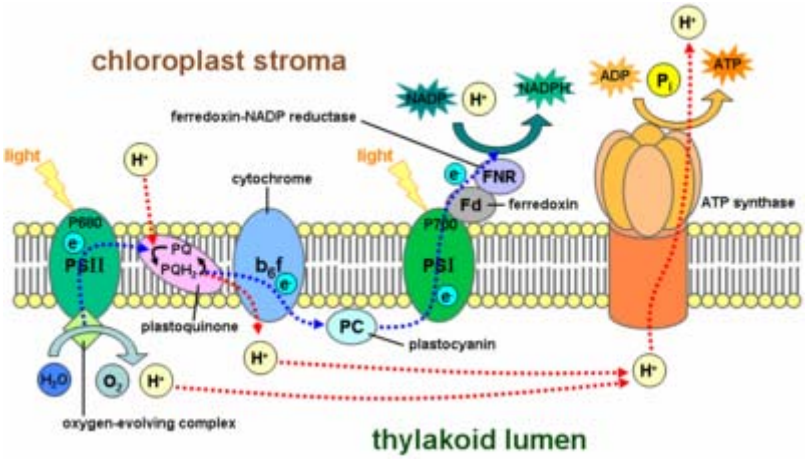


*Figure 5: Les différents acteurs de la chaîne de transfert des électrons dans le chloroplaste*

continuer à créer du pouvoir réducteur sous forme de NADPH.

Chez *C.reinhardtii*, la modification des antennes photosynthétiques du PSI lors de la carence en fer est la première étape conduisant à la dégradation du PSI (Naumann *et al.*, 2005)

### (2) Les antennes photosynthétiques

Lorsque le phytoplancton est soumis à une carence en fer, l'efficacité photosynthétique diminue, les protéines composant le PSI et le Cyt b6/f sont réprimées, et les antennes

photosynthétiques sont remaniées. Les antennes des photosystèmes I et II, respectivement appelées LHCI et LHCII (Light Harvesting Complex), sont constituées d'un assemblage de différentes protéines (Lhc) qui organisent les pigments afin de récolter l'énergie nécessaire à la photosynthèse. Les Lhc ont une structure similaire, 3 hélices transmembranaires et 1 ou 2 hélices amphiphiles, et ont des sites spécifiques pour la fixation des chlorophylles et des caroténoïdes (Kühlbrandt *et al.*, 1994; Liu *et al.*, 2004; Ben-Shem *et al.*, 2003). La majorité des protéines du LHCI sont réprimées et la partie N-terminale de la protéine Lhca3 est dégradée (Naumann *et al.*, 2005). La protéine PSI-K, impliquée dans la connexion entre le PSI et les LHCI (Jensen *et al.*, 2000), est réprimée lors d'une carence en fer (Moseley *et al.*, 2002). Cette modification de Lhca3 et la répression de PSI-K altèrent la structure des LHC1 et diminuent l'efficacité du transfert d'énergie entre les LHC1 et le PSI, permettant ainsi de minimiser les dommages oxydatifs dans la membrane thylacoïdale (Moseley *et al.*, 2002). Les protéines composant les LHCII (lhcb) ne sont peu ou pas réprimées en carence de fer, par contre Lhcbm1 et Lhcbm3, qui représentent la majeur partie des LCHII sont fortement induites (Naumann *et al.*, 2007). La taille des LHCII augmente beaucoup (Naumann *et al.*, 2007; Strzepek and Harrison, 2004; Strzepek *et al.*, 2012), ce qui conduit à un taux de photo inhibition élevé. D'autres Lhc appartenant à la famille LI818 (Zhu and Green, 2010), spécifiquement associées à l'acclimatation aux lumières fortes, sont aussi exprimés lors de carence en fer, notamment LhcSR3 chez *C.reinhardtii* (Naumann *et al.*, 2007). Chez *T.oceanica*, et *P.tricornutum*, la majeure partie des gènes codant pour les protéines liées à la fucoxanthine et aux chlorophylles a/c (FCPs), sont induits lors d'une carence en fer. Chez ces deux espèces , il existe deux FCPs appartenant à la famille LI818 qui sont abondamment exprimées dans des conditions de carence (Lommer *et al.*, 2012; Allen *et al.*, 2008).

Les caroténoïdes participent aussi à l'acclimatation à la carence en fer. Après réduction du nombre de photosystèmes, la viola-xanthine est de-époxydée en zéa-xanthine, le caroténoïde impliqué dans la protection contre les stress lumineux dans la lignée verte (Figure 6). Ainsi ils protègent le nombre réduit de centres réactionnels en dissipant le surplus d'énergie collecté par les chlorophylles. Chez les diatomées ce sont les caroténoïdes diadinoxanthine et diatoxanthine qui remplacent respectivement viola-xanthine et zéa-xanthine dans la photo-acclimatation (Wu *et al.*, 2012). Chez *T.oceanica*, la viola-xanthine dé-époxydase est fortement induite (x 3.1) lors d'une carence en fer (Lommer *et al.*, 2012), ce qui permet de transformer rapidement la diadinoxanthine en diatoxanthine. De la même façon, la zéa-xanthine époxydase est nettement réprimée chez *P.tricornutum* permettant ainsi

l'accumulation de diatoxanthine et l'augmentation du NPQ (Non Photochemical Quenching) (Allen *et al.*, 2008).

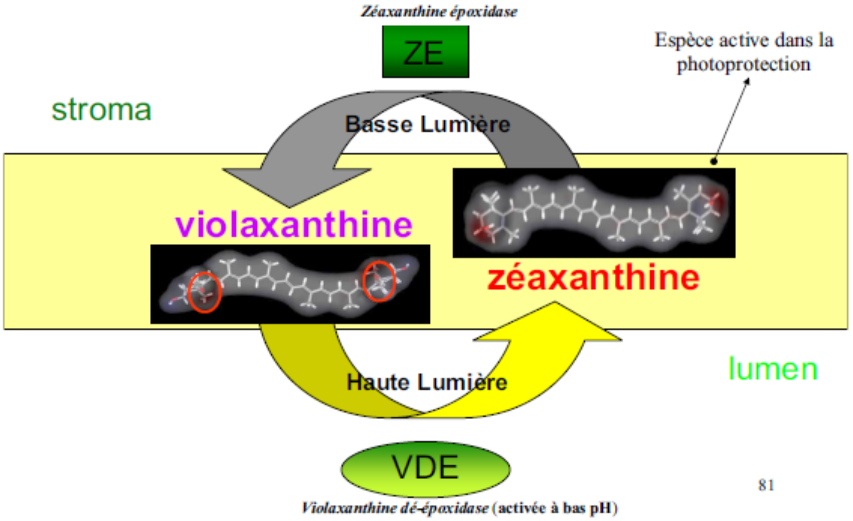


*Figure 6: Cycle des xanthophylles face au stress lumineux d'après (Tardy, 1997)*

### *b) Les enzymes de détoxification*

Face aux espèces réactives de l'oxygène (ROS) produites à proximité des chaînes de transfert d'électron (respiration et photosynthèse), les organismes disposent d'un panel d'enzymes de détoxification : super oxyde dismutase (SOD), ascorbate peroxydase, catalase et hème oxydase, pour empêcher ou arrêter les réactions de Fenton (Figure 7) (Mittler, 2002). Ces enzymes contiennent du fer et sont réprimées en carence en fer. Par contre, pour remplacer la Fe-SOD, des équivalents utilisant d'autres métaux tels le cuivre, le zinc et le manganèse sont fortement exprimés. De même, les péroxyrédoxines, qui fonctionnent sans fer, sont induites lors des carences en fer (Allen *et al.*, 2008; Lommer *et al.*, 2012; Edgar *et al.*, 2012).

Afin de contrebalancer la répression des enzymes de défense contre les ROS lors de la carence en fer, la production de molécules anti-oxydantes comme le tocophérol (Vitamine E) et le dehydroascrobate (Vitamine C oxydée) est fortement induite.

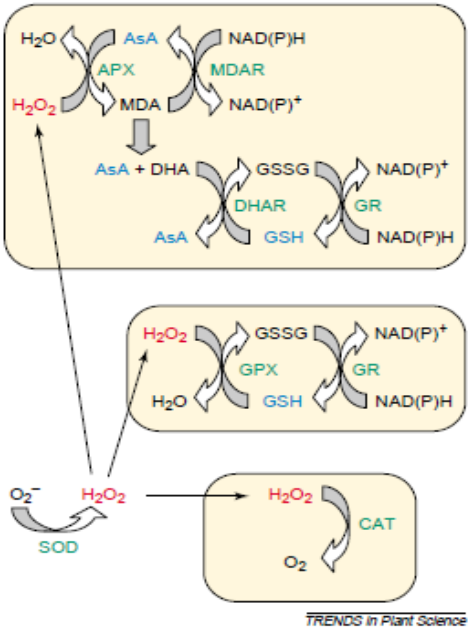


*AsA, ascorbate;*

*DHA, dehydroascorbate;*

*SOD, superoxide dismutase;*

*CAT, catalase;*

*APX, ascorbate peroxidase;*

*MDA, monodehydroascorbate;*
*MDAR, MDA reductase;*
*DHAR, DHA reductase;*
*GR, glutathione reductase;*
*GSH glutathione;*
*GSSG, glutathione disulphide.*

*Figure 7: Les différents mécanismes de détoxifications des ROS (Mittler, 2002).*

Chez *P.tricornutum*, la transcription des hème-oxydases et super-oxyde-dismutases à fer (Fe-SOD) est fortement réprimée lors d'une carence en fer et ce sont les Cu/Zn-SOD ou les Mn-SOD qui les remplacent. La production de tocophérol (Vitamine E) et de dehydroascrobate (Vitamine C oxydée) est fortement induite (Allen *et al.*, 2008).

### 3. Recyclage du fer :

Chez les cyanobactéries diazotrophes, une partie du transcriptome est régulée par l'alternance jour/nuit (Johnson and Egli, 2014). Les gènes associés à la photosynthèse et à la fixation de l'azote, dont la nitrogénase, sont exprimés à des moments différents du cycle jour/nuit. La nitrogénase est un complexe protéique riche en fer composé par NifH (4 atomes de fer par homodimère) et NifDK (15 atomes de fer par homodimère) (Shi *et al.*, 2007). Cette protéine est extrêmement sensible à la présence de dioxygène ($O_2$) qui peut irrémédiablement détruire son site actif (Fay, 1992). La séparation temporelle ou spatiale de la photosynthèse, productrice d'$O_2$, et de la fixation de l'azote atmosphérique ($N_2$), catalysée par la nitrogénase est donc indispensable. Chez *Crocosphaera watsonii,* une cyanobactérie diazotrophe isolée en zone oligotrophe, les photosystèmes, les enzymes de synthèse des pigments et les protéines du cycle de Calvin-Benson-Bassham (CBB) sont induits en fin de nuit et réprimés en fin de journée. Les gènes associés à la respiration, au cycle de Krebs et à la glycolyse sont, quant à eux, exprimés en fin de journée et réprimés à la fin de la nuit. Les gènes codant pour les protéines de fixation de l'azote comme la nitrogénase sont exprimés pendant la nuit, il y a

donc une séparation temporelle entre la photosynthèse et la fixation du $N_2$ (Shi *et al.*, 2010). Une étude protéomique chez *Crocosphaera watsonii*a a montré une forte variation du niveau des métallo-enzymes au cours d'un cycle jour/nuit, en accord avec les variations du transcriptome. Ainsi, chez cette cyanobactérie, les protéines photosynthétiques sont traduites à l'aube et dégradées au crépuscule, ce qui pourrait permettre la récupération du fer contenu dans les photosystèmes. Les enzymes impliquées dans la fixation de l'azote, et notamment la nitrogénase, sont traduites au début de la nuit et pourraient potentiellement utiliser le fer provenant des photosystèmes. Ces enzymes sont dégradées à l'aube et le fer serait à nouveau disponible pour la néosynthèse des photosystèmes. En alternant la photosynthèse oxygénique et la fixation de $N_2$, deux voies métaboliques très demandeuses en fer, cette cyanobactérie peut potentiellement recycler son pool de fer et réduire ses besoins (Figure 8) (Saito *et al.*, 2011). Cette stratégie, combinée à un nombre réduit de métallo-enzymes dans le génome, pourrait expliquer le succès écologique de *Crocosphaera watsonii* dans des parties de l'océan pauvres en fer (>0.3nM Fe) (Saito *et al.*, 2011).

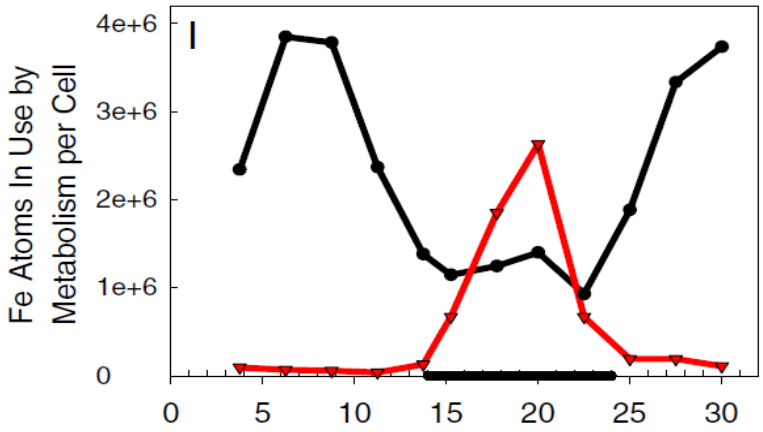


*Figure 8: Allocations putatives des atomes de fer aux différentes voies métaboliques au cours d'un cycle jour/nuit : En rouge : la fixation de l'azote, en noir : la photosynthèse (Saito et al., 2011)*

### 4. La ferritine

La ferritine est le principal complexe protéique de stockage du fer utilisée par les êtres vivants, des plantes aux animaux en passant par les bactéries et les cyanobactéries. Elle permet de concentrer et stocker le fer en toute sécurité, réduisant ainsi les dommages cellulaires potentiels dus aux espèces réactives de l'oxygène et au stress oxydatif (Elizabeth C. Theil, 2003; Arosio *et al.*, 2009). Cette protéine de 24kDa est composée de 4 hélices α et

d'un centre ferroxidase. Les monomères de ferritine s'assemblent en un complexe de maxi-ferritine de 24-mer ou de mini-ferritine de 12-mer. Les ferritines eucaryotes s'assemblent en 24-mer, formant des nano-cages capables de stocker jusqu'à 4500 atomes de $Fe^{3+}$ chez les animaux et les plantes supérieures. L'assemblage de la ferritine nécessite de nombreuses interactions entre ses différentes sous-unités et le complexe de maxi-ferritine présente des symétries par rotation d'ordre 4, 3, 2. Des pores de 3 Å de large sont présents au niveau des symétries d'ordre 3 et 4 (Harrison and Arosio, 1996; Douglas and Ripoll, 1998). Ces pores sont hydrophiles chez les plantes (Briat *et al.*, 2010), par contre, chez les animaux, les pores au niveau de la symétrie d'ordre 4 sont hydrophobes (Douglas and Ripoll, 1998) . Ces pores permettent l'entrée du fer dans le complexe avant oxydation au niveau des centres ferroxydase puis stockage sous forme d'oxyde ferrique hydraté minéral chez les animaux et d'un cristal amorphe contenant beaucoup de phosphate chez les plantes (Wade *et al.*, 1993; Waldo *et al.*, 1995). Cette réaction utilise du dioxygène et produit du $H_2O_2$ (Arosio *et al.*, 2009; Harrison and Arosio, 1996). Chez l'homme, les protéines de liaison au poly(rC) (PCBP), sont des métallochaperonnes cytoplasmiques qui permettent de transporter le fer jusqu'au complexe de ferritine (Shi *et al.*, 2008). Le processus permettant de récupérer le fer après stockage au sein de la ferritine est encore mal connu, plusieurs modèles sont proposés : soit une dégradation complète du complexe de ferritine via un lysosome pour en extraire le noyau ferrique (Figure 9) (Konijn *et al.*, 1999), soit un relargage contrôlé du fer par l'intervention de petites molécules réductrices (Liu *et al.*, 2007). L'implication de métallochaperonnes dans la décharge contrôlée de la ferritine est aussi envisagée (Carmona *et al.*, 2013).

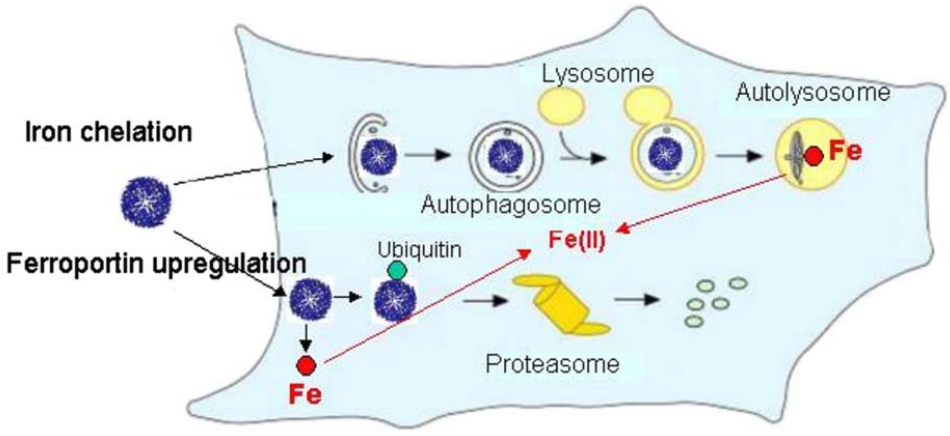


*Figure 9: Possibles voies de dégradation du complexe ferritine pour récupérer le noyau ferrique*(Arosio *et al.*, 2009)

### *a) Rôle et régulation de la ferritine chez les plantes supérieures*

Chez *A.thaliana* il existe 4 gènes codant pour une ferritine qui sont exprimés différemment. Les ferritines 1, 3 et 4 (codées par les génes *AtFer1, AtFer3, AtFer4*) sont présentes dans les feuilles, les tiges et les fleurs alors que la ferritine 2 (*AtFer2*) est seulement trouvée dans les graines (Briat *et al.*, 2010). En absence de *AtFer2* la viabilité des graines est réduite et les germes sont très sensibles au stress oxydatif. Chez un triple mutant *AtFer1-3-4*, les fleurs ont un contenu en fer élevé et l'activité des enzymes de détoxification est accrue, sans doute pour contre-balancer la surproduction de ROS. Lorsque la concentration en fer est élevée dans le milieu de culture, la biomasse des feuilles diminue, et les fleurs sont stériles. Dans des conditions en fer normales, la concentrations en ROS augmente fortement dans tous les organes, le taux de fixation de $CO_2$ diminue dans les feuilles, et la concentration en fer diminue dans les tiges. L'expression des transporteurs de métaux est dérégulée dans les tiges et les fleurs (Briat *et al.*, 2010). Les génes *AtFer1, AtFer3* et *AtFer4* sont induits par l'excés de fer, seul *AtFer1* est induit en présence de $H_2O_2$ et serait donc aussi impliqué dans la réponse au stress oxydatif.

### *b) Rôle et régulation de la ferritine chez les micro-algues*

En 2009, Marchetti et al. ont mis en évidence que les diatomées du genre *Pseudo-nitzschia* possèdent une ferritine qui est adressée au chloroplaste et s'assemble en complexe de 24-mer. Le gène codant cette ferritine est transcrit en présence de fer extracellulaire, et son induction est proportionnelle à la concentration en fer dans le milieu. Cette nano-cage de ferritine serait capable de stocker 600 atomes de Fe. Lorsque les cellules de *Pseudo-nitzschia granii* sont transférées vers un milieu sans fer, après une préculture dans un milieu supplémenté en fer, elles continuent à se diviser pendant plus longtemps, et dans de meilleures conditions, que d'autres diatomées océaniques, comme *Thalassiosira oceanica,* qui ne possèdent pas le gène codant pour la ferritine. Le rendement photochimique maximal du PSII (Fv/Fm) reste stable pendant 5 jours chez *P.grannii* alors qu'il diminue dès le deuxième jour chez *T.oceanica*. Les auteurs de cette étude ont émis l'hypothèse que la capacité de survie à la carence en Fer chez *Pseudo-nitzschia* de serait liée à la présence de la ferritine.

Les espèces océaniques du genre *Pseudo-Nitzschia* ont un ratio Fe/Carbone (Fe :C en µmol par mol) très variable selon qu'elles ont été cultivées en présence ou en absence de fer dans le milieu. Le rapport entre le ratio Fe/C entre ces deux conditions est beaucoup plus élevé chez

les espèces océaniques du genre Pseudo-Nitzschia (3 à 12 x) que chez d'autres diatomées océaniques comme *Thalassiosira oceanica*. Si l'on compare ce rapport chez des écotypes côtiers de *Pseudo-Nitzschia* et de *Thalassiosira* on retrouve cette différence, mais amoindrie (1,5 à 5,5 x). Ceci suggère que le genre *Pseudo-Nitzschia*, et plus particulièrement les espèces océaniques, i) utilise le fer plus efficacement lors d'une carence, ii) importe et stocke beaucoup plus de fer (Marchetti *et al.*, 2006). L'implication de la ferritine dans cette survie a été également proposée. Si cette hypothèse est séduisante, elle manque de preuves expérimentales. *La capacité de Pseudo-Nitzschia à gérer la carence en fer pourrait également s'expliquer par d'autres mécanismes comme ceux décrits dans la section 2, ci-dessus.*

# 4 Les liens entre l'horloge circadienne et l'homéostasie du fer.

La rotation de la terre sur elle-même en 24 heures est à l'origine des alternances jour/nuit. De plus l'inclinaison de l'axe des pôles, qui varie au cours de la rotation autour du Soleil, influe sur la longueur relative du jour par rapport à la nuit, engendrant des saisons marquées aux hautes latitudes. Ceci se traduit par des jours plus courts et des températures plus faibles en hiver qu'en été. La majorité des êtres vivants se sont adaptés à ces variations rythmées de leur environnement au cours du cycle diurne (24 heures) et annuel (365 jours), en coordonnant de nombreux processus biochimiques, physiologiques et comportementaux en fonction des cycles journaliers et saisonniers. Un rythme biologique est caractérisé par trois paramètres principaux : sa période, sa phase et son amplitude. La période libre des oscillations (ou FRP pour Free Running Period) est utilisée comme paramètre pour classer les différents types de rythmes biologiques. Ainsi on regroupe les rythmes biologiques selon trois grandes classes, ultradien (haute fréquence), circadien (période entre 20 et 28h) et infradien (périodicité mensuelle ou annuelle).

La persistance des rythmes biologiques en l'absence de variations de l'environnement (lumière continue ou température stable) implique la présence d'une horloge biologique interne autonome, capable de coordonner les processus biologiques en l'absence de signaux extérieurs, que l'on appelle l'horloge circadienne. Cette capacité à mesurer le temps permet d'anticiper les variations cycliques prédictibles comme les transitions entre le jour et la nuit à l'aube et au crépuscule.

Si l'horloge circadienne est un donneur de temps autonome qui oscille avec une période d'environ 24 heures, elle est entrainable par les cycles environnementaux journaliers de lumière et/ou de température.

De façon schématique, l'horloge biologique peut être décomposée en trois compartiments : 1) un oscillateur central, qui est capable de maintenir un rythme de 24h de manière autonome, 2) des voies d'entrée vers l'oscillateur central, qui permettent de renseigner l'oscillateur sur les variations de l'environnement afin de le synchroniser. 3) les voies de sortie, régulées par l'oscillateur central qui contrôlent la rythmicité de nombreux processus biologiques tels que le métabolisme, la photosynthèse ou la division cellulaire (Figure 10). Cependant, même si cette représentation permet d'appréhender la nature de l'horloge, elle n'intègre pas les interconnections complexes entre les différents compartiments qui permettent, par exemple à l'oscillateur central de réguler la voie d'entrée des signaux lumière ou température, processus dénommé« gating » en anglais.

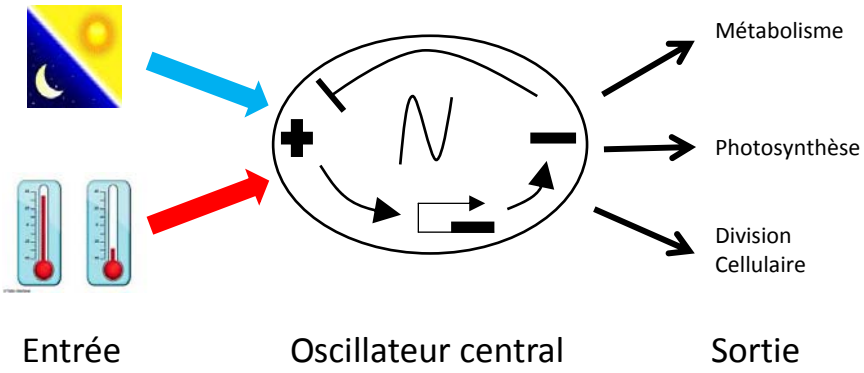


*Figure 10: Représentation schématique des trois compartiments de l'horloge circadienne*

### 1. Les acteurs moléculaires de l'oscillateur central

De manière générale, l'oscillateur central est composé de boucles de rétrocontrôle couplées, chacune faisant intervenir des éléments répresseurs qui répriment leur propre expression en inhibant leurs activateurs (Figure 10). Si ce schéma générique a été retrouvé chez de multiples organismes, des cyanobactéries aux animaux, champignons et plantes, en revanche les acteurs de l'horloge ne sont pas conservés. Seule l'horloge des plantes est présentée ci-dessous.

Chez *A.thaliana*, les principaux acteurs moléculaires de l'horloge circadienne ont été identifiés à l'aide de mutants présentant des défauts de l'horloge circadienne ou de photopériodisme. TOC1 (Timing of CAB expression 1*)* est un pseudo régulateur de réponse (Strayer *et al.*, 2000), ce gène central de l'horloge réprime la transcription de CCA1 (Circadian Clock Associated 1) (Wang and Tobin, 1998) et LHY (Late elongated HYpocotyl) (Schaffer *et al.*, 1998). Ces trois gènes constituent le cœur de l'horloge circadienne

d'*A.thaliana*, CCA1 et LHY sont des facteurs de transcription de type MYB qui répriment l'expression de *toc1*(Mizoguchi *et al.*, 2002). Des approches expérimentales couplées à des modélisations mathématiques ont montré que l'horloge d'*A.thaliana* repose sur au moins 3 boucles interconnectés. La boucle du matin est composée des gènes *prr7/prr9* qui répriment leurs activateurs CCA1/LHY le matin. La boucle de rétrocontrôle centrale est constituée du gène *toc1* transcrit le soir, qui réprime l'expression de ses répresseurs: les gènes *cca1* et *lhy* (Huang *et al.*, 2012; Gendron *et al.*, 2012), exprimés en fin de nuit et le matin. La boucle du soir comprend TOC1, GI et ZTL. GI est un activateur de *toc1* qui est réprimé par CCA1/LHY et TOC1. ZTL est un répresseur de la transcription de *toc1* qui est inactivé en présence de GI et TOC1. Il existe une forte redondance génétique entre les gènes de l'horloge avec 9 facteurs de transcription de type MYB SANT de la famille de CCA1/LHY et 5 de type PRR (TOC1), impliqués à divers degrés dans l'horloge circadienne (Carre, 2002; Harmer, 2009)

## 2. Influence de la lumière sur l'entrainement de l'horloge circadienne

L'une des fonctions fondamentales des voies d'entrée est de renseigner l'horloge circadienne sur le temps externe par rapport au temps interne de l'oscillateur central. Dans la nature, le temps externe est donné par l'alternance jour/nuit qui recale l'horloge chaque jour. Bien que de nombreux signaux environnementaux comme la température participent à la synchronisation du temps externe et du temps interne, le signal lumineux est l'un des plus importants, notamment chez les organismes photosynthétiques.

La coïncidence entre le temps interne donné par l'oscillateur central et le temps externe (photopériode) permet de réguler des processus annuels comme le déclenchement de la floraison chez *A.thaliana.* La lumière est un donneur de temps externe qui influe directement sur la période et la phase de l'horloge circadienne (Millar, 2004). Ainsi lorsque les espèces diurnes sont soumises à des augmentations d'intensité lumineuse dans des conditions de FRP, leur période libre diminue. Inversement, chez les espèces nocturnes placées dans les mêmes conditions, on observe un allongement de la période libre lorsqu'on augmente l'intensité lumineuse. Cette propriété a été décrite de manière empirique par la loi d'Aschoff (Aschoff, 1979).

La sensibilité de l'horloge circadienne à la lumière varie en fonction du moment du cycle, l'horloge étant plus sensible aux variations lumineuses lors des transitions jour/nuit alors qu'elle est peu affectée au cours de la journée. Cette sensibilité se traduit par des modifications de la phase de l'horloge, illustrées par les Courbes de Réponse de Phase (PRC).

En général, ces PRC montrent une avance de phase en début de jour, un retard de phase en fin de journée et une zone morte, « Dead-zone » en anglais, en milieu de journée indiquant une faible sensibilité au recalage.

### 3. Influence de l'homéostasie du fer sur l'horloge circadienne d'A.thaliana

Le gène *TIC (TIme for Coffee),* impliquée dans la perception de la lumière au sein de l'horloge circadienne, régule l'expression rythmique de la ferritine. Les signaux lumineux sont indispensables à cette régulation. En cycle jour/nuit, la ferritine est fortement exprimée à la fin de la nuit alors qu'en condition de lumière continue elle est fortement exprimée à la fin de la journée. La transcription de *Atfer1* continue à être induite par l'excès de fer dans un mutant *tic*, il y a donc un autre élément qui régule l'expression de *Atfer1*et le signal qui renseigne la plante sur l'homéostasie du fer ne passe pas par *tic* (Duc *et al.*, 2009). La perméase spécifique de l'importation du $Fe^{2+}$, *irt1* est transcrite en milieu de journée sous contrôle de l'horloge circadienne, mais seulement si les stocks de fer sont insuffisants (Hong *et al.*, 2013). Le facteur de transcription BHLH39, fortement induit lors d'une carence en fer, est lui aussi régulé par l'horloge circadienne, avec un maximum d'expression en fin de nuit.

Chez *A.thaliana* la concentration en fer disponible dans le milieu (sous forme de hème ou de fer complexé à un ligand hexadendate) influence directement la FRP des principaux gènes de l'horloge, qui augmente en absence de fer (Chen *et al.*, 2013; Salomé *et al.*, 2013; Hong *et al.*, 2013). De même, dans des mutants *irt* et *firt* (Facteur de transcription d'IRT) qui ont une assimilation du fer fortement réduite et présentent un déficit en fer constitutif, le gène *cca1*a une période plus longue (Hong *et al.*, 2013). Seul les mutants de l'horloge *cca1lhy* et *gi* ne répondent pas à la carence en fer en allongeant leur FRP, ce qui montre leur rôle dans l'intégration du signal du manque de fer à l'oscillateur central (Chen *et al.*, 2013). En l'absence de phytochromophores (mutant *phyAphyB*) ou suite la mutation de leurs voies de biosynthèse (mutants *hy6* et *hy2*), l'allongement de la FRP n'est plus observée en réponse à la carence en fer (Salomé *et al.*, 2013). Le mutant *hmr*, incapable de transporter les phytochromophores (comme phyA et phyB) réduits vers le noyau, n'ajuste plus sa période en fonction du fer disponible, ce qui suggère que la réponse de l'horloge circadienne au fer nécessite le transport de phytochromes photo-activés vers le noyau. Chez des plantes traitées avec des inhibiteurs de la biogénèse du chloroplaste (erythromicine, chloramphénicol, lincomycine), et des semis étiolées (sans chloroplaste) qui sont moins sensibles à l'apport en fer, la période de l'horloge ne varie pas en fonction du fer disponible (Salomé *et al.*, 2013).

Les activités transcriptionnelle et traductionnelle du chloroplaste seraient donc nécessaire pour renseigner l'horloge nucléaire sur le niveau de fer disponible (Figure 11).

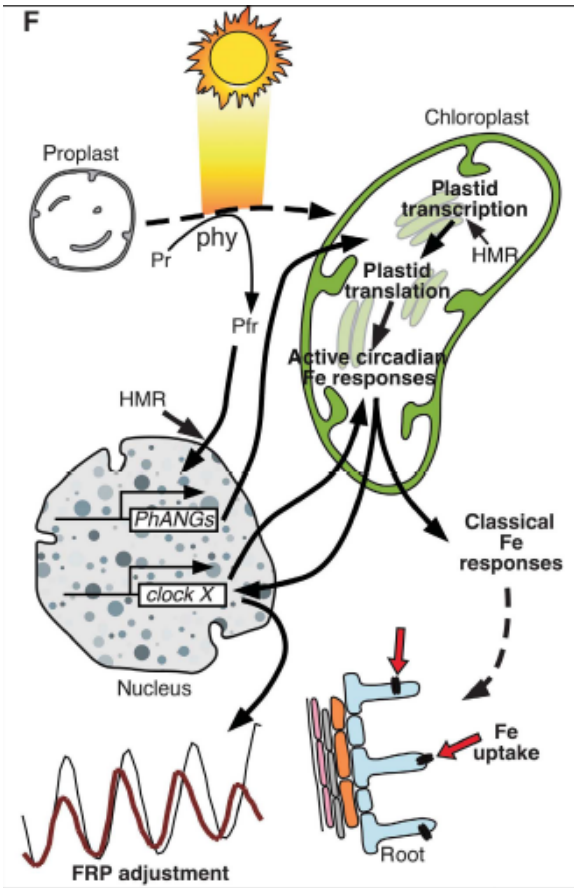


Pr : phytochromophores,
Pfr: phytochromophores photo réduit
HMR :HEMERA,
PhANGs : Photosynthesis-associated nuclear genes,
FRP : Free Running Period.
Fléche rouge: Import de fer.

*Figure 11: Schéma des réponses à la carence en fer chez A.thaliana (Salomé et al., 2013)*

# 5 *Ostreococcus tauri*, une algue modèle

## 1. Caractéristiques/Présentation

*Ostreococcus tauri* est un pico-eucaryote phytoplanctonique isolé dans l'étang de Thau (Courties *et al.*, 1994), appartenant à la classe des Prasinophyceae dans l'infra-règne des chlorophytes qui a divergé à la base de la lignée verte (Courties *et al.*, 1998; Baldauf, 2003; Waters, 2003). Cet unicellulaire est considéré comme le plus petit eucaryote libre découvert à ce jour, avec un diamètre inférieur à 1µm. L'organisation cellulaire d'*O.tauri* est particulièrement simple, avec un noyau, une mitochondrie, un appareil de golgi, un peroxysome et un seul chloroplaste qui occupe environ 45% du volume cellulaire (Figure 12). *O.tauri* est dépourvu de paroi cellulaire et de flagelle (Chrétiennot-Dinet *et al.*, 1995; Henderson *et al.*, 2007)

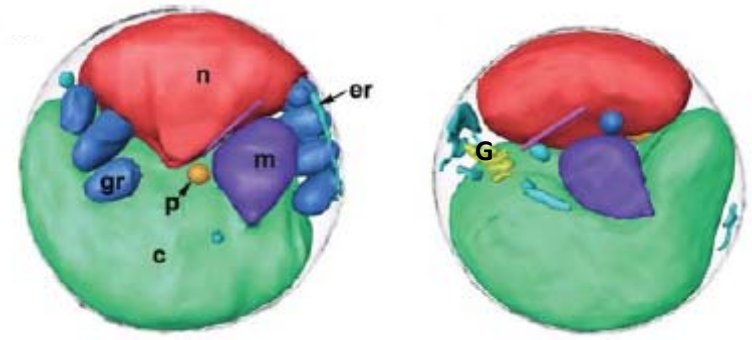


*Figure 12: Organisation cellulaire d'O.tauri. n : noyau, mt : mitochondrie, c : chloroplaste, p :peroxysome, G : appareil de Golgi, gr : grana ; er : réticulum endoplasmique d'après Henderson et al., 2007*

Le genre *Ostreococcus* est répandu dans l'océan mondial, à l'exception des zones les plus oligotrophes. Il existe une grande variété d'espèces encore appelés écotypes d'*Ostreococcus* adaptés à de nombreuses niches écologiques différentes du point de vue de la lumière (Six *et al.*, 2008; Rodríguez *et al.*, 2005), des nutriments, de la salinité, de la température (Demir-Hilton *et al.*, 2011). Certains écotypes, comme *Ostreococcus lucimarinus* ou *RCC809* ont été caractérisés et séquencés ce qui les rend particulièrement attractifs pour des études de génomique comparative dans un contexte d'adaptation à l'environnement.

## 2. Propriétés du génome d'*Ostreococcus tauri*

*Ostreococcus tauri* possède un génome haploïde de petite taille (12.6 Mb), contenant de l'ordre de 8000 gènes répartis sur 20 chromosomes. Son génome est extrêmement compact, avec 81.6% de séquences codantes, soit une densité génétique de 1,54 kb par gène et des

régions intergèniques d'une taille inférieure à 200pb (Derelle *et al.*, 2002; Derelle *et al.*, 2006). Ce génome contient peu de familles multigéniques, ce qui suggère une faible redondance fonctionnelle entre les gènes. Ainsi *O.tauri* contient moins de 200 facteurs de transcription au total. Les génomes de la mitochondrie et du chloroplaste d'*O.tauri* ont aussi été séquencés (Robbens *et al.*, 2007). Le génome mitochondrial est particulièrement dense, il contient 65 gènes avec des régions intergèniques d'à peine 42 pb. Son génome chloroplastique est l'un des plus petits chez les Viridiplantae avec une taille de 71 kb pour 86 gènes (Robbens *et al.*, 2007). La faible redondance génétique, la compaction du génome, la simplicité de l'organisation cellulaire et un nombre limité de facteurs de transcription font de cet organisme un très bon modèle pour l'étude fonctionnelle de processus complexes impliquant des réseaux de gènes. Une étude transcriptomique au cours du cycle jour/nuit a mis en évidence la co-régulation de clusters fonctionnels de gènes associés à des processus biologiques tel que la traduction et la réplication de l'ADN (Monnier *et al.*, 2010).

### 3. Outils génétiques

Le développement de la transformation génétique stable chez *O.tauri* a permis de promouvoir cet organisme comme nouveau modèle biologique afin d'étudier le picophytoplancton marin. Cette technique, qui a été développée par l'équipe de FY Bouget, permet d'introduire et insérer de l'ADN de façon stable dans le génome d'*O.tauri*. Ainsi, des gènes fusionnés à celui codant pour la luciférase de luciole ont pu être insérés dans le génome pour suivre l'expression de ces gènes *in vivo* en temps réel. Il est possible d'utiliser des rapporteurs transcriptionnels (promoteurs d'intérêt fusionnés à la luciférase) et traductionnels (gènes complets en amont du codon stop fusionnés en phase de lecture à celui de la luciférase). L'utilisation du promoteur *HAPT*, (High Affinity Phosphate Transporteur), dont l'expression est modulable en fonction de la concentration en phosphate dans le milieu, permet de sur-exprimer ou de réprimer un transgène. Il est aussi possible de moduler l'expression d'un gène en insérant une construction génétique codant pour un ARN complémentaire au transcrit du gène que l'on veut réprimer, sous contrôle du promoteur HAPT. (Corellou *et al.*, 2009)

### 4. Horloge circadienne

#### *a) Horloge transcriptionnelle*

Des analyses *in silico* du génome d'*Ostreococcus tauri* ont permis de mettre en évidence la présence de gènes ayant des domaines similaires aux acteurs de l'horloge circadienne chez les

végétaux supérieurs. Seul deux gènes candidats ont été identifiés, un homologue de *toc1* et un homologue de *cca1*, présents à l'état de simple copie. Il y aurait donc un nombre réduit de gènes impliqués dans l'horloge d'*O.tauri* comparé aux plantes supérieures. L'expression de ces deux gènes est rythmique dans des conditions de lumière continue, et la surexpression de l'un entraîne l'arythmie de l'autre (Corellou *et al.*, 2009). Les profils d'expression et les analyses fonctionnelles de TOC1 et de CCA1 sont compatibles avec l'existence d'une boucle de rétrocontrôle à deux gènes. Dans cette boucle TOC1 active l'expression de *cca1*au crépuscule et CCA1 réprime l'expression de *toc1*. Pour valider cette boucle de rétrocontrôle, un modèle mathématique simple de la transcription et de la traduction de TOC1/CCA1 a été développé. Ce modèle permet de reproduire avec précision les profils de transcription et de traduction de TOC1/CCA1, confirmant l'existence de cette boucle de rétrocontrôle (Thommen *et al.*, 2010; Morant *et al.*, 2010). D'après ces modèles mathématiques, l'horloge d'*Ostreococcus* est à la fois robuste et flexible. Robuste car elle est peu perturbée par des variations lumineuses au cours de la journée, et flexible car elle reste sensible aux variations lors des transitions jour/nuit (i.e. aube/crépuscule) et peut s'acclimater à un large éventail de photopériodes (Pfeuty *et al.*, 2012)

### *b) Horloge non-transcriptionnelle*

Il a été observé que les rythmes circadiens se maintenaient dans des cellules énucléées (hématie, cellules végétales (Woolum, 1991)), suggérant l'existence d'horloges non-transcriptionnelles. Chez *Synechococcus* et *Ostreococcus* des cellules placées en obscurité constante arrêtent leur transcription (O'Neill *et al.*, 2011). Les rythmes reprennent des phases différentes en fonction du moment où les cellules gardées à l'obscurité sont de nouveau placées à la lumière. Ceci indique l'existence d'un mécanisme de « gating » qui serait sous contrôle d'une horloge non transcriptionnelle. . Chez *Ostreococcus tauri* et plusieurs autres eucaryotes et cyanobactéries, la sulfonylation des péroxyrédoxines présente un rythme circadien à l'obscurité, ce qui suggère la présence de cycles d'oxydo-réduction ayant une période d'environ 24h en l'absence de transcription (Edgar *et al.*, 2012). En revanche ces rythmes sont absents en lumière continue, ce qui pose la question de la connexion entre les horloges transcriptionnelle et non transcriptionnelle (Bouget *et al.*, 2014).

## 5. Objectifs de la thèse :

Le milieu marin se distingue du milieu terrestre par des concentrations en fer faibles, souvent limitants pour le phytoplancton. Au cours de ma thèse, je me suis attaché à répondre aux questions suivantes :

**Quels sont les mécanismes d'assimilation et de stockage du fer chez les microalgues marines et en particulier chez *Ostreococcus tauri* ?**

Ce travail mené en parallèle sur plusieurs microalgues a été développé en collaboration avec Emmanuel Lesuisse et Robert Sutak. Je me suis concentré principalement sur *O. tauri.* Parmi les questions abordées, j'ai étudié l'assimilation de différentes sources de fer, l'influence du cycle jour/nuit sur l'assimilation du fer ainsi que les principales protéines de stockage du fer chez *O. tauri* et *P. tricornutum*. L'une des conclusions de ce travail est que l'importation du Fer est régulée par le cycle jour/nuit et que la ferritine est la principale protéine qui lie le fer chez *O. tauri*. Dès lors je me suis focalisé sur l'étude de cette protéine.

**Quel est le rôle de la régulation circadienne de la ferritine chez *Osterococcus tauri ?***

Chez *Ostreococcus tauri* l'expression de la majorité des gènes est régulée par l'alternance jour/nuit aussi bien en laboratoire (Monnier *et al.*, 2010) qu'*in situ* (Ottesen *et al.*, 2013). Ainsi les protéines associées à la photosynthèse sont exprimées en début de journée, alors que la ferritine est exprimée au crépuscule. Compte tenu du rôle supposé de la ferritine dans la gestion de la carence en fer chez les diatomées (Marchetti *et al.*, 2009) et de l'importance du recyclage du fer en cycle jour/nuit chez les cyanobactéries (Saito *et al.*, 2011), la question de l'importance de la régulation de la ferritine par le cycle jour/nuit se pose, en particulier dans *(i)* l'importation du fer extracellulaire au cours du cycle jour/nuit,*(ii)*la gestion du pool de fer au cours du cycle jour/nuit dans des cellules limitées en fer, *(iii)* la survie cellulaire dans des conditions de carence en fer.

Par la suite, j'ai exploité la diversité naturelle du genre *Ostreococcus* pour étudier les mécanismes mis en œuvre lors de l'exposition à la carence en fer.

**Quelles stratégies ont adopté différents écotypes d'*Ostreococcus* provenant d'environnements variés ?**

Je me suis intéressé à plusieurs écotypes d'*Ostreococcus* provenant d'environnements très variés du point de vue de la biodisponibilité en fer, afin de comprendre quelles sont les différentes solutions adoptées par le genre *Ostreococcus* pour gérer la limitation en fer. La réduction de la biomasse semble être une stratégie fructueuse pour survivre à la carence en fer. Pour tester cette hypothèse, j'ai étudié la réponse à la carence d'un mutant d'*Ostreococcus* présentant des biomasses cellulaires plus faibles.

# II. **Résultats**

# 1 Chapitre 1 : Caractérisation des systèmes d'assimilation et de stockage du fer

Dans un premier temps, en collaboration avec Robert Sutak et Emmanuel Lessuisse, nous nous sommes intéressés aux stratégies d'assimilation du fer de différentes micro-algues, appartenant à des phylums écologiquement importants : les diatomées *Phaeodactylum tricornutum* et *Thalassiosira pseudonana*, les prasinophyceae *Ostreococcus tauri* et *Micromonaspusilla*, et un coccolithophore *Emilianiahuxleyi*. Nous avons montré que toutes ces micro-algues assimilent aussi bien le fer ferreux ($Fe^{2+}$) que le fer ferrique ($Fe^{3+}$) mais l'assimilation du fer ferreux est plus rapide. Parmi ces micro-algues, seules les deux diatomées sont capables de réduire le fer à l'aide d'un système de réductase ferrique, inductible chez *P.tricornutum* et constitutif chez *T.pseudonana*. Ce type de système est similaire à celui découvert chez *S.cerevisiae*. Chez toutes ces micro-algues, la variation de la charge en fer après dilution isotopique lors des expériences de chasse suggère que le fer est fortement lié à la membrane cellulaire avant d'être assimilé.

Pour ma part, j'ai utilisé une approche biochimique pour identifier les principales protéines de liaison du fer. Pour cela, j'ai réalisé des gels natifs à partir d'extraits de protéines natives de cellules ayant incorporé du fer radioactif ($^{55}Fe$) chez plusieurs micro-algues. J'ai détecté en autoradiographie une bande majoritaire à 480 kDa chez *O. tauri*. L'analyse par spectrométrie de masse MS/MS a révélé la présence de ferritine dans cette bande mais seulement en 25éme position (score Mascot). Cette bande correspondrait au complexe 24-mer de ferritine qui serait la principale protéine de stockage du fer chez *O.tauri*. A court terme, ce complexe se charge plus rapidement en fer ferreux. Chez *E. huxleyi*, le fer semble se fixer de façon uniforme sur les membranes et aucune protéine de liaison au fer n'a pu être identifiée. L'analyse chez la diatomée *P.tricornutum* n'a pas permis de détecter la ferritine mais la protéine ISIP2, codée par un gène surexprimé en réponse à la carence en Fer. J'ai participé à un travail de caractérisation de cette protéine, qui fait l'objet d'un article en cours de révision dans Current Biology dont je suis coauteur.

L'ensemble de ces résultats font partie d'un article publié dans Plant Physiology dont je suis second auteur.

### 1. Article 1:

A comparative study of iron uptake mechanisms in marine microalgae: iron binding at the cell surface is a critical step.

Sutak, R, Botebol, H, Blaiseau, P.-L., Léger, T., Bouget, F.-Y., Camadro, J.-M., & Lesuisse, E. (2012). *Plant Physiology*, *160*(4), 2271–84.

# A Comparative Study of Iron Uptake Mechanisms in Marine Microalgae: Iron Binding at the Cell Surface Is a Critical Step[1][W][OA]

**Robert Sutak, Hugo Botebol, Pierre-Louis Blaiseau, Thibaut Léger, François-Yves Bouget, Jean-Michel Camadro, and Emmanuel Lesuisse***

Department of Parasitology, Faculty of Science, Charles University, 12844 Prague, Czech Republic (R.S.); Université Pierre et Marie Curie (Paris 06), Centre National de la Recherche Scientifique Unité Mixte de Recherche 7621, Laboratoire d'Océanographie Microbienne, F–66651 Banyuls/Mer, France (H.B., F.-Y.B.); and Université Paris Diderot (Paris 07), Centre National de la Recherche Scientifique, Institut Jacques Monod, F–75013 Paris, France (P.-L.B., T.L., J.-M.C., E.L.)

We investigated iron uptake mechanisms in five marine microalgae from different ecologically important phyla: the diatoms *Phaeodactylum tricornutum* and *Thalassiosira pseudonana*, the prasinophyceae *Ostreococcus tauri* and *Micromonas pusilla*, and the coccolithophore *Emiliania huxleyi*. Among these species, only the two diatoms were clearly able to reduce iron, via an inducible (*P. tricornutum*) or constitutive (*T. pseudonana*) ferrireductase system displaying characteristics similar to the yeast (*Saccharomyces cerevisiae*) flavohemoproteins proteins. Iron uptake mechanisms probably involve very different components according to the species, but the species we studied shared common features. Regardless of the presence and/or induction of a ferrireductase system, all the species were able to take up both ferric and ferrous iron, and iron reduction was not a prerequisite for uptake. Iron uptake decreased with increasing the affinity constants of iron-ligand complexes and with increasing ligand-iron ratios. Therefore, at least one step of the iron uptake mechanism involves a thermodynamically controlled process. Another step escapes to simple thermodynamic rules and involves specific and strong binding of ferric as well as ferrous iron at the cell surface before uptake of iron. Binding was paradoxically increased in iron-rich conditions, whereas uptake per se was induced in all species only after prolonged iron deprivation. We sought cell proteins loaded with iron following iron uptake. One such protein in *O. tauri* may be ferritin, and in *P. tricornutum*, Isip1 may be involved. We conclude that the species we studied have uptake systems for both ferric and ferrous iron, both involving specific iron binding at the cell surface.

There are two main strategies for iron uptake by terrestrial microorganisms and plants, and both have been characterized in the yeast *Saccharomyces cerevisiae* (for review, see Kosman, 2003; Philpott and Protchenko, 2008; Blaiseau et al., 2010). The first is the reductive mechanism of uptake. Extracellular ferric complexes are dissociated by reduction via transplasma membrane electron transfer catalyzed by specialized flavohemoproteins (Fre). In yeast, free ferrous iron is then imported as such, or by a high-affinity permease system (Ftr) coupled to a copper-dependent oxidase (Fet), allowing iron to be channeled through the plasma membrane (this reoxidation step is not found in higher plants). In the second strategy, the siderophore-mediated mechanism, siderophores excreted by the cells or produced by other bacterial or fungal species are taken up without prior dissociation via specific, copper-independent high-affinity receptors. The iron is then dissociated from the siderophores inside the cells, probably by reduction (for review, see Philpott, 2006; Blaiseau et al., 2010). *Chlamydomonas reinhardtii* is a model photosynthetic eukaryotic freshwater organism for the study of iron homeostasis and shares with yeast the first strategy of iron uptake (iron reduction followed by uptake involving reoxidation of iron by a multicopper oxidase; Merchant et al., 2006; Allen et al., 2007).

Much less is known about the strategies used by marine phytoplankton to acquire iron. There is evidence that these two strategies are used by some marine microalgae (for review, see Morrissey and Bowler, 2012). A yeast-like reductive uptake system has been suggested in the marine diatoms *Thalassiosira pseudonana* (Armbrust et al., 2004) and *Phaeodactylum tricornutum* (Kustka et al., 2007; Allen et al., 2008; Bowler et al., 2008) on the basis of gene

[1] This work was supported by the French Agence Nationale de la Recherche (grant no. ANR 11 BSV7 018 02 "PhytoIron"), by the Ministry of Education of the Czech Republic (grant no. MSM 0021620858), by a Marie Curie European Reintegration Grant (within the 7th European Community Framework Program) project no. UNCE 204017, and by the Centre National de la Recherche Scientifique (Centre National de la Recherche Scientifique fellowship to H.B).

* Corresponding author; e-mail lesuisse.emmanuel@ijm.univ-paris-diderot.fr.

The author responsible for distribution of materials integral to the findings presented in this article in accordance with the policy described in the Instructions for Authors (www.plantphysiol.org) is: Emmanuel Lesuisse (lesuisse.emmanuel@ijm.univ-paris-diderot.fr).

[W] The online version of this article contains Web-only data.

[OA] Open Access articles can be viewed online without a subscription.

www.plantphysiol.org/cgi/doi/10.1104/pp.112.204156

  

sequence homology and transcriptomic analyses, and copper-dependent reductive uptake of iron has been demonstrated for *Thalassiosira oceanica* (Maldonado et al., 2006). The existence of marine siderophores has also been established (Butler, 1998, 2005; Mawji et al., 2008), and their use by certain microalgae as an iron source, through reductive or nonreductive mechanisms, has been documented (Soria-Dengg and Horstmann, 1995; Naito et al., 2008; Hopkinson and Morel, 2009). However, for most marine unicellular eukaryotes, the mechanisms of iron assimilation are completely unknown. The strategies used by these organisms to acquire iron must have evolved to adapt to the very particular conditions that prevail in their surrounding natural environment: the transition metal composition of the ocean differs greatly from that of terrestrial environments (Butler, 1998). The form in which iron exists in ocean water remains unclear. Morel et al. (2008) suggested that unchelated iron may be an important source of iron for phytoplankton, whereas other authors have suggested that most of the ferric iron in ocean water is complexed to organic ligands, with conditional stability constants in the range of $10^{11}$ to $10^{22}$ $M^{-1}$ (Rue and Bruland, 1995; Butler, 1998). Colloidal iron has been identified as a major form of iron at the surface of the ocean (Wu et al., 2001). In any case, iron levels in surface seawater are extremely low (0.02–1 nM; Turner et al., 2001). Most existing research supports the general model of iron uptake by marine eukaryotic phytoplankton, involving membrane transporters that directly access dissolved monomeric inorganic iron species (Sunda, 2001): in *T. pseudonana*, for example, iron uptake is related to the concentration of unchelated ferric iron species (Fe′) and is independent of the concentration of iron chelated to synthetic ligands (Sunda, 2001; Morel et al., 2008). We found that this also applies to *Chromera velia* (Sutak et al., 2010). Depending on the ligands present in the system, the equilibrium free ferric ion (Fe′) concentration is in the range of $10^{-16}$ to $10^{-19}$ M, a concentration that seems incompatible with the functioning of any classic metal transport system. No classic iron uptake system with a $K_d$ in the nanomolar range has ever been found. A strategy of iron uptake operating efficiently in a terrestrial environment that contains iron at micromolar concentrations may thus be ineffective in a marine environment. Additionally, the marine environment imposes physical limits on the classic strategies of uptake, including the high diffusion rate of the species of interest, notably siderophores and reduced iron (Völker and Wolf-Gladrow, 1999). Therefore, there are likely to be completely different mechanisms of iron uptake in phytoplanktonic algae that have not yet been discovered. Photoreductive dissociation of natural ferric chelates or ferric colloids in seawater could increase the "free" iron (Fe′) concentration available for transport by over 100-fold (Sunda, 2001). Consequently, dark/light cycles may be relevant to the regulation of these postulated iron uptake systems in phytoplanktonic species.

The fate of intracellular iron in marine microalgae is also poorly understood. As in all plants, iron is primarily involved in the electron transfers required for photosynthesis and respiration, but little is known about how phytoplanktonic species adapt to iron scarcity. In chronically low-iron regions, the lack of iron in seawater, and the resulting decrease in iron uptake, could theoretically trigger two kinds of metabolic responses in addition to the changes observed in cell morphology (Allen et al., 2008; Marchetti et al., 2009). The cells may mobilize intracellular iron stores, if present, or adapt their metabolism to reduce the requirement for iron for electron transfer and energy production. Intracellular iron stores, in the form of ferritin, have only been evidenced in pennate diatoms (Marchetti et al., 2009), although ferritin genes have now been detected in several species (Allen et al., 2008; Monnier et al., 2010). Different kinds of metabolic responses of eukaryotic phytoplankton to iron starvation have also been proposed, mainly on the basis of whole-genome analyses (Finazzi et al., 2010), but very few experimental data are available, and when available, the authors generally used ferric EDTA as the only iron source. Ferric EDTA is widely used as the iron source for studies of iron uptake by marine microalgae (Anderson and Morel, 1982; Shaked et al., 2005; Shaked and Lis, 2012), because EDTA buffers an easily calculated pool of unchelated iron (Fe′) in the medium (Shaked et al., 2005). However, the stability constants ($\log K_1$) of ferric and ferrous EDTA are both very high (25.7 and 14.3, respectively); thus, using ferric EDTA as an iron source in experiments of iron uptake does not allow discrimination between reductive and nonreductive uptake. Most ferric ligands, unlike EDTA, have a much lower stability constant for ferrous iron than for ferric iron, and this is the reason why the reductive iron uptake system is so powerful: it catalyzes the dissociation of ferric iron from most of its ligands by reduction, allowing ferrous iron to be taken up by a unique system from very different ferric chelates. The estimated stability constant for the monoiron(III) dicitrate complex is in the range (log) 19.1 to 38.7 (Silva et al., 2009), and for the ferrous complex it is about (log) 3. This explains how yeast cells can take up ferric citrate and different ferri-siderophore complexes reductively, but not ferric EDTA (Lesuisse and Labbe, 1989). Intermediates of the Kreb's cycle have been shown to be good candidates for iron ligation in seawater (Vukosav and Mlakar, 2010). We thus used ferric citrate as the main source of ferric iron and ferrous ascorbate as the main source of ferrous iron (the iron sources generally used in the yeast model), although we also studied other iron sources but in less detail.

We tried to determine experimentally the main features of iron uptake from these iron sources by five phylogenetically unrelated microalgae species representative of the marine and oceanic eukaryotic phytoplankton. We chose species that have their genomes sequenced and that are living in different ecological niches. Among the picoplanktonic prasinophytes, we studied the widespread coastal species *Ostreococcus tauri*, the smallest eukaryotic organism described until

now, and *Micromonas pusilla*, which is the dominant photosynthetic picoeukaryote in the western English Channel (Not et al., 2004). Among the important group of diatoms, we studied the centric diatom *T. pseudonana* and the pennate diatom *Phaeodactylum tricornutum*, because genomic studies on both species allowed the identification of genes putatively involved in iron metabolism and in the response to iron starvation (Armbrust et al., 2004; Allen et al., 2008). Finally, the oceanic species *Emiliania huxleyi* was chosen for this study, as it is the most abundant coccolithophore found in the Earth's oceans. The position of each species on a eukaryotic phylogenetic tree (Cepicka et al., 2010) is shown in Figure 1.

Our main goal was to identify the strategies of iron uptake (reductive or nonreductive) in these different species and the differences between them. We also examined the conditions, if any, of induction of the mechanisms of iron uptake.

## RESULTS

### Iron Requirement and Storage

We compared the iron requirements of the selected species by growing each of them with a series of concentrations of ferric citrate or in the presence of the hydroxamate siderophores ferrioxamine B (FOB) or ferrichrome (FCH), with a 100-fold excess of the desferri-siderophores desferrichrome and desferri-ferrioxamine B (DFOB) to ensure that all of the iron medium was complexed by the siderophores (Supplemental Table S1). We evaluated their ability to accumulate and store iron when added as ferric citrate (0.1 or 1 $\mu$M) to the growth medium (Table I). The five species showed nearly maximum growth rate (in exponential growth phase) with iron concentration as low as 0.01 $\mu$M in the medium, although this iron concentration was limiting for biomass production, except for *E. huxleyi* (Supplemental Fig. S1). This is indicative of very-high-affinity iron uptake systems and of high iron requirements. The diatom *T. pseudonana* showed the highest iron requirement, both in terms of maximum growth rate in the exponential growth phase and of biomass production: this species grew nearly 2-fold faster in the exponential phase (first 3 d of culture) and produced 4.5-fold more cells in the stationary phase (after 10 d of culture) when the iron concentration in the medium was shifted from 1 nM to 1 $\mu$M (Supplemental Table S1). In contrast, even the lowest iron concentration tested (1 nM) did not slow the growth of the coccolithophore *E. huxleyi*, and maximum biomass production (cell yield) by this species was reached at 0.01 $\mu$M (Supplemental Table S1). Iron concentrations of 1 $\mu$M or higher were toxic (as assessed from the growth rate; data not shown) for *E. huxleyi.* The growth rate of *T. pseudonana* continued to increase with increasing iron concentration up to 10 $\mu$M (the highest concentration we tested; data not shown). Thus, these two species have very different physiological responses to changes in the concentration of iron in the medium. The other species tested showed intermediate iron requirements in the order *O. tauri* > *M. pusilla* > *P. tricornutum* (Supplemental Table S1). The green algae *O. tauri* and *M. pusilla* showed generally similar behavior in terms of iron requirement and storage: the effects of iron concentration on the growth rate and biomass yield were very similar (Supplemental Table S1), and both species accumulated nearly identical amounts of iron (Table I).

Addition of the hydroxamate siderophore FCH or FOB (0.01 $\mu$M) with a large excess of the corresponding desferri-siderophores (1 $\mu$M) strongly or completely inhibited the growth of *O. tauri*, *M. pusilla*, and *T. pseudonana* but inhibited the growth of *E. huxleyi* and *P. tricornutum* more weakly, as reported previously (Soria-Dengg and Horstmann, 1995; Supplemental Table S1). Thus, two of the species were able to use iron initially bound to hydroxamate siderophores for growth (see below).

All the species were able to accumulate iron from the medium very efficiently (Table I). For comparison, yeast cells show optimum growth rate and cell yield when the concentration of iron in the medium is about 10 $\mu$M, leading to an intracellular concentration of iron of about 100 to 200 $\mu$M (Seguin et al., 2010). Clearly, the enrichment factor (cell-associated versus extracellular iron) was much higher in all the microalgae species tested, indicating the expression of very efficient mechanisms of iron uptake and concentration, as already described (for review, see Morrissey and Bowler, 2012). The two species of diatom overaccumulated iron more than the other species in the presence of excess iron (1 $\mu$M): a 10-fold increase in the concentration of iron in the medium led to a nearly 10-fold increase of iron associated with *T. pseudonana* cells (Table I). *T. pseudonana* cells in stationary phase (with a mean volume of 100 $\mu m^3$ per cell)

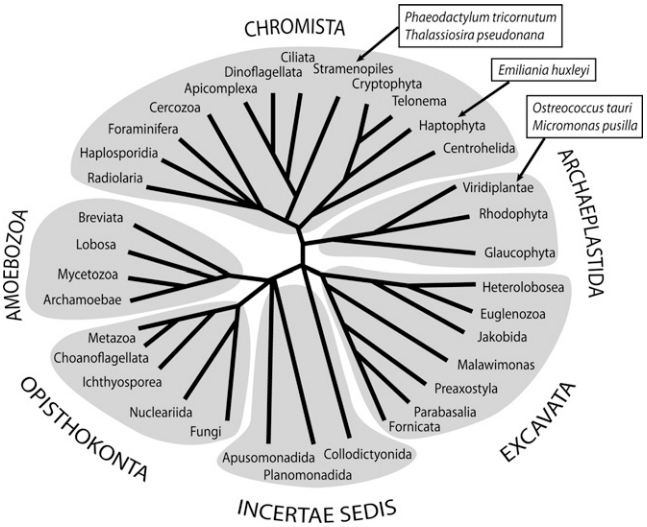


**Figure 1.** Eukaryotic phylogenetic tree showing the positions of the five marine microalgae species selected in this work.

**Table I.** *Iron associated with the cells as a function of the iron concentration in the medium*

Cells were grown with either 0.1 or 1 $\mu$M ferric citrate, harvested in the stationary phase, and washed with strong iron chelators as described in "Materials and Methods." Iron associated with the cells was then determined. Values are expressed in pmol iron 1 million cells$^{-1}$ and in $\mu$M iron within the cells (values in parentheses). Values shown are means ± SD from three experiments.

| Species | Fe 0.1 $\mu$M | Fe 1 $\mu$M |
|---|---|---|
| *P. tricornutum* | 10.2 ± 0.8 (65) | 52.3 ± 12.3 (350) |
| *T. pseudonana* | 5.99 ± 0.54 (50) | 53.56 ± 6.48 (450) |
| *O. tauri* | 0.59 ± 0.12 (400) | 0.99 ± 0.07 (670) |
| *M. pusilla* | 0.40 ± 0.02 (150) | 1.02 ± 0.16 (390) |
| *E. huxleyi* | 11.99 ± 0.72 (80) | 34.54 ± 7.65 (240) |

had accumulated about 70% of the total iron present in the culture medium (1 $\mu$M). In contrast, the smallest species, *O. tauri* (1 $\mu m^3$), increased its cellular iron content by only about 1.6-fold when the iron concentration was increased from 0.1 to 1 $\mu$M and accumulated about 10% of the iron present in the medium at this latter concentration (Supplemental Tables S1 and S2). In all species, the amount of iron accumulated by the cells clearly exceeded the cellular iron requirements, which implies the existence of iron storage mechanisms. These preliminary experiments show that the patterns of iron acquisition and accumulation differ between phylogenetically unrelated marine microalgae, suggesting different mechanisms of iron uptake and responses to iron starvation and iron excess.

### General Methodology

We investigated whether the uptake of ferric and/or ferrous ions and/or iron chelates could be induced/repressed by growth conditions. We also tested whether the species studied used a reductive mechanism of iron uptake, involving the expression of an inducible or a constitutive ferrireductase activity. The cells were precultured in either low-iron modified f (Mf) medium (0.01 $\mu$M) or in high-iron Mf medium (1 $\mu$M) for 1 week, harvested, and washed. The cells were then distributed equally into fresh high-iron Mf medium (2 $\mu$M) and into fresh iron-deficient Mf medium (no iron added). Cells were harvested from samples of these new cultures every day for 10 to 15 d and examined for ferrireductase and iron uptake activities. When cells reached late exponential or stationary phase, they were diluted in the same iron-rich and iron-deficient media. An example of the growth curves and ferrireductase activities obtained in one such experiment is shown in Figure 2.

### Cell Ferrireductase Activity and Transplasma Membrane Electron Transfer

*P. tricornutum* exhibited a ferrireductase activity that was induced after prolonged iron starvation (Fig. 1), whereas *T. pseudonana* showed constitutive ferrireductase activity (Fig. 2). The activity of this ferrireductase was in the same order of magnitude as that of the Fre1-dependent ferrireductase in iron-deficient yeast cells (0.5–2 nmol h$^{-1}$ 1 million cells$^{-1}$). Transcriptomic analyses, comparative genomic studies, and direct measurements of reductase activity have indicated the presence of a reductive system of iron uptake in diatoms (Shaked et al., 2005; Maldonado et al., 2006; Allen et al., 2008). Here, we show that the ferrireductase activity is regulated by iron availability in one diatom and constitutively expressed in another. In *P. tricornutum*, induction of ferrireductase activity was rapid but delayed by 7 d after the shift from high-iron medium to iron-deficient medium (Fig. 2). This lag period was decreased to 3 d when the cells were precultured in low-iron medium (0.01 $\mu$M) and shifted to iron-deficient medium (data not shown).

The green algae *M. pusilla* and *O. tauri* exhibited very low or undetectable ferrireductase activity (Fig. 2): in *M. pusilla*, the ferrireductase activity was iron independent and at least 1,000-fold weaker than that in diatoms; and in *O. tauri* and *E. huxleyi*, no ferrireductase activity was detected under any growth conditions (Fig. 2). Note that the sensitivity of the colorimetric assay we used may be too low to evidence very weak, but possibly significant, reductase activity. We previously showed that the transplasma membrane electron transport involved in the reduction of extracellular ferric complexes by yeast cells could be measured with a highly sensitive fluorometric assay based on reduction of the nonpermeant (blue) resazurin dye (electron acceptor) to resorufin (fluorescent red; Lesuisse et al., 1996). The inducible yeast reductase activity (using either resazurin or $Fe^{3+}$ as electron acceptor) is strongly inhibited by diphenylene iodonium (DPI), a powerful inhibitor of the neutrophil

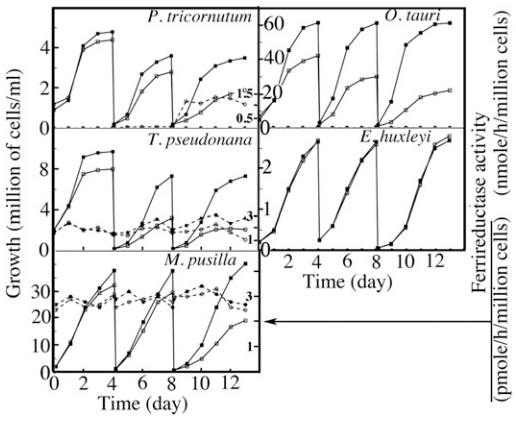


**Figure 2.** Iron-dependent growth and ferrireductase activity of the five marine microalgae species selected in this work. The cells were precultured in iron-rich medium (1 $\mu$M) for 1 week and washed, and aliquots were shifted to iron-rich medium (closed symbols) and iron-deficient medium (open symbols). Growth (squares) and ferrireductase activity (circles) were determined daily. When the cells reached the end of the exponential growth phase, they were diluted in the same medium. Data are from one representative experiment.

NADPH oxidase (Doussière and Vignais, 1992) and more generally of flavohemoproteins (Lesuisse et al., 1996). Therefore, we tested whether the algae species were able to reduce resazurin and measured the effect of DPI on resazurin reduction, using yeast cells as a reference (Fig. 3). The diatom species showed transplasma membrane electron transfer to resazurin, and this activity was inducible by iron deprivation in *P. tricornutum* and was constitutive in *T. pseudonana*, in agreement with the results of the colorimetric assay for iron reduction (Fig. 3). In both species, resazurin reduction was strongly inhibited by DPI, as in yeast, suggesting that flavohemoproteins (like Fre1 in yeast) are responsible for the ferrireductase activity in diatoms, as suggested previously (Allen et al., 2008; Morrissey and Bowler, 2012). Surprisingly, the green algae *M. pusilla* and *O. tauri* showed significant resazurin reductase activity (Supplemental Fig. S1), although ferrireductase activity in both species was very low or undetectable (Fig. 2). In these species, transplasma membrane electron transfer to resazurin was not induced by iron deprivation and was not inhibited by DPI (Supplemental Fig. S1). This suggests that the proteins involved in this activity are not related to the Fre family. *E. huxleyi* failed to reduce resazurin (Supplemental Fig. S1), consistent with findings for the alveolate *C. velia* (Sutak et al., 2010). Our results strongly support the hypothesis that diatoms can use a reductive mechanism for iron uptake, as suggested previously (Shaked et al., 2005; Allen et al., 2008).

### Kinetics of Iron Uptake from Ferric and Ferrous Iron Sources

We investigated iron uptake from the following iron sources: ferric citrate, ferrous ascorbate, ferric EDTA, and hydroxamate siderophores (FOB and FCH). We recorded the kinetics of iron uptake by cells harvested daily 6 h after the beginning of the light period in a night/day cycle of 8/16 h (for 10–15 d) from iron-rich and iron-deficient media (Fig. 2). Uptake kinetics were recorded either in the dark or in the light (3,000 lux). We will present selected representative results.

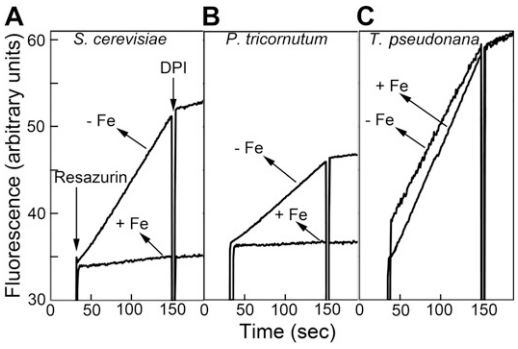


**Figure 3.** Reductase activity of yeast and diatoms with resazurin as the electron acceptor. A, Transplasma membrane electron transfer by whole cells was monitored by fluorimetric analysis of the formation of resorufin from resazurin (10 $\mu$M). Yeast was used as a control. Yeast cells were grown overnight in iron-rich (10 $\mu$M; + Fe) or iron-deficient (−Fe) medium. B and C, *P. tricornutum* (B) and *T. pseudonana* (C) were grown for 1 week in iron-rich (1 $\mu$M; +Fe) or iron-deficient (−Fe) medium. Yeast and diatoms were suspended at 100 million cells $mL^{-1}$ in citrate/Glc buffer and in Mf medium, respectively, and the formation of resorufin was monitored. The inhibitor DPI was added to a final concentration of 10 $\mu$M as indicated.

We did not observe major differences in short-term (2-h) iron uptake kinetics (from either ferric citrate or ferrous ascorbate) recorded in the dark or in the light (Supplemental Fig. S2). This suggests that photoreduction of ferric citrate was negligible under our experimental conditions, and most of the iron uptake kinetics were thus followed in the light.

Figure 4 shows typical kinetics of uptake from ferric citrate (1:20), ferric EDTA (1:1.2), and ferrous ascorbate (1:50) by the five selected species after 1 and 7 d (or 11 d for *E. huxleyi*) of growth in iron-rich and iron-deficient media (according to the pattern presented in Fig. 2). In all species, iron was taken up much more rapidly from ferric citrate than from ferric EDTA, and ferrous iron (ferrous ascorbate) was generally taken up more rapidly than ferric iron (ferric citrate). Both ferric and ferrous iron uptake activities were inducible by iron deprivation in all species, but there was a lag between shifting the cells from iron-rich to iron-deficient conditions and induction: this lag period was 3 d for *T. pseudonana*, 4 to 5 d for *O. tauri* and *M. pusilla*, 7 d for *P. tricornutum*, and 11 to 12 d for *E. huxleyi* (Fig. 4; data not shown). This lag could have been the consequence of iron bound to the cell surface when shifted, although the cells were washed with strong ferric and ferrous chelators before inoculation of the iron-deficient medium (see below). More surprisingly, species shifted from high-iron Mf medium (1 $\mu$M) to fresh high-iron Mf medium (2 $\mu$M) exhibited higher iron uptake activities (especially during the first 30–60 min of the kinetics) than cells shifted to iron-deficient medium (Fig. 4). A similar transient induction of iron uptake activities (which lasted for several days) occurred following a shift from low-iron medium (0.01 $\mu$M) to high-iron medium (2 $\mu$M; data not shown). This is suggestive of two different mechanisms of induction of iron uptake and/or binding, one responding rapidly to iron-rich conditions and the other responding after a prolonged period of iron deprivation.

Although some species were able to grow with hydroxamate siderophores as iron sources (Supplemental Table S1), the rate of iron uptake from FOB and FCH by all the species tested was similar to (for FCH) or slower than (for FOB) the rate of iron uptake from ferric EDTA and very much slower than that from ferric citrate (data not shown). Direct transport of hydroxamate siderophores mediated by specific receptors, therefore, is unlikely, although a gene encoding a putative FCH transporter has been found in *P. tricornutum* (Allen et al., 2008). Iron uptake from hydroxamate siderophores probably occurred either reductively (in diatoms) or after nonreductive dissociation of $Fe^{3+}$ from its ligands (as is probably the case for iron uptake from ferric EDTA).

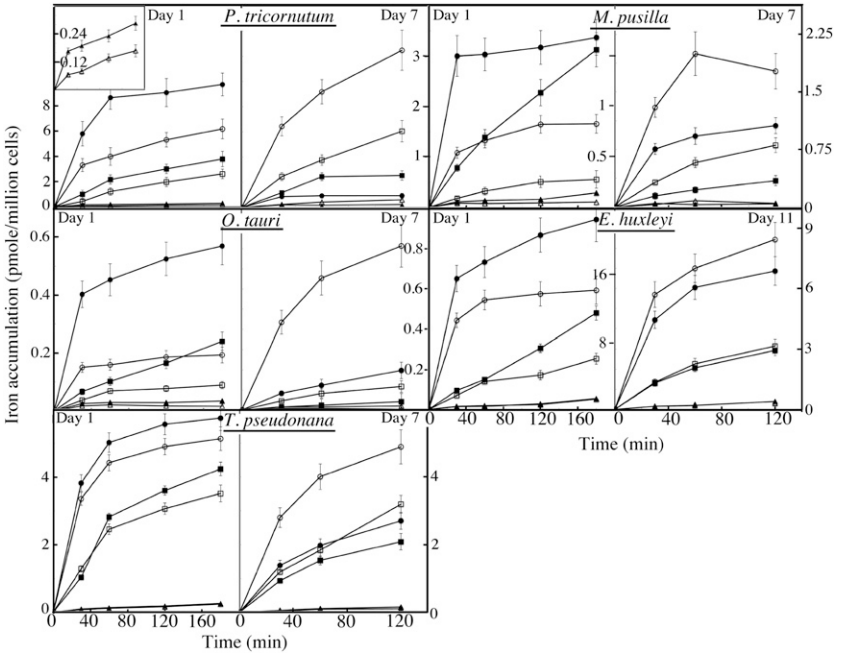


**Figure 4.** Iron uptake from various iron sources (1 $\mu$M) by the five marine microalgae species selected in this work, harvested after 1, 7, or 11 d of growth in iron-rich (closed symbols) or iron-deficient (open symbols) medium. Squares represent ferric citrate (1:20), circles represent ferrous ascorbate (1:50), and triangles represent ferric EDTA (1:1.2). The insert in the top left panel shows iron uptake from ferric EDTA at a different *y* scale. Values shown are means ± SD from four experiments.

In all species we tested, the rate of iron uptake from citrate, EDTA, or hydroxamate (siderophore) ferric complexes decreased substantially as the ligand-to-$Fe^{3+}$ ratio increased, as observed previously for the alveolate *C. velia* (Sutak et al., 2010) and for *Thalassiosira weissflogii* (Shaked et al., 2005). An example is shown in Figure 5 for ferric citrate. This observation strongly suggests that iron uptake is dissociative in all five species studied (i.e. that iron must be dissociated from its ligands prior to uptake by the cells). This observation also suggests that at least one limiting step of iron uptake is controlled thermodynamically rather than kinetically and does not involve a mechanism of iron channeling through the membrane, unlike what is observed in the high-affinity reductive iron uptake system of yeast (Kwok et al., 2006).

### Iron Reduction Is Not a Prerequisite for Iron Uptake

The results presented above and previous observations (Shaked et al., 2005; Allen et al., 2008; Morrissey and Bowler, 2012) suggest that some phytoplanktonic algae use a reductive mechanism for iron uptake. This is particularly evident for the diatom *P. tricornutum*, because both iron uptake and ferrireductase activity were induced by iron deprivation in this species. However, all of the species we studied were able to take up both ferric and ferrous iron, although ferrous iron was the preferred substrate in terms of uptake rate, regardless of the ferrireductase activity of the cells. For example, *P. tricornutum* acquired iron from ferric chelates even when its ferrireductase system was completely repressed (compare Figs. 2 and 4). Therefore, iron reduction may not be essential for iron uptake, unlike the situation in yeast. To evaluate the contribution of iron reduction to iron uptake from a ferric iron source, we measured the effect of a large excess (200 $\mu$M) of the strong ferrous chelator bathophenanthroline disulfonic acid (BPS) on initial iron uptake rates from ferric citrate (1 $\mu$M). The experiments were done in the dark to avoid photoreduction of ferric citrate, which is strongly promoted by BPS addition. After 15 min, BPS inhibited iron uptake

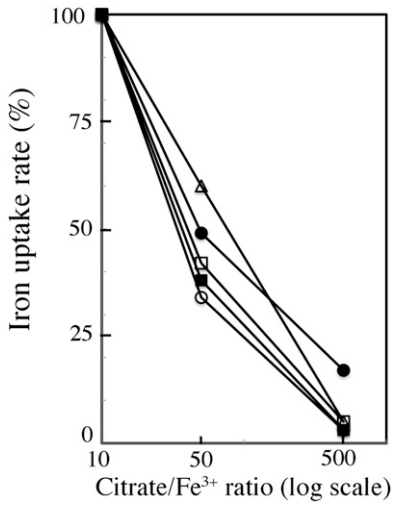


**Figure 5.** Effect of increasing the ligand (citrate)-$Fe^{3+}$ ratio on iron uptake. The cells (grown under standard conditions) were incubated for 1 h in uptake buffer with 1 $\mu$M $Fe^{3+}$ complexed with 10, 50, or 500 $\mu$M citrate, and iron taken up by the cells was determined. Results are expressed as percentage of the maximal uptake rate for each species. Open circles represent *P. tricornutum*, closed circles represent *T. pseudonana*, open squares represent *O. tauri*, closed squares represent *M. pusilla*, and triangles represent *E. huxleyi*. Values shown are means from four experiments. Error bars are not shown for the sake of clarity, but SD values in all cases were 7% or less.

by 71% ± 3% in *P. tricornutum*, 78% ± 6% in *T. pseudonana*, 61% ± 3% in *O. tauri*, 65% ± 8% in *M. pusilla*, and 15% ± 2% in *E. huxleyi* (mean ± SD from three experiments; cells were cultured for 1 week in Mf medium without iron to induce iron uptake systems before uptake experiments). In yeast, for which iron reduction is a prerequisite for uptake, inhibition of ferric citrate uptake (1 μM) by BPS (200 μM) was 95% ± 2%, as shown previously (Sutak et al., 2010). The inhibitory effect of BPS on ferric citrate uptake was weakest for *E. huxleyi*, the only species studied to have no system for transplasma membrane electron transfer. Therefore, this species must have a nonreductive uptake system for ferric iron, as described previously for *C. velia* (Sutak et al., 2010). The inhibitory effect of BPS was highest for *P. tricornutum* and *T. pseudonana*, consistent with the rapid reduction of iron by these species, which can then be trapped by BPS. However, even in these species, BPS did not inhibit ferric citrate uptake as strongly as it does in yeast (95%). This difference could be due to ferrous iron being less available to BPS in marine microalgae than yeast suspensions for some unknown reason. However, it is more likely that all the algae species we studied are able to take up both ferric and ferrous iron, maybe via independent transporters.

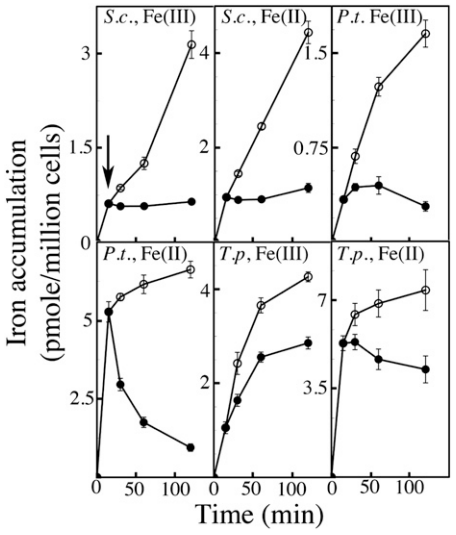


**Figure 6.** Pulse-chase uptake of iron (1). Yeast (*S.c.*), *P. tricornutum* (*P.t.*), and *T. pseudonana* (*T.p.*) cells (grown in Mf medium containing 0.1 μM iron) were incubated in citrate/Glc buffer (yeast) or uptake buffer (microalgae) with either 1 μM $^{55}$ferric citrate [1:20; Fe(III)] or 1 μM $^{55}$ferrous ascorbate [1:50; Fe(II)]. At 15 min (arrow), a 10-fold excess (10 μM) of cold iron (in the same chemical form) was added (closed symbols) or not (open symbols). Accumulation of $^{55}$Fe by the cells was followed. Values shown are means ± SD from four experiments.

### Evidence That There Is an Iron-Binding Step at the Cell Surface Prior to Uptake

We used pulse-chase experiments to study the kinetics of iron uptake. Cells were grown for 1 week in standard conditions (Mf medium with 0.1 μM iron), in high-iron conditions (Mf medium with 1 μM iron), or in low-iron conditions (Mf medium with 2 nM iron). The yeast *S. cerevisiae* was used as a control. They were then incubated in the presence of $^{55}$Fe (ferric citrate or ferrous ascorbate) for 15 min, and a 10- to 100-fold excess of cold ferric or ferrous iron (in the same chemical form) was added (Figs. 6 and 7). As expected, uptake of $^{55}$Fe by yeast stopped (or substantially decreased) immediately upon addition of excess cold iron (Fig. 6), indicating that iron uptake occurs directly from iron in solution, without any intermediate step. Iron uptake by *T. pseudonana* from $^{55}$Fe(III)-citrate continued after the addition of a large excess of cold Fe(III)-citrate (Figs. 6 and 7). Similarly labeled ferrous iron uptake by *P. tricornutum* grown in low-iron medium continued after the chase (Fig. 7). Similar findings have been reported for *Pleurochrysis carterae* (Hudson and Morel, 1990), and the authors concluded that iron was taken up from the surface of the cells without reentering solution (Hudson and Morel, 1990). This appears to be the case for the species we analyzed: according to the redox state of iron, to the algae species, and to the growth conditions, addition of excess cold iron after that of $^{55}$Fe resulted in either an increase or a decrease of $^{55}$Fe associated with the cells, but never in complete arrest of $^{55}$Fe uptake, as would be expected for simple isotopic dilution (Figs. 6 and 7). As a control experiment, we tested the addition of excess cold iron simultaneously with that of $^{55}$Fe. In all cases, we observed a simple effect of isotopic dilution (data not shown). Thus, presumably, a few minutes after addition of $^{55}$Fe, a significant proportion of this iron was not in solution but was bound to the surface of the cells, preventing isotopic dilution by excess cold iron. As the experimental procedure included washing with strong ferrous and ferric chelators before counting $^{55}$Fe associated with the cells (see "Materials and Methods"), these putative binding sites appear to have high affinity. Two different effects of adding excess cold iron at 15 min on uptake of $^{55}$Fe were observed according to the algae species, to the redox state of iron, and to the growth conditions. In some cases, the amount of $^{55}$Fe associated with the cells continued to increase after the addition of cold iron (Figs. 6 and 7). This is consistent with the $^{55}$Fe binding to high-affinity binding sites at the cell surface prior to internalization during the chase and with surface iron being removed by the iron chelators during the washing step. In other conditions (depending on the species and on the amount of iron in the growth medium), addition of cold iron resulted in a decrease of $^{55}$Fe associated with the cells (Figs. 6 and 7). This was evident, for example, for ferrous iron uptake by diatoms grown in Mf medium containing 0.1 μM iron (Fig. 6) or for ferric iron uptake by *O. tauri* and *E. huxleyi* grown in low-iron (2 nM) Mf medium (Fig. 7). This effect is more difficult to interpret. Possibly, $^{55}$Fe bound to the cell surface was not removed by the iron chelators during the washing step but could be displaced by excess cold iron, leading to a net decrease of $^{55}$Fe associated with the cells after

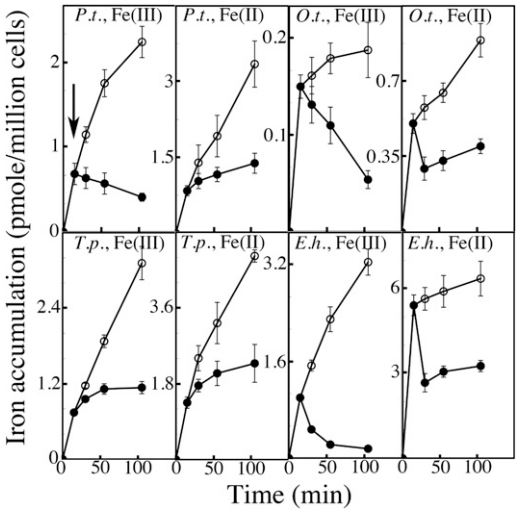


**Figure 7.** Pulse-chase uptake of iron (2). *P. tricornutum* (*P.t.*), *O. tauri* (*O.t.*), *T. pseudonana* (*T.p.*), and *E. huxleyi* (*E.h.*) cells grown for 1 week in low-iron Mf medium (2 nM iron) were incubated in uptake buffer with either 1 $\mu$M $^{55}$ferric citrate [1:20; Fe(III)] or 1 $\mu$M $^{55}$ferrous ascorbate [1:50; Fe(II)]. At 15 min (arrow), a 100-fold excess (100 $\mu$M) of cold iron (in the same chemical form) was added (closed symbols) or not (open symbols). Accumulation of $^{55}$Fe by the cells was followed. Values shown are means ± SD from three experiments.

cold iron addition. Alternatively, iron may be exported from the cells to the medium: net uptake would result from equilibrium between iron influx and efflux. This possibility was not investigated further.

These pulse-chase experiments indicate that iron uptake by marine microalgae is not a simple process in which iron in the bulk solution directly accesses the uptake sites. It is likely that there is an iron-binding step at the cell surface prior to uptake, as suggested previously (Hudson and Morel, 1990; Sutak et al., 2010). This binding step differed between algae species and varied according to the cell iron status. For example, the patterns of pulse-chase uptake of ferrous iron by *P. tricornutum* differed between cells grown in high-iron and in low-iron media (Figs. 6 and 7), suggesting that the ability of cells to bind iron at the cell surface depends on the cell iron status.

### Iron Bound to the Cell Surface Is Poorly Exchangeable by Iron Chelators

Cells of the various species were incubated at 0°C for 5 min with 1 $\mu$M $^{55}$Fe(III)-citrate or $^{55}$Fe(II)-ascorbate and then washed with various iron chelators. All five species specifically bound large amounts of both ferric and ferrous iron; the proportion of this bound iron displaced by strong iron chelators depended on the species (Supplemental Fig. S3). For example, most of the iron bound to *E. huxleyi* within 5 min remained bound after repeated washing with strong iron chelators (Supplemental Fig. S3); however, in pulse-chase experiments, about 50% (ferrous iron) to more than 90% (ferric iron) of the $^{55}$Fe bound to *E. huxleyi* cells was removed by cold iron chasing (Fig. 7). This experiment suggests that the rapid phase of iron uptake observed especially for ferrous iron following a shift to high-iron medium (see day 1 in Fig. 2) involved high-affinity iron binding at the cell surface.

We followed the percentage of iron that remained in solution in a growth medium containing 0.1 $\mu$M $^{55}$Fe (III)-citrate (Fig. 8). Most of the iron rapidly became associated with the cells, and for some species (namely both diatom species), only a few percent of the iron remained in solution after 24 h. This confirms that the cells bind and concentrate iron at the cell surface.

### Proteins Involved in Iron Uptake/Binding

Next, we investigated whether some of the iron associated with cells during iron uptake kinetics was bound to proteins and/or accumulated into protein(s). Cells were grown under standard conditions and then incubated for 1 and 3 h with $^{55}$Fe(III)-citrate or $^{55}$Fe(II)-ascorbate. Total protein extracts were prepared and subjected to native gel electrophoresis. The gels were dried and autoradiography was used to identify iron-containing bands (Fig. 9 for *P. tricornutum*, *O. tauri*, and *E. huxleyi*). In *P. tricornutum*, some of the iron from both ferric citrate and ferrous ascorbate accumulated, with the same efficiency, in a protein (or a protein

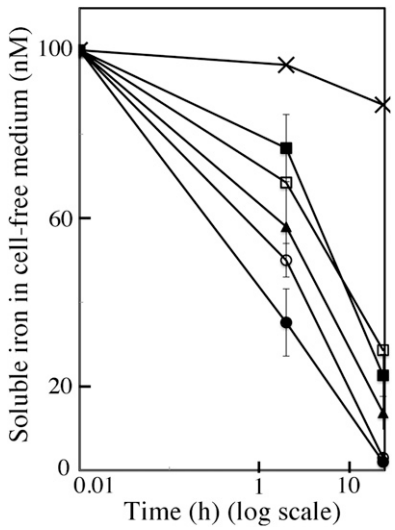


**Figure 8.** Evolution of soluble iron in the growth medium. Mf medium containing 100 nM $^{55}$Fe(III)-citrate (1:20) was left free of cells (crosses) or was inoculated at time 0 with 5 million cells mL$^{-1}$ (open circles, *P. tricornutum*; closed circles, *T. pseudonana*; triangles, *E. huxleyi*) or 50 million cells mL$^{-1}$ (open squares, *O. tauri*; closed squares, *M. pusilla*). Before inoculation, cells were precultured for 1 week in Mf medium containing 0.1 $\mu$M iron, harvested, washed once with uptake buffer containing 1 mM BPS, 1 mM DFOB, and 50 mM EDTA, and then washed twice with iron-free Mf medium. Aliquots of the media were taken at 2 and 24 h, centrifuged for 20 min at 10,000*g*, and the supernatant was assayed for iron. Values shown are means ± SD from three experiments.

complex) of high molecular mass (although the ferrireductase of cells was not induced). Similarly, in *O. tauri*, some of the iron accumulated in a high-molecular-mass protein, but to a greater extent from ferrous ascorbate than ferric citrate. In *E. huxleyi*, most of the iron bound to proteins was associated with high-molecular-mass complexes (greater than 1,000 kD), and possibly photosystems and respiratory chain complexes, although two faint bands were visible, one between the 242- and 480-kD markers and another around the 66-kD marker. None of these bands increased in intensity between 1 and 3 h of incubation of the cells with iron, inconsistent with the corresponding proteins being iron storage proteins. The amount of iron associated with *E. huxleyi* proteins did not differ according to whether the iron source was ferric or ferrous iron, although there was a very faint additional band when ferric iron was the iron source (Fig. 9). The main *P. tricornutum* and *O. tauri* bands associated with iron were excised from the gels, and the proteins contained were analyzed by mass spectrometry (MS; Supplemental Table S2). Separation of proteins by native gel electrophoresis allows much less resolution than separation by SDS-PAGE; therefore, we identified numerous proteins from the excised bands (Supplemental Table S2). Among these, we looked for proteins putatively involved in iron metabolism. The *O. tauri* proteins loaded with iron included ferritin (band around 480 kD in Fig. 9; Mascot score of 60.4). The major *P. tricornutum* band loaded with iron (between 242 and 480 kD in Fig. 9) did not contain ferritin or any other protein with known iron-binding properties, but it did contain Isip1 (for iron starvation-induced protein; with a high Mascot score of 181.6). *ISIP1* is induced by iron starvation in *P. tricornutum* (Allen et al., 2008) and other marine microalgae (Marchetti et al., 2012), but its role remains unknown. Our results suggest that this protein could play a role in iron uptake by *P. tricornutum*. However, these results are still preliminary: further purification steps will be required to identify unambiguously ferritin and Isip1 as the main proteins loaded with iron during iron uptake kinetics in *O. tauri* and *P. tricornutum*, respectively (and to identify iron-binding proteins in other species). This work is in progress in our laboratories.

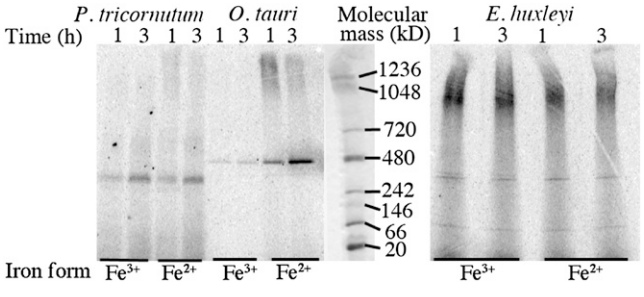


**Figure 9.** Autoradiography of dried gels after separation of whole-cell extracts on blue native PAGE. *P. tricornutum*, *O. tauri*, and *E. huxleyi* cells were incubated in uptake buffer with either 1 $\mu$M $^{55}$ferric citrate ($Fe^{3+}$) or 1 $\mu$M $^{55}$ferrous ascorbate ($Fe^{2+}$) for 1 and 3 h as indicated. Cells were washed twice with Mf medium by centrifugation, and whole-cell extracts were prepared as described in "Materials and Methods." After native PAGE (about 25 $\mu$g of protein per lane), the gels were dried and autoradiographed. Major iron-containing bands in *P. tricornutum* and *O. tauri* extracts were excised from the gel and analyzed by MS.

Although these experiments do not allow one to determine which part of total iron associated with the cells was bound to proteins, our findings are consistent (qualitatively) with the iron uptake kinetics for whole cells (compare Figs. 4 and 9): *P. tricornutum* can take up iron from ferric and from ferrous iron sources even when the ferrireductase activity of the cells is not induced; *O. tauri* preferentially uses ferrous iron, despite no clear evidence of ferrireductase activity in this species; *E. huxleyi*, which has no reductase activity, can use both ferric and ferrous iron with comparable efficiency. This correspondence between enzymological and biochemical data is consistent with the notion that iron binding cannot be dissociated from iron uptake per se in a large panel of marine microalgae: iron binding to the cell surface is probably part of the uptake process itself, regardless of the ability of cells to reduce iron or not.

## DISCUSSION

Interest in the iron uptake mechanisms used by marine phytoplankton is increasing due to the importance of phytoplankton in the carbon cycle and in primary oxygen production. The number of species for which the genome is sequenced is also increasing, facilitating the analysis of the molecular basis of iron uptake (for review, see Morrissey and Bowler, 2012; Shaked and Lis, 2012). Here, we report investigations into iron uptake from different iron sources by marine microalgae species belonging to different phyla and from different ecological niches. We aimed to establish experimentally whether different strategies are used preferentially by different species to acquire iron from the medium and to determine the conditions, if any, in which iron uptake mechanisms are induced/repressed. The main strategies of iron uptake by unicellular eukaryotes include reductive and nonreductive uptake of iron (see introduction). Both strategies are used in yeast (Lesuisse and Labbe, 1989) and have been well characterized. The nonreductive strategy of iron uptake generally involves the use of siderophores but may also involve the direct uptake of aqueous ferric ions (Sutak et al., 2010), although no such mechanism has been described at the molecular level. However, it is unclear whether the known mechanisms are relevant to the marine environment. Iron levels in surface seawater are generally extremely low (0.02–1 nM; Turner et al., 2001), and no mechanism of iron uptake (reductive or nonreductive) with affinity constants in the nanomolar range has ever been described. The marine environment also has other characteristics, relevant to uptake, including, in particular, the high diffusion rate

of the relevant species (siderophores or reduced iron; Völker and Wolf-Gladrow, 1999).

Genes homologous to those encoding yeast/plant ferrireductases (*FRE/FRO* family), the yeast multicopper ferroxidase (*FET*), and the yeast/plant ferrous ions transporters (*NRAMP*, *ZIP* family) have been identified in several marine microalgae (Armbrust et al., 2004; Allen et al., 2008; for review, see Morrissey and Bowler, 2012). However, there is a lack of experimental data concerning how these components may contribute to the very efficient iron uptake mechanisms required by marine microalgae.

Ferrous iron was taken up more rapidly than ferric iron by all the species we studied, suggestive of reductive iron uptake. However, direct measurement identified cell ferrireductase activities only for the diatoms *P. tricornutum* and *T. pseudonana*. In *P. tricornutum*, this activity was induced only under strict iron starvation conditions, as expected from transcriptomic analyses (Allen et al., 2008). By contrast, ferrireductase appeared to be constitutive and highly active (comparable to the activity of iron-deprived yeast cells) in *T. pseudonana*, and this was not predicted by transcriptomic analyses (Kustka et al., 2007). The ferrireductase activity of both diatoms was inhibited by DPI, a powerful inhibitor of the yeast ferrireductase (Lesuisse et al., 1996) and of the human neutrophil NADPH oxidase (Doussière and Vignais, 1992), which suggests that these proteins of the Fre family are conserved flavohemoproteins. We found no clear evidence of ferrireductase activity in the other three species, although the green algae *O. tauri* and *M. pusilla* were able to transfer electrons to the nonpermeant dye resazurin, and this activity was not inhibited by DPI. Therefore, the transplasma membrane electron transfer in these species does not appear to be catalyzed by a member of the Fre family. The coccolithophore *E. huxleyi* showed no transplasma membrane electron transfer activity at all, like the alveolate *C. velia* (Sutak et al., 2010). All the species we studied were thus able to use $Fe^{2+}$ as an iron source, regardless of the presence and/or induction of a ferrireductase system.

Systems for ferrous uptake in the species that are unable to reduce iron may serve to acquire iron naturally reduced by photoreduction (Sunda, 2001; Sunda and Huntsman, 2003). All the species we studied were also able to use ferric iron, although ferrous iron was clearly the preferred iron source in some species (e.g. *O. tauri*). Experimental evidence and comparative genomics studies led several authors to propose the yeast reductive iron uptake system as a paradigm for iron uptake by some diatoms (Allen et al., 2008; Morrissey and Bowler, 2012) or even more generally for the eukaryotic phytoplankton (Shaked et al., 2005). However, in yeast, iron reduction is a prerequisite for iron uptake, such that the flux of iron entering the cells from a ferric complex is directly dependent on the cell ferrireductase activity (except for siderophores, for which yeast cells have specific receptors) and does not depend on the stability constants of the ferric complex (Lesuisse et al., 1987). In addition, iron uptake in yeast by the high-affinity mechanism is controlled kinetically, via the channeling of iron through the Fet3/Ftr1 complex (Kwok et al., 2006), meaning that the rate of iron uptake does not decrease when the concentration of ferric ligands increases. This is not what we observed in marine microalgae, even in diatoms expressing inducible or constitutive ferrireductase activity. Consistent with previous reports (Hudson and Morel, 1990; Sunda, 2001), the rate of iron uptake from any ferric iron source (citrate, EDTA, desferrichrome, DFOB) by the species we studied decreased sharply with increasing ligand-Fe (III) ratio. This is not what is observed in yeast but similar to *C. velia* (Sutak et al., 2010). This suggests that iron uptake is dissociative: $Fe^{3+}$ ions bound to the putative permease or to surface binding sites equilibrate with the bulk phase. In this model (called the "Fe′ model"), the rate of iron uptake is controlled thermodynamically and is limited by the concentration of unchelated iron (Fe′) in the medium (Morel et al., 2008).

The situation is thus complicated: our data and previous findings (Morel et al., 2008) indicate that the limiting step for iron uptake is controlled thermodynamically, depending on the concentration of unchelated iron (Fe′). However, this raises an "insoluble" biological problem: the solubility of iron is very low, so how do cells acquire an ionic species (Fe′) in solution at concentrations ranging from $10^{-16}$ to $10^{-19}$ M? Reduction greatly increases the solubility of iron and, thus, the concentration of iron available to the cells (Shaked et al., 2005; Shaked and Lis, 2012). Thus, even if we did not observe, in any of the species we studied, that iron reduction was a prerequisite for uptake, the presence of a ferrireductase system is expected to increase the amount of aqueous iron available to the cells. However, the ability of some species to reduce iron does not solve the problem of iron acquisition in a very-low-iron environment: if the ferrous species generated were in equilibrium with the bulk solution, reduction would not help cells in an environment where iron is present in nanomolar concentrations, unless iron reduction would be tightly coupled to a ferrous iron uptake system controlled kinetically and with a $K_d$ ($K_a$) in the nanomolar range.

Experiments comparing the well-characterized iron uptake systems of yeast with iron uptake systems in marine microalgae can help resolve this issue. Yeast cells take up iron directly from the bulk solution, as shown by pulse-chase experiments. In contrast, analogous experiments show that in all the microalgae we studied, iron uptake involved an additional step of binding at the cell surface. Addition of cold iron during $^{55}Fe$ uptake never resulted in simple isotopic dilution, indicating that iron uptake is preceded by binding to the cell surface. Iron bound to the cells was not readily displaced by strong iron chelators, as observed previously in *P. carterae* (Hudson and Morel, 1990), indicating that it was specific and high affinity. This is in apparent contradiction with the observation that an increase in the ligand-to-iron ratio resulted in a large decrease in iron uptake; however, this observation only shows that

iron equilibrates with the bulk phase at some stage of the uptake process. One possibility, which we propose as a general model (Fig. 10), is that binding of iron from the medium at the cell surface would be controlled thermodynamically, and in a further step this bound iron would escape simple thermodynamics rules, being no more in equilibrium with the bulk solution. This would account for this striking paradox: (1) in all the species we studied, iron associated with the cells decreased dramatically with increasing the concentration of ligand and the stability constant of ferric complexes; and (2) iron bound to the cells was not readily displaced by strong iron chelators.

Different mechanisms could account for the strong binding of iron at the cell surface. In *T. pseudonana*, there is an interconnection between the genes regulated by iron and by silicon, and it has been suggested that iron could be incorporated with silicon into the cell wall (Mock et al., 2008; Morrissey and Bowler, 2012). Iron may also bind to specific iron-binding proteins at the surface, as in the complex mechanism described in *Dunaliella salina*, where two transferrin-like proteins form a complex with a multicopper ferroxidase and a glycoprotein at the surface to take up iron (Paz et al., 2007). Whatever the mechanism involved, accumulation of iron at the surface of the cells as such would not facilitate uptake if this iron were still in equilibrium with the bulk solution, as we noted previously (Sutak et al., 2010). Iron binding at the cell surface might be controlled thermodynamically and iron-binding components might specifically interact with uptake proteins (possibly homologous to proteins found in yeast and higher plants, like Fet3, Fetr1, Nramp, or Irt-like proteins, or alternatively completely undescribed proteins), involving a cooperative, kinetically controlled process. Further work is required to identify the molecular components involved in the binding and uptake of iron by the different species. We started to do so by a proteomic approach, which allows one to propose that ferritin and Isip1 are involved in iron uptake/storage in *O. tauri* and *P. tricornutum*, respectively. This is a fruitful approach that we are currently developing in our laboratories.

The critical surface binding step may explain the apparent paradox we observed concerning the induction/repression of uptake as a function of the growth conditions: iron uptake rates appeared higher for the first few days following a shift to high-iron medium than to low-iron medium. Induction of iron uptake occurred only after several days in iron-deficient medium. But the pattern of kinetics also changed between the first stage (early induction in high-iron medium) and the second stage (later induction in iron-deficient medium): in the first stage of induction under high-iron conditions, the iron uptake rate increased most during the first 30 to 60 min after iron addition, and then uptake slowed down; in the second stage of induction under iron limitation, less iron associated with the cells within the first 30 to 60 min after iron addition, but iron uptake progressed continuously over the following 2 h (Fig. 4). This might reflect a change in the iron-binding capacity of the cells between the two situations. Excess iron may result in specific binding of iron at the surface, whereas iron limitation may induce iron incorporation into the cells. This effect of an increased capacity of iron binding induced by iron addition is similar to findings for *E. huxleyi* (Boye and van den Berg, 2000). As pointed out by the authors, this increase in the capacity of cells to

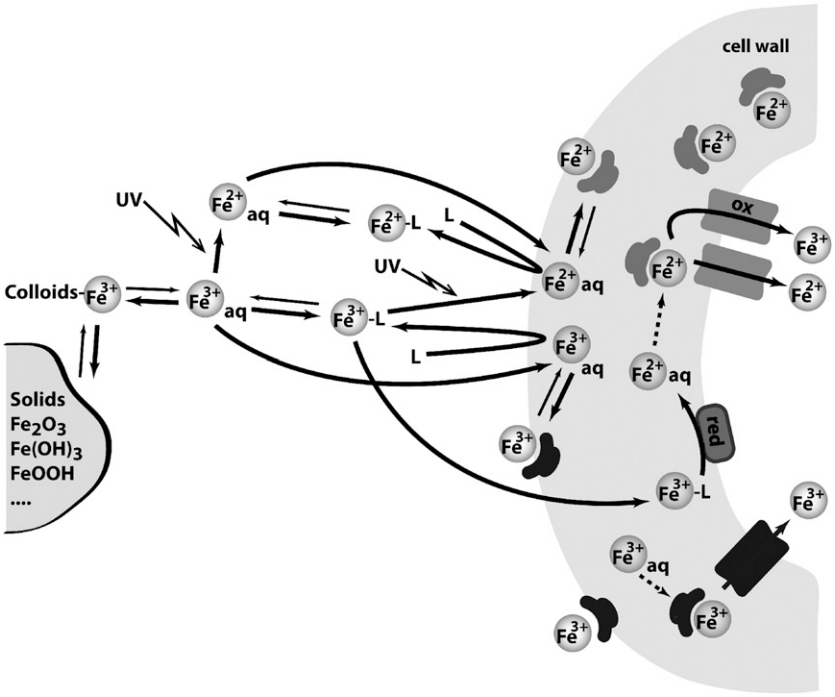


**Figure 10.** Tentative model of iron uptake by marine microalgae. Several different iron species interact in the ocean (solid iron, colloid iron, liganded [L] iron, or aqueous ferric and ferrous species), some of which are theoretically accessible for transport by the phytoplankton. Aqueous $Fe^{3+}$ and $Fe^{2+}$ (generated either by photoreduction or via the cell ferrireductase activity) bind to the cell wall of the cells (black and gray symbols, respectively), resulting in a higher local concentration of this element near the transport sites. This iron equilibrates with the bulk phase in a first stage (binding sites oriented toward the exterior) but becomes poorly exchangeable with ferric and ferrous chelators in a second stage (binding sites oriented toward the interior). Uptake of iron per se occurs via unknown interactions between binding sites and transport sites, which can involve proteins homologous to that described in yeast and plants (Fet, Nramp, Irt-like proteins, etc.) and/or uncharacterized proteins.

bind iron induced by iron itself is contrary to the concept of siderophores, which are normally synthesized when iron is limiting (Boye and van den Berg, 2000). Possibly, marine microalgae have developed an adaptation allowing large quantities of iron to be bound when the iron concentration increases transiently in their environment, which can be used subsequently during periods of iron scarcity.

In conclusion, this work strengthens two main hypotheses. Our first hypothesis is that iron uptake in marine microalgae can only be understood if a cell surface binding step is considered. We are currently trying to identify iron-binding components at the surface of various microalgae. Our second hypothesis is that most microalgae can take up both ferric and ferrous iron, regardless of the presence/absence of a ferrireductase system, and therefore that nonreductive uptake of iron as described previously for *C. velia* (Sutak et al., 2010) is probably common in marine microalgae.

## MATERIALS AND METHODS

### Strains, Cell Culture, and Media

The yeast *Saccharomyces cerevisiae* YPH499 was grown at 30°C in iron-rich (yeast nitrogen base) or iron-deficient (yeast nitrogen base + 0.1 mM BPS) medium as described previously (Lesuisse et al., 2001). Microalgae were grown at 20°C under a 16/8-h light (3,000 lux)/dark regime in a filtered Mf medium as described previously (Sutak et al., 2010). The composition of Mf medium (standard medium used for cell growth) was as follows (for 1 L of medium): sea salts (Sigma) 40 g (composition: $Cl^-$ 19.29 g, $Na^+$ 10.78 g, $SO_4^{2-}$ 2.66 g, $Mg^{2+}$ 1.32 g, $K^+$ 420 mg, $Ca^{2+}$ 400 mg, $CO_3^{2-}/HCO_3^-$ 200 mg, $Sr^{2+}$ 8.8 mg, $BO_2^-$ 5.6 mg, $Br^-$ 56 mg, $I^-$ 0.24 mg, $Li^+$ 0.3 mg, $F^-$ 1 mg); MOPS 250 mg (pH 7.3); $NH_4NO_3$ 2.66 mg; $NaNO_3$ 75 mg; $Na_2SiO_3 0.5H_2O$ 22.8 mg; $NaH_2PO_4$ 15 mg; 1 mL of vitamin stock (thiamine-HCl 20 mg $L^{-1}$, biotin 1 mg $L^{-1}$, B12 1 mg $L^{-1}$); 1 mL of trace metal stock ($MnCl_2 0.4H_2O$ 200 mg $L^{-1}$, $ZnSO_4 0.7H_2O$ 40 mg $L^{-1}$, $Na_2MoO_4 0.2H_2O$ 20 mg $L^{-1}$, $CoCl_2 0.6H_2O$ 14 mg $L^{-1}$, $Na_3VO_4.nH_2O$ 10 mg $L^{-1}$, $NiCl_2$ 10 mg $L^{-1}$, $H_2SeO_3$ 10 mg $L^{-1}$); and 1 mL of antibiotic stock (ampicillin sodium and streptomycin sulfate 100 mg $mL^{-1}$). Iron was added in the form of ferric citrate (1:20). Under standard conditions of growth (for routine maintenance of the cultures), iron concentration was 0.1 μM.

The composition of uptake medium (buffer used to measure iron uptake kinetics) was as follows: 480 mM NaCl, 20 mM KCl, 0.1 mM $MgCl_2$, 0.1 mM $CaCl_2$, and 10 mM MOPS (pH 7.3). Uptake medium was used instead of Mf medium to measure iron uptake in order to minimize the interactions of iron ligands with $Ca^{2+}$ and $Mg^{2+}$ ions (the concentrations of which are 10 and 54 mM, respectively, in the Mf medium). The chemical speciation of iron was estimated using GEOCHEM-EZ software (http://www.plantmineralnutrition.net/Geochem/geochem%20home.htm; Shaff et al., 2010). The algae species used were obtained from the Roscoff culture collection (http://www.sb-roscoff.fr/Phyto/RCC/index.php): *Phaeodactylum tricornutum* RCC69, *Thalassiosira pseudonana* RCC950, *Ostreococcus tauri* RCC745, *Micromonas pusilla* RCC827, and *Emiliania huxleyi* RCC1242. To analyze the responses of cells to a sudden decrease or increase in the iron concentration in the medium, we proceeded as follows. Cells from standard cultures (0.1 μM iron as ferric citrate) were harvested and washed twice with iron-free Mf medium. They were resuspended in Mf medium containing either 0.01 μM iron (low-iron condition) or 1 μM iron (high-iron condition) and grown for 1 week. The cells were harvested by centrifugation and washed once with a buffer containing 480 mM NaCl, 20 mM KCl, 0.1 mM $MgCl_2$, 0.1 mM $CaCl_2$, 1 mM BPS, 1 mM DFOB, 50 mM EDTA, and 10 mM MOPS (pH 7.3) and twice with iron-free Mf medium to remove traces of iron chelators. Aliquots were resuspended in 500 mL of high-iron medium (2 μM iron) and 500 mL of iron-deficient medium (no iron added). Cells were harvested from samples of 50 to 100 mL collected every day, washed with strong iron chelators as described above, and used for uptake and ferrireductase assays. When the cultures reached the end of the exponential growth phase, they were diluted to 500 mL with the same iron-rich or iron-deficient medium.

### Iron Uptake Assays

Iron uptake by yeast was assayed on microtiter plates as described previously (Lesuisse et al., 2001). Iron uptake by microalgae was assayed on microtiter plates under shaking in the light or in the dark at 20°C. Iron uptake assays were performed with concentrated cell suspensions (50–250 million cells per 100 μL) incubated in the uptake medium described above. $^{55}Fe$ (29,600 MBq $mg^{-1}$) was added to the appropriate concentration in the form of ferrous ascorbate, ferric citrate, ferric EDTA, ferrioxamine B, or ferrichrome. Iron uptake was stopped after various periods by adding 0.1 mM BPS, 0.1 mM DFOB, and 5 mM EDTA (final concentrations) to the cell suspensions and incubating for 2 min. The cells were then collected with a cell harvester (Brandel), washed three times on the filter with the uptake buffer containing 10 mM EDTA and 1 mM salicyl hydroxamic acid, and counted in a Wallac 1450 Micro Beta TriLux scintillation counter. To avoid quenching, cell pigments were bleached with sodium hypochlorite before scintillation counting. Determination of iron storage and binding under various conditions was also performed by using $^{55}Fe$ (29,600 MBq $mg^{-1}$).

### Reductase Assays

Whole-cell ferrireductase activity expressed by microalgae was measured as described previously (Lesuisse and Labbe, 1989) with Fe(III)-EDTA (0.5 mM) as the iron source. The cells (50–500 million cells per mL) were incubated in Mf medium at 20°C in the dark in the presence of iron (0.5 mM) and ferrozine (1.5 mM) for various times and then centrifuged at 10,000*g* for 10 min. The absorbency (562 nm) of the supernatant was then measured ($\epsilon$ = 25.7 $mM^{-1}$ $cm^{-1}$). Transplasma membrane electron transfer was assessed for whole cells with resazurin as the electron acceptor. Reductase activity was recorded as the appearance of resorufin at 30°C with a Jobin Yvon JY3D spectrofluorimeter ($\lambda_{ex}$ = 560 nm, $\lambda_{em}$ = 585 nm, slit widths of 2 nm for both excitation and emission). The incubation mixture was 50 mM sodium citrate buffer (pH 6.5; yeast) or Mf medium (algae) containing 10 mM resazurin and was stirred magnetically.

### Electrophoresis

Cells were disrupted by sonication, and proteins were solubilized with 0.5% digitonin. Samples were analyzed by blue native PAGE using the Novex Native PAGE Bis-Tris Gel System (3%–12%) according to the manufacturer's (Invitrogen) protocol. The gels were vacuum dried and autoradiographed.

### MS Analysis

Gel plugs were rehydrated with 20 μL of 25 mmol $L^{-1}$ $NH_4HCO_3$ containing sequencing-grade trypsin (12.5 μg $mL^{-1}$; Promega) and incubated overnight at 37°C. The resulting peptides were sequentially extracted with 30% acetonitrile, 0.1% trifluoroacetic acid and 70% acetonitrile, 0.1% trifluoroacetic acid. Digests were analyzed with a LTQ Velos Orbitrap (Thermo Fisher Scientific) coupled to an Easy nano-LC Proxeon system (Thermo Fisher Scientific). Peptides were separated chromatographically on a Proxeon C18 Easy Column (10 cm, 75 μm i.d., 120 A), at 300 nL $min^{-1}$ flow, with a gradient rising from 95% solvent A (water-0.1% formic acid) to 25% B (100% acetonitrile, 0.1% formic acid) in 20 min, then to 45% B in 40 min, and finally to 80% B in 10 min. The peptides were analyzed in the Orbitrap in full ion scan mode at a resolution of 30,000, a mass range of 400 to 1,800 mass-to-charge ratio, and with a MS full scan maximum ion time of 100 ms. Fragments were obtained with collision-induced dissociation activation with a collisional energy of 35%, an activation collisional endothermicity of 0.250 for 10 ms, and analyzed in the LTQ in a second scan event. The ion-trap MS/MS maximum ion time was 50 ms. MS/MS data were acquired in a data-dependent mode in which the 20 most intense precursor ions were isolated, with a dynamic exclusion of 20 s and an exclusion mass width of 10 ppm. Data were processed with Proteome Discoverer 1.3 software (Thermo Fisher Scientific) coupled to an in-house Mascot search server (Matrix Science; version 2.3.02). The mass tolerance of fragment ions was set to 10 ppm for precursor ions and 0.6 D for fragments. The following modifications were used in variable parameters: oxidation (Met) and phosphorylations (Ser/Thr/Tyr). The maximum number of missed cleavages was limited to two for trypsin digestion. MS/MS data were compared with the *Ostreococcus* and *Phaeodactylum* sequence databases extracted from the National Center for Biotechnology Information nonredundant database. A reversed database approach was used for the false discovery rate estimation. A threshold of 5% was chosen for this rate.

Sequence data from this article can be found in the GenBank/EMBL data libraries under accession numbers listed in Supplemental Table S2.

## Supplemental Data

The following materials are available in the online version of this article.

**Supplemental Figure S1.** Reductase activity of *O. tauri, M. pusilla,* and *E. huxleyi* with resazurin as the electron acceptor.

**Supplemental Figure S2.** Iron uptake recorded in the dark and in the light.

**Supplemental Figure S3.** Iron binding by the microalgae cells at 0°C.

**Supplemental Table S1.** Effect of iron concentration on growth rate and cell yield.

**Supplemental Table S2.** Mass spectrometry results corresponding to Figure 9.

## ACKNOWLEDGMENTS

We thank Régis Chambert for fruitful discussions and for his help with interpreting data.

Received July 23, 2012; accepted September 28, 2012; published October 2, 2012.

## LITERATURE CITED

**Allen AE, Laroche J, Maheswari U, Lommer M, Schauer N, Lopez PJ, Finazzi G, Fernie AR, Bowler C** (2008) Whole-cell response of the pennate diatom Phaeodactylum tricornutum to iron starvation. Proc Natl Acad Sci USA **105:** 10438–10443

**Allen MD, del Campo JA, Kropat J, Merchant SS** (2007) FEA1, FEA2, and FRE1, encoding two homologous secreted proteins and a candidate ferrireductase, are expressed coordinately with FOX1 and FTR1 in iron-deficient Chlamydomonas reinhardtii. Eukaryot Cell **6:** 1841–1852

**Anderson MA, Morel FMM** (1982) The influence of aqueous iron chemistry on the uptake of iron by the coastal diatom Thalassiosira weissflogii. Limnol Oceanogr **27:** 789–813

**Armbrust EV, Berges JA, Bowler C, Green BR, Martinez D, Putnam NH, Zhou S, Allen AE, Apt KE, Bechner M, et al** (2004) The genome of the diatom Thalassiosira pseudonana: ecology, evolution, and metabolism. Science **306:** 79–86

**Blaiseau P-L, Seguin A, Camadro JM, Lesuisse E** (2010) Iron uptake in yeasts. *In* P Cornelis, SC Andrews, eds, Iron Uptake and Homeostasis in Microorganisms. Caister Academic Press, Brussels, pp 265–284

**Bowler C, Allen AE, Badger JH, Grimwood J, Jabbari K, Kuo A, Maheswari U, Martens C, Maumus F, Otillar RP, et al** (2008) The Phaeodactylum genome reveals the evolutionary history of diatom genomes. Nature **456:** 239–244

**Boye M, van den Berg CMG** (2000) Iron availability and the release of iron-complexing ligands by Emiliania huxleyi. Mar Chem **70:** 277–287

**Butler A** (1998) Acquisition and utilization of transition metal ions by marine organisms. Science **281:** 207–210

**Butler A** (2005) Marine siderophores and microbial iron mobilization. Biometals **18:** 369–374

**Cepicka I, Elias M, Hampl V** (2010) Řád z Chaosu. Vesmír **89:** 464–469

**Doussière J, Vignais PV** (1992) Diphenylene iodonium as an inhibitor of the NADPH oxidase complex of bovine neutrophils: factors controlling the inhibitory potency of diphenylene iodonium in a cell-free system of oxidase activation. Eur J Biochem **208:** 61–71

**Finazzi G, Moreau H, Bowler C** (2010) Genomic insights into photosynthesis in eukaryotic phytoplankton. Trends Plant Sci **15:** 565–572

**Hopkinson BM, Morel FM** (2009) The role of siderophores in iron acquisition by photosynthetic marine microorganisms. Biometals **22:** 659–669

**Hudson RJM, Morel FMM** (1990) Iron transport in marine phytoplankton: kinetics of cellular and medium coordination reactions. Limnol Oceanogr **35:** 1002–1020

**Kosman DJ** (2003) Molecular mechanisms of iron uptake in fungi. Mol Microbiol **47:** 1185–1197

**Kustka AB, Allen AE, Morel FMM** (2007) Sequence analysis and transcriptional regulation of iron acquisition genes in two marine diatoms. J Phycol **43:** 715–729

**Kwok EY, Severance S, Kosman DJ** (2006) Evidence for iron channeling in the Fet3p-Ftr1p high-affinity iron uptake complex in the yeast plasma membrane. Biochemistry **45:** 6317–6327

**Lesuisse E, Blaiseau PL, Dancis A, Camadro JM** (2001) Siderophore uptake and use by the yeast Saccharomyces cerevisiae. Microbiology **147:** 289–298

**Lesuisse E, Casteras-Simon M, Labbe P** (1996) Evidence for the Saccharomyces cerevisiae ferrireductase system being a multicomponent electron transport chain. J Biol Chem **271:** 13578–13583

**Lesuisse E, Labbe P** (1989) Reductive and non-reductive mechanisms of iron assimilation by the yeast *Saccharomyces cerevisiae*. J Gen Microbiol **135:** 257–263

**Lesuisse E, Raguzzi F, Crichton RR** (1987) Iron uptake by the yeast *Saccharomyces cerevisiae*: involvement of a reduction step. J Gen Microbiol **133:** 3229–3236

**Maldonado MT, Allen AE, Chong JS, Lin K, Leus D, Karpenko N, Harris SL** (2006) Copper-dependent iron transport in coastal and oceanic diatoms. Limnol Oceanogr **51:** 1729–1743

**Marchetti A, Parker MS, Moccia LP, Lin EO, Arrieta AL, Ribalet F, Murphy ME, Maldonado MT, Armbrust EV** (2009) Ferritin is used for iron storage in bloom-forming marine pennate diatoms. Nature **457:** 467–470

**Marchetti A, Schruth DM, Durkin CA, Parker MS, Kodner RB, Berthiaume CT, Morales R, Allen AE, Armbrust EV** (2012) Comparative metatranscriptomics identifies molecular bases for the physiological responses of phytoplankton to varying iron availability. Proc Natl Acad Sci USA **109:** E317–E325

**Mawji E, Gledhill M, Milton JA, Tarran GA, Ussher S, Thompson A, Wolff GA, Worsfold PJ, Achterberg EP** (2008) Hydroxamate siderophores: occurrence and importance in the Atlantic Ocean. Environ Sci Technol **42:** 8675–8680

**Merchant SS, Allen MD, Kropat J, Moseley JL, Long JC, Tottey S, Terauchi AM** (2006) Between a rock and a hard place: trace element nutrition in Chlamydomonas. Biochim Biophys Acta **1763:** 578–594

**Mock T, Samanta MP, Iverson V, Berthiaume C, Robison M, Holtermann K, Durkin C, Bondurant SS, Richmond K, Rodesch M, et al** (2008) Whole-genome expression profiling of the marine diatom Thalassiosira pseudonana identifies genes involved in silicon bioprocesses. Proc Natl Acad Sci USA **105:** 1579–1584

**Monnier A, Liverani S, Bouvet R, Jesson B, Smith JQ, Mosser J, Corellou F, Bouget FY** (2010) Orchestrated transcription of biological processes in the marine picoeukaryote Ostreococcus exposed to light/dark cycles. BMC Genomics **11:** 192

**Morel FMM, Kustka AB, Shaked Y** (2008) The role of unchelated Fe in the iron nutrition of phytoplankton. Limnol Oceanogr **53:** 400–404

**Morrissey J, Bowler C** (2012) Iron utilization in marine cyanobacteria and eukaryotic algae. Front Microbiol **3:** 43

**Naito K, Imai I, Nakahara H** (2008) Complexation of iron by microbial siderophores and effects of iron chelates on the growth of marine microalgae causing red tides. Phycol Res **56:** 58–67

**Not F, Latasa M, Marie D, Cariou T, Vaulot D, Simon N** (2004) A single species, Micromonas pusilla (Prasinophyceae), dominates the eukaryotic picoplankton in the Western English Channel. Appl Environ Microbiol **70:** 4064–4072

**Paz Y, Katz A, Pick U** (2007) A multicopper ferroxidase involved in iron binding to transferrins in Dunaliella salina plasma membranes. J Biol Chem **282:** 8658–8666

**Philpott CC** (2006) Iron uptake in fungi: a system for every source. Biochim Biophys Acta **1763:** 636–645

**Philpott CC, Protchenko O** (2008) Response to iron deprivation in Saccharomyces cerevisiae. Eukaryot Cell **7:** 20–27

**Rue EL, Bruland KW** (1995) Complexation of iron(III) by natural organic ligands in the Central North Pacific as determined by a new competitive ligand equilibration/adsorptive cathodic stripping voltammetric method. Mar Chem **50:** 117–138

**Seguin A, Sutak R, Bulteau AL, Garcia-Serres R, Oddou JL, Lefevre S, Santos R, Dancis A, Camadro JM, Latour JM, et al** 2010) Evidence that yeast frataxin is not an iron storage protein in vivo. Biochim Biophys Acta **1802:** 531–538

**Shaff JE, Schultz BA, Craft EJ, Clark RT, Kochian LV** (2010) GEOCHEM-EZ: a chemical speciation program with greater power and flexibility. Plant Soil **330:** 207–214

**Shaked Y, Kustka AB, Morel FMM** (2005) A general kinetic model for iron acquisition by eukaryotic phytoplankton. Limnol Oceanogr **50:** 872–882

**Shaked Y, Lis H** (2012) Disassembling iron availability to phytoplankton. Front Microbiol **3:** 123

**Silva AMN, Le Kong X, Parkin MC, Cammack R, Hider RC** (2009) Iron(III) citrate speciation in aqueous solution. Dalton Trans **40:** 8616–8625

**Soria-Dengg S, Horstmann U** (1995) Ferrioxamines B and E as iron sources for the marine diatom Phaeodactylum tricornutum. Mar Ecol Prog Ser **127:** 269–277

**Sunda W, Huntsman S** (2003) Effect of pH, light, and temperature on Fe-EDTA chelation and Fe hydrolysis in seawater. Mar Chem **84:** 35–47

**Sunda WG** (2001) Bioavailability and bioaccumulation of iron in the sea. *In* DR Turner, KA Hunter, eds, The Biogeochemistry of Iron in Seawater. John Wiley & Sons, Chichester, UK, pp 41–84

**Sutak R, Slapeta J, San Roman M, Camadro JM, Lesuisse E** (2010) Non-reductive iron uptake mechanism in the marine alveolate *Chromera velia*. Plant Physiol **154:** 991–1000

**Turner DR, Hunter KA, de Baar HJW** (2001) Introduction. *In* DR Turner, KA Hunter, eds, The Biogeochemistry of Iron in Seawater. John Wiley & Sons, Chichester, UK, pp 1–7

**Völker C, Wolf-Gladrow DA** (1999) Physical limits on iron uptake mediated by siderophores or surface reductases. Mar Chem **65:** 227–244

**Vukosav P, Mlakar M** (2010) Iron(III)-organic complexes dissolved in seawater: characterization of iron(III)-succinate and iron(III)-malate complexes in aqueous solution. Rapp Comm Int Mer Médit **39:** 321

**Wu J, Boyle E, Sunda W, Wen LS** (2001) Soluble and colloidal iron in the oligotrophic North Atlantic and North Pacific. Science **293:** 847–849

Dans un second temps nous avons étudié plus spécifiquement l'utilisation des différentes sources de fer par différentes micro-algues représentatives de la diversité du phytoplancton, et notamment par *O.tauri*, par des approches physiologiques et biochimiques. Ce travail, réalisé en collaboration avec E. Lesuisse et R. Sutak, a montré que le citrate-ferrique et l'ascorbate-ferreux sont des sources de fer rapidement absorbés par les micro-algues, particulièrement utiles pour des expériences à court terme comme la détermination de la vitesse d'assimilation du fer et le marquage des protéines liant le fer. En revanche, le Fe-EDTA est une meilleure source de fer pour des expériences de croissance cellulaire où la concentration en fer doit être maintenue constante dans le temps.

Nous avons pu mesurer la vitesse d'assimilation du fer ferreux ($Fe^{2+}$) et du fer ferrique ($Fe^{3+}$) au cours d'un cycle jour/nuit. La cinétique d'assimilation du $Fe^{3+}$et $Fe^{2+}$ est similaire au cours de la nuit et la vitesse d'importation est maximale en fin de nuit chez *O. tauri*. Par contre, l'incorporation maximale du fer ferreux le jour a lieu 6h après l'aube lorsque l'absorption de fer ferrique est minimale. Le $Fe^{3+}$ présente un maximum d'absorption en fin de journée. Ces différences entre les profils d'assimilation la journée, suggèrent la présence de deux systèmes indépendants pour chaque forme de fer.

Nous avons mis en évidence que l'assimilation du fer ferreux était réduite en l'absence de cuivre. L'absorption du fer ferreux dépendrait donc d'un système d'absorption différent de celui du fer ferrique. Ce système pourrait faire intervenir une ferroxydase à cuivre chez *O.tauri*.

Ces résultats font l'objet d'un article publié dans Biométal dont je suis co-premier auteur.

### 2. Article 2:

Different iron sources to study the physiology and biochemistry of iron metabolism in marine micro-algae.

Botebol, H. , Sutak, R. , Scheiber, I. F., Blaiseau, P.-L., Bouget, F.-Y., Camadro, J.-M., & Lesuisse, E. (2014. *Biometals : An International Journal on the Role of Metal Ions in Biology, Biochemistry, and Medicine*, *27*(1), 75–88.

Biometals
DOI 10.1007/s10534-013-9688-1

# Different iron sources to study the physiology and biochemistry of iron metabolism in marine micro-algae

**Hugo Botebol · Robert Sutak · Ivo F. Scheiber · Pierre-Louis Blaiseau · François-Yves Bouget · Jean-Michel Camadro · Emmanuel Lesuisse**

Received: 26 September 2013 / Accepted: 13 November 2013


**Abstract** We compared ferric EDTA, ferric citrate and ferrous ascorbate as iron sources to study iron metabolism in *Ostreococcus tauri*, *Phaeodactylum tricornutum* and *Emiliania huxleyi*. Ferric EDTA was a better iron source than ferric citrate for growth and chlorophyll levels. Direct and indirect experiments showed that iron was much more available to the cells when provided as ferric citrate as compared to ferric EDTA. As a consequence, growth media with iron concentration in the range 1–100 nM were rapidly iron-depleted when ferric citrate—but not ferric EDTA was the iron source. When cultured together, *P. tricornutum* cells overgrew the two other species in iron-sufficient conditions, but *E. huxleyi* was able to compete other species in iron-deficient conditions, and when iron was provided as ferric citrate instead of ferric EDTA, which points out the critical influence of the chemical form of iron on the blooms of some phytoplankton species. The use of ferric citrate and ferrous ascorbate allowed us to unravel a kind of regulation of iron uptake that was dependent on the day/night cycles and to evidence independent uptake systems for ferrous and ferric iron, which can be regulated independently and be copper-dependent or independent. The same iron sources also allowed one to identify molecular components involved in iron uptake and storage in marine micro-algae. Characterizing the mechanisms of iron metabolism in the phytoplankton constitutes a big challenge; we show here that the use of iron sources more readily available to the cells than ferric EDTA is critical for this task.

Hugo Botebol and Robert Sutak have contributed equally to this work.

**Electronic supplementary material** The online version of this article (doi:10.1007/s10534-013-9688-1) contains supplementary material, which is available to authorized users.

H. Botebol · F.-Y. Bouget
LOMIC, UMR7621, Centre National de la Recherche Scientifique, Universite Pierre et Marie Curie (Paris 06), 66651 Banyuls/Mer, France

R. Sutak · I. F. Scheiber
Department of Parasitology, Faculty of Science, Charles University in Prague, Prague, Czech Republic

P.-L. Blaiseau · J.-M. Camadro · E. Lesuisse (✉)
Institut Jacques Monod, Centre National de la Recherche Scientifique, Universite Paris Diderot (Paris 07), 75013 Paris, France
e-mail: lesuisse.emmanuel@ijm.univ-paris-diderot.fr

E. Lesuisse
Institut Jacques Monod, CNRS, Université Paris Diderot, Bât. Buffon, 15 rue Hélène Brion, 75205 Paris Cedex 13, France

Published online: 27 November 2013

**Keywords** Iron · Marine micro-algae · Ferric citrate · Ferric EDTA · *Ostreococcus* · *Phaeodactylum* · *Emiliania*

## Introduction

Iron is vital for most living organisms. This element is abundant in the terrestrial environment but often poorly available due to its chemical properties. Iron has a strong tendency to oxidize in aerobiosis to form insoluble precipitates of ferric hydroxides and oxy-hydroxides. As a result, most organisms developed specific and high affinity mechanisms to acquire this element. Iron involved in a Fenton reaction can be toxic and so the specific mechanisms for iron uptake are tightly regulated in most organisms. In terrestrial unicellular eukaryotes, the mechanisms of iron uptake are well documented [reviewed in (Sutak et al. 2008)]. Two main strategies of iron uptake have been described at the molecular level, mostly based on studies of the yeast *Saccharomyces cerevisiae* [reviewed in (Kosman 2003; Philpott and Protchenko 2008; Blaiseau et al. 2010)]. The reductive strategy of iron uptake involves the dissociation of extracellular ferric complexes by reduction and the uptake of ferrous iron through specific or non-specific permeases, or via a high-affinity permease system (Ftr) coupled to a copper-dependent oxidase (Fet). This enables iron to be channeled through the plasma membrane. The nonreductive strategy of iron uptake involves the direct uptake of ferric complexes, without prior dissociation, via specific transporters. The mechanisms of nonreductive iron uptake mostly involve the use of siderophores.

*Chlamydomonas reinhardtii* is a model photosynthetic eukaryotic freshwater organism for the study of iron metabolism which has the same reductive strategy of iron uptake (Merchant et al. 2006; Allen et al. 2007) as yeast. Seawater microorganisms often face very different conditions of iron availability as the transition metal composition of oceans differ greatly from that of terrestrial environments (Butler 1998), and iron levels in surface seawater [for example, in the form of colloidal iron (Wu et al. 2001)] are extremely low (0.02–1 nM) (Turner et al. 2001). It is therefore likely that phytoplankton species use very high affinity uptake systems to capture iron from seawater.

Interest in marine phytoplankton iron uptake mechanisms, and their adaptation to extreme iron scarcity, is increasing due to the importance of phytoplankton in the carbon cycle and in primary oxygen production. The number of species with a sequenced genome is also increasing, facilitating the analysis of the molecular basis of iron uptake [for recent reviews, see (Morrissey and Bowler 2012; Shaked and Lis 2012)]. Different metabolic responses of eukaryotic phytoplankton to iron starvation have been proposed, mainly on the basis of whole genome analyses (Finazzi et al. 2010). Iron uptake models for marine micro-algae have been proposed based on experimental data (Sunda 2001; Shaked et al. 2005; Morel et al. 2008) and on genome analysis (Kustka et al. 2007; Allen et al. 2008; Bowler et al. 2008). Data supports a general model where unchelated iron ($Fe'$) is taken up directly by cells via a thermodynamically controlled process (Morel et al. 2008). Genome analyses have revealed genes encoding putative proteins which are homologous to the yeast Fre proteins (involved in reductive iron uptake), and models which are similar to the reductive uptake system of yeast have also been proposed (Shaked et al. 2005; Shaked and Lis 2012).

In a recent study of five micro-algae species, we showed that some species were able to reduce iron at the cell surface but that reduction was not a prerequisite for uptake, unlike in yeast (Sutak et al. 2012). Iron binding for uptake is controlled thermodynamically, bound iron then escapes to simple thermodynamic rules (Sutak et al. 2012). Most of the species studied seemed to have both iron uptake systems for ferrous iron and nonreductive uptake systems for ferric iron, independently on their ability to reduce iron (Sutak et al. 2010, 2012). No mechanism allowing the direct uptake of ferric ions without the involvement of siderophores has ever been described in eukaryotic cells. Here, we aim to identify which tools are best to assist the complex task of characterize such systems at the molecular level.

There are several considerations to take into account when considering which iron source should be used to grow marine micro-algae and study iron uptake when iron concentration and availability in the medium must be controlled. Iron should be maintained in a soluble form with a high ferric chelate stability constant (log $K_1$): this is required to avoid precipitation of ferric hydroxides and oxy-hydroxides in an aerobic alkaline medium containing high amounts of $Ca^{2+}$ and $Mg^{2+}$ ions (more than 10 mM each) which often compete with iron for its ligands. The ligand/iron ratio can also be increased to push the thermodynamic equilibrium

towards the formation of the iron chelate. However, increasing the stability constant of a ferric chelate reduces the pool of unchelated iron (Fe′) in the medium, with the possible consequence of iron becoming unavailable to the cells. This is typically the case when iron is bound to siderophores for which the cells have no specific receptors (Sutak et al. 2012). Ferric EDTA has often been the only source used for studies of iron uptake by marine micro-algae (Anderson and Morel 1982; Shaked et al. 2005; Shaked and Lis 2012). We previously used ferric citrate and ferrous ascorbate as alternative iron sources (Sutak et al. 2010, 2012), but did not systematically compare the benefits and disadvantages of using these sources for different purposes. Here, we compare ferric EDTA with ferric citrate and ferric ascorbate in different experiments to understand when different sources might be preferable. We show that, if ferric EDTA is a good iron source for cell grow, it is a poor source to study the enzymology of iron uptake, the regulation of iron uptake and storage, and to characterize the molecular components involved in these processes. We focused on three algae species exhibiting different characteristics in their iron uptake systems, as previously described (Sutak et al. 2012). The pennate diatom *Phaeodactylum tricornutum* has a ferrireductase system that is induced under iron starvation, the oceanic coccolithophore *Emiliania huxleyi* has no ferrireductase activity at all, and the picoplanktonic prasinophyte *Ostreococcus tauri* has some very low trans-plasma membrane electron transfer activity which is constitutive and does not seem to have a specific role in iron uptake (Sutak et al. 2012). These three species have uptake systems for both ferric and ferrous iron and the following different affinities for iron: *E. huxleyi* > *P. tricornutum* > *O. tauri* (Sutak et al. 2012) (opposite order for their iron requirement for growth). The experiments with these three species illustrate the usefulness of different iron sources readily available to cells and highlights promising methods for further characterization of iron uptake and storage mechanisms in marine micro-algae.

## Materials and methods

### Strains, cell culture and media

Micro-algae were grown at 20 °C under a 12:12 light (3,000 lux) dark regime in a filtered modified f (Mf) medium as described previously (Sutak et al. 2010, 2012). The composition of Mf medium (standard medium used for cell growth) was the following (for 1 l medium): sea salts (Sigma) 40 g (composition: $Cl^-$ 19.29 g, $Na^+$ 10.78 g, $SO_4^{2-}$ 2.66 g, $Mg^{2+}$ 1.32 g, $K^+$ 420 mg, $Ca^{2+}$ 400 mg, $CO_3^{2-}/HCO_3^-$ 200 mg, $Sr^{2+}$ 8.8 mg, $BO_2^-$ 5.6 mg, $Br^-$ 56 mg, $I^-$ 0.24 mg, $Li^+$ 0.3 mg, $F^-$ 1 mg); MOPS 250 mg (pH 7.3); $NH_4NO_3$ 2.66 mg; $NaNO_3$ 75 mg; $Na_2SiO_3.5H_2O$ 22.8 mg; $NaH_2PO_4$ 15 mg; 1 ml of vitamin stock (thiamine HCl 20 mg/l, biotin 1 mg/l, B12 1 mg/l); 1 ml of trace metal stock ($MnCl_2.4H_2O$ 200 mg/l, $ZnSO_4.7H_2O$ 40 mg/l, $Na_2MoO_4.2H_2O$ 20 mg/l, $CoCl_2.6H_2O$ 14 mg/l, $Na_3VO_4.nH_2O$ 10 mg/l, $NiCl_2$ 10 mg/l, $H_2SeO_3$ 10 mg/l); and 1 ml of antibiotic stock (ampicillin sodium and streptomycin sulfate 100 mg/ml). The Mf medium was buffered with 1 g/l HEPES (pH 7.5). Iron was added in the form of ferric citrate (1:20) or ferric EDTA (1:20). Iron was added as 0.1 µM ferric citrate under standard growing conditions (for routine maintenance of the cultures). We refer to "no iron" medium when no iron was added to the medium; in this condition, we estimated experimentally that the concentration of contaminating iron was less than 1 nM.

Cell growth and chlorophyll fluorescence were determined with a flow cytometer (BD Accury C6). The chemical speciation of iron was estimated using the GEOCHEM-EZ software (http://www.plantmineralnutrition.net/Geochem/Geochem%20Download.htm) (Shaff et al. 2010) and the MINEQL+4.62.2 software (http://www.mineql.com/) (Kraepiel et al. 1999). The algae species used were obtained from the Roscoff culture collection (http://www.sb-roscoff.fr/Phyto/RCC/index.php): *P. tricornutum* RCC69, *O. tauri* RCC745 and *E. huxleyi* RCC1242 (a calcifying strain of *E. huxleyi*).

### Iron uptake assays

Iron uptake by micro-algae was assayed in microtiter plates or in 2 ml micro-centrifuge tubes as previously described (Sutak et al. 2012). Iron uptake assays were performed with concentrated cell suspensions (from 50 to 250 million cells/100 µl) incubated in the Mf medium described above. $^{55}Fe$ (29,600 MBq/mg) was added to the appropriate concentration in the form of ferrous ascorbate, ferric citrate or ferric EDTA. Iron uptake was stopped at certain time points by adding 0.1 mM BPS, 0.15 mM DFOB and 50 mM EDTA

(final concentrations) to the cell suspensions and incubating for 2 min. The cells were collected with a cell harvester (microtiter plates) or by centrifugation (micro-centrifuge tubes), and washed three times on the filter or by centrifugation with washing buffer containing strong iron chelators. The composition of the washing buffer was as follows: 480 mM NaCl, 20 mM KCl, 0.1 mM $MgCl_2$, 0.1 mM $CaCl_2$, 1 mM BPS (Bathophenanthroline sulfonate), 1 mM DFOB (desferrioxamine B), 50 mM EDTA, 1 mM salicyl hydroxamic acid (SHAM) and 10 mM HEPES (pH 7.5). The washed samples were counted for radioactivity in a Wallac 1450 Micro Beta TriLux scintillaton counter. Cell pigments were bleached with sodium hypochlorite before scintillation counting to avoid quenching. Determination of iron storage and binding under various conditions was also carried out using $^{55}Fe$ (29,600 MBq/mg).

### Electrophoresis

Cells were disrupted by sonication and proteins were solubilized with 0.5 % digitonin. Samples were analyzed by blue native PAGE using the Novex Native PAGE Bis–Tris Gel System (3–12 %) according to the manufacturer's (Invitrogen) protocol. The gels were vacuum-dried and autoradiographed.

## Results

### Iron speciation

The theoretical speciation of iron (0.1 μM), added as ferric citrate (1:20) or ferric EDTA (1: 1.1) in a medium containing 10 mM $CaCl_2$ and 10 mM $MgSO_4$ at pH 7.5 is as follows [estimations based on the use of the GEOCHEM-EZ software (Shaff et al. 2010)]: 97.45 % of the iron is expected to precipitate when added as ferric citrate (1:20), with only 2.03 % soluble iron-citrate complex and 0.52 % of iron complexed with $OH^-$; 88.58 % of the iron would precipitate when added as ferric EDTA (1:1.1, i.e. a 10 % excess of the EDTA ligand), with 10.9 % soluble ferric EDTA complex and 0.52 % of iron complexed with $OH^-$. The ligand/iron ratio of ferric EDTA (using 25.1 as the $\log_K$ for ferric EDTA) has to be increased to twenty for the theoretical concentration of soluble ferric EDTA to increase to 99.93 % total iron (with 0.02 % iron-$OH^-$ complex). These theoretical values are, however, difficult to transpose to real experimental conditions. Iron forms different complexes with citrate, the stability constants of which are not precisely determined. For example, estimated stability constants for the monoiron (III) dicitrate complex is in the range of (log) 19.1–38.7 (Silva et al. 2009). Moreover, theoretical speciation values represent concentrations of the different species when the thermodynamic equilibrium is reached, which depends on the kinetic constants of the reactions. We previously determined experimentally that more than 90 % of iron remained soluble in seawater 30 min after addition of 1 μM ferric citrate (1:20) (Sutak et al. 2010). This suggests that the stability constant of ferric citrate used by most speciation software is underestimated and/or that precipitation of iron from ferric citrate to form ferrihydryie and hematite is limited by the kinetic constants of the reactions.

We compared the effects of using ferric citrate and ferric EDTA sources on cell physiology and biochemistry. Both complexes were in a 1:20 stoichiometry and were mostly soluble (as determined experimentally) in our experimental conditions. A third species, ferrous ascorbate (1:100), was used for short-term experiments. Ferrous iron does not form a stable complex with ascorbate as ascorbate continuously reduces ferric iron into the soluble $Fe^{2+}$ species which is re-oxidized by oxygen. Ferrous ascorbate thus forms a redox system that allows iron to remain soluble in the reduced form until the pool of ascorbate is fully oxidized.

### Effect of the iron source on cell yields and chlorophylls

We compared ferric EDTA and ferric citrate (1:20) in a wide range of concentrations (1 Nm–10 μM), for their ability to sustain growth of *O. tauri*, *P. tricornutum* and *E. huxleyi*. We also measured the mean fluorescence intensity of chlorophylls ("FL3" channel, excitation 488 nm, emission ≥670 nm), at different time points, as an indication of the amount of cell chlorophylls. Full data are presented in Table S1. Figure 1a shows selected growth curves of *O. tauri* precultured for 1 week in a medium with no iron and then inoculated in media containing various amounts of either ferric EDTA or ferric citrate (full data are presented in Table S1). Cells of this species progressively died a few days

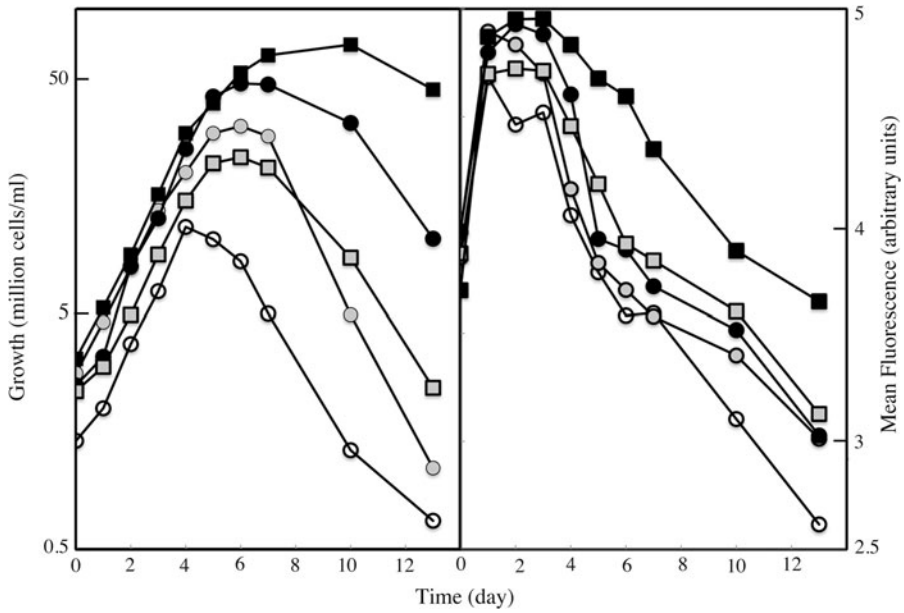


**Fig. 1** Iron-dependent growth (**a**) and iron-dependent chlorophyll fluorescence (**b**) of *O. tauri*. The cells were precultured for one week in iron-free medium and then inoculated in media containing 0–10 µM ferric citrate (*circles*) or 0–10 µM ferric EDTA (*squares*). Selected *curves* are shown for the following concentrations of iron added to the media: 0 (*empty symbols*), 10 nM (*grey symbols*) and 100 nM (*black symbols*). Values obtained for other iron concentration are presented in Table S1. The cells were grown under a 12:12 light–dark regime, and the number and fluorescence of cells were measured everyday by flow cytometry in the middle of the day. Fluorescence was recorded at ≥670 nm (emission) with excitation at 488 nm (FL3). Data represents mean results from three experiments. Error bars are not shown for the sake of clarity, but SE values were ≤ 9 % for Fig. 1a and ≤ 11 % for Fig. 1b. Full data with SE values are presented in Table S1

after strict iron deprivation (no iron added, Fig. 1a). We had not previously observed this phenotype (Sutak et al. 2012), and this is probably related to both the stringency of the experimental conditions (here, we precultured the cells in iron-free medium) and to the method used to count the cells (this method enables viable cells to be separated from dead cells and cell debris by flow cytometry). In all conditions (ferric citrate or ferric EDTA from 1 nM–10 µM), ferric EDTA was a better iron source than ferric citrate in terms of cell yield. At low iron concentration (1–10 nM), ferric citrate promoted a higher growth rate than ferric EDTA during the first days, and then the cells rapidly died (Fig. 1a). This result suggests that iron was more readily available when provided as ferric citrate than as ferric EDTA, resulting in a boost of growth followed by iron depletion in the medium. At higher iron concentrations (>10 nM) growth rates in exponential growth phase were similar with both mediums but the cells stopped growing earlier when ferric citrate was the iron source (in the range 1–100 nM; Fig. 1a), and the cells then started to die, suggesting that iron became limiting earlier when utilizing ferric citrate. Ferric EDTA also generated higher cell fluorescence intensity scores than ferric citrate for all concentrations of iron tested (Fig. 1b and Table S1): fluorescence intensity increased in a similar way with both sources during the first few days of growth but then decreased more rapidly when using ferric citrate, suggesting again that iron was more rapidly limiting when present as ferric citrate, leading to chlorosis.

We performed the same experiments with the diatom *P. tricornutum* (Fig. S1 and Table S1) and the coccolithophore *E. huxleyi* (Table S1). The growth rates and cell yields of *P. tricornutum* did not differ significantly according to the iron source, but the mean intensity of chlorophyll fluorescence was higher for all the concentrations of iron when using ferric EDTA as the iron source (Fig. S1). No significant difference in growth rates, cell yields or chlorophyll fluorescence was observed with the different iron sources for *E.*

*huxleyi* (Table S1). Overall, we observed that ferric EDTA was a better iron source than ferric citrate for the growth of different marine micro-algae (or equivalent in the case of *E. huxleyi*). The severity of cell preference for ferric EDTA was proportional to the general iron requirements of the species previously determined [*O. tauri* > *P. tricornutum* > *E. huxleyi*; (Sutak et al. 2012)].

## Effect of the iron source on inter-specific competition

Our results suggest that iron availability to the cells is not the same at all points of growth when iron is provided as ferric citrate or as ferric EDTA; iron becomes more rapidly limiting when provided as ferric citrate. This notion is strengthened by inter-specific competition experiments. Cells of the three species were precultured separately for 1 week in iron-deficient medium (no iron added) and then mixed together and grown in media containing ferric citrate or ferric EDTA in the range 1 nM–10 µM. Growth of the three mixed cell populations was measured using flow cytometry on the basis of cell size and fluorescence of each species (Fig. S2). In iron-deficient medium (no iron added), the *O. tauri* population was rapidly outcompeted by the *P. tricornutum* and *E. huxleyi* populations (Fig. 2a). The addition of further iron (as ferric citrate or ferric EDTA) to the medium resulted in complex evolution patterns of the three cell populations (Fig. 2, S3). In iron-rich conditions, the *O. tauri* population decreased continuously to reach zero after a few days, the *E. huxleyi* population showed a transient bloom and then also rapidly decreased to zero, and the *P. tricornutum* population started to increase after a few days until completely outcompeting the two other cell populations (Fig. 2f, S3). This general pattern was observed when the medium contained excess iron (>100 nM) either in the form of ferric citrate or ferric EDTA. However, at lower iron concentrations, there was a clear difference in the evolution of the *E. huxleyi* population with the different iron sources (Fig. 2). When ferric citrate was the iron source, the *E. huxleyi* population continued to increase (1–10 nM iron) or to stabilize (100 nM) alongside the growing *P. tricornutum* population (Fig. 2b, d, e). When ferric EDTA was the iron source, the *E. huxleyi* population stabilized at 1 nM iron (Fig. S3), but rapidly decreased to zero at higher concentrations (Fig. 2b, f). *E. huxleyi* has the lowest iron requirement of the three species (Sutak et al. 2012) which is probably one of the reasons why this species was able to survive together with *P. tricornutum* when no iron was added to the medium (Fig. 2a). This species was able to survive in the presence of the diatom at concentrations of up to 100 nM iron as ferric citrate but not as ferric EDTA, probably because iron depletion of the medium occurred earlier with ferric citrate than with ferric EDTA (supporting our suggestions in the paragraph above).

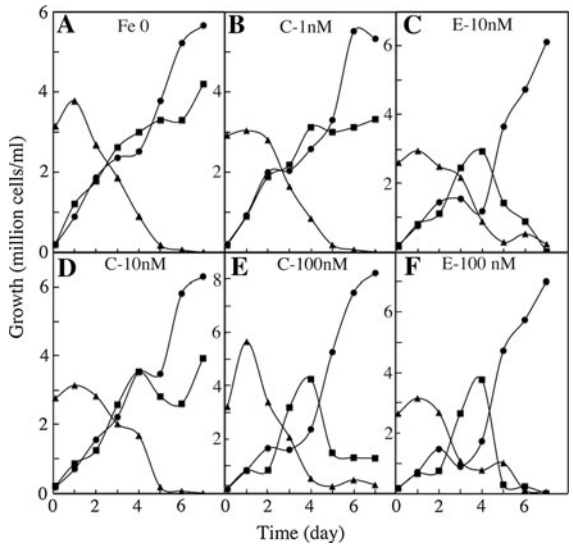


**Fig. 2** Effect of the concentration and source of iron on the growth of *O.tauri*, *E. huxleyi* and *P. tricornutum* (inter-specific competition). Cells of each species were grown separately for 1 week in iron-free medium and then inoculated together in media containing no iron (Fe 0) or different concentrations (1 nM–10 µM) of ferric citrate (C-XnM) or ferric EDTA (E-XnM). The number of cells of each species in the inoculum was inversely proportional to the estimated value of the cell surface. The cells were grown under a 12:12 light–dark regime, and the number of cells of each species was measured everyday by flow cytometry in the middle of the day. *O. tauri*: triangles; *E. huxleyi*: *squares*; *P. tricornutum*: *circles*. Data are from one representative experiment out of two independent experiments. Other conditions of growth are presented in Fig. S3

## Iron uptake from ferric citrate and ferric EDTA

In a previous study of short-term kinetics (between 1 and 3 h) under resting conditions (cells suspended in an isotonic buffer), iron was taken up much more rapidly (between 10 and 50 times faster) from ferric

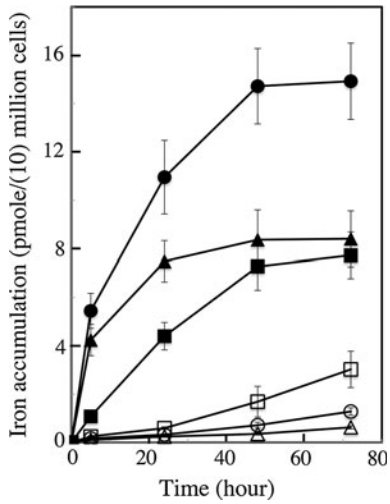


**Fig. 3** Iron uptake from ferric citrate (*closed symbols*) or ferric EDTA (*open symbols*) during growth of *O. tauri* (*triangles*), *E. huxleyi* (*squares*) and *P. tricornutum* (*circles*). The cells of each species were precultured for 1 week in iron-free medium and then inoculated at 15 million cells/ml (*O. tauri*) or 1 million cells/ml (*E. huxleyi* and *P. tricornutum*) in a medium containing 0.1 μM $^{55}$Fe-labeled ferric citrate or ferric EDTA (1:20). The cells were grown under a 12:12 light–dark regime. Aliquots of cells were harvested at different points in time during growth, washed three times with a buffer containing strong iron chelators, and the amount of cell-associated iron was determined by liquid scintillation. Results are expressed in p mol/million cells (*E. huxleyi* and *P. tricornutum*) or in p mol/10 million cells (*O. tauri*). Mean±SE from three experiments

citrate than from ferric EDTA (Sutak et al. 2012) in five tested species. Here, we quantified the amount of cell-associated iron during growth in ferric citrate or ferric EDTA mediums. Figure 3 shows the amount of iron associated with each of the three types of cells (and non-removable by washing with strong iron chelators, see methods) during the first 3 d of growth when the cells (1 week iron-free precultures) were inoculated in a medium containing either 0.1 μM ferric citrate or 0.1 μM ferric EDTA. After only two days of growth, *P. tricornutum* and *O. tauri* cells took up more than 90 % of the iron present as ferric citrate in the medium, and only about 2 % of the iron present as ferric EDTA; the values for *E. huxleyi* were about 70 and 10 %, respectively (data not shown). These data strongly support the notion proposed above: when ferric citrate is the iron source for growth, iron is rapidly removed from the medium by the cells in such a way that iron becomes limiting after a few generations, at least when iron is not added in large excess. In contrast, iron is taken from ferric EDTA at a much slower rate, enabling the cells to grow in a medium where the concentration of iron remains nearly constant. This justifies the use of ferric EDTA as an iron source for growth. Several authors have suggested that EDTA buffers an easily calculated pool of unchelated iron (Fe′) in the medium (Shaked et al. 2005; Shi et al. 2010) and allows cells to take up iron from this pool that remains constant throughout growth. The question remaining is as to whether there are any conditions in which other iron sources would be preferable.

## Ferric citrate and ferrous ascorbate as a tool to study the physiology and enzymology of iron uptake

To study the mechanisms and regulation of iron uptake by cells, it is essential to measure initial rates of iron uptake. If cells are harvested rapidly at a given moment of their growth, and if iron uptake rates by these cells are measured for a short period of time (10–15 min), the results should reflect the ability of cells to take up iron at this given moment of their growth. This kind of experiment would be difficult to carry out with ferric EDTA, using $^{55}$Fe with specific activity within the range of commercially available radionuclides (15–100 mCi/mg), as iron uptake from ferric EDTA for short periods of time could be beyond the limit of detection. Moreover, the use of ferric EDTA does not allow one to discriminate between the use of putative ferric and ferrous iron transporters by cells (Sutak et al. 2012). Ferric citrate and ferrous ascorbate may be useful tools to investigate the detailed kinetics parameters of iron uptake and the regulation of iron uptake systems as they can be taken up by cells very rapidly (as shown for *O. tauri* and *E. huxleyi* in Fig. 4). We harvested cells in exponential phase of growth every 3 h over a 24 h day/night cycle (12/12 h), and measured initial (15 min) iron uptake rates by the cells from ferric citrate and ferrous ascorbate. Figure 4 shows that the ability of the cells to take up ferric and ferrous iron varied greatly according to the period of the day or night: peaks of ferrous iron uptake capacity by *O. tauri* occurred in the middle of the day (6 h) and at the end of the night (21 h) (Fig. 4a). Strikingly, the peak of ferrous iron uptake during the day corresponded to the lowest rates of ferric iron uptake. Both ferrous and ferric iron

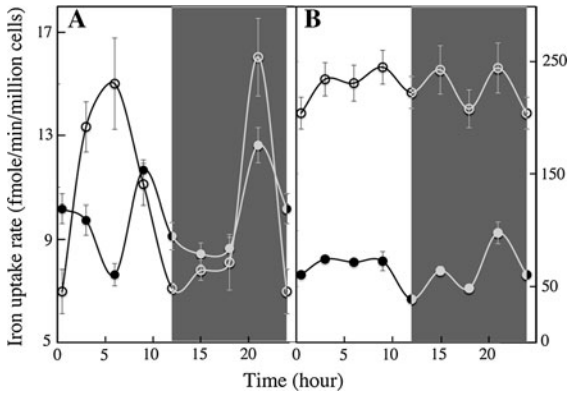


**Fig. 4** Regulation of iron uptake according to the day/night cycles. *O. tauri* (**a**) and *E. huxleyi* (**b**) cells were grown for 5 d under standard conditions (Mf medium + 0.1 µM ferric citrate) and a 12:12 light–dark regime in two growing chambers programmed in opposition of phase (day started at 10 a.m. in one chamber while night started at 10 a.m. in the second chamber). When the cells were in exponential growth phase, 50 ml of the cultures in both chambers were harvested every 3 h. The cells were washed once with iron-free medium, re-suspended in 1 ml of the same medium and distributed in two micro-centrifuge tubes (2 × 500 µl). $^{55}$Fe (1 µM) was added as ferric citrate (1:20) (*closed circles*) in one tube and as ferrous ascorbate (1:100) (*open circles*) in the second tube. After 15 min incubation at 20 °C in the light, the cells were washed three times by centrifugation with the washing buffer containing strong iron chelators. Iron associated to the cells was counted by liquid scintillation. *White parts* of the graph shows the iron uptake rates during the day and *dark parts* of the graphs show the iron uptake rates during the night. Mean±SE from three experiments

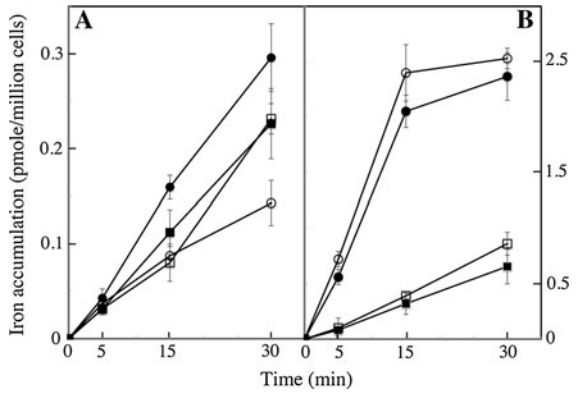


**Fig. 5** Copper-dependence of iron uptake. *O. tauri* (**a**) and *E. huxleyi* (**b**) cells were grown for 3 d under a 12:12 light–dark regime in Mf medium containing 0.1 µM ferric citrate and either 0.1 µM $CuSO_4$ (*closed symbols*) or 0.1 mM of the copper-chelating agent, bathocuproin sulfonate (*open symbols*). Cells were harvested 2 h after dawn, washed once with iron-free and copper-free Mf medium, and tested for iron uptake from 1 µM ferrous ascorbate (*circles*) or 1 µM ferric citrate (*squares*) in microtiter plates (see Sect. 2). Mean±SE from three experiments

uptake was induced at the end of the night (Fig. 4a). We found no significant change in the capacity of *E. huxleyi* to take up ferrous iron as a function of the day/night cycle, but a significant peak of ferric iron uptake also occurred at the end of the night (Fig. 4b). Results obtained with *P. tricornutum* will be presented in a further study focused on this diatom. These results suggest that some marine micro-algae iron uptake systems are regulated according to the photoperiod, and this is particularly clear for *O. tauri* (Fig. 4a). The results also indicate that ferric and ferrous iron uptake depends on separate systems that are regulated differently. We previously suggested that there might be independent uptake systems for ferrous and ferric iron in the various species studied (Sutak et al. 2012). The present data indicates that it is the case, at least for *O. tauri*. We then carried out a further experiment, which indicated that there are at least two independent iron uptake systems in *O. tauri*. We grew *O. tauri* (and *E. huxleyi*) cells in copper-containing medium (0.1 µM) and copper-depleted medium (medium containing 100 µM of the specific copper chelator, bathocuproin sulfonic acid) for 3 d; the cells were harvested in the middle of the day, washed with copper-free and iron-free medium and used for iron uptake assays with either ferric citrate or ferrous ascorbate. Figure 5a shows that ferrous iron uptake was copper-dependent whereas ferric iron uptake was not. In contrast, neither ferric nor ferrous iron uptake showed copper-dependence in *E. huxleyi* (Fig. 5b).

## Ferric citrate and ferrous ascorbate as a tool to study the biochemistry of iron uptake

We previously showed that iron-binding proteins of marine micro-algae could be identified by mass spectrometry: cells were incubated for various periods of time with $^{55}$Fe(III)-citrate or $^{55}$Fe(II)-ascorbate, total protein extracts were prepared and subjected to native gel electrophoresis, and autoradiography of dried gels was used to identify iron-containing bands (Sutak et al. 2012). In the present study, we performed similar experiments and included $^{55}$Fe(III)-EDTA as an iron source. Cells from different species were harvested during the exponential growth phase either in the middle of the day or in the middle of the night and incubated (in the light) for 1.5–2.5 h in iron-free

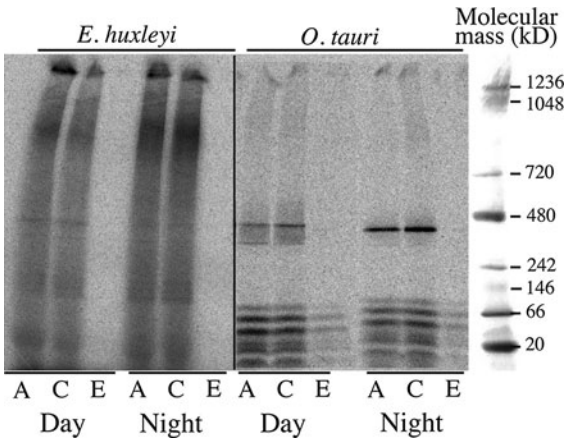


**Fig. 6** Autoradiography of dried gels after separation of whole cell extracts on blue native PAGE. *O. tauri* and *E. huxleyi* cells were grown for 5 d under standard conditions (Mf medium+0.1 µM ferric citrate) and a 12:12 light–dark regime. Cells in exponential growth phase were harvested in the middle of the day ("Day") or in the middle of the night ("Night"), washed once by centrifugation with iron-free Mf medium and incubated in the same medium for 2.5 h (*E. huxleyi*) or 1.5 h (*O. tauri*) in the light at 20 °C with either 2 µM $^{55}$ferrous ascorbate (1:100; "A"), 2 µM $^{55}$ferric citrate (1:20; "C") or 2 µM $^{55}$ferric EDTA (1:20; "E"). Cells were then washed once by centrifugation with iron-free Mf medium (*E. huxleyi*) or (*O. tauri*) with a medium containing strong iron chelators (see Sect. 2), and whole cell extracts were prepared by sonication. After native PAGE (about 25 µg protein per lane), the gels were dried and autoradiographed

growth medium supplemented with either 2 µM $^{55}$Fe(III)-citrate, 2 µM $^{55}$Fe(II)-ascorbate or 2 µM $^{55}$Fe(III)-EDTA. The cells were washed and disrupted by sonication before submitting total cell extracts to native gel electrophoresis. Results of autoradiography are shown in Fig. 5 for *E. huxleyi* and *O. tauri*. Our results show that iron from both ferric citrate and ferrous ascorbate was rapidly bound to molecular components of the cells, unlike iron from ferric EDTA (Fig. 6). We previously identified the main band of iron-containing proteins in *O. tauri* as ferritin (Sutak et al. 2012), and this protein was more efficiently loaded with iron when ferrous ascorbate was the iron source than when ferric citrate was the iron source. We obtained the opposite result in the experiment presented in Fig. 6. Iron loading of ferritin was more efficient for cells harvested during the night than for those harvested during the day, and ferric citrate was the preferred iron source in both cases (Fig. 6). When compared with Fig. 4, and with the previously published data (Sutak et al. 2012), the results presented in Fig. 6 suggest that there is no direct relationship between the iron uptake capacity of the cells and the loading of ferritin. In the middle of the day, the ability of *O. tauri* cells to take up ferrous iron was much higher than their ability to take up ferric iron (Fig. 4), but more iron was incorporated into ferritin when ferric citrate was the iron source (Fig. 6).

The pattern of iron-binding components produced by native gel electrophoresis was more complicated for *E. huxleyi* than for *O. tauri* (Fig. 6). A strong background of iron appeared throughout of the gels from which only faint discrete bands could be detected. This background of iron (distributing from the top to the bottom of the gels) was stronger in cells harvested during the night, and was mainly related to specific, non-reversible binding of iron. An important pool of bound iron remained present, even if the cells were washed with strong iron chelators (see Sect. 2) before being disrupted (Fig. S4). In this case, the background of bound iron was stronger when the cells were incubated with ferrous ascorbate than when they were incubated with ferric citrate before washing (Fig. S4). This suggests that iron (especially ferrous iron) is rapidly incorporated into non-protein structures of the cell surface that do not migrate as discrete bands on gels. No background of iron or discrete band appeared when ferric EDTA was the iron source (Fig. 6). Interestingly, a faint band was detected at the same molecular mass as the ferritin band of *O. tauri*. We are currently trying to identify the corresponding protein by mass spectrometry.

This biochemical approach to characterizing the molecular components involved in iron metabolism in marine micro-algae was found to be a powerful assessment tool. Ferric citrate and/or ferrous ascorbate must be used in the place of ferric EDTA for such an approach.

## Discussion

Experimental protocols are often influenced by custom and tradition. The first uptake experiments in baker yeast were performed using ferric citrate and ferrous ascorbate as iron sources (Lesuisse et al. 1987), and these sources have been used in most of the studies that followed. In the field of plant iron metabolism, ferric EDTA has been frequently used (Moog et al. 1995), and is almost exclusively used by

oceanographers (Anderson and Morel 1982; Shaked et al. 2005; Shaked and Lis 2012). There is of course a rationale for this choice: seawater contains huge amounts of $Ca^{2+}$ and $Mg^{2+}$ ions, which compete with iron for most of its putative ligands, and so the general problem of iron insolubility in aerobic media is more acute in seawater. It is thus necessary to use iron complexes with relatively high affinity constants to prevent iron precipitation in seawater. It has long been observed that iron uptake by eukaryotic phytoplankton was related to the concentration of unchelated ferric iron species (Fe′) and was independent of the concentration of iron chelated to synthetic ligands (Sunda 2001; Morel et al. 2008). This observation gave rise to a model (called the "Fe′ model") in which the rate of iron uptake is controlled thermodynamically and is limited by the concentration of unchelated iron (Fe′) in the medium (Morel et al. 2008). In this model, it is critical to control the pool of unchelated iron (Fe′) in the medium. This is easily done using EDTA, because this ligand forms complexes with divalent and trivalent cations which have stability constants that are clearly and precisely defined (Shaked et al. 2005).

Genes encoding putative proteins homologous to proteins involved in yeast iron uptake were identified (Fre, Fet and Ftr proteins) after the genome of several marine micro-algae has been sequenced. This gave rise to new models of iron uptake by marine micro-algae (by diatoms) involving a reduction step and a kinetic control of uptake, as in yeast (Shaked et al. 2005; Allen et al. 2008; Morrissey and Bowler 2012). In this model, it would be paradoxical to continue to use ferric EDTA for iron uptake studies, since the very principle of reductive iron uptake is that the cells dissociate iron from its ligands by reduction at the cell surface: the role of the reduction step is to facilitate ligand exchange (De Luca and Wood 2000). EDTA is one of the very few ligands of iron that forms complexes with both ferric and ferrous iron with very high affinity: the stability constant (log $K_1$) of ferric EDTA is 25.7 and the stability constant of ferrous EDTA is 14.3 (in comparison, the respective values are more than 20 for ferric citrate and only three for ferrous citrate (Silva et al. 2009)). In a reductive model of iron uptake, reduction of ferric EDTA would not help the cells to take up iron and so ferric EDTA cannot be used as an iron source by yeasts.

We have already used ferric citrate and ferrous ascorbate to study iron uptake in marine micro-algae (Sutak et al. 2010, 2012). However, we did not systematically compare the benefits and drawbacks of using the different iron sources. In this paper we aimed to establish clear rationale for the use of particular iron sources in order to open new perspectives in the field of iron metabolism in marine micro-algae. This work will be followed by other studies where we will apply the techniques developed here to decipher more specific questions (namely, the mechanisms of iron uptake by diatoms, the role of ferritin in *O. tauri*, the iron-copper connection and the role of iron in interspecific competition).

Our main conclusion is that ferric EDTA remains the best iron source in terms of growth and cell yield, but is not a good tool to study the enzymology and biochemistry of iron uptake by marine micro-algae. Paradoxically, ferric EDTA is a good iron source for growth because it is a poor iron source for uptake. Marine micro-algae generally face problems of iron scarcity rather than iron excess, thus phytoplankton probably did not develop efficient mechanisms to repress their iron uptake systems when iron is in excess, in the way that most terrestrial organisms did (Sutak et al. 2008). When more iron is available, more is taken up by the cells. Iron from ferric citrate is much more available to cells, but as the cells take up most of the iron present in the medium very rapidly, it soon becomes limiting in the growth medium. We showed this both directly (by measuring growth rates and cell-associated iron in different conditions), and indirectly (by studying the competition between three species in the presence of ferric citrate and ferric EDTA in a wide range of concentrations). These last experiments will need further work to be fully interpreted. The observation that *O. tauri* "lost" when in competition with the two other species is probably related to the fact that it has the lowest affinity iron uptake systems (Sutak et al. 2012). However, we still do not understand why an increase in iron availability causes the species with the highest affinity iron uptake systems (*E. huxleyi*) to die in the presence of the diatom *T. tricornutum*. One notion to be tested is that the diatom dominates in iron-rich medium through the induction of nitrate assimilation (Marchetti et al. 2012). The competition effect was even more pronounced when these only two species were grown together (data not shown). In the presence of *O. tauri*, there was a transient bloom of *E. huxleyi* before dominance by *P. tricornutum*, but this transient increase in the *E. huxleyi* population did not

appear when this species was grown with *P. tricornutum* only In that case, *E. huxleyi* was only able to grow with the diatom in iron-deficient medium (<1 nM; data not shown). The behavior of *E. huxleyi* was clearly related to the availability of iron, allowing us to show that ferric citrate was more available as an iron source than ferric EDTA in a micro-environment model. This model will be developed and studied further by our group, using additional species, different iron sources and other sources and amounts of nutrients like nitrogen and phosphate. The iron supply in oceanic high-nitrate, low-chlorophyll environments exerts controls on the dynamics of phytoplankton blooms, which in turn affect the biogeochemical cycles (for example, of carbon, nitrogen, silicon) (Boyd et al. 2007). Large-scale iron fertilization of the ocean was therefore proposed as a possible tool to decrease atmospheric carbon dioxide and help to mitigate climate change (Buesseler and Boyd 2003). Iron fertilization of the ocean can however stimulate growth of toxigenic species (Silver et al. 2010; Trick et al. 2010). As previously reported for *E. huxleyi* (Muggli and Harrison 1996), the bloom of given species depends on several factors which we have shown includes the chemical form of the iron.

We found that the iron uptake systems of marine micro-algae can be regulated according to the day/light cycles. Particular interesting is the observation that *O. tauri* cells to take up ferrous iron best around the middle of the day, when their ability to take up ferric iron is decreasing. As *O. tauri* does not show clear ferrireductase activity (Sutak et al. 2012), this regulation could reflect an adaptation of the cells to facilitate iron uptake after photoreduction, which is expected to be maximal at the middle of the day. Iron naturally reduced by photoreduction might represent a critical pool of iron for some species (Sunda 2001; Sunda and Huntsman 2003). This peak of ferrous iron uptake was neither observed in the coccolithophore *E. huxleyi* nor in the diatom *P. tricornutum* (data not shown; a further study will be devoted to iron uptake by this species), suggesting that this regulation of the ferrous iron uptake system may be specific to some phylogenetic groups. It is worth noting that, whereas *E. huxleyi* has no ferrireductase activity, *P. tricornutum* does have an inducible ferrireductase activity (Park et al. 2011), meaning that photoreduction is not a prerequisite for ferrous iron uptake by this species. *E. huxleyi* will be discussed further below.

The circadian clock regulates genes involved in photo-protection of *O. tauri* cells, in the defense against oxidative stress and the gene encoding ferritin (Monnier et al. 2010). The co-regulation of genes involved in iron uptake could seem plausible as ferrous iron can generate oxidative stress through the Fenton reaction and iron is loaded into ferritin rapidly after its uptake in *O. tauri* [as shown here and in (Sutak et al. 2012)]. Moreover, redox-sensitive proteins and redox-active cofactors are themselves involved in modulating the circadian oscillator and/or relaying the light/dark information to the oscillator in cyanobacteria and terrestrial plants (Dong and Golden 2008; Silver et al. 2010; Carre and Veflingstad 2013). Studying the regulation of iron metabolism as a function of day/night cycles is thus particularly relevant and we are currently working on these specific questions. Such studies could not be undertaken with ferric EDTA as the iron source: forms of iron that are rapidly taken up by the cells and incorporated into proteins and cofactors are required to follow the detailed changes in iron uptake and storage as a function of the moment of the day/night cycle.

Uptake experiments realized with ferric citrate and ferrous ascorbate showed that, at least in *O. tauri*, there are distinct systems for the uptake of ferric and ferrous iron. The ferrous uptake system of *O. tauri*, but not that of *E. huxleyi*, is copper-dependent whereas ferric iron uptake is copper-independent. The iron-copper connection is well documented in yeast, and more generally in terrestrial eukaryotes (Kaplan and O'Halloran 1996). The multi-copper oxidase Fet3 (or functional homologues like ceruloplasmin and hephaestin in human) is required by yeast to re-oxidize iron during its uptake by a mechanism involving the interaction between Fet3 and the permease Ftr1 (Askwith et al. 1994). Little is known about such a putative connection in eukaryotic phytoplankton. Copper-dependence of iron uptake has been shown in diatoms (Maldonado et al. 2006), but the molecular bases of the iron-copper connection in marine micro-algae remain unclear. In yeast, copper-mediated oxidation of iron is part of the iron uptake process itself via a channeling, kinetically controlled mechanism (Kwok et al. 2006). Some phytoplankton species including *O. tauri*, and *P. tricornutum* have genes encoding putative multi-copper oxidases. Homologues of Fet3 could thus play a similar role in marine micro-algae as in yeast (Allen et al. 2008; Morrissey

and Bowler 2012). This notion remains questionable, however. The mechanisms of iron uptake by several marine micro-algae is thermodynamically controlled (Morel et al. 2008), at least in a first step of surface iron binding (Sutak et al. 2012). It is therefore unlikely that putative homologues of Fet3 could function in the same way in yeast and in algae since there is no known evidence of a channeling mechanism in marine micro-algae (Sutak et al. 2012). The molecular bases of the iron-copper connection in some phytoplankton species is yet to be understood.

The use of ferric citrate and ferrous ascorbate, unlike ferric EDTA, enables the molecular components that rapidly bind iron in cells of marine micro-algae to be identified by native gel electrophoresis and mass spectrometry. This approach provides future opportunities to study the regulation of ferritin iron loading/unloading and to identify other proteins involved in iron uptake and storage in different species. It has enabled us to study the role of ferritin in *O. tauri* and the molecular mechanisms involved in iron uptake in *P. tricornutum* (these studies will be presented separately). This biochemical approach gave striking results in the case of *E. huxleyi.* Unlike other species which rapidly bind iron to specific proteins (resulting in discrete bands in autoradiography on native gels), *E. huxleyi* seems to rapidly bind iron to molecular components that does not migrate as discrete bands on native gels. This bound iron (especially ferrous iron) is mostly non-exchangeable with strong iron chelators. A strong, non-reversible binding of ferrous iron to the surface of *E. huxleyi* cells has been previously observed (Sutak et al. 2012). Other authors also observed strong iron-binding components in this species (Rodgher et al. 2010) or organic iron-binding components excreted by this species (Boye and van den Berg 2000). The strong iron-binding properties of *E. huxleyi* cells could be part of a strategy used by this organism to take up iron with huge efficiency. No iron binding was observed when ferric EDTA was the iron source. This observation is paradigmatic of the apparent paradox which seems to be specific to marine micro-algae: iron uptake/binding by cells is inversely proportional to the stability constants of the iron complexes and the ligand/iron ratio (and directly proportional to the pool of unchelated iron Fe′), which indicates a thermodynamically controlled step. However, once iron is bound to the cell surface, it escapes simple thermodynamic rules and becomes non-exchangeable, even by strong iron chelators. Understanding the molecular bases of such new iron uptake mechanisms remains a substantial challenge.

**Acknowledgments** We thank William Schecher (Environmental Research Software) for his help in the use of MINEQL software. This work was funded by the French "Agence Nationale de la Recherche" (grant "PhytoIron" ANR 11 BSV7 018 02), Czech Science Foundation (13-25349S), Marie Curie European Reintegration Grant (within the 7th European Community Framework Program), the European Social Fund and the state budget of the Czech Republic (CZ.1.07/2.3.00/30.0061), by the project "BIOCEV – Biotechnology and Biomedicine Centre of the Academy of Sciences and Charles University" (CZ.1.05/1.1.00/02.0109), from the European Regional Development Fund and by CNRS BDI fellowship (to HB).



## References

Allen MD, del Campo JA, Kropat J, Merchant SS (2007) FEA1, FEA2, and FRE1, encoding two homologous secreted proteins and a candidate ferrireductase, are expressed coordinately with FOX1 and FTR1 in iron-deficient *Chlamydomonas reinhardtii*. Eukaryot Cell 6:1841–1852

Allen AE, Laroche J, Maheswari U, Lommer M, Schauer N, Lopez PJ, Finazzi G, Fernie AR, Bowler C (2008) Whole-cell response of the pennate diatom *Phaeodactylum tricornutum* to iron starvation. Proc Natl Acad Sci USA 105:10438–10443

Anderson MA, Morel FMM (1982) The influence of aqueous iron chemistry on the uptake of iron by the coastal diatom *Thalassiosira weissflogii*. Limnol Oceanogr 27:789–813

Askwith C, Eide D, Van Ho A, Bernard PS, Li L, Davis-Kaplan S, Sipe DM, Kaplan J (1994) The FET3 gene of *S. cerevisiae* encodes a multicopper oxidase required for ferrous iron uptake. Cell 76:403–410

Blaiseau P-L, Seguin A, Camadro JM, Lesuisse E (2010) Iron uptake in yeasts. In: Cornelis P, Andrews SC (eds) Iron uptake and homeostasis in microorganisms. Caister Academic Press, Brussels & Reading, pp 265–284

Bowler C, Allen AE, Badger JH, Grimwood J, Jabbari K, Kuo A, Maheswari U, Martens C, Maumus F, Otillar RP, Rayko E, Salamov A, Vandepoele K, Beszteri B, Gruber A, Heijde M, Katinka M, Mock T, Valentin K, Verret F, Berges JA, Brownlee C, Cadoret JP, Chiovitti A, Choi CJ, Coesel S, De Martino A, Detter JC, Durkin C, Falciatore A, Fournet J, Haruta M, Huysman MJ, Jenkins BD, Jiroutova K, Jorgensen RE, Joubert Y, Kaplan A, Kroger N, Kroth PG, La Roche J, Lindquist E, Lommer M, Martin-Jezequel V, Lopez PJ, Lucas S, Mangogna M, McGinnis K, Medlin LK, Montsant A, Oudot-Le Secq MP, Napoli C, Obornik M, Parker MS, Petit JL, Porcel BM, Poulsen N, Robison M, Rychlewski L,

Rynearson TA, Schmutz J, Shapiro H, Siaut M, Stanley M, Sussman MR, Taylor AR, Vardi A, von Dassow P, Vyverman W, Willis A, Wyrwicz LS, Rokhsar DS, Weissenbach J, Armbrust EV, Green BR, Van de Peer Y, Grigoriev IV (2008) The Phaeodactylum genome reveals the evolutionary history of diatom genomes. Nature 456:239–244

Boyd PW, Jickells T, Law CS, Blain S, Boyle EA, Buesseler KO, Coale KH, Cullen JJ, de Baar HJ, Follows M, Harvey M, Lancelot C, Levasseur M, Owens NP, Pollard R, Rivkin RB, Sarmiento J, Schoemann V, Smetacek V, Takeda S, Tsuda A, Turner S, Watson AJ (2007) Mesoscale iron enrichment experiments 1993–2005: synthesis and future directions. Science 315:612–617

Boye M, van den Berg CMG (2000) Iron availability and the release of iron-complexing ligands by *Emiliania huxleyi*. Mar Chem 70:277–287

Buesseler KO, Boyd PW (2003) Climate change. Will ocean fertilization work? Science 300:67–68

Butler A (1998) Acquisition and utilization of transition metals ions by marine organisms. Science 281:207–209

Carre I, Veflingstad SR (2013) Emerging design principles in the *Arabidopsis circadian* clock. Semin Cell Dev Biol 24:393–398

De Luca NG, Wood PM (2000) Iron uptake by fungi: contrasted mechanisms with internal or external reduction. Adv Microb Physiol 43:39–74

Dong G, Golden SS (2008) How a cyanobacterium tells time. Curr Opin Microbiol 11:541–546

Finazzi G, Moreau H, Bowler C (2010) Genomic insights into photosynthesis in eukaryotic phytoplankton. Trends Plant Sci 15:565–572

Kaplan J, O'Halloran TV (1996) Iron metabolism in eukaryotes: mars and venus at it again. Science 271:1510–1512

Kosman DJ (2003) Molecular mechanisms of iron uptake in fungi. Mol Microbiol 47:1185–1197

Kraepiel AML, Keller K, Morel FMM (1999) A Model for metal adsorption on montmorillonite. J Colloid Interface Sci 210:43–54

Kustka AB, Allen AE, Morel FMM (2007) Sequence analysis and transcriptional regulation of iron acquisition genes in two marine diatoms. J Phycol 43:715–729

Kwok EY, Stoj CS, Severance S, Kosman DJ (2006) An engineered bifunctional high affinity iron uptake protein in the yeast plasma membrane. J Inorg Biochem 100:1053–1060

Lesuisse E, Raguzzi F, Crichton RR (1987) Iron uptake by the yeast *Saccharomyces cerevisiae*: involvement of a reduction step. J Gen Microbiol 133:3229–3236

Maldonado MT, Allen AE, Chong JS, Lin K, Leus D, Karpenko N, Harris SL (2006) Copper-dependent iron transport in coastal and oceanic diatoms. Limnol Oceanogr 51:1729–1743

Marchetti A, Schruth DM, Durkin CA, Parker MS, Kodner RB, Berthiaume CT, Morales R, Allen AE, Armbrust EV (2012) Comparative metatranscriptomics identifies molecular bases for the physiological responses of phytoplankton to varying iron availability. Proc Natl Acad Sci USA 109:E317–E325

Merchant SS, Allen MD, Kropat J, Moseley JL, Long JC, Tottey S, Terauchi AM (2006) Between a rock and a hard place: trace element nutrition in *Chlamydomonas*. Biochim Biophys Acta 1763:578–594

Monnier A, Liverani S, Bouvet R, Jesson B, Smith JQ, Mosser J, Corellou F, Bouget FY (2010) Orchestrated transcription of biological processes in the marine picoeukaryote *Ostreococcus* exposed to light/dark cycles. BMC Genomics 11:192

Moog PR, van der Kooij TA, Bruggemann W, Schiefelbein JW, Kuiper PJ (1995) Responses to iron deficiency in *Arabidopsis thaliana*: the Turbo iron reductase does not depend on the formation of root hairs and transfer cells. Planta 195:505–513

Morel FMM, Kustka AB, Shaked Y (2008) The role of unchelated Fe in the iron nutrition of phytoplankton. Limnol Oceanogr 53:400–404

Morrissey J, Bowler C (2012) Iron utilization in marine cyanobacteria and eukaryotic algae. Front Microbiol 3:43

Muggli DL, Harrison PJ (1996) Effects of nitrogen source on the physiology and metal nutrition of *Emiliania huxleyi* grown under different iron and light conditions. Mar Ecol Prog Ser 130:255–267

Park YJ, Yang JK, Lee SM, Choi SI (2011) Applicability of poorly crystalline aluminum oxide for adsorption of arsenate. J Environ Sci Health A 46:1376–1384

Philpott CC, Protchenko O (2008) Response to iron deprivation in *Saccharomyces cerevisiae*. Eukaryot Cell 7:20–27

Rodgher S, Espindola EL, Lombardi AT (2010) Suitability of *Daphnia similis* as an alternative organism in ecotoxicological tests: implications for metal toxicity. Ecotoxicology 19:1027–1033

Shaff JE, Schultz BA, Craft EJ, Clark RT, Kochian LV (2010) GEOCHEM-EZ: a chemical speciation program with greater power and flexibility. Plant Soil 330:207–214

Shaked Y, Lis H (2012) Disassembling iron availability to phytoplankton. Front Microbiol 3:123

Shaked Y, Kustka AB, Morel FMM (2005) A general kinetic model for iron acquisition by eukaryotic phytoplankton. Limnol Oceanogr 50:872–882

Shi D, Xu Y, Hopkinson BM, Morel FM (2010) Effect of ocean acidification on iron availability to marine phytoplankton. Science 327:676–679

Silva AMN, Le Kong X, Parkin MC, Cammack R, Hider RC (2009) Iron(III) citrate speciation in aqueous solution. Dalton Trans 28(40):8616–8625

Silver MW, Bargu S, Coale SL, Benitez-Nelson CR, Garcia AC, Roberts KJ, Sekula-Wood E, Bruland KW, Coale KH (2010) Toxic diatoms and domoic acid in natural and iron enriched waters of the oceanic Pacific. Proc Natl Acad Sci USA 107:20762–20767

Sunda WG (2001) Bioavailability and bioaccumulation of iron in the sea. In: Turner DR, Hunter KA (eds) The biogeochemistry of iron in seawater. Wiley, Chichester, pp 41–84

Sunda W, Huntsman S (2003) Effect of pH, light, and temperature on Fe-EDTA chelation and Fe hydrolysis in seawater. Mar Chem 84:35–47

Sutak R, Lesuisse E, Tachezy J, Richardson DR (2008) Crusade for iron: iron uptake in unicellular eukaryotes and its significance for virulence. Trends Microbiol 16: 261–268

Sutak R, Slapeta J, San Roman M, Camadro JM, Lesuisse E (2010) Nonreductive iron uptake mechanism in the marine alveolate *Chromera velia*. Plant Physiol 154:991–1000

Sutak R, Botebol H, Blaiseau PL, Leger T, Bouget FY, Camadro JM, Lesuisse E (2012) A comparative study of iron uptake mechanisms in marine microalgae: iron binding at the cell surface is a critical step. Plant Physiol 160:2271–2284

Trick CG, Bill BD, Cochlan WP, Wells ML, Trainer VL, Pickell LD (2010) Iron enrichment stimulates toxic diatom production in high-nitrate, low-chlorophyll areas. Proc Natl Acad Sci USA 107:5887–5892

Turner DR, Hunter KA, de Baar HJW (2001) Introduction. In: Turner DR, Hunter KA (eds) The biogeochemistry of iron in seawater. Wiley, Chichester, pp 1–7

Wu J, Boyle E, Sunda W, Wen LS (2001) Soluble and colloidal iron in the oligotrophic North Atlantic and North Pacific. Science 293:847–849

# 2 Chapitre 2: Rôle de la ferritine dans l'assimilation et le recyclage du fer au cours du cycle jour/nuit chez *Ostreococcus tauri*

Avec moins de 8000 gènes et une organisation cellulaire simple, *O.tauri* est l'un des eucaryotes photosynthétiques les plus simples. Les caractéristiques du génome d'*O.tauri* (petit, haploïde, peu de redondance, transposons rares) et les outils moléculaires développés tel que la surexpression et/ou la répression inductible de gènes, ont promu *O.tauri* comme un nouveau modèle pour les études de génomique fonctionnelle et de biologie systémique dans la lignée verte et plus globalement pour le picophytoplancton eucaryote.

La technique de répression des gènes par ARN anti-sens a été utilisée avec succès pour étudier des gènes de l'horloge, des photorécepteurs ou encore du cycle cellulaire (Corellou *et al.*, 2009; Moulager *et al.*, 2010; Djouani-tahri *et al.*, 2011; Heijde *et al.*, 2010). Néanmoins sa mise en œuvre n'est pas toujours aisée. En effet, les phénotypes observés ne sont pas toujours corrélés aux niveaux de transcrits dans les lignées anti-sens. De plus, le niveau d'expression des transgènes rapporteurs luciférase dépend de l'endroit d'intégration dans le génome et l'insertion aléatoire s'effectue fréquemment à différents loci, ce qui peut induire des mutations par disruption de gènes au site d'insertion. Aussi l'équipe s'est attelé à développer les techniques de knock-out par recombinaison homologue. Ce travail mené par Jean Claude Lozano et Philippe Schatt a d'abord ciblé le gène de la *nitrate réductase (NR)*. *O. tauri* possède un seul gène de NR et est haploïde, ce qui permet d'identifier directement des mutants knock-out (croissance sur ammonium mais pas sur nitrate). Ce travail a permis de démontrer que le remplacement de gènes par recombinaison homologue est réalisable chez *Ostreococcus*. De plus, la fréquence de recombinaison dépend de la longueur des régions homologues et aussi de l'historique de recombinaison au locus. Ainsi, lorsque le locus de la *NR* contenant un gène de sélection est ciblé par le gène sauvage de la *NR*, on observe exclusivement une intégration du construit par recombinaison homologue.

Pour ma part, j'ai participé à l'établissement de lignées *ko ferritine* par recombinaison homologue. Des mutants knock-out ont été obtenus démontrant ainsi que cette technique fonctionne pour d'autres *loci* que la *NR*. Pour étudier la régulation de la ferritine au niveau traductionnel, nous avons construit par recombinaison homologue des rapporteurs traductionnels luminescents de ferritine. La construction utilisée comprend le gène complet de la ferritine fusionné à celui de la luciférase, suivi d'un marqueur de sélection et de la séquence en 3' en aval du gène de ferritine. La stratégie vise à introduire la luciférase en fusion C-ter par recombinaison homologue au locus de la ferritine. J'ai obtenu deux types de

transformants : des insertions par recombinaison homologue dans lesquelles l'insert a été intégré au locus de la ferritine (RH) dans 35% des cas et des lignées dans lesquelles l'insert s'est intégré de manière aléatoire dans le génome (RI). L'étude de l'expression de la ferritine est donc possible dans deux contextes génétiques différents : dans les RH où il n'y a plus de ferritine native (comme pour le *KoFer*) et dans les RI où la ferritine native est toujours présente. L'absence de ferritine fonctionnelle dans les RH a été vérifiée par autoradiographie (voir second article du chapitre). Ce travail fait l'objet d'un article technique publié dans Plant Journal dont je suis le troisième auteur.

### 1. Article 3:

Efficient gene targeting and removal of foreign DNA by homologous recombination in the picoeukaryote Ostreococcus.

Lozano, J.-C., Schatt, P., Botebol, H., Vergé, V., Lesuisse, E., Blain, S., Carré, I. and Bouget, F.-Y. (2014).*The Plant Journal : For Cell and Molecular Biology*, *78*(6), 1073–83. doi:10.1111/tpj.12530

the plant journal

SEB Society for Experimental Biology

*The Plant Journal* (2014) **78,** 1073–1083 doi: 10.1111/tpj.12530

TECHNICAL ADVANCE

# Efficient gene targeting and removal of foreign DNA by homologous recombination in the picoeukaryote *Ostreococcus*

**Jean-Claude Lozano[1,2,†], Philippe Schatt[1,2,†], Hugo Botebol[1,2], Valérie Vergé[1,3], Emmanuel Lesuisse[4], Stéphane Blain[1,2], Isabelle A. Carré[5] and François-Yves Bouget[1,2,*]**

[1]*Sorbonne Universités, UPMC Univ Paris 06, UMR 7621, Laboratoire d'Océanographie Microbienne, Observatoire Océanologique, F-66650 Banyuls/mer, France,*

[2]*CNRS, UMR 7621, Laboratoire d'Océanographie Microbienne, Observatoire Océanologique, F-66650 Banyuls/mer, France,*

[3]*Unité Mixte de Service, UMS2348, F-66651 Banyuls/Mer, France,*

[4]*Lab Mitochondria Metals and Oxidative Stress, Institut Jacques Monod, CNRS-Université Paris Diderot, Paris, France, and*

[5]*School of Life Sciences, University of Warwick, Coventry, UK*

Received 18 July 2013; revised 14 February 2014; accepted 31 March 2014; published online 3 April 2014.

*For correspondence (e-mail fy.bouget@obs-banyuls.fr).

[†]These authors contributed equally.

## SUMMARY

**With fewer than 8000 genes and a minimalist cellular organization, the green picoalga *Ostreococcus tauri* is one of the simplest photosynthetic eukaryotes. *Ostreococcus tauri* contains many plant-specific genes but exhibits a very low gene redundancy. The haploid genome is extremely dense with few repeated sequences and rare transposons. Thanks to the implementation of genetic transformation and vectors for inducible overexpression/knockdown this picoeukaryotic alga has emerged in recent years as a model organism for functional genomics analyses and systems biology. Here we report the development of an efficient gene targeting technique which we use to knock out the *nitrate reductase* and *ferritin* genes and to knock in a luciferase reporter in frame to the ferritin native protein. Furthermore, we show that the frequency of insertion by homologous recombination is greatly enhanced when the transgene is designed to replace an existing genomic insertion. We propose that a natural mechanism based on homologous recombination may operate to remove inserted DNA sequences from the genome.**

**Keywords: *Ostreococcus*, homologous recombination, gene targeting, microalgae, genetic transformation, technical advance.**

## INTRODUCTION

Over the past 20 years the extensive development of genetic transformation technologies in model organisms has revealed different mechanisms of transgene integration. Gene targeting by homologous recombination (HR) is the method of choice for deleting a gene, introducing a selected mutation or fusing a tag to a protein. In bacteria and in a few eukaryotic model organisms, such as the yeast *Saccharomyces cerevisiae*, HR occurs preferentially over random integration of homologous sequences; however for most eukaryotes, transgene integration occurs almost exclusively in a random fashion.

Random insertion (RI) of transgenes and targeted insertion by HR are based on distinct mechanisms of DNA repair. Random insertion is based on non-homologous end joining (NHEJ) repair of double-strand breaks (DSBs) in DNA (Heyer *et al.*, 2010). Targeted insertion is mediated by the recombinase Rad51, which catalyzes the exchange of DNA strands between damaged DNA and intact, homologous DNA sequences (Shinohara *et al.*, 1992). This mechanism is conserved between bacteria and eukaryotes (Heyer *et al.*, 2010). The Spo11 protein mediates an additional mechanism of HR specific to eukaryotes, which allows the formation of crossovers between homologous chromosome pairs at meiosis to ensure their proper segregation (Keeney *et al.*, 1997). This is of crucial importance in allowing exchanges of

DNA between homologous chromosomes and the shuffling of genetic information.

Gene targeting by HR remains difficult in most photosynthetic eukaryotes, with the exception of mosses (Schaefer and Zryd, 1997). Most attempts to knock out genes by HR in algae and higher plants were designed to disrupt the *nitrate reductase* gene (*NR*). This strategy greatly simplified the identification of HR events, as knock-out mutants grew on ammonium but failed to grow in the presence of nitrate. Gene knock-out by HR in algae was first reported 20 years ago in the chlorophyte *Chlamydomonas*, but gene targeting by HR remains very difficult in this model organism (Sodeinde and Kindle, 1993; Zorin *et al.*, 2009). In contrast, efficient gene targeting has been reported for two unicellular algae: the thermophilic acidophilic red alga *Cyanidioschizon merolae* and the heterokontophyte *Nannochloropsis* sp. (Minoda *et al.*, 2004; Kilian *et al.*, 2011).

*Ostreococcus tauri* (Prasinophyceae) has recently emerged as model marine organism. This tiny unicellular alga has a minimalist organization that allows approaches such as whole cell imaging by electron cryotomography (Gan *et al.*, 2011). Its haploid genome is compact and gene dense, with very little genetic redundancy (Derelle *et al.*, 2006). Functional genetic analyses in this organism are facilitated by an efficient genetic transformation protocol. This enabled, for example, the study of phenotypes caused by constitutive or inducible overexpression or knockdown of gene expression, or the monitoring of gene activity by *in vivo* imaging of luciferase reporter constructs (Corellou *et al.*, 2009; Moulager *et al.*, 2010; Djouani-Tahri *et al.*, 2011b). These tools were used in our research to analyze the genetic circuits and light signaling pathways of the circadian clock (Heijde *et al.*, 2010; Monnier *et al.*, 2010; Djouani-Tahri *et al.*, 2011a; Pfeuty *et al.*, 2012) and to demonstrate the presence of a non-transcriptional circadian clock shared with human red blood cells (O'Neill *et al.*, 2011).

However, antisense silencing of gene expression proved difficult in *O. tauri.* In our experience, phenotypes were not always correlated with reduced transcript levels, and RNA interference (RNAi) approaches are unlikely to be successful because *O. tauri* lacks key components of the RNA-induced silencing complex such as Dicer and Argonaute. However, homologues of Rad51 and Spo11 were identified in this organism, suggesting the presence of HR mechanisms involved in DSB repair and meiosis (Derelle *et al.*, 2006). This suggested that targeted gene disruption by HR might be achievable.

In this paper we describe a method for efficient transgene insertion by HR. This was used to knock out two different genes, *NR* and *ferritin*, and in a knock-in experiment to insert a luciferase reporter gene in-frame at the *ferritin* locus. Interestingly the frequency of transgene insertion by HR varied between 1 and 100% depending on whether the construct was designed to replace wild-type (Wt) DNA sequences or to replace an existing transgene insertion. We propose that HR may normally operate in *Ostreococcus* to eliminate foreign DNA sequences from the genome.

## RESULTS

### Knock-out of the *NR* gene by homologous recombination

*Ostreococcus tauri* is normally able to grow on Artificial Seawater (ASW) containing either nitrate or ammonium as the sole source of nitrogen (nitrate-ASW and ammonium-ASW, respectively). However, loss of NR function in *NR knock-out* ($NR^{KO}$) lines should result in the loss of ability to grow on nitrate-ASW. This provided us with a simple and efficient method for identifying HR events.

*Ostreococcus tauri* is haploid, and *NR* is encoded by a single gene located on chromosome 10. We designed a disruption cassette containing about 2 kbp of sequence homologous to the *NR* locus. This was interrupted by the *KanMx* selection marker, which confers resistance to the antibiotic G418. The *Kan-Mx* marker was inserted either in a sense or an antisense orientation relative to the *NR* sequence to produce the *KanMx-s* and *KanMx-as* constructs (Figure 1a). This was used to determine whether the orientation of the *KanMx* gene relative to the *NR* gene affected the frequency of insertion by HR. These constructs were introduced into Wt cells using the standard electroporation protocol (Corellou *et al.*, 2009). Transformants were selected on semi-solid ammonium-ASW agarose plates containing 1 mg $ml^{-1}$ G418. G418-resistant transformants were then tested for their ability to grow in nitrate-ASW. Clones that did not grow under these conditions identified putative HR events (Figure 1b).

Four G418-resistant *KanMx-s* transformants out of 193, and eight G418-resistant *KanMx-as* transformants out of 425 failed to grow in nitrate-ASW (Table 1). Cell growth of Wt and putative *NR* knock-out lines was monitored by flow cytometry (Figure 1c). Noticeably, Wt cells grew better in nitrate-ASW than in ammonium-ASW. Furthermore, *NR* knock-out lines reached higher concentrations in ammonium-ASW. These results suggest that *O. tauri* uses nitrate more efficiently than ammonium and that nitrate regulates the uptake and/or the assimilation of ammonium.

The first generations of *KanMx-as* and *KanMx-s* HR lines were denoted HR1 *KanMx-as* and HR1 *KanMx-s*, respectively. The nomenclature used to describe these lines and the lineages of subsequent HR lines are summarized in Figure 2(a). Polymerase chain reaction and Southern blot analysis were carried out to confirm the mechanism of transgene insertion in these putative HR lines (Figure 2, Table 1). The primers F1 and R1 were used to test for the presence of an intact *NR* locus. A 0.6 kbp fragment was amplified from Wt cells. The same fragment was amplified from all of the *KanMx-as* transformants that grew in

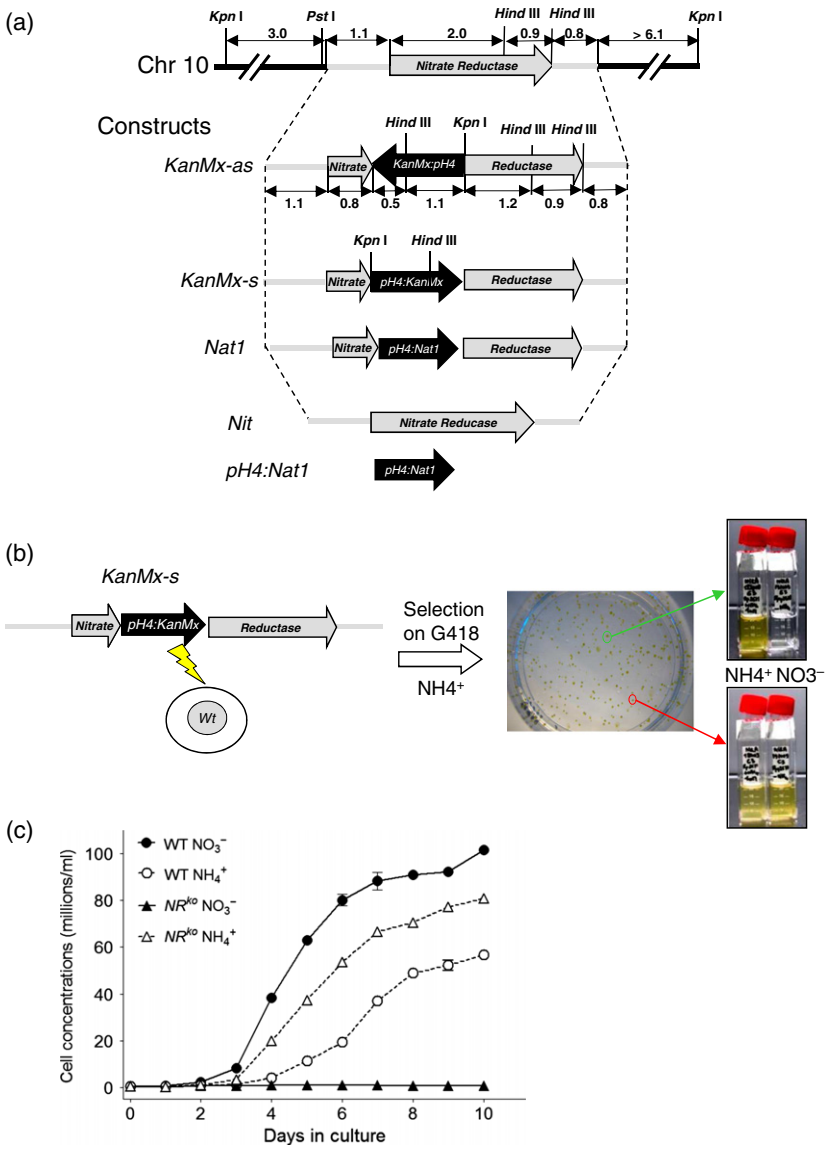


**Figure 1.** Strategy for the targeted disruption of the *nitrate reductase* (*NR*) gene in *Ostreococcus tauri*.

(a) Physical map of the *NR* locus and of the constructs used in the study. Homologous sequences are highlighted in grey and selection genes in black. The *pH4:Nat1* construct shares promoter and terminator sequences with the *pH4:KanMx* sequence of *KanMx-as* and *KanMx-s* constructs.

(b) Identification of a putative *NR* knock-out line. The *KanMx-as* construct was electroporated into *O. tauri* cells. Transformants resistant to G418 were selected in Artificial Seawater (ASW) agarose medium containing $NH_4^+$. Their growth was further tested in liquid ASW medium containing $NO_3^-$ as the sole source of nitrogen. Most of the clones also grew on $NO_3^-$ (bottom). However, those that grew on $NH_4^+$ but failed to grow on $NO_3^-$ identified putative *NR* disruptants (top).

(c) Growth curves of wild type (Wt) and putative *NR* knock-out lines in $NO_3^-$ and $NH_4^+$ ASW medium.

nitrate-ASW, confirming that they were the product of RI in the genome (Figure 2c). In contrast this fragment was not amplified from lines that failed to grow in nitrate-ASW, showing that the *NR* gene had been disrupted by insertion of the transgene. This was confirmed by the amplification of a 3-kbp product in all HR lines using a combination of primers, F2 in the selection gene and R2 in the *NR* sequence.

Southern blot analyses were carried out to check the number and pattern of transgene insertions in the HR lines. Genomic DNA was digested with *Kpn*I, which cleaved the insertion cassette immediately upstream of the *KanMx* resistance gene (Figure 2c). Hybridization of a *NR*-specific probe (P1) revealed a single band around 20 kbp in Wt and RI cells, corresponding to the intact *NR* locus. In contrast, a 6.5-kbp band was detected in HR lines, indicating the presence of the additional *Kpn*I site resulting from insertion of the *KanMx* gene at the *NR* locus. No additional band was detected, indicating that no additional insertions had occurred in the HR lines. A similar 6.5-kbp band was detected in HR lines using a probe specific to the *KanMx* transgene (P2) whereas a 15-kbp band was observed in the single RI line tested, corresponding to a RI of the transgene.

Similar experiments were performed in the lines resulting from the *KanMx-s* transformation (Figure S1 in Supporting Information). Polymerase chain reaction products were obtained at the expected size for HR, i.e. 3.2 and 2.2 kbp using (F3, R2) and (F1, R1) primer pairs, respectively. Hybridization of genomic DNA digested with *Kpn*I to the *NR* P1 probe revealed a band at a size (4.9 kbp) consistent with HR of the *KanMx-s* construct at the *NR* locus (Figure S1).

**Table 1** Effect of construct orientation on the frequency of homologous recombination (HR) at the *NR* locus

| | Transformants | | | | |
|---|---|---|---|---|---|
| Construct (recipient Wt) | Selection | Growth on $NH_4^+$ (HR + RI) | No growth on $NO_3^-$ (%) | HR lines confirmed by PCR analyses (no. of tested lines) | Name of HR lines |
| *KanMx-as* | G418 | 425 | 8[a] (about 2%) | 8 (20) | HR1 *KanMx-as* |
| *KanMx-s* | G418 | 193 | 4[a] (about 2%) | 4 (20) | HR1 *KanMx-s* |

Wt, wild type; RI, random insertion.
[a]Lines were all analyzed by PCR.

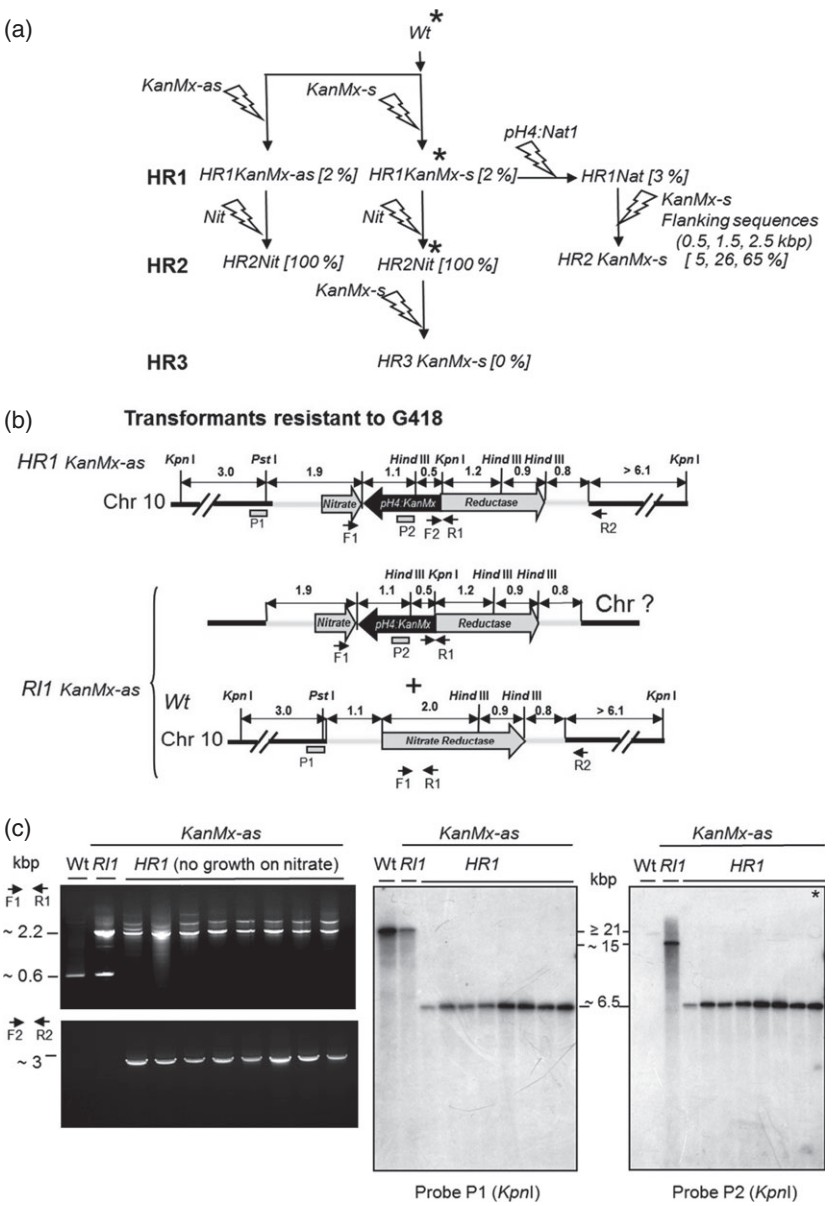


**Figure 2.** Targeted disruption of the nitrate reductase (*NR*) gene by homologous recombination (HR) using antisense *KanMx* constructs.
(a) Summary of the *NR* targeting experiments showing the history of each of the lines. Lines marked with asterisks were used for the chromatin immunoprecipitation experiments in Figure S4. The percentage of HR is given in brackets. The length of the homologous sequences used in Figure 4 is shown in parenthesis.
(b) Expected physical maps of homologous recombinants (*HR1KanMx-as*) and random insertion lines (*RI1KanMx-as*). The wild-type (Wt) *NR* locus is expected to remain intact if insertion takes place at a random genomic location.
(c) Analysis of *HR1KanMx-as* lines. Left: PCR analyses using either internal *NR* (F1,R1) or external and *KanMx* (F2,R2) primers. Right: Southern blot analysis. DNA was digested with *Kpn*I and hybridized to either *NR*- or *KanMx*-specific probes P1 and P2, respectively. All of the clones that failed to grow on nitrate had patterns of amplification and hybridization consistent with disruption of *NR* by HR.

In summary, the molecular characterization of HR events at the *NR* locus indicated that HR occurred at frequency of around 1–2%, regardless of orientation of the antibiotic resistance cassette (Table 1). No additional insertion took place through a random process in any of the HR lines analysed.

### Complementation of the NR mutation by HR occurs at a very high frequency

In order to confirm that the lack of growth on nitrate-ASW was due to the disruption of the *NR* gene, we tested whether replacement of the disrupted copy of the *NR* gene in *HR1* lines with the Wt sequence restored a Wt phenotype. One *HR1KanMx-s* line and one *HR1KanMx-as* line were transformed with a 4.2-kbp *Nit* fragment comprising the full *NR* gene (see Figure 1). Transformants that had acquired a Wt copy of the *NR* gene were selected on nitrate-ASW medium. These transformants (denoted *HR2NitKanMx-s* or *HR2NitKanMx-as* depending on the parental HR1 *KanMx-s* or *KanMx-as* lines) were expected to arise either from replacement by HR of the disrupted copy of the *NR* gene or by RI of the *Nit* fragment elsewhere in the genome. The latter scenario should result in retention of the *KanMx* cassette at the *NR* locus and therefore resistance to the antibiotic G418. Surprisingly, none of the *HR2NitKanMx-s* and *HR2NitKanMx-as* transformants ($n = 54$ and 219, respectively) grew in the presence of G418 (Table 2). This suggested that the native *NR* locus had been restored in all of these transformants by HR. This was confirmed by PCR and Southern blot analyses as above (Figure 3).

### The HR frequency is increased at loci containing foreign DNA

The very high frequency of HR in the complementation experiment contrasted with that of the original transformation experiments (100% compared with 1–2%). We first hypothesized that the frequency of HR might be affected by the different types of selection used in these experiments. In order to test this hypothesis, we generated *HR1Nat* lines that contained a *Nat1* insertion at the *NR* locus (see Figure S2). The *KanMx* and *Nat1* selection cassettes share the *histone H4* promoter and *Tef* terminator sequences (0.4 and 0.25 kbp long, respectively). We therefore transformed the *pH4:Nat1* construct into the *HR1KanMx-s* line in order to target the selection cassette (Figure S2a). Four out of 122 transformants showed a phenotype expected from HR, i.e. resistance to CloNat and sensitivity to G418 (Table 2). These were designated *HR1Nat* (Figure 1c). Polymerase chain reaction analysis using *PH4*- and *Tef*-specific primers confirmed that the *KanMx* marker had been replaced by *Nat1* in these lines. We were also able to replace the *Nat* selection cassette with *KanMx* in a subsequent experiment (Figure S2b). Transformation of a *HR1Nat* line using the *KanMx-s* construct to replace the *Nat1* resistance gene in *HR1Nat* line resulted in 39 transformants out of 60 becoming sensitive to CloNat (Table 2). The loss of the *Nat1* marker in these lines suggested that they were the product of HR, and this was confirmed in PCR analyses (Figure S2). The frequency of HR in this experiment was comparable with that obtained using the *Nit* construct in the complementation experiment above (approximately 65%). As acquisition of the *KanMx-s* and the *Nit* sequences is selected for using different mechanisms, this showed that the efficiency of HR was unrelated to the selection mechanism. However, the frequency of HR was much greater when transforming the *KanMx*-s construct into *H1RNat* than in wild-type cells (65% compared with 1–2%). This suggested that the frequency of HR was linked to the recipient line rather than to the specific construct used in the transformation experiment. We hypothesized that the interruption of the *NR* locus by a foreign sequence may increase the rate of HR, whether to restore the native DNA sequence or to replace one foreign DNA insertion

**Table 2** Gene replacement at the *NR* locus. All transformants were analyzed by PCR

| | Transformants | | | | | | | | |
|---|---|---|---|---|---|---|---|---|---|
| | Homology length (kbp) | | | | | | | | |
| Construct | 5′ | 3′ | Recipient strain | Selection | $NO_3^-$ growth (%) | G418 growth (%) | CloNat growth (%) | PCR HR lines (% HR/RI) | Name of HR lines |
| *Nit* | 1.9 | 2.5 | *HR1 KanMx-s* | $NO_3^-$ | 219 (100%) | 0 | N/A | 20 (20) (100%) | *HR2Nit KanMx-s* |
| *Nit* | 1.9 | 2.5 | *HR1 KanMx-as* | $NO_3^-$ | 54 (100%) | 0 | N/A | 54 (54) (100%) | *HR2Nit KanMx-as* |
| *pH4Nat* | 0.5 | 0.25 | *HR1 KanMx-s* | CloNat | N/A | 122 | 4 (3%) | 4 (122) (3%) | *H1RNat* |
| *KanMx-s* | 1.9 | 2.5 | *HR1Nat* | G418 | N/A | 60 | 21 (35%) | 39 (60) (65%) | *HR2 KanMx-s* |
| *KanMx-s* | 1.9 | 2.5 | *HR2Nit* | G418 | 0 (0%) | 192 | N/A | 0 (192) (0%) | *HR3 KanMx-s* |

HR, homologous recombination; RI, random insertion; N/A, not applicable.

 

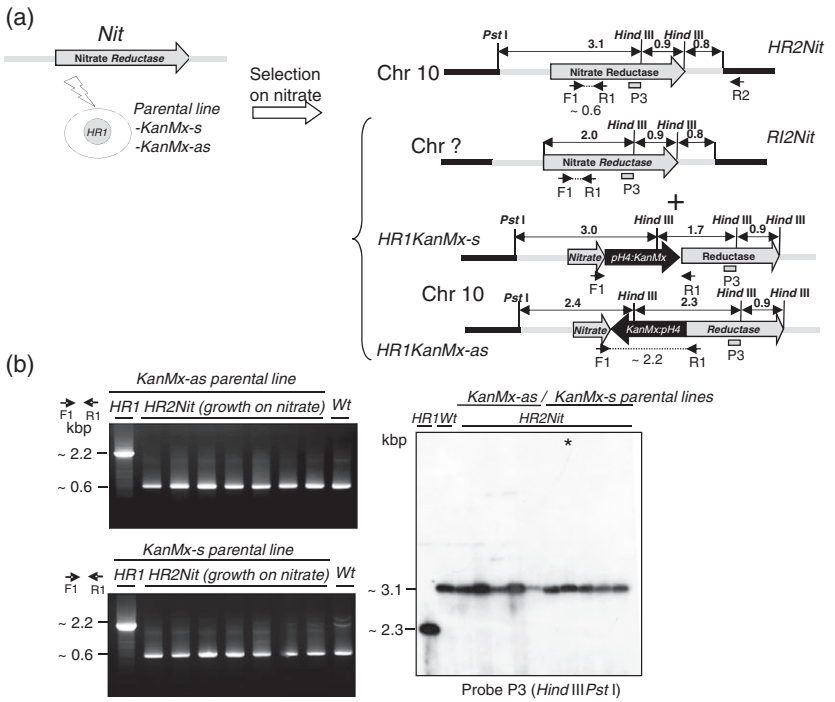


**Figure 3.** High-frequency transgene removal from the nitrate reductase (NR) locus by homologous recombination (HR).
*HR1KanMx-s* or *-as* cell lines were transformed using a wild-type (Wt) *NR* sequence fragment and selected on nitrate-Artificial Seawater (ASW).
(a) Expected physical maps of homologous recombinants (*HR2Nit*) and random insertion (RI) lines (*RINit*). Homologous recombination between the Wt transgene and the disrupted locus in the parental cell lines should lead to restoration of the Wt locus. However, RI of the *NR* sequence should introduce an additional copy of the *NR* locus elsewhere in the genome (indicated by Chr?).
(b) Analysis of transformants. Left: PCR analysis using the F1 and R1 primers. All transformants that grew on nitrate gave 0.6-kbp PCR bands typical of the Wt *NR* locus. Right: Southern blot analysis. Genomic DNA from transformants, from the HR1 recipient and from a Wt cell line was digested with *Hin*dIII and *Pst*I and hybridized to the *NR* probe P3. The line marked with an asterisk was used for the chromatin immunoprecipitation experiments in Figure S4.

with another. According to this hypothesis, HR frequencies should return to very low levels upon removal of the foreign DNA sequence. Thus, when *HR2Nit* cells (produced by complementation of the *HR1 NR* knock-out lines) were transformed using the *KanMx-s* construct, all of the 192 transformants were the product of RI rather than HR (Figure S3, Table 2). These results indicate that HR frequencies are low whether targeting the native or the restored *NR* gene, and are high when targeting a disrupted *NR* locus.

### Importance of the length of homologous sequences

Homologous recombination occurred at frequencies ranging between 65 and 100% when targeting the disrupted *NR* locus using the *Nit* and *KanMx-s* constructs, which both contain 2.5 kbp of flanking sequences homologous to *NR*. In contrast the HR frequency was much lower (4%) using the *pH4:Nat1* construct (see Figure 1), which only comprises 0.25 and 0.5 kbp of sequence homologous to the *KanMx* cassette (Table 2). This suggests that the length of the homologous sequence may be a critical parameter in the efficiency of HR. This possibility was explored by systematically testing the effect of the length of homologous sequences on the efficiency of gene targeting. *HR1Nat* cells were transformed with a *KanMX-s* construct that contained *NR* flanking sequences of various lengths (0.5–2.5 kbp). The HR frequency with the full-length construct (approximately 65%) decreased to 26 and 5% when using homologous sequences of length 1 and 0.5 kbp, respectively (Figure 4). This result indicates that a length of homologous sequence >2.5 kbp is required for optimal gene targeting by HR.

### Role of chromatin structure and transcription

There is evidence that chromatin packing regulates HR at immunoglobulin loci in *Drosophila* (Cummings *et al.*, 2007). Furthermore, histone acetyl transferase activity was required for HR in HeLa cells, suggesting a role for chromatin structure in this process (Kotian *et al.*, 2011). We therefore hypothesized that the dramatic increase in recombination frequencies upon insertion of the *KanMx* cassette in HR1 lines may be due to remodeling of the local chromatin. This effect would then be reversed upon removal of the *KanMx* cassette, leading to lower recombination rates in complemented, HR2 lines. We tested for changes in nucleosome density at the *NR* locus by quantifying the *in vivo* binding of histone H3 in chromatin immunoprecipitation (ChIP) experiments. In addition we tested for changes in histone H3 modifications that either open up the chromatin (H3 acetyl K9) or that result in a more compact structure (H3 trimethyl K4). Three different regions surrounding the insertion site were assayed, including the *NR* promoter (Region 2), the 3′ end of the *NR* coding region (Region 1) and Region 3, which falls outside the homologous sequence used in our *KanMx-s* construct. The CpG methylation of DNA was assayed by restriction enzyme digestion using the *Hpa*II/*Msp*I pair, followed by PCR analysis (Figure S4). No consistent reversible change was observed across any region that would support our hypothesis that one of the specific histone modifications

or DNA methylations tested could regulate the frequency of HR (Figure S4).

Integration of foreign DNA by HR interrupts the transcription of the *NR* gene. The effect of inhibition of transcription on the targeting efficiency was tested by growing Wt cells in ammonium-ASW prior to genetic transformation to repress the transcription of the *NR* gene. Polymerase chain reaction analysis using *NR*- and *KanMx*-specific primers (as described in Figure 2) revealed that all of the 192 transformants arose from RI of the *KanMx-s* transgene.

### Knocking-out and tagging of the native *ferritin* gene

Experiments so far have focused on the *NR* locus, which is especially attractive because of the ease with which knock-out mutants can be identified. To determine whether the use of HR-mediated gene targeting could be generalized to other loci in *O. tauri*, we tested its application to the *ferritin* gene which does not have a selectable phenotype.

In *O. tauri* the ferritin is encoded by a single gene that is located on chromosome 2 (Figure 5). A similar approach to that described for *NR* was used to disrupt the *ferritin* gene. Wild-type cells were transformed with the gene interrupted by the *KanMx* selection marker. Ninety-six transformants were obtained after selection on G418 medium. These were subsequently screened by PCR to identify lines resulting from HR events (Figure 5a). Two HR lines (denoted *HRFe*) were identified by the production of a PCR band at 0.9 kbp using a *KanMx*-specific primer (FFt) and a reverse primer located in the *Ferritin* sequence (RFo). In addition, the 0.9-kbp band amplified from Wt cells using *ferritin* internal primers (FFe and RFe) was replaced by a band at 2.5 kbp indicating that the *KanMx* sequence had inserted into the endogenous *ferritin* locus. The frequency of recombination (2%) was in the range observed when targeting the Wt *NR* gene.

Gene targeting by HR is useful for generating gene knock-outs, but also for knock-in sequences such as epitope tags downstream of protein-coding sequences. Translational reporter fusions to the firefly luciferase reporter gene have been extensively used to monitor circadian changes in gene expression in *Ostreococcus* (Corellou *et al.*, 2009; Moulager *et al.*, 2010; Djouani-Tahri *et al.*, 2011b). We designed a knock-in construct to insert the luciferase sequence downstream of, and in frame with, the ferritin-coding region. The construct comprised the *luciferase-KanMx* flanked upstream by the ferritin-coding region (lacking a stop codon) and on the other side by downstream sequences of the *ferritin* gene (Figure 5b). A 1.2-kbp product indicative of HR was amplified from 10 out of 42 transformants using the *KanMx*-specific primer FH4 and the external primer RFi (24%). These 10 *HRFlu* lines also failed to yield a product at 0.27 kbp using the *ferritin*-specific primers FFo and RFo which was detected in Wt and RI lines (Figure 5b). Western blot analysis using an anti-luciferase antibody revealed a protein band at about 85 kDa in both *RIFlu* and *HRFLu* lines (Figure 5b), confirming the production of a *Ferritin-luc* fusion protein. These results indicate that HR can be used to generate not only knock-out but also knock-in recombinants in *Ostreococcus tauri*.

## DISCUSSION

### Efficient gene targeting by homologous recombination in *Ostreococcus tauri*

The ability to target DNA constructs to specific homologous regions of the genome provides a tool for functional genomics analysis that is available in only a few eukaryotic model systems and even fewer photosynthetic organisms.

Here we report the successful targeting of the *NR* locus in *O. tauri* in more than 10 independent experiments. We further demonstrate the knock-out of a non-selectable gene, *ferritin*, at a similar frequency. Southern blot experiments indicated that no illegitimate integration occurred in HR lines, suggesting that HR which occurs by DSB repair and RI (which occurs by NHEJ) are mutually exclusive in *O. tauri*. In contrast to previous reports in the moss *Physcomitrella patens* (Kamisugi *et al.*, 2006), we observed no

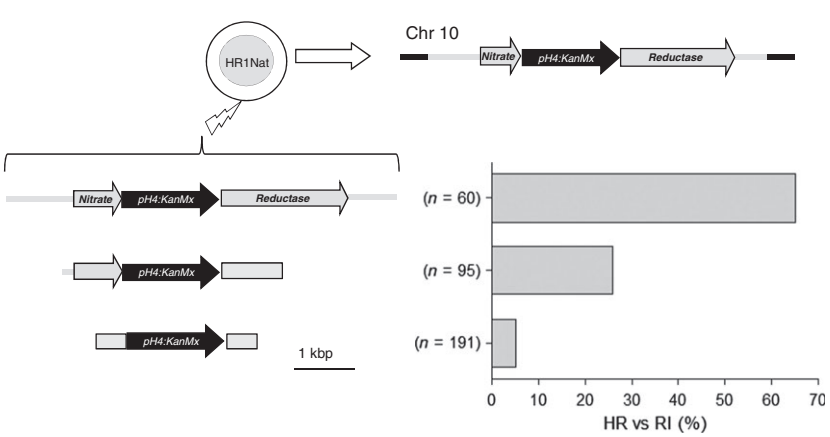


**Figure 4.** Effect of the length of homologous sequences on the efficiency of gene targeting. A cell line resistant to CloNat (*HR1Nat*) was transformed using constructs containing either 2.5, 1 or 0.5 kbp of sequence homologous to *nitrate reductase* (*NR*) on either side of the *KanMx-s* resistance cassette. The percentage of transgene insertion by homologous recombination (HR) is plotted on the *x*-axis (RI, random insertion).

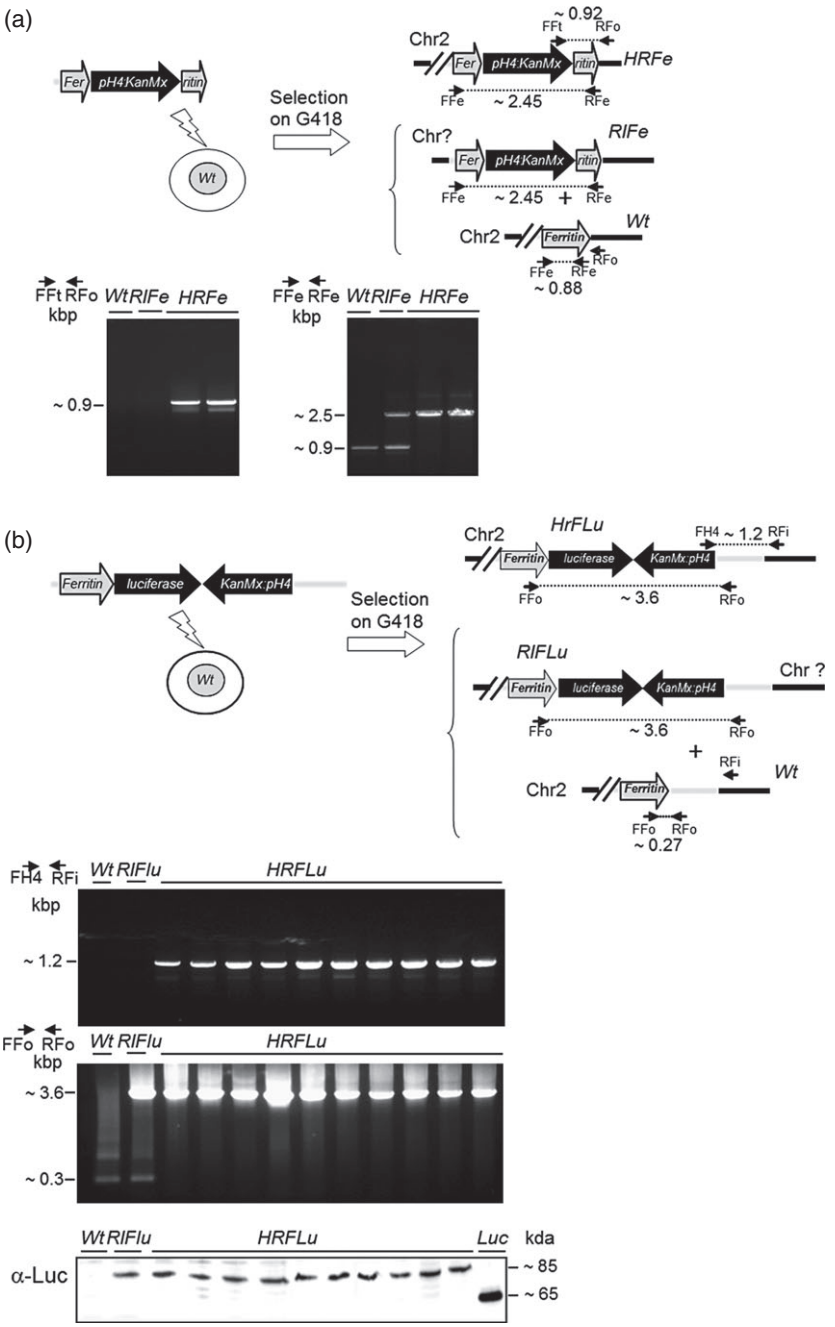


**Figure 5.** Targeted knock-out and knock-in of the *luciferase* reporter at the *ferritin* locus.
(a) Knock-out of the *ferritin* gene. Wild-type (Wt) cells were transformed using a *ferritin* sequence fragment disrupted by the *KanMx* selection marker. Transformants were identified by selection on G418. Homologous recombination (HR) was confirmed by obtaining a 0.9-kbp PCR product using the primers FFe and RFo, and a 2.5-kbp PCR product using the primers FFe and RFe. RIFe indicates *ferritin* random insertion (RI) lines and *HRFe*, homologous insertion lines.
(b) In-frame knock-in of the *luciferase* reporter. A construct in which the *luciferase* reporter gene was inserted in frame downstream of the *ferritin* open reading frame was electroporated into *Ostreococcus tauri* cells. Knock-in lines (*HRFlu*) were identified by PCR using either a combination of the selection marker FH4 and external primer RFi, or using the *ferritin*-specific primers FFo and RRFo. *RIFlu* indicates RI of the *ferritin-luc* construct. Bottom: Western blot analysis using an anti-luc (α-luc) antibody detected a protein at 85 kDa in *HRFlu* and *RiFlu* lines. *Luc* indicates recombinant luciferase protein (65 kDa), expressed in *O. tauri* under control of the *high affinity phosphate transporter* promoter.

concatenation of transgenes during HR. Taken together our results suggest that HR will be the method of choice for targeted gene disruption for the knock-in of transgenes in *Ostreococcus*.

Homologous recombination was observed at frequencies varying between 1 and 100% depending on the construct and the recipient strain. The length of homology was a key factor in determining the efficiency of gene targeting, but the mechanism of transgene selection had no effect. The GC content of the transgene was not important, as shown by the similar rates of recombination of the *KanMx* and *Nat1* sequences (40 and 60% GC, respectively) with the Wt gene.

The identification of HR events could be made even more effective by the use of a counter-selection marker to select against RI events. For example, the use of chlorate facilitated the selection of *NR* knock-out mutants in *Chlamydomonas* despite the very low frequencies of HR in this green microalga (Sodeinde and Kindle, 1993). However, our attempts to use chlorate as a counter-selection marker in *Ostreococcus* failed, all chlorate-resistant clones being false positives and able to grow on nitrate.

### A memory of recombination events at the *nitrate reductase* locus?

To our surprise, gene integration occurred exclusively by HR when the native *NR* sequence was used to replace the disrupted *NR* sequence in *HR1KanMx* lines. Rates of HR were also high (65%) when a construct containing a *KanMx* selection marker was used to replace the *Nat1* sequence in *HR1Nat* lines. This contrasted with the much lower rates of HR when transforming Wt cells with the *KanMx* disruption cassette. The restored *NR* locus resulting from the complementation of the *NR* knock out by the Wt gene also displayed low rates of HR. On the basis of these observations, it is tempting to speculate that elevated rates of HR in HR1 *HR1KanMx* and *HR1Nat* lines result from the presence of insertions at the *NR* locus. In budding yeast, similarly, the insertion of the prokaryotic Tn3-beta lactamase into the genome resulted in a hotspot for meiotic recombination (Stapleton and Petes, 1991).

The genome of *O. tauri* has one of the highest gene densities known for a free-living eukaryote, and contains very few repeated and transposon-like sequences (Derelle *et al.*, 2006). This suggests that efficient mechanisms may operate to remove foreign DNA from the genome. One such mechanism may be based on HR. This would require the pairing of homologous DNA sequences. *Ostreococcus tauri* is haploid in culture, but pairing of homologous chromosomes may occur during mating. Comparison of *O. tauri* strains supports the existence of cryptic sex, although this remains to be demonstrated under laboratory conditions (Grimsley *et al.*, 2010). Whether HR takes place during sexual reproduction or not and how inserted DNA may be recognized as foreign and marked as a recombination hotspot is currently unknown.

We hypothesized that this may be mediated through changes in chromatin structure, because histone modifications such as H3K4Me can modulate the rate of recombination, and meiotic hotspots are usually associated with an open chromatin structure (Berchowitz and Hanlon, 2009; Borde *et al.*, 2009). We did not observe any obvious correlation between the abundance of H3 trimethyl K4, H3 acetyl K9, nucleosome density at the *NR* locus and the rate of HR in *Ostreococcus.* In addition, DNA CpG methylation did not promote HR at the *NR* locus. Transcription inhibition had a slightly positive effect on the efficiency of HR (0/192 in $NH_4^+$ versus 4/193 in $NO_3^-$ Wt cultures) but these rates were much lower than those observed when targeting the *NR* disrupted locus (Figures 3 and S2).

Our results indicate that recombination frequencies vary with chromosomal location, which may reflect different states of the chromatin. For example, while the rate of HR to replace the ferritin open reading frame with a selection marker was only 1%, it was 25% for the knock-in construct which was targeted 500 bp downstream. This suggests that the recombination rate is dependent on the locus and the chromatin state, which can vary along chromosomes. At this stage, further investigations would be required to determine how inserted DNA sequences are efficiently removed from the *Ostreococcus* genome.

## CONCLUSION

For most model organisms, like the plant *Arabidopsis thaliana*, large insertion collections of mutants are used to compensate for the lack of efficient gene targeting technologies. Our results indicate that in *O. tauri* gene targeting by HR can be used to knock out specific genes, or to fuse a protein using an epitope tag or a reporter gene. The whole process of gene targeting, from transformation of the transgene to the identification of haploid knock-out lines by PCR, takes about 3 weeks. In the future, this technology could be used to introduce mutations at selected positions in the DNA. When combined with the use of an inducible promoter (Djouani-Tahri *et al.*, 2011b), this should facilitate the controlled and inducible expression of recombinant proteins from specific loci. These tools promise a bright future for *Ostreococcus* as a 'green yeast' for functional genomics, systems biology and biotechnological developments.

## EXPERIMENTAL PROCEDURES

### Algal culture, genetic transformation and biological tests

*Ostreococcus tauri* strain 0TTH0595 was grown in flasks (Sarstedt, http://www.sarstedt.com/) or white 96-well microplates (Nunc, Perkin Elmer, http://www.perkinelmer.com/) under constant light at an intensity of 20 μmol quanta $cm^{-2}$ $sec^{-1}$. Cells were grown in standard Keller medium, which contained natural seawater supplemented with trace metals and vitamins unless otherwise stated. Cell counting was performed by flow cytometry using a Cell Lab Quanta® SC MPL (Beckman Coulter, https://www.beckmancoulter.com/). Cells were fixed in 0.25% glutaraldehyde for 20 min before flow cytometric analysis.

Genetic transformation was carried out by electroporation as previously described (Corellou *et al.*, 2009). Stable transformant colonies were selected in semi-solid medium at 0.2% w/v agarose (low-melting-point agarose; Invitrogen, http://www.invitrogen.com/) in Keller medium supplemented with an appropriate antibiotic, G418 at 1 mg $ml^{-1}$ (Merck Chemicals, http://www.merckmillipore.com) or CloNat (nourseothricin) at 2 mg $ml^{-1}$ (WERNER BioAgents, http://www.webioage.de/). For the *NR* targeting experiments a Keller-based ASW (WERNER BioAgents) medium was used. This modified Keller medium contained 24.55 g $L^{-1}$ NaCl, 0.75 g $L^{-1}$ KCl, 4.07 g $L^{-1}$ $MgCl_2$ $6H_2O$, 1.47 g $L^{-1}$ $CaCl_2$ $2H_2O$, 6.04 g $L^{-1}$ $MgSO_4$ $7H_2O$, 0.21 g $L^{-1}$ $NaHCO_3$, 0.138 g $L^{-1}$ $NaH_2PO_4$ and 0.75 g $L^{-1}$ $NaNO_3$. $NR^{KO}$ were selected on this medium supplemented with 0.534 g $L^{-1}$ $NH_4Cl$. In *NR* complementation experiments, $NaNO_3$ was the only source of nitrogen.

$NR^{KO}$ transformants were identified by their ability to grow on ASW lacking ammonium in microplates and confirmed by PCR tests (see below). Disruption of *Nat1* or *KanMx* genes was identified by the inability to grow on G418 at 1 mg $ml^{-1}$ or on CloNat at 2 mg $ml^{-1}$. These tests were carried out with individual transformants grown on microplates.

 

### Cloning strategy for gene targeting experiments

The PCR amplifications were performed on *O. tauri* genomic DNA using the Triple Master polymerase mix (Eppendorf, http://www.eppendorf.com/). Primer sequences are given in Table S1. The *Bgl*II and *Nco*I sites were added to the 5′ and 3′ ends of the 1102-bp *ferritin* PCR product to allow subsequent cloning. A subcloning step was performed in the pGEMT-easy vector (Promega, http://www.promega.com/). The *pH4::KanMx::Tef* selection cassette from the pOtluc vector (Corellou *et al.*, 2009) was introduced into the coding sequence of *NR* and *ferritin* by blunt-end ligation into *Afe*I (AGC/GCT) or *Nru*I (TCG/CGA) sites, respectively. The same strategy was used to introduce pH4::CloNat::Tef selection gene from the pOtox vector (Corellou *et al.*, 2009) into the *NR* sequence. The *ferritin-luc* knock-in construct was generated by cloning the full-length *ferritin* gene into the *Bgl*II–*Nco*I sites of the pOT-Luc vector, in frame with *luciferase*. A 1102-bp fragment corresponding to the 3′ end of the *ferritin* gene was then ligated into the *Sma*I site of pOtluc. The resulting construct (5462 bp) comprised the full-length *ferritin* gene fused in frame with *luciferase*, upstream of the *KanMx* selection gene. Prior to transformation, plasmids were digested with appropriate restriction enzymes and purified onto a NucleoSpin® Gel and PCR Clean-up kit (Macherey Nagel, http://www.mn-net.com/).

### Molecular analysis of transformants

*Ostreococcus* transformants were analyzed by PCR using transgene-specific primers (see Table S1) and/or by Southern blot analysis. Genomic DNA was extracted using the DNeasy Plant Minikit (Qiagen, http://www.qiagen.com/). For DNA blots, 1 μg of DNA was digested with appropriate enzymes, migrated in a 0.8% 2-amino-2-(hydroxymethyl)-1,3-propanediol (TRIS)-acetate-EDTA (TAE) agarose gel and transferred onto Hybond N+ membrane (GE HEALTHCARE Life sciences, http://www.gelifesciences.com) as previously described (Corellou *et al.*, 2009). DNA probes were generated by PCR amplification using primers described in Table S1, except for the P3 probe corresponding to the *KanMx* sequence, which was excised from the pOtluc vector using *Hin*dIII and *Eco*RI. All probes were radiolabelled by random priming. Hybridization and washing of the membranes were performed as previously described (Corellou *et al.*, 2009).

### Chromatin immunoprecipitation

Cultures were grown in constant light until late log-phase. Cells were fixed by the addition of formaldehyde to the medium to a concentration of 1% (v/v). Glycine was added after 10 min to a 125 mM concentration. After 5 min cells were washed twice with ice-cold PBS. Cell pellets were frozen in liquid nitrogen then stored at −80°C until extraction. In order to extract chromatin, cells were resuspended in extraction buffer (50 mM TRIS-HCl pH 8, 10 mM EDTA, 1% SDS) containing a protease inhibitor cocktail (Roche, http://www.roche.com/) prior to sonicating three times for 10 sec at 50-sec intervals using a Branson sonicator. The cell lysate was centrifuged at 10 000 ***g*** for 10 min and the supernatant containing the chromatin was frozen at −80°C. For ChIP analyses, 200 μl of chromatin was diluted to 2 ml using ChIP dilution buffer (167 mM NaCl, 16.7 mM TRIS-HCl pH 8, 1.2 mM EDTA, Triton X-100, 1 mM phenylmethylsufonyl fluoride and protease inhibitors). After pre-clearing with protein A Dynabeads (Invitrogen), samples were incubated overnight at 4°C with either anti-H3 (1:200), anti H3-Acetyl K9 or anti-H3 trimethyl K4 antibodies (Abcam, http://www.abcam.com/). The immunocomplexes were isolated by incubation with protein A Dynabeads for 2 h at 4°C. The beads were washed as described (Haring *et al.*, 2007) with the addition of three extra-high-salt buffer washes. The DNA to be analysed by quantitative PCR was eluted from the beads in the presence of 10% Chelex according to Nelson *et al.* (2006). Real-time PCR was carried out on a LightCycler 1.5 (Roche Diagnostics, http://www.roche.com/) with LightCycler DNA Master SYBR Green I (Roche Molecular Biochemicals) Putative target loci in immunoprecipitated samples were amplified using specific primers (Table S1). Results were analysed using the comparative critical threshold ($\Delta\Delta C_T$) method, quantified relative to the original input chromatin sample and presented as percentage of input DNA.

### DNA methylation analysis

To analyze the DNA methylation status, 0.25 μg of genomic DNA was digested with *Msp*I and *Hpa*II restriction enzymes (Promega) overnight prior to PCR amplification of the regions of interest. These two enzymes have different sensitivities to CpG methylation. When the internal CpG in the 5′-CCGG-3′ tetranucleotide sequence is methylated, cleavage with *Hpa*II is blocked, but cleavage with *Msp*I is not affected. Polymerase chain reaction analysis was performed on DNA regions containing *Msp*I/*Hpa*II sites (see Table S1) so that cytosine demethylation of any of the CpG target sites would impair the amplification of *Hpa*II-cut DNA. *Msp*I-digested DNA was used as a negative control. A fragment lacking CpG *Msp*I/*Hpa*II sites was used as positive control (c).

### Western blot analysis

Cells were harvested by centrifugation in conical bottles (10 000 ***g***, 4°C, 10 min), after addition of Pluronic-F68 (0.1%) to the medium. Pellets were frozen in liquid nitrogen and stored at −80° C until extraction. Cells were ground in lysis buffer (100 mM potassium phosphate pH 7.8, 1 mM EDTA, 1 mM DTT, 1% Triton® X-100, 10% glycerol) using a RNA tissue lyser.

Protein concentration was determined by the Bradford method (Sigma, http://www.sigmaaldrich.com/) and the same amount of protein was loaded in each well on a 10% SDS-polyacrylamide denaturing gel with 4× Laemmli buffer. Western blot analysis was performed as follows: the gel was liquid-transferred onto a nylon membrane (PVDF, Amersham Life Sciences). The membranes were blocked in TRIS buffer saline (TBS) containing 5% milk powder antibody for 1 h and then incubated with an anti-luciferase antibody (sc-74548, Santa Cruz Biotechnology, http://www.scbt.com/) at a 1/2000 dilution The membranes were washed three to six times in TBS containing 0.1% Tween 20 and the bound antibody was detected with a goat anti-mouse antibody (sc-2005). Immunodetection was performed using the ECL+ reagent (Amersham Life Science). Recombinant luciferase from *Photinus pyralis* (Sc-32896) was used as a positive control.

## ACKNOWLEDGEMENTS

This work was supported by ASSEMBLE EU Project to FYB and IC and ANR Phytoiron to EL and FYB. Thanks to Charles White for helpful discussions and advice.

## SUPPORTING INFORMATION

Additional Supporting Information may be found in the online version of this article.

**Figure S1.** Targeted disruption of the *NR* gene by homologous recombination using sense *KanMx-s* constructs.

**Figure S2.** Selection marker replacements by homologous recombination.

**Figure S3.** Targeting of the *NR* restored line.

**Figure S4.** Chromatin remodeling and DNA CpG methylation during successive homologous recombination events.

**Table S1.** List and sequences of oligonucleotides used in cloning and PCR experiments. The size (in bp) of the PCR products is indicated.

## REFERENCES


**Berchowitz, L. and Hanlon, S.** (2009) A positive but complex association between meiotic double-strand break hotspots and open chromatin in Saccharomyces cerevisiae. *Genome Res.* **19**, 2245–2257.

**Borde, V., Robine, N., Lin, W., Bonfils, S., Géli, V. and Nicolas, A.** (2009) Histone H3 lysine 4 trimethylation marks meiotic recombination initiation sites. *EMBO J.* **28**, 99–111.

**Corellou, F., Schwartz, C., Motta, J.-P., Djouani-Tahri, E.B., Sanchez, F. and Bouget, F.-Y.** (2009) Clocks in the green lineage: comparative functional analysis of the circadian architecture of the picoeukaryote *Ostreococcus*. *Plant Cell*, **21**, 3436–3449.

**Cummings, W.J., Yabuki, M., Ordinario, E.C., Bednarski, D.W., Quay, S. and Maizels, N.** (2007) Chromatin structure regulates gene conversion. *PLoS Biol.* **5**, e246.

**Derelle, E., Ferraz, C., Rombauts, S. *et al.*** (2006) Genome analysis of the smallest free-living eukaryote Ostreococcus tauri unveils many unique features. *Proc. Natl Acad. Sci. USA* **103**, 11647–11652.

**Djouani-Tahri, E.-B., Christie, J.M., Sanchez-Ferandin, S., Sanchez, F., Bouget, F.-Y. and Corellou, F.** (2011a) A eukaryotic LOV-histidine kinase with circadian clock function in the picoalga Ostreococcus. *Plant J.* **65**, 578–588.

**Djouani-Tahri, E.B., Sanchez, F., Lozano, J.-C. and Bouget, F.-Y.** (2011b) A phosphate-regulated promoter for fine-tuned and reversible overexpression in Ostreococcus: application to circadian clock functional analysis. *PLoS ONE*, **6**, e28471.

**Gan, L., Ladinsky, M. and Jensen, G.** (2011) Organization of the smallest eukaryotic spindle. *Curr. Biol.* **21**, 1578–1583.

**Grimsley, N., Péquin, B., Bachy, C., Moreau, H. and Piganeau, G.** (2010) Cryptic sex in the smallest eukaryotic marine green alga. *Mol. Biol. Evol.* **27**, 47–54.

**Haring, M., Offermann, S., Danker, T., Horst, I., Peterhansel, C. and Stam, M.** (2007) Chromatin immunoprecipitation: optimization, quantitative analysis and data normalization. *Plant methods*, **3**, 11.

**Heijde, M., Zabulon, G., Corellou, F. *et al.*** (2010) Characterization of two members of the cryptochrome/photolyase family from Ostreococcus tauri provides insights into the origin and evolution of cryptochromes. *Plant, Cell Environ.* **33**, 1614–1626.

**Heyer, W.-D., Ehmsen, K.T. and Liu, J.** (2010) Regulation of homologous recombination in eukaryotes. *Annu. Rev. Genet.* **44**, 113–139.

**Kamisugi, Y., Schlink, K., Rensing, S.A., Schween, G., Von Stackelberg, M., Cuming, A.C., Reski, R. and Cove, D.J.** (2006) The mechanism of gene targeting in Physcomitrella patens: homologous recombination, concatenation and multiple integration. *Nucleic Acids Res.* **34**, 6205–6214.

**Keeney, S., Giroux, C.N. and Kleckner, N.** (1997) Meiosis-specific DNA double-strand breaks are catalyzed by Spo11, a member of a widely conserved protein family. *Cell*, **88**, 375–384.

**Kilian, O., Benemann, C.S.E., Niyogi, K.K. and Vick, B.** (2011) High-efficiency homologous recombination in the oil-producing alga Nannochloropsis sp. *Proc. Natl Acad. Sci. USA* **108**, 21265–21269.

**Kotian, S., Liyanarachchi, S., Zelent, A. and Parvin, J.D.** (2011) Histone deacetylases 9 and 10 are required for homologous recombination. *J. Biol. Chem.* **286**, 7722–7726.

**Minoda, A., Sakagami, R., Yagisawa, F., Kuroiwa, T. and Tanaka, K.** (2004) Improvement of culture conditions and evidence for nuclear transformation by homologous recombination in a red alga, Cyanidioschyzon merolae 10D. *Plant Cell Physiol.* **45**, 667–671.

**Monnier, A., Liverani, S., Bouvet, R., Jesson, B., Smith, J.Q., Mosser, J., Corellou, F. and Bouget, F.-Y.** (2010) Orchestrated transcription of biological processes in the marine picoeukaryote Ostreococcus exposed to light/dark cycles. *BMC genomics*, **11**, 192.

**Moulager, M., Corellou, F., Vergé, V., Escande, M.-L. and Bouget, F.-Y.** (2010) Integration of light signals by the retinoblastoma pathway in the control of S phase entry in the picophytoplanktonic cell Ostreococcus. *PLoS Genet.* **6**, e1000957.

**Nelson, J. D., Denisenko, O., Sova, P. and Bomsztyk, K.** (2006) Fast chromatin immunoprecipitation assay. *Nucleic Acids Res.* **34**, e2.

**O'Neill, J.S., Van Ooijen, G., Dixon, L.E., Troein, C., Corellou, F., Bouget, F.-Y., Reddy, A.B. and Millar, A.J.** (2011) Circadian rhythms persist without transcription in a eukaryote. *Nature*, **469**, 554–558.

**Pfeuty, B., Thommen, Q., Corellou, F., Djouani-Tahri, E.B., Bouget, F.-Y. and Lefranc, M.** (2012) Circadian clocks in changing weather and seasons: lessons from the picoalga Ostreococcus tauri. *BioEssays*, **34**, 781–790.

**Schaefer, D.G. and Zryd, J.-P.** (1997) Efficient Gene targeting in the moss Physcomirella patens. *Plant J.* **11**, 1195–1206.

**Shinohara, A., Ogawa, H. and Ogawa, T.** (1992) Rad51 protein involved in repair and recombination in S. cerevisiae is a RecA-like protein. *Cell*, **69**, 457–470.

**Sodeinde, O.A. and Kindle, K.L.** (1993) Homologous recombination in the nuclear genome of. *Proc. Natl Acad. Sci. USA* **90**, 9199–9203.

**Stapleton, A. and Petes, T.D.** (1991) The Tn3 beta-lactamase gene acts as a hotspot for meiotic recombination in yeast. *Genetics*, **2**, 39–51.

**Zorin, B., Lu, Y., Sizova, I. and Hegemann, P.** (2009) Nuclear gene targeting in Chlamydomonas as exemplified by disruption of the PHOT gene. *Gene*, **432**, 91–96.


 

Une étude transcriptomique sur des cultures d'*O. tauri* a révélé que le gène de ferritine est exprimé de façon rythmique avec un pic d'expression en fin de journée au cours du cycle jour/nuit (Monnier *et al.*, 2010). J'ai analysé les profils d'expression de la ferritine et des principales protéines de liaison du fer (photosystème, métabolisme de l'azote) dans un jeu de données méta-transcriptomiques collectées au cours de cycles jour/nuit sur du pico-plancton dominé par le genre *Ostreococcus* (Ottesen *et al.*, 2013). Ces données, en accord avec l'étude sur culture, ont révélé une expression anti-phasique de la ferritine (en fin de journée) par rapport aux gènes codant pour les protéines riches en Fer du photosystème I, du cytochrome $b_{6/f}$ et du métabolisme de l'azote.

J'ai mesuré l'expression de la ferritine-luc en cycle jour/nuit (LD) à l'aide d'un luminomètre couplé à un système automatisé de contrôle de la lumière par LED développé au laboratoire. Dans les deux types de lignées j'ai observé une forte accumulation de la ferritine-luc à partir du crépuscule suivie d'une chute brutale de la luminescence à l'aube. Ces résultats montrent que la traduction de la ferritine est régulée par l'alternance jour/nuit

Pour déterminer si l'horloge circadienne est impliquée dans la régulation de l'expression de la ferritine, les lignées RH et RI ont été placées en condition de lumière continue (LL) après un entrainement en cycle jour/nuit. De façon surprenante, dans ces conditions, les lignées RI et RH ne se comportent pas de la même manière. On observe en lumière constante un rythme d'environ 24 h qui indique un contrôle circadien de l'expression de la ferritine dans les lignées RI. Dans les mêmes conditions, aucun rythme n'est observé dans les lignées RH et la luminescence semble varier uniquement en fonction de l'intensité lumineuse. Ces résultats suggèrent que, soit la ferritine native est indispensable à sa propre régulation (circadienne) soit le fait de déréguler l'homéostasie du fer affecte l'horloge circadienne

Afin de déterminer l'effet du fer extracellulaire sur l'expression de la ferritine, j'ai cultivé des cellules RH et RI dans un milieu avec une concentration en fer contrôlée avant de les transférer dans des milieux contenant des concentrations variables en Fer-EDTA. On remarque dans les lignées RI une augmentation de la luminescence uniquement pour les concentrations en fer supérieures à la condition de pré acclimatation. En revanche la luminescence ne varie pas en fonction de la concentration en fer dans les lignées RH. Ces résultats suggèrent que l'expression de la ferritine est induite par le fer et qu'un complexe fonctionnel de ferritine est essentiel à cette réponse.

L'analyse par spectrométrie de masse suggère que le principal complexe protéique liant le fer (à 480 kDa) est la ferritine. J'ai pu valider cette hypothèse en montrant que le complexe à 480 kDa disparaît dans la lignée ko ferritine (*KoFer*). Pour étudier l'importance de la ferritine dans l'assimilation du fer, nous avons comparé la vitesse d'assimilation du fer dans les cellules Wt et *KoFer*. La lignée *KoFer* est fortement impactée dans sa capacité à assimiler le fer comme en témoignent des contenus en fer moindre. Nous avons ensuite comparé l'assimilation du fer au cours d'un cycle jour/nuit. Les cellules *KoFer* présentent des vitesses d'importation du fer réduites (3 à 7 fois). En cycle jour/nuit, les profils des cinétiques d'assimilation du Fe-citrate sont quasiment plats même si il y a une légère augmentation en fin de journée et de nuit. De plus, la bande de ferritine fixe plus rapidement le fer au cours de la nuit. Ces résultats indiquent que la ferritine joue un rôle clé dans la régulation de l'assimilation de fer au cours du cycle jour/nuit.

Dans un second temps, j'ai étudié les variations de charge de la ferritine en cycle jour/nuit dans des cellules en phase stationnaire qui n'incorporent plus de fer (Botebol, Sutak, *et al.*, 2014). J'ai réalisé des gels natifs en prélevant des cellules à intervalles réguliers au cours d'un cycle jour/nuit. L'autoradiographie des gels révèle une forte baisse du $^{55}$Fe fixé à la ferritine à l'aube, avec un minimum de marquage radioactif au milieu de la journée. Le signal commence à augmenter en fin de journée et atteint un maximum à la fin de la nuit. Ces résultats tendent à montrer que la ferritine est impliquée dans le recyclage du pool de fer intracellulaire en phase stationnaire. Les principales protéines liant le fer ont été caractérisées par spectrométrie de masse ESI MS/MS. Parmi les meilleurs scores MASCOT pour chaque bande analysée, nous avons identifié la Nitrite réductase (meilleur score) et la Glutamate synthase (GOGAT, troisième score). La Nitrate réductase (NR), protéine à hème, a également été identifiée avec un score moins bon (25). L'utilisation d'un mutant KO de *NR* a permis de confirmer que cette bande correspond bien à la nitrate réductase. De façon surprenante, la nitrate réductase est la principale protéine qui lie le fer dans le mutant ko ferritine ce qui suggère un lien entre le métabolisme du fer et celui de l'azote.

Pour préciser l'importance de la ferritine dans la gestion de la carence en fer, des suivis de croissance du mutant *KoFer* ont été réalisés dans des milieux contrôlés en fer en cycle jour/nuit et en lumière continue. Pour acclimater les cellules au milieu et réduire leur stock de fer, elles sont pré-cultivées dans un milieu (5.4 nM Fe-EDTA), puis transférées dans différents concentrations de Fe-EDTA (de 5.4 à 5400 nM). En lumière continue, les taux de croissance des cellules Wt et *KoFer* sont comparables quelle que soit la concentration en fer

utilisée. En cycle jour/nuit, le *KoFer* présente des taux de croissance légèrement inférieurs mais les différences ne sont pas significatives.

Etant donné le rôle de la ferritine dans le recyclage du fer, nous avons pré-cultivé en 1µM $Fe^{3}$+-citrate les souches Wt et *KoFer* puis nous les avons transférées en présence de différentes concentrations de DesFerriOxamine B (DFOB). En présence de DFOB, les cellules ne sont pas capables d'importer le fer extracellulaire. En cycle jour/nuit, les cellules *KoFer* survivent moins bien que le Wt, même en absence de DFOB. Lorsque les cellules sont transférées en lumière continue après un entrainement en cycle jour/nuit 12 :12, la synthèse de la ferritine est contrôlée uniquement par l'horloge circadienne. La survie des cellules *KoFer* diminue pour des concentrations en DFOB de 1.5µM et 2 µM. Ainsi lorsqu'un chélateur fort du fer extracellulaire est ajouté, la survie du mutant est plus fortement impactée, ce qui montre l'importance de la ferritine dans la survie en conditions de carence en fer.

Pour conclure cette étude, nous nous sommes intéressés à un site de fertilisation naturelle par le fer sur le plateau des îles Kerguelen. Des échantillons ont été prélevés au cours de la campagne KEOPSII le jour et la nuit sur deux sites : un de référence, l'autre fertilisé par le fer. Les ARNms ont été extraits et l'analyse RNAséq est en cours en collaboration avec Chris Bowler (ENS Paris). Ces travaux font l'objet d'un manuscrit soumis.

### 2. Article 4:

Iron saving in marine phytoplankton: a central role of ferritin in the day/night regulation of uptake, recycling and survival under iron limitation

Botebol, H.‡, Lesuisse, E.‡, Sutak, R., Lozano, J., Schatt, P., Vergé, V., Bowler, C., Morrissey, J., Gueunegues, A., Blain, S. and Bouget, F-Y. (2014).Prochainement soumis à PlosBiology.

‡ : Contribution equivalente

# Iron saving in marine phytoplankton: a central role of ferritin in the day/night regulation of iron uptake, recycling and survival under iron limitation

Hugo Botebol[1,2,‡], Emmanuel Lesuisse[3,‡], Robert Sutak[4], Christophe Six[5], Jean-Claude Lozano[1,2], Philippe Schatt[1,2], Valérie Vergé[1,6], Chris Bowler[7], Joe Morrissey[7], Thibault Léger, Audrey Gueunegues[1,2], Stéphane Blain[1,2,§], and François-Yves Bouget[1,2,§]

1- Sorbonne Universités, UPMC Univ Paris 06, UMR 7621, Laboratoire d'Océanographie Microbienne, Observatoire Océanologique, F-66650 Banyuls/mer, France

2- CNRS, UMR 7621, Laboratoire d'Océanographie Microbienne.
Microbienne, Observatoire Océanologique, F-66650 Banyuls/mer, France

3- Université Paris Diderot (Paris 07), Centre National de la Recherche Scientifique, Institut Jacques Monod, F–75013 Paris, France.

4- Department of Parasitology, Faculty of Science, Charles University, 12844 Prague, Czech Republic5- Unité Mixte de Service, UMS2348,F-66651, Banyuls/Mer, France.

5- CNRS, UPMC Univ Paris 06, UMR 7144, Groupe Plancton Océanique, BP 74, 29682 Roscoff Cedex,

6- Unité Mixte de Service, UMS2348,F-66651, Banyuls/Mer, France.

7- Institut de Biologie de l'Ecole Normale Supérieure (IBENS), CNRS UMR8197 Inserm U1024, 75005 Paris, France

‡ Equal contribution

§ -Corresponding authors

E-mail: fy.bouget@obs-banyuls.fr; blain@obs-banyuls.fr

**Running title: Reinvestigating the role of ferritin in marine phytoplankton**

**SUMMARY**

In open oceans, iron is one of the main limiting factor to primary production as revealed by artificial and natural iron fertilization experiments and observations. Phytoplankton species have developed diverse strategies to cope with iron limitation and sporadic iron supply, such as iron storage into Ferritin in pennate diatoms or day/night recycling of iron in diazotroph cyanobacteria. Survey of gene expression under day/night condition in the field and in the lab have revealed a genome-wide regulation of gene expression in the picoeukaryote *Ostreococcus sp*. Here we demonstrate, combining biochemical and physiological experiments on *Ostreococcus* wild type and knock out mutants, that ferritin plays a central role in the diel regulation of iron uptake in exponential phase and iron recycling in early stationary phase cells. Furthermore, ferritin is important for cell survival under iron limitation. Ferritin and iron binding proteins of Photosystem and nitrate assimilation pathway show, both in the lab and in the field, opposite expression patterns, ferritin being maximally expressed at night. We conclude that a key function of ferritin is to regulate iron homeostasis under day/night conditions and this strategy contributes to improved survival under iron limitation.

## INTRODUCTION

Iron is a cofactor involved in numerous redox-based biological processes such as DNA synthesis, photosynthesis, nitrogen fixation, mitochondrial respiration or the detoxification of reactive oxygen species (Lukianova and David, 2005; Müh *et al.*, 2012; McHugh *et al.*, 2003; Rueter and Ades., 1987; Tortell *et al.*, 1999; Mittler, 2002). Although iron is essential for living organisms, it is also highly reactive and toxic via the Fenton reaction (Halliwell and Gutteridge, 1992). The homeostasis of iron must therefore be tightly regulated in the cell.

In one third of open oceans, iron bioavailability limits phytoplankton growth. This is well illustrated in high nutrient low chlorophyll (HLNC) regions of austral oceans that suffer of chronically low iron concentrations. Natural sporadic iron supply or artificial iron fertilization experiments induce massive phytoplanktonic blooms in these HLNC areas (Blain *et al.*, 2007; Coale *et al.*, 1996). Phytoplanktonic species have evolved several strategies to cope with iron limiting conditions and sporadic iron supply, so that iron cellular quotas are optimized. Earlier studies have shown that the uptake rates per unit of cell surface are similar between species with different iron requirements and as a consequence smaller cells with higher surface to volume ratio are favored under iron limitation (Sunda and Huntsman, 1997). Acclimation to low iron induces rapid changes in the Photosystem II (PSII) to Photosystem I (PSI) ratio and a global remodeling of photosynthetic machinery (Lommer *et al.*, 2012), the down-regulation of nitrogen reducing enzymes such as nitrate and nitrite reductase and the up-regulation of enzymes involved in nitrogen recycling (Nunn *et al.*, 2013). Metabolic adaptation to iron limitation involves a decrease of Photosystem I and cytochrome *b6/f* requirement in oceanic diatoms (Strzepek and Harrison, 2004) and the utilization of copper-dependent plastocyanin instead of cytochrome *c6* (Peers and Price, 2006). The ability to take up and store iron under high iron conditions for subsequent use under low iron conditions represents another strategy that would be successful when iron supply is sporadic. Ferritin, the main iron-storage protein in eukaryotes, has been found in a number of microalgae including several diatoms and picoeukaryotes (Marchetti *et al.*, 2009). In particular, the ferritin-containing diatom *Pseudo-nitzschia* survive better to iron limitation than diatoms lacking ferritin (Marchetti *et al.*, 2009). It was therefore proposed that long term-storage of iron into ferritin is a strategy to cope with iron variable supplies. In the land plant Arabidopsis, however, ferritin is regulated by the circadian clock component Time for coffee (TIC)

suggesting that its function may be to regulate iron homeostasis during the day/night cycle (Duc *et al.*, 2009).

Day/night recycling of iron was suggested indirectly by a proteomic study in the diazotroph cyanobacteria *Crocosphera watsonii* (Saito *et al.*, 2011). While the main iron-binding proteins of PSI and Cytochrome b6/f involved in photosynthesis are expressed during the day, the metalloproteins involved in nitrogen reduction are expressed at night, consistent with an internal recycling of iron between metalloproteins over the day/night cycle. The occurrence of such diel recycling of iron remains to be determined in non-diazotrophs phytoplanktonic species.

An automated Lagrangian approach on microbial communities has revealed strong diel rhythms of gene transcripts in picoplankton dominated by the genus *Ostreococcus* (Ottesen *et al.*, 2013). These results, in agreement with those conducted on *Ostreococcus tauri* cultures, identified cluster of genes associated to specific biological processes such as cell division which are expressed at specific times of the day (Monnier *et al.*, 2010; Moulager *et al.*, 2007). *O. tauri* was originally isolated from the Thau Lagoon less than 20 years ago. This minute-size picoalga (1 micrometer) described as the smallest free-living eukaryote has a minimalist cellular organization (Courties et al., 1995). *Ostreococcus* (Prasinophyceae) falls into the order of Mamiellales which also includes the genera *Micromonas* and *Bathycococcus*. Mamiellales have a world wide geographic distribution, predominantly in costal ecosystems where they contribute significantly to primary production and carbon flow to higher trophic levels since they are subjected to intense grazing (Bec *et al.*, 2005). *Ostreococcus* blooms have been reported in several locations including the Thau lagoon (Vaquer *et al.*, 1996; Bec *et al.*, 2005), the West Neck bay (O' Kelly *et al.*, 2003), the Chilean Upwelling ecosystem (Collado-Fabbri *et al.*, 2011). *In situ* studies revealed that the two main *Ostreococcus*-clade partitions occurs between nutrient rich coastal waters versus more oligotrophic open ocean waters (Demir-Hilton *et al.*, 2011).

*O. tauri* has emerged as a model organism thanks to the ease of culture and techniques for functional analysis such a genetic transformation and gene targeting by homologous recombination (Bouget *et al.*, 2014; Corellou *et al.*, 2009; Lozano *et al.*, 2014). In *O. tauri* cultures, radiolabelled $^{55}Fe$ accumulated in a protein complex around 480 kDa, which was attributed to a ferritin complex by mass spectrometry (Sutak *et al.*, 2012). The uptake of iron appeared to be differentially regulated over the diurnal cycle, the maximal uptake occurring before dusk and before dawn (Botebol *et al.*, 2014). Furthermore the ferritin transcript

exhibited a strong diel rhythm of expression in cultures (Monnier *et al.*, 2010). Here, we investigated the diel regulation of ferritin and iron-binding proteins in the field and in the lab. Furthermore, functional approaches were conducted to determine importance of ferritin in the regulation of iron homeostasis and for cell survival under iron limitation.

## RESULTS

### Day/night and circadian regulation of genes encoding iron-containing proteins

We first analysed expression patterns of genes encoding iron-containing proteins in an environmental data set collected during day/night cycles in an open ocean environment (Ottesen *et al.*, 2013). Within the phytoplankton community the unique genus *Ostreococcus* was dominant and exhibited robust rhythms of gene expression. *Ostreococcus* genes encoding the main (Fe)-sulphur (S) cluster proteins of Photosystem I (PSI) such as PsaC, Photosystem II (PSII) such as PsbE, Cytochrome b6/f (Cytb6/f) and Ferredoxin (Fdx) and of nitrogen metabolism such as the ferredoxin-dependent glutamate synthase (Fd-GOGAT) had similar patterns of expression during day-night cycles. Transcripts peaked in late morning and decreased during the afternoon. Low levels of mRNA persisted during all the night (Fig 1A and Fig.S1A). In contrast the gene encoding the main iron storage protein ferritin had an opposite pattern of expression with a maximum level of transcript around dusk.

Similar expression patterns were observed for genes encoding photosynthesis Fe-S proteins and ferritin in cultures of *Ostreococcus tauri* grown under day/night conditions (Figure S1B).

The protein levels of the main iron-containing protein (PsaC) and ferritin was determined in *O. tauri* cultures exposed to day/night cycles. Western blot analysis confirmed a rhythmic expression of PsAC with a maximum in the middle of the day (Fig 1B). A Ferritin-luciferase (FTN-luc) translational reporter line (corresponding to a random insertion in the genome of the full ferritin gene fused to luciferase) was used to estimate *O. tauri* ferritin protein regulation in living cells (Fig. 1C). Under day/night cycle, FTN-luc reporter lines show rhythmic luminescence patterns. The luminescence raised abruptly after dusk and remained high during the night. A rapid drop in luminescence was observed at dawn, followed by a slow decrease until the end of the day. Rhythmic patterns of luminescence of FTN-luc were still observed when cells entrained under 12:12 day/night cycle were transferred to free running conditions of constant light (Figure 1D). The period of oscillation was close to 24 hours indicating that the expression of ferritin is regulated by the circadian clock.

### Ferritin in the regulation of cellular iron content and uptake

Iron binding capacity of *O. tauri* ferritin was demonstrated using short term (1 to 3 hours) incubations of WT cells and a ΔFtn knock out lines (Lozano *et al.*, 2014) in the presence of 1µM $^{55}$Fe(III)-citrate. Autoradiography of labelled proteins resolved on a native gel revealed in WT a major band around 480 kDa, which was not detected in ΔFtn cells, suggesting that this band corresponds to a functional ferritin complex (Figure 2A). Under these conditions, the cellular content of $^{55}$Fe was higher in WT than in ΔFtn, by 2 fold after only 30 min incubation with the radionuclide and by 3.5 fold after 120 min incubation indicating that ferritin complex contributes significantly to the cellular iron content (Figure 2B). Between 0 and 30 min, iron uptake rate was about two fold higher in WT (2.57 fmol/min/million cells) than in ΔFtn cells (1.18 fmol/min/million cells). Furthermore between 30 and 120 min, virtually no uptake was measured ΔFtn (0,05 fmol/min/million cells) while a continuous uptake was still detected in WT cells (0.73 fmol/min/million cells).

The regulation of ferritin synthesis in response to extracellular iron is determined by using luciferase reporter lines in two different genetic background; FTN-luc (WT FTN) described above and FTN-luc (*ΔFtn*) a line in which the luciferase is fused in frame to ferritin (24 kDa) at the native locus giving rise to a 90 kDa protein (Lozano et al., 2014). A radiolabelled band at the expected size for the ferritin complex (480 kDa) was observed in FTN-luc (WT FTN) but not in FTN-luc (*ΔFtn*) cells grown in the presence of 1µM $^{55}$Fe(III)-citrate (Figure 2C). This result confirmed that the FTN-luc (*ΔFtn*) lacks a functional ferritin complex but that the FTN-luc fusion protein did not prevent the formation of a functional ferritin complex in the FTN-luc (WT FTN) line. Figure 2D shows the luminescence levels of the two FTN-Luc reporter lines in response to changes in extracellular iron concentration. To buffer precisely iron in the culture medium, iron was provided as Fe(III)-EDTA (the reasons for choosing either ferric citrate or ferric EDTA as iron sources were explained in a previous publication; Botebol et al, 2014). Cells were first acclimated in a medium containing 270 nM EDTA since this concentration is limiting but does not prevent cell growth. Cells were then shifted to media containing various concentrations of Fe(III)-EDTA. In the FTN-luc (WT FTN) cell line, luminescence increased gradually with increasing concentration of ferric EDTA. In contrast, no variation of the luminescence was observed in the FTN-luc (*ΔFtn*) cell line when varying the Fe(III)-EDTA concentration. These results suggest that a functional ferritin is required for the iron-dependent induction of ferritin synthesis.

**Ferritin in the day/night regulation of iron uptake in growing cells**

The results presented in Figure 2 show that ferritin plays a role in iron uptake. Furthermore the rate of iron uptake varies along the day/night cycle (Botebol *et al.*, 2014). Since ferritin is regulated by the day/night cycle (Figure 1), we measured the rate of iron uptake by ΔFtn exponentially growing cells versus WT cells under day/night conditions (Figure 3A). WT cells displayed two main peaks in the rate of Fe uptake, one at the end of the day (8 fmol/min/million cells) and one at the end of the night (12 fmol/min/ million cells) as previously described (Botebol *et al.*, 2014). ΔFtn cells showed drastically reduced uptake rates compared to WT cells, with maximal peaks of uptake rates of 2.4 and 1.9 pmole/min/$10^6$ cells, corresponding to 3 and 6 fold reductions compared to WT at 9 and 21 hours respectively (Figure 3A). Notably the rate of iron uptake was much lower in ΔFtn cells than in WT cells during all of the night, but these rates were similar in ΔFtn and WT cells during the first part of the day.

The kinetics of ferritin iron loading was assessed in the same conditions (Figure 3B). WT cells were incubated with $^{55}$Fe either from dawn or dusk (Figure 3B). Incorporation of $^{55}$Fe into ferritin increased progressively from 3 hours after dawn until the end of the day, when iron was provided at dawn. Loading of ferritin, on the other hand was continuous during the night when iron was supplied at dusk. In addition, the relative rate of incorporation of $^{55}$Fe during the night was two-fold higher than during the day.

**Day night rhythms of iron binding proteins in iron-loaded cells**

In the following experiments, cells were grown for one week in a medium containing 1 μM $^{55}$Fe (III)-citrate under 12:12 light-dark cycle. Under these conditions, most of the iron was removed from the medium by the cells after two days (Botebol *et al.*, 2014). After one week (early stationary phase) we analysed the fate of iron (total cell iron, ferritin iron and iron associated to other proteins) over one day/night cycle (Figure 4). Analysis on non-denaturing gel revealed that ferritin was the most prominently $^{55}$Fe-labelled protein. While total cell iron did not significantly change (Figure 4B), strong variations were observed in the level of ferritin iron over the 24h period, with maximal level of ferritin iron reaching more than 10-fold its minimal level (Figure 4B). Ferritin iron was maximal at dawn, and then decreased sharply until midday before increasing progressively again until dusk and more markedly during the night until dawn (Fig 4A). As total cell iron did not change much, the changes in ferritin iron content as a function of day/night periods (increased during the night) probably reflected changes in intracellular iron distribution, more than new iron intake during the night.

Several iron bands of lower molecular weights were also detected when we tried to get better resolution (see lower panels). Proteins from these bands were analysed by ESI- MS/MS mass spectrometry (Table S1). Best Mascot score for Band 2 in Figure 4 (around 150 kDa) was attributed to a ferredoxin-dependent glutamate synthase (Fd-GOGAT) with 58 unique peptides. Around 100 kDa the plastid-targeted nitrite reductase (NiR) was also the first putative iron binding Fe-S protein ($4^{th}$ Mascot score, 42 unique peptides). The $4^{th}$ band around 75 kDa may correspond to the iron binding protein sulfite reductase ($7^{th}$ score, 27 peptides). Nitrate reductase (NR) was identified in band 1 around 350 kDa, which was confirmed by the absence of this band in the ΔNR nitrate reductase knock-out line (Fig 4C). Interestingly, the NR labelled band was more labelled in the ΔFtn line (Figure 4C). All these protein bands except for NR, showed a day night variation in their iron content (Fig 4D). The amount of iron associated with NiR and Fd-GOGAT was higher during the day than during the night.

**Ferritin is required for cell survival under iron starvation conditions in day/night and circadian conditions**

The importance of ferritin for cell survival under day/night conditions was investigated by exposing WT and ΔFtn cells to strict iron deprivation conditions. For that purpose, we added various concentrations of Desferrioxamin B (DFOB), a siderophore that cannot be used as an iron source by *O. tauri* (data not shown). Under control conditions the ΔFtn cell line reached a cellular density corresponding to about 80% of that reached by the WT cell line (48 million cells/ml, n=3, $P<0.01$) (Figure 5). Addition of DFOB to the growth medium compromised cell survival to a much larger extend in ΔFtn than in WT cell lines: the density of cells lacking ferritin reached only 35% of WT cell density with 2µM DFOB (5.4 millions/ml, n=3, $P<0.0001$) (Figure 5).

The same experiment was done under constant light after an initial entrainment under 12:12 light/dark cycles. In these free running conditions the synthesis of ferritin is driven only by the circadian clock (Figure 2). Cell survival was 50% lower in ΔFtn than in WT cells (6.8 millions/ml, n=3, $P<0.001$) at concentrations of 1.5µM DFOB, and 60% lower at 2µM (3.1 millions/ml, n=3, $P<0.001$) (Figure 5).

DFOB was added at dawn or dusk to cells that were previously loaded with $^{55}Fe$ for one week as described above (Figure 4A). Ferritin iron decreased sharply after 1 hour to reach undetectable level in less than 6 hours when DFOB was added at dawn (Figure S2). In

contrast, ferritin iron remained constant or only slightly decreased when DFOB was added at dusk. These results further suggest that the activity (mobility) of ferritin iron is not the same during the day and during the night, in agreement with the results presented above (Figure 4): when any external supply of iron is blocked by DFOB, iron is rapidly released from ferritin during the day, not during the night.

The monitoring of the levels of the Fe-S protein PsaC in ΔFtn cells, revealed similar day/night rhythms as in WT cells (Figure S3 and Figure 1) indicating that the turnover of the PsaC protein occurs even in the absence of ferritin.

## DISCUSSION

### Ferritin in the day/night regulation of of iron homeostasis

Both in situ meta-transcriptomic data and RNA microarray studies indicate that in the genus *Ostreococcus*, *ferritin* is regulated by the day/night cycle with a peak of transcript at the end of the day. The profile of FTN-luc translational reporter further suggests that the ferritin protein is translated during the night and is degraded soon after the dark/light transition. In cultures of iron-limited cells, iron-binding to the ferritin also decreases dramatically after dawn. Comparison of FTN-luc levels and iron binding to ferritin suggest that the low level of ferritin labelling after dawn may result of a light-dependent degradation of ferritin that ultimately results in lower amount of ferritin complex per cell. Maximal Iron-binding to ferritin, in contrast, is observed a few hours before dawn, that is, after a sustained synthesis of ferritin during the night as inferred by FTN-luc reporter. In other words our results suggest that transcriptional, translational and light-dependent regulation of ferritin contributes strongly to the level of ferritin and ultimately of intracellular iron storage into the ferritin complex. This key role of ferritin level in the regulation of iron homeostasis is illustrated in ΔFtn which displayed 3-4 fold reduced iron content compared to Wt cells (Figure 2B).

In exponentially growing cells of *O. tauri*, the uptake of iron is regulated by the day/night cycle with maximal uptakes before dawn and dusk. Under the same conditions, iron binding to ferritin increases progressively from midday to dusk and markedly during the whole night, suggesting that the variations in the iron binding to ferritin does not result only from differential iron uptake over the day night cycle. Internal ferritin-dependent recycling of iron may also operates in exponential phase. In support of this of hypothesis, the ferritin and most of iron-binding protein encoding genes are regulated under day/night cycle in exponentially growing cell cultures (see figure 1). It would be difficult, however, to monitor iron recycling in growing cells because of iron uptake interference.

ΔFtn cells displayed 3 to 6 fold lower rates of iron uptakes but the biphasic profile with maximal uptakes before dawn and dusk is observed, though with a much more reduced amplitude, indicating that ferritin itself is not the primary component in the diel regulation of iron uptake. The lower uptake rate and ultimately iron content is most likely to arise from a misregulation of iron homeostasis in ΔFtn cells. The addition of DFOB, at dusk, has no effect on ferritin iron-loading during the night but when added at dawn DFOB leads to a complete

unloading of ferritin during the day. DFOB, which is an extracellular iron chelator, would trap free iron only when it is released from ferritin or from other iron binding proteins and exported out of the cell at specific times of the day/night cycle.

**Significance of the ferritin-dependent diel recycling of iron**

In iron-limited cells which do not take up extracellular iron, 24 hour cycles of iron loading and unloading on ferritin are observed, with a maximum iron binding at night. Under the same conditions, the main iron binding proteins identified are involved in nitrogen reduction, among which *Fe*-S cluster proteins nitrite reductase and GOGAT are expressed during the day. Other iron-rich proteins such as PsaC, cytochrome b6/f and ferredoxin were not detected on blue native gels, most likely because their native protein complex are not preserved during the extraction and/or electrophoresis processes. PsaC protein, however, also exhibit 24 hour rhythms of expression with a maximum level at day. Taken together these data suggest that iron contained in PSI and nitrogen reducing enzymes during the day is transferred and stored into ferritin at night. At dawn, the ferritin complex is degraded, and the released iron becomes available to daily expressed iron-containing proteins of PSI and nitrogen metabolism. Such a mechanism of iron conservation operates in the diazotroph cyanobacteria *Crocosphera wastsoonii* and it has been proposed that iron is transferred from PSI proteins during the day to Nif proteins involved in nitrogen reduction, at night (Saito *et al.*, 2011).

The importance of ferritin-dependent recycling of intracellular iron is highlighted in cells grown in the presence of the extracellular chelator of iron DFOB. While, under standard conditions of iron, no difference is observed between Wt and ΔFtn cells, in the presence of DFOB, cell survival is more severely compromised in ΔFtn cells. In these mutant cells, day/night regulation of iron-binding proteins still occurs as shown for PsaC. The most plausible explanation is that because of the high toxicity of iron through the Fenton reaction which generates reactive oxygen species, in cells lacking ferritin (1) iron uptake is reduced, (2) iron is exported out of the cells during day/night recycling of iron. In the plant Arabidopsis, similarly, *ferritin* triple mutant show a massive accumulation of iron in the apoplastic space, suggesting that in the absence of iron buffering cells activate iron efflux and/or repress iron influx to limit the amount of free iron in the cell (Roschzttardtz *et al.*, 2013). Since *O. tauri* is unicellular, it is more likely that at dusk in ΔFtn cells, iron is exported outside of the cell where it is either bound to the plasma membrane (Sutak *et al.*, 2012) or to

exopolysaccharides (Gledhill and Buck, 2012), thus remaining bioavailable for later uptake before dawn and dusk. In the presence of DFOB, extracellular iron would be irreversibly chelated and therefore unavailable to the cells. This would suggest that the main function of ferritin in *O. tauri* is not so much the long-term storage of iron, as the temporal storage of iron over the day/night cycle. Such a mechanism would be efficient to repair and recycle damaged /oxidized iron-binding proteins, while keeping the intracellular stock of iron intact for the following day.

Studies in plant and in the green alga *Chlamydomonas*, confirmed that organisms lacking ferritin are more sensitive to oxidative stress such as photo-oxidation (Long *et al.*, 2008; Ravet *et al.*, 2009). Day/night recycling of iron would be particularly important in iron-limited cells that are exposed to oxidative stress. Recently enzymes composing the nitrogen assimilation pathway, including, nitrite reductase and GOGAT were found to be redox-regulated in the diatom *Phaeodactylum tricornutum*. (Rosenwasser *et al.*, 2014). Iron is an essential cofactor of ROS detoxifying enzymes and therefore iron intracellular level plays an essential role in maintaining the cellular redox balance (Outten and Theil, 2009). Ferritin day/ night regulation could therefore be important not only for recycling iron but also for fine tuning of the intracellular level of iron and ROS, which are key regulators of the nitrogen assimilation pathway during the day night/cycle.

## EXPERIMENTAL PROCEDURES

### Algal strains and cell culture

Ferritin knock-out (ΔFtn), FTN-Luc knock in translational reporters (WT and KO background) and Nitrate Reductase knock-out (ΔNR) have been previously described (Lozano *et al.*, 2014). Cell were grown at 20 °C under a 12:12 light dark regime or under constant light for monitoring circadian rhythms in modified F (Mf) medium (Sutak *et al.*, 2010; Botebol *et al.*, 2014; Sutak *et al.*, 2012) unless otherwise stated. For short term uptake and protein radiolabelling experiments, iron was provided as ferric citrate (1:20) at a 0.1 µM final concentration since the uptake is much faster with ferric citrate compared to Ferric-EDTA. The chemical speciation of iron was estimated using the GEOCHEM-EZ software (http://www.plantmineralnutrition.net/Geochem/Geochem%20Download.htm) (Shaff *et al.*, 2009) and the MINEQL+4.62.2 software (http://www.mineql.com/) (Kraepiel *et al.*, 1999).

For long term monitoring of the iron effect of on the expression of FTN-luc reporter, AQUIL medium was used to controlled precisely the level of iron in the culture media (Price *et al.*, 1988). All culture work and subsampling were conducted in a clean room (class 10,000) equipped with a laminar flow hood (class 100). We used polycarbonate bottles and plastic-ware soaked in 10% HCl for 24 h and subsequently soaked overnight with ultrapure water (18.2 Mohm resistivity, Elga). All the lab-ware was sterilized three times by microwaving (5 min, power 750 W) and then dried under the laminar flow hood before use. Synthetic ocean water (SOW; Price et al., 1988) and solutions of inorganic nutrients ($NO_3^-$ and $PO_4^{3-}$) were separately purified by removing trace metals using a Chelex 100 ion exchange resin (Bio-Rad). All solutions were filtered through metal-free 0.2 mm syringe Acrodisc filters (Pall Corporation) before use.

Cell number and chlorophyll red fluorescence (FL3 parameter) were determined with a flow cytometer (BD Accury C6).

### Luminescence recording and analysis of circadian rhythms

For luminescence recording, FTN-luc cultures were transferred to 96-well microplates at a density of 5 x $10^6$ cells $ml^{-1}$ and entrained for 24h under 12:12 light/dark cycle at 20 µmol.quanta.$cm^{-2}$.$s^{-1}$ before recording luminescence under 12:12 light/dark cycle or constant light corresponding to circadian clock free running condition. Luminescence was

acquired for 5 sec every hour using an automated microplate luminometer (LB Centro, Berthold Technologies, http://www.berthold.com). Statistical analyses were performed using BRASS (biological rhythms analysis software system software; P. E. Brown, Warwick University, UK). Fast Fourier transform nonlinear least square (FFT-NLLS) analysis was used to estimate the RAE (a measure of goodness of fit to a theoretical sine wave) and FRP, which were taken as objective measures of the rhythmicity of bioluminescence traces (Hastings *et al.*, 2008).

**Iron uptake assays**

Iron uptake by micro-algae was assayed in microtiter plates or in 2 ml micro-centrifuge tubes as previously described (Sutak *et al.*, 2012). Iron uptake assays were performed with concentrated cell suspensions (from 50 to 250 million cells/100 µl) incubated in Mf medium (synthetic seawater, the composition of which was described previously (Sutak *et al.*, 2012)). $^{55}$Fe (29,600 MBq/mg) was added as 1 µM ferric citrate (1:20), ferric ascorbate (1:100) or ferric EDTA (1:1.2) as we described previously (Botebol et al., 2014). Iron uptake was stopped at chosen intervals by adding a mixture of strong iron chelators (1 mM Bathophenanthroline sulfonate (BPS), 0.15 mM desferrioxamine B (DFOB), 50 mM EDTA) to the cell suspensions. After 2 min cells were harvested and washed on filters with a cell harvester (Brandel), or harvested and washed by centrifugation. In either cases, the cells were washed three times with a washing buffer containing strong iron chelators (480 mM NaCl, 20 mM KCl, 0.1 mM $MgCl_2$, 0.1 mM $CaCl_2$, 0.1 mM BPS, 0.15 mM DFOB, 50 mM EDTA, 1 mM salicyl hydroxamic acid (SHAM) and 10 mM HEPES pH 7.5). Cell pigments were bleached with sodium hypochlorite before scintillation counting in a Wallac 1450 Micro Beta TriLux scintillation counter.

**Electrophoresis and identification of iron-binding proteins**

Cells grown in the presence of 1 µM $^{55}$Fe(III)-citrate (1:20) were disrupted by sonication on ice. Proteins were solubilised with 0.7% digitonin and resolved in a blue native PAGE using the Novex Native PAGE Bis-Tris Gel 3%–12% System (Invitrogen) according to the manufacturer protocol. The gels were vacuum dried and autoradiographed for 2-10 days using a TyphoonTrio Phosphorimager (Amersham).$^{55}$Fe signals were quantified using the ImageJ software (Abràmoff *et al.*, 2004). The main labelled proteins were cut from the gel. Plugs were reduced with 10 mM dithiothreitol (DTT), alkylated with 55 mM iodoacetamide

(IAA) and incubated with 20 µL of 25 mmol $L^{-1}$ $NH_4HCO_3$ containing sequencing-grade trypsin (12.5 µg $mL^{-1}$; Promega) overnight at 37°C. The resulting peptides were sequentially extracted with 30% acetonitrile, 0.1% formic acid and 70% acetonitrile, 0.1% formic acid. Peptide analyzes were performed by a LTQ Velos Orbitrap (Thermo Fisher Scientific, San Jose, CA) coupled to an Easy-nLC Proxeon 1000 chromatographic system (Thermo Fisher Scientific, San Jose, CA). Chromatographic separation of peptides was performed with the following parameters : Acclaim Pepmap100 pre-column (5mm, 300 µm i.d., C18, 5 µm, 100 Å) and Acclaim PepMap-RSLC Proxeon column (50 cm, 75 µm i.d., C18, 2 µm, 100 Å), 300nl/min flow, gradient rising from 90 % solvent A (2 % acetonitrile, 0,1% formic acid) to 40% solvent B (100 % acetonitrile, 0,1% formic acid) in 100 minutes then rising to 80% B in 5 minutes. The peptides were analyzed in the Orbitrap in full ion scan mode at a resolution of 30,000 (at m/z 400), a mass range of 400 to 1,800 mass-to-charge ratio, and with a MS full scan maximum ion time of 100 ms. Fragments were obtained with collision-induced dissociation activation with a collisional energy of 35%, an activation collisional endothermicity of 0.250 for 10 ms, and analyzed in the LTQ in a second scan event. The ion-trap MS/MS maximum ion time was 50 ms. MS/MS data were acquired in a data-dependent mode in which the 20 most intense precursor ions were isolated, with a dynamic exclusion of 20 s and an exclusion mass width of 10 ppm. Data were processed with Proteome Discoverer 1.4 software (Thermo Fisher Scientific) coupled to an in-house Mascot search server (Matrix Science; version 2.4). The mass tolerance of fragment ions was set to 7 ppm for precursor ions and 0.5 Da for fragments. The following modifications were used in variable parameters: oxidation (Met) phosphorylation (Ser/Thr/Tyr), carbamidomethylation (Cys), acetylation (Lys/N-term) and deamidation (Asp/Asn). The maximum number of missed cleavages was limited to two for trypsin digestion. MS/MS data were compared with the *Ostreococcus tauri* sequence database extracted from the National Center for Biotechnology Information nonredundant database. Q-values of peptides were calculated using the percolator algorithm and a 5% filter was applied as False Discovery Rate (FDR) threshold.

**Quantization of PsaC protein by immunoblotting**

Cells were harvested in 50mL batch by centrifugation at 8,000.x g for 10 min in order to remove medium, resuspended in 1.5 mL micro-tubes and centrifuged at 10,000 g for 15 min to remove the remaining medium. Then dry pellets were frozen in liquid nitrogen before conservation at -80°C. All manipulations were carried out on ice. Cells pellets were grinded in

400µL extraction buffer (50mM Tris-HCl pH7.4, 100mM NaCl, 5mM EDTA, 0.5% (v/v) NP40 (sigma), 10% (v/v) Glycerol ) using Tissue Lyser (Quiagen). The samples were centrifuged at 10,000 g for 10 min to remove filter debris. The supernatant was collected, and the total protein concentration was determined using Bicinchoninic Acid assay (Smith *et al.*, 1985). Sample buffer was added to a final concentration of 62.5mM Tris-HCL pH6.8, 2% Sodium Dodecyl Sulfate, 1.5µM Bromophenol blue, 10% glycerol, 50mM DTT. Samples were heated for 5 min at 70°C, and loaded on a 4-12% acrylamide precast NuPAGE mini-gel (Invitrogen). PsaC protein standard (Agrisera) was used as a calibration standard curve. Samples were resolved for 40 min at 200 V in a 2-[N- morpholino]ethanesulfonic acid (MES)-sodium dodecyl sulfate (SDS) running buffer (Invitrogen). Proteins were transferred onto a methanol prehydrated polyvinylidene di-fluoride (PVDF) membrane (Sigma-Aldrich) using a liquid transfer system (Invitrogen) for 70 min at 30 V in a transfer buffer of consisting 1.25 mmol $L^{-1}$ N,N-bis (2- hydroxyethyl) glycine (Bicine), 1.25 mmol $L^{-1}$ Bis(2-hydroxyethyl)iminotris (hydroxymethyl) methane (Bis-tris), 0.05 mmol $L^{-1}$ EDTA, 5 mmol $L^{-1}$ DTT, 2.5 mmol $L^{-1}$ chlorobutanol, and 10% methanol) pH 7.2., The membrane was immediately immersed in Tween 20-tris-buffered saline (Tween-TBS (Sigma-Aldrich)) buffer pH 7.6 (0.1% Tween 20, 350 mmol $L^{-1}$ sodium chloride, 20 mmol $L^{-1}$ Trizma base) containing 2% (w:vol) blocking agent (Amersham Biosciences) overnight at 4°C. Primary antibody PsaC (photosystem I [PSI] core subunit; Agrisera) was diluted at 1 : 50,000 in Tween-TBS in the presence of 2% blocking agent and the membrane was soaked in this solution for 1 h with slow agitation at room temperature. The primary antibody solution was then discarded and the blot was extensively washed in Tween-TBS. Anti-rabbit secondary antibody coupled to horseradish peroxidase (Biorad) diluted at 1: 50,000 in Tween-TBS buffer containing 2% blocking agent was added for 1 h. The membrane was washed three times for minutes in Tween-TBS buffer prior to revelation using The Enhanced Chemiluminescent Reagent (ECL) Advance reagent (Amersham Biosciences). Signals were measured using the Quantity One software (Biorad). Protein standard curves were generated by fitting a two-factor polynomial function, and the protein concentrations were determined by fitting the sample signal values on the standard curve. Pilot experiments were performed to ensure that sample signals fell within the range spanned by the standard curve.

## REFERENCES


**Abràmoff, M.D., Magalhães, P.J. and Ram, S.J.** (2004) Image processing with ImageJ. *Biophotonics Int.*, **11**, 36–42.

**Bec, B., Husseini-Ratrema, Collos, Y., Souchu, P. and Vaquer, A.** (2005) Phytoplankton seasonal dynamics in a Mediterranean coastal lagoon: emphasis on the picoeukaryote community. *J. Plankton Res.*, **27**, 881–894.

**Blain, S., Quéguiner, B., Armand, L., et al.** (2007) Effect of natural iron fertilization on carbon sequestration in the Southern Ocean. *Nature*, **446**, 1070–4.

**Botebol, H., Sutak, R., Scheiber, I.F., Blaiseau, P.-L., Bouget, F.-Y., Camadro, J.-M. and Lesuisse, E.** (2014) Different iron sources to study the physiology and biochemistry of iron metabolism in marine micro-algae. *Biometals*, **27**, 75–88.

**Bouget, F.-Y., Lefranc, M., Thommen, Q., Pfeuty, B., Lozano, J.-C., Schatt, P., Botebol, H. and Vergé, V.** (2014) Transcriptional versus non-transcriptional clocks: A case study in Ostreococcus. *Mar. Genomics*, **14**, 17–22.

**Coale, K., Fitzwater, S. and Gordon, R.** (1996) Control of community growth and export production by upwelled iron in the equatorial Pacific Ocean. *Nature*.

**Collado-Fabbri, S., Vaulot, D. and Ulloa, O.** (2011) Structure and seasonal dynamics of the eukaryotic picophytoplankton community in a wind-driven coastal upwelling ecosystem. *Limnol. Oceanogr.*, **56**, 2334–2346.

**Corellou, F., Schwartz, C., Motta, J.-P., Djouani-Tahri, E.B., Sanchez, F. and Bouget, F.-Y.** (2009) Clocks in the green lineage: comparative functional analysis of the circadian architecture of the picoeukaryote ostreococcus. *Plant Cell*, **21**, 3436–49.

**Courties, C., Perasso, R., Chrétiennot-Dinnet, M., Gouy, M., Guillou, L. and Troussellier, M.** (1998) Phylogenetic analysis and genome size of Ostreococcus tauri (Chlorophyta). *J. Phycol.*, **34**, 844–849.

**Demir-Hilton, E., Sudek, S., Cuvelier, M.L., Gentemann, C.L., Zehr, J.P. and Worden, A.Z.** (2011) Global distribution patterns of distinct clades of the photosynthetic picoeukaryote Ostreococcus. *ISME J.*, **5**, 1095–107.

**Duc, C., Cellier, F., Lobréaux, S., Briat, J.-F. and Gaymard, F.** (2009) Regulation of iron homeostasis in Arabidopsis thaliana by the clock regulator time for coffee. *J. Biol. Chem.*, **284**, 36271–81.

**Gledhill, M. and Buck, K.N.** (2012) The organic complexation of iron in the marine environment: a review. *Front. Microbiol.*, **3**, 69.

**Halliwell, B. and Gutteridge, J.** (1992) Biologically relevant metal ion-dependent hydroxyl radical generation An update. *Febs Lett.*, **307**, 108–112.

**Hastings, M.H., Maywood, E.S. and O'Neill, J.S.** (2008) Cellular circadian pacemaking and the role of cytosolic rhythms. *Curr. Biol.*, **18**, R805–R815.

**Kraepiel, A., Keiler, K.C. and Morel, F.M.M.** (1999) A Model for Metal Adsorption on Montmorillonite. *J. Colloid Interface Sci.*, **210**, 43–54.

**Lommer, M., Specht, M., Roy, A.-S., et al.** (2012) Genome and low-iron response of an oceanic diatom adapted to chronic iron limitation. *Genome Biol.*, **13**, R66.

**Long, J.C., Sommer, F., Allen, M.D., Lu, S.-F. and Merchant, S.S.** (2008) FER1 and FER2 encoding two ferritin complexes in Chlamydomonas reinhardtii chloroplasts are regulated by iron. *Genetics*, **179**, 137–47.

**Lozano, J.-C., Schatt, P., Botebol, H., Vergé, V., Lesuisse, E., Blain, S., Carré, I. a and Bouget, F.-Y.** (2014) Efficient gene targeting and removal of foreign DNA by homologous recombination in the picoeukaryote Ostreococcus. *Plant J.*, **78**, 1073–83.

**Lukianova, O. a and David, S.S.** (2005) A role for iron-sulfur clusters in DNA repair. *Curr. Opin. Chem. Biol.*, **9**, 145–51.

**Marchetti, A., Parker, M.S., Moccia, L.P., Lin, E.O., Arrieta, A.L., Ribalet, F., Murphy, M.E.P., Maldonado, M.T. and Armbrust, E.V.** (2009) Ferritin is used for iron storage in bloom-forming marine pennate diatoms. *Nature*, **457**, 467–70.

**McHugh, J.P., Rodríguez-Quinoñes, F., Abdul-Tehrani, H., Svistunenko, D. a, Poole, R.K., Cooper, C.E. and Andrews, S.C.** (2003) Global iron-dependent gene regulation in Escherichia coli. A new mechanism for iron homeostasis. *J. Biol. Chem.*, **278**, 29478–86.

**Mittler, R.** (2002) Oxidative stress, antioxidants and stress tolerance. *Trends Plant Sci.*, **7**, 405–410.

**Monnier, A., Liverani, S., Bouvet, R., Jesson, B., Smith, J.Q., Mosser, J., Corellou, F. and Bouget, F.-Y.** (2010) Orchestrated transcription of biological processes in the marine picoeukaryote Ostreococcus exposed to light/dark cycles. *BMC Genomics*, **11**, 192.

**Moulager, M., Monnier, A., Jesson, B., Bouvet, R., Mosser, J., Schwartz, C., Garnier, L., Corellou, F. and Bouget, F.-Y.** (2007) Light-dependent regulation of cell division in Ostreococcus: evidence for a major transcriptional input. *Plant Physiol.*, **144**, 1360–9.

**Müh, F., Glöckner, C., Hellmich, J. and Zouni, A.** (2012) Light-induced quinone reduction in photosystem II. *Biochim. Biophys. Acta*, **1817**, 44–65.

**Nunn, B.L., Faux, J.F., Hippmann, A. a, Maldonado, M.T., Harvey, H.R., Goodlett, D.R., Boyd, P.W. and Strzepek, R.F.** (2013) Diatom proteomics reveals unique acclimation strategies to mitigate fe limitation. *PLoS One*, **8**, e75653.

**O' Kelly, C.J., Sieracki, M.E., Thier, E.C. and Hobson, I.C.** (2003) A transient bloom of Ostreococcus (Chlorophyta, Prasinophyceae) in West Neck Bay, Long Island, New York. *J Phycol*, **854**, 850–854.

**Ottesen, E. a, Young, C.R., Eppley, J.M., Ryan, J.P., Chavez, F.P., Scholin, C. a and Delong, E.F.** (2013) Pattern and synchrony of gene expression among sympatric marine microbial populations. *Proc. Natl. Acad. Sci. U. S. A.*, **110**, E488–E497.

**Outten, F.W. and Theil, E.C.** (2009) Iron-based redox switches in biology. *Antioxid. Redox Signal.*, **11**, 1029–46.

**Peers, G. and Price, N.M.** (2006) Copper-containing plastocyanin used for electron transport by an oceanic diatom. *Nature*, **441**, 341–4.

**Price, N.M., Harrison, G.I., Hering, J.G., Hudson, R.J., Nirel, P.M., Palenik, B. and Morel, F.M.M.** (1988) Preparation and chemistry of the artificial algal culture medium Aquil. *Biol. Oceeanography*, **6**, 443–461.

**Ravet, K., Touraine, B., Boucherez, J., Briat, J.-F., Gaymard, F. and Cellier, F.** (2009) Ferritins control interaction between iron homeostasis and oxidative stress in Arabidopsis. *Plant J.*, **57**, 400–12.

**Roschzttardtz, H., Conéjéro, G., Divol, F., Alcon, C., Verdeil, J.-L., Curie, C. and Mari, S.** (2013) New insights into Fe localization in plant tissues. *Front. Plant Sci.*, **4**, 350.

**Rosenwasser, S., Graff van Creveld, S., Schatz, D., et al.** (2014) Mapping the diatom redox-sensitive proteome provides insight into response to nitrogen stress in the marine environment. *Proc. Natl. Acad. Sci.*, **111**, 2740–2745.

**Rueter, J.G. and Ades., D.R.** (1987) The role of iron nutrition in photosynthesis and nitrogen assimilation in Scenedesmus quadricauda (Chlorophyceae). *J. Phycol.*, **23**, 452–457.

**Saito, M. a, Bertrand, E.M., Dutkiewicz, S., Bulygin, V. V, Moran, D.M., Monteiro, F.M., Follows, M.J., Valois, F.W. and Waterbury, J.B.** (2011) Iron conservation by reduction of metalloenzyme inventories in the marine diazotroph Crocosphaera watsonii. *Proc. Natl. Acad. Sci. U. S. A.*, **108**, 2184–9.

**Shaff, J.E., Schultz, B. a., Craft, E.J., Clark, R.T. and Kochian, L. V.** (2009) GEOCHEM-EZ: a chemical speciation program with greater power and flexibility. *Plant Soil*, **330**, 207–214.

**Smith, P., Krohn, R. and Hermanson, G.** (1985) Measurement of protein using bicinchoninic acid. *Anal. Biochem.*, **150**, 76–85.

**Strzepek, R.F. and Harrison, P.J.** (2004) Photosynthetic architecture differs in coastal and oceanic diatoms. *Nature*, **431**, 689–692.

**Sunda, W.G. and Huntsman, S.A.** (1997) Interrelated influence of iron, light and cell size on marine phytoplankton growth. *Nature*, **2051**, 1193–1197.

**Sutak, R., Botebol, H., Blaiseau, P.-L., Léger, T., Bouget, F.-Y., Camadro, J.-M. and Lesuisse, E.** (2012) A comparative study of iron uptake mechanisms in marine microalgae: iron binding at the cell surface is a critical step. *Plant Physiol.*, **160**, 2271–84.

**Sutak, R., Slapeta, J., San Roman, M., Camadro, J.-M. and Lesuisse, E.** (2010) Nonreductive iron uptake mechanism in the marine alveolate Chromera velia. *Plant Physiol.*, **154**, 991–1000.

**Tortell, P.D., Maldonado, M.T., Granger, J. and Price, N.M.** (1999) Marine bacteria and biogeochemical cycling of iron in the oceans. *FEMS Microbiol. Ecol.*, **29**, 1–11.

**Vaquer, A., Troussellier, M., Courties, C. and Bibent, B.** (1996) Standing stock and dynamics of picophytoplankton in the Thau Lagoon (northwest Mediterranean coast). *Limnol. Oceanogr.*, **41**, 1821–1828.

## FIGURE LEGENDS

Figure 1

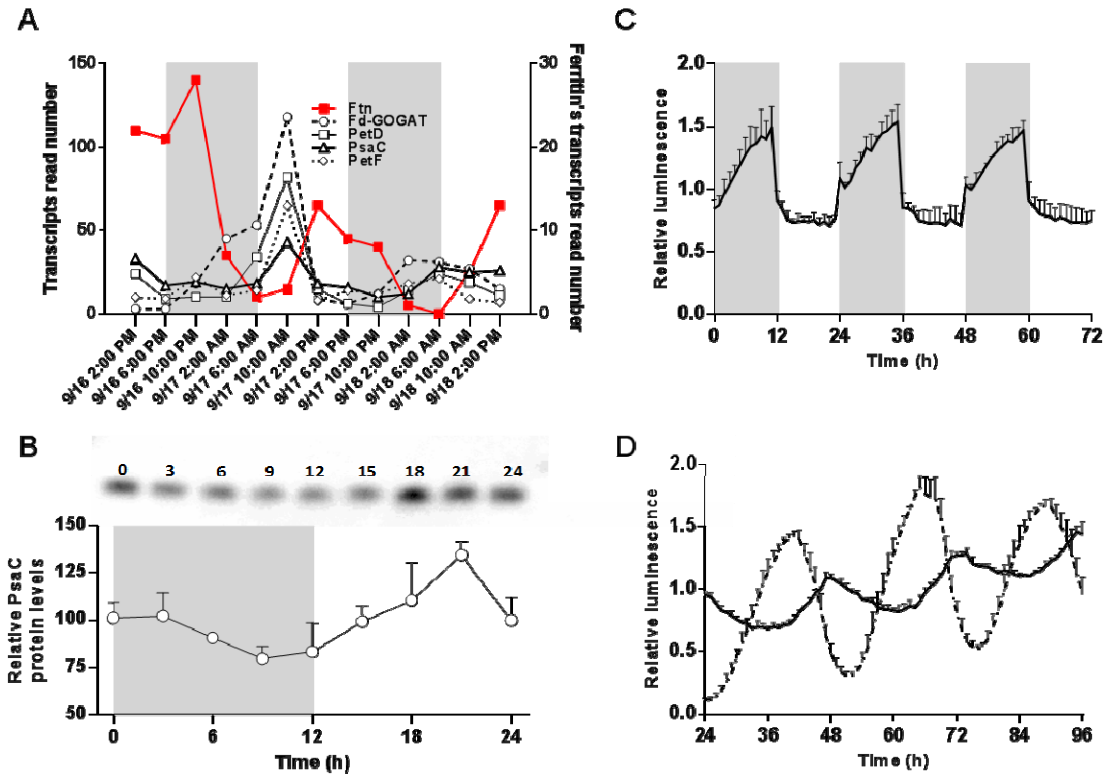


**Figure 1 Day/night and circadian regulation of ferritin and iron-containing protein.(A) relative** transcript abundance of ferritin and iron-containing proteins of photosystem PSI (PsaC), Cytochrocrome b6/f (PetD), ferredoxin (PetF) and nitrogen assimilation pathway (ferredoxin GOGAT) during two complete day-night cycles. Environmental dataset sampled on western U.S.A. coast between 9/16 and 9/18 2010 (Ottesen *et al.*, 2013). Grey layers correspond to PAR=0 light condition.

**(B)** Day-night changes in the level of PsaC protein. Upper part: western blot analysis of PsaC under 12:12 light/dark condition. Lower part: normalised density quantization of PsaC levels normalized to the mean signal (mean ± SD, n=3). **(C)** Day-night changes in the level of ferritin as inferred from the relative luminescence of ferritin-luc (FTN-luc)translational reporter normalised to the mean signal (mean ± SD, n=3). **(D)** Circadian regulation of Ferritin expression. Translational reporters of FTN-luc (solid line) and circadian clock associated 1 protein (CCA1-Luc, dashed line) were placed into constant light after entrainment under 12:12 light-dark condition. Normalised luminescence to the mean signal is shown (mean ± SD, n=3).

Figure 2

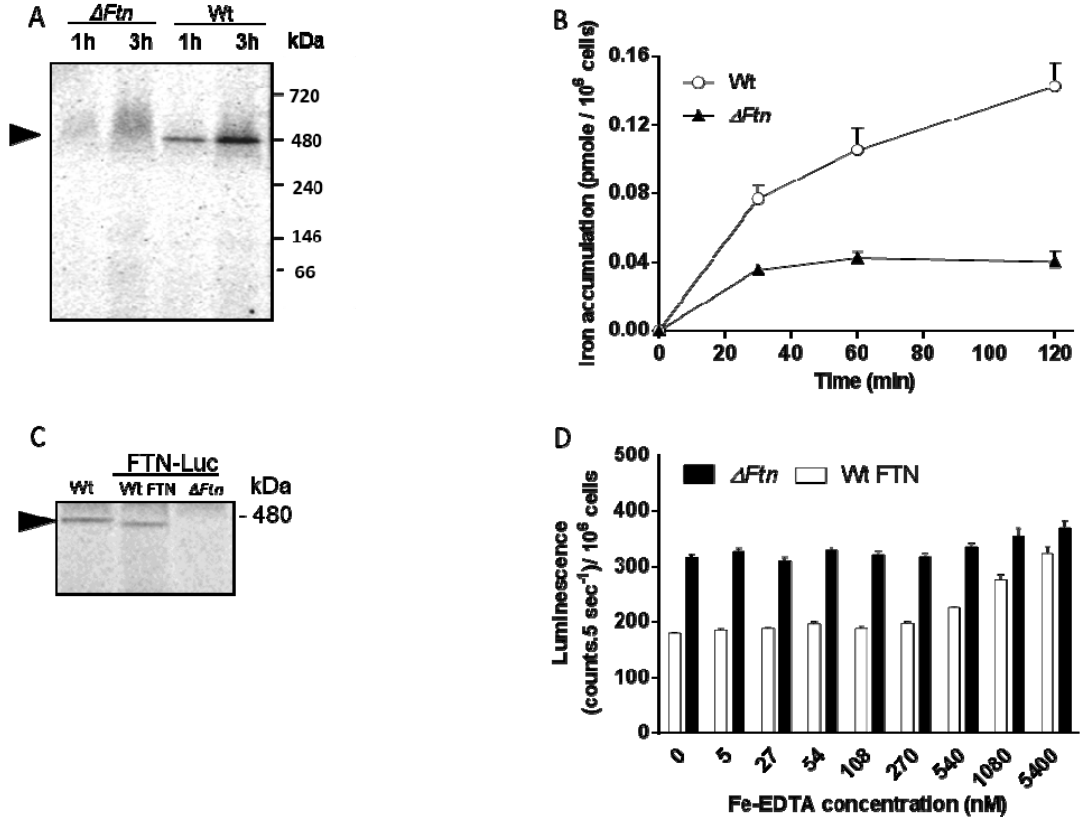


**Figure 2: Functional analysis of ferritin in *O. tauri*. (A)** Identification of ferritin on blue native PAGE. WT and *ΔFtn* cells were incubated in uptake buffer with 1 µM $^{55}$Fe for 1 and 3h and washed twice with Mf medium. Protein extracts (25 µg per lane) were separated in blue native PAGE. Autoradiography of dried gel reveals one band at 480 kDa (black arrow) in WT but not ΔFtn protein extracts. (B) Iron accumulation in WT and *ΔFtn* cells incubated with $^{55}Fe^{3+}$ citrate (1 µM). Values shown are means ± SD from four experiments. **(C)** Iron binding to ferritin in FTN-Luc (*ΔFtn*) knock in and in FTN-Luc (WT-FTN). $^{55}$Fe labelled proteins were analysed in blue native PAGE as described in (A). **(D)** Iron-dependent regulation of ferritin in FTN-Luc (*ΔFtn*) knock in and FTN-Luc (WT-FTN). Cells preacclimated for 7 days in 270nM Fe-EDTA were transferred to Aquil medium containing various amount of Fe-EDTA. *In vivo* luminescence of reporter lines is plotted as a function of Fe-EDTA concentration. Means ± SD from three experiments ( n=3 ).

Figure 3

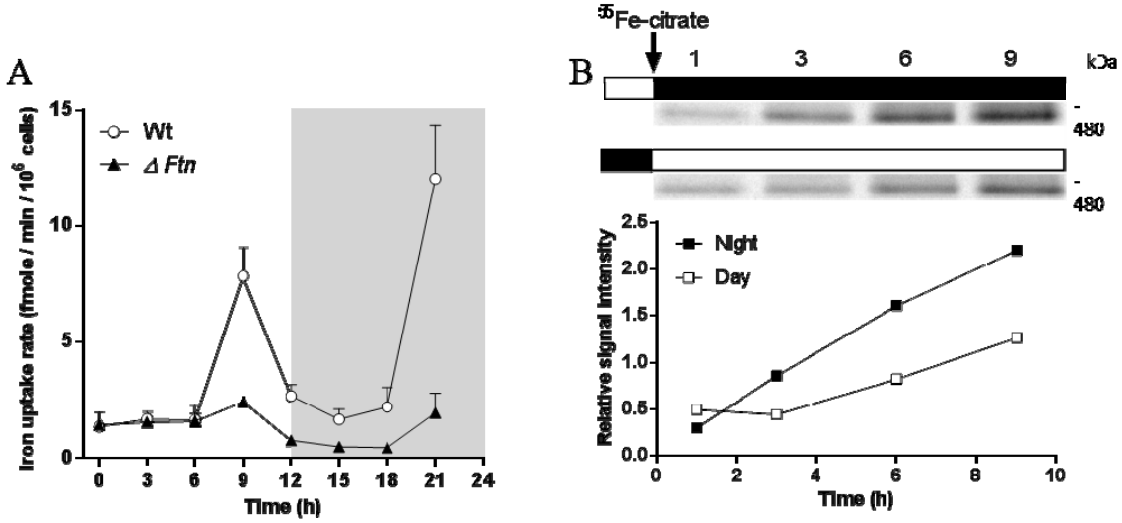


**Figure 3: Role of Ferritin in the day night regulation of iron uptake in exponentially growing cells.**

**(A)** Regulation of iron uptake along the day/night cycle. WT and *ΔFtn* cells were grown for 5 days in Mf medium containing 0.1 µM ferric citrate under day/night conditions. 50 ml of cells in exponential growth phase were harvested every 3 h, washed with iron-free medium, re-suspended in 1 ml of the same medium and incubated with $^{55}$Fe citrate(1 µM) for 15 minutes. Iron content determined by liquid scintillation as in Figure 2, was used to calculate iron uptake. Means ± SD from three experiments. **(B)** Kinetics of ferritin loading. WT cells grown as described in (A) were incubated from dawn or dusk with 1 µM $^{55}$Fe citrate. Ferritin was detected by autoradiography on blue native PAGE at 480 kDa (Top).Quantization of ferritin band intensity normalised to the mean signal (bottom).

Figure 4

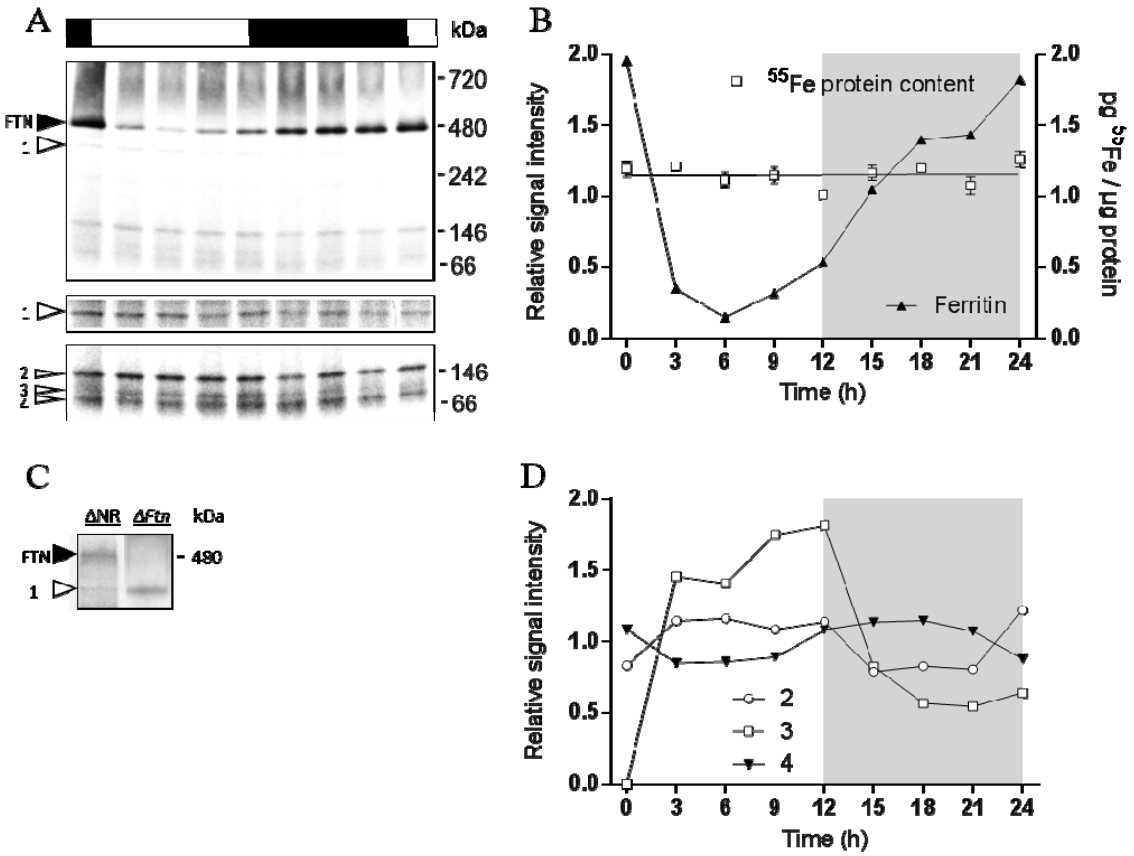


**Figure 4: Iron binding proteins under day/night cycle in stationary phase cells**

Proteins (25 µg par sample) from WT cells in early stationary phase grown for seven days in 1µM $^{55}$Fe under 12:12 light-dark cycle were separated on blue native PAGE. **(A)** Autoradiography of dried gel. Black and white boxes represent night and day respectively; the two lower panels correspond to longer exposure time of the same gel. Arrows indicate the main iron binding proteins, identified as ferritin (FTN) and putative nitrate reductase (1), ferredoxin dependent glutamate synthase (2), nitrite reductase (3) and sulphite reductase (4). See Supplementary Table 1. **(B)** Quantization of ferritin bands intensity, normalised to the mean signal reveal strong variation of radiolabelling over the day/night cycle. Total count of the whole protein content measured by liquid scintillation remains constant in the same samples. **(D)** Blue native PAGE (25 µg of protein per lane) of (ΔFtn) and nitrate reductase knock-out (ΔNR) proteins from cells frown in Mf medium containing 1µM $^{55}$ferric citrate. The band 1 is absent of (ΔNR) but present in (*ΔFtn*) cells which lack ferritin. **(C)**

Quantization of the main iron binding proteins from panel (A). The signal intensity is normalised to the mean signal.

Figure 5

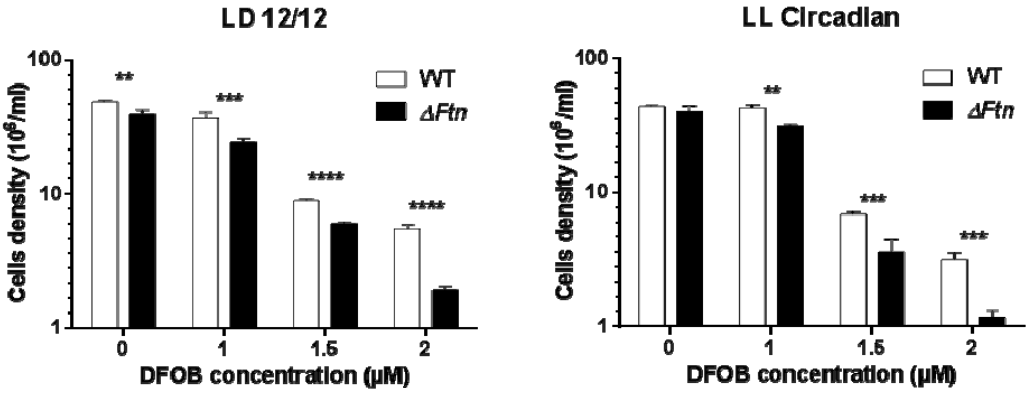


**Figure 5: The role of ferritin in cell survival under iron limitation**

Cell survival of WT and *ΔFtn* cells grown in Mf medium containing 1 mM Fe citrate in the presence of increasing concentrations of desferrioxamine B (DFOB). Cell number was determined by flow cytometry. **(A)** Cells were grown under 12:12 light-dark condition. **(B)** Cells entrained under 12:12 light-dark condition for 5 days were transferred under constant light corresponding to circadian free running conditions of constant light. Mean ± SD (n=3). Significant differences in cell number betwwen WT and *ΔFtn* were determined using a Student multivariate distribution test (**, P<0.01; ***, P<0.001; ****, P<0.0001).

**SUPPLEMENTARY INFORMATION**

Figure S1

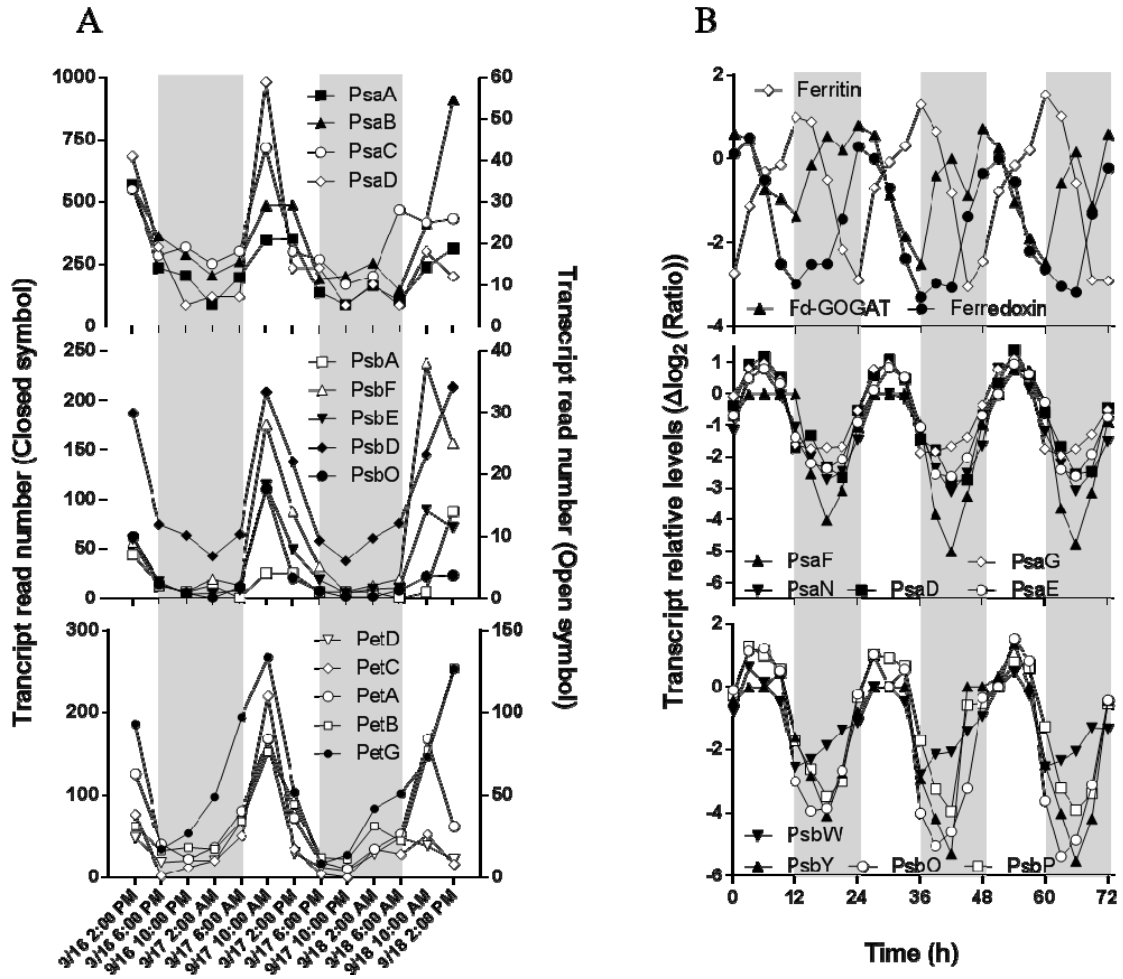


**Supplementary Figure 1: Comparison of day/night pattern of transcripts between environment metatranscriptomic data and *O. tauri* cultures.**

**(A)** Transcripts abundance of *Ostreococcus sp* in a western U.S.A. coast environmental dataset (Ottesen *et al.*, 2013). From top to bottom, PSI, PSII and $Cyt_{b/6f}$ genes. **(B)** Gene expression profiles from microarray data of *O.tauri* cells grown under day/night conditions. From top to bottom: Ferritin/Ferredoxin, PSII and PSI genes. Changes in gene expression are expressed in $\Delta log_2$ (ratio). In each panel grey layers represent night time, for in situ experiment night time correspond to periods when PAR=0

Figure S2

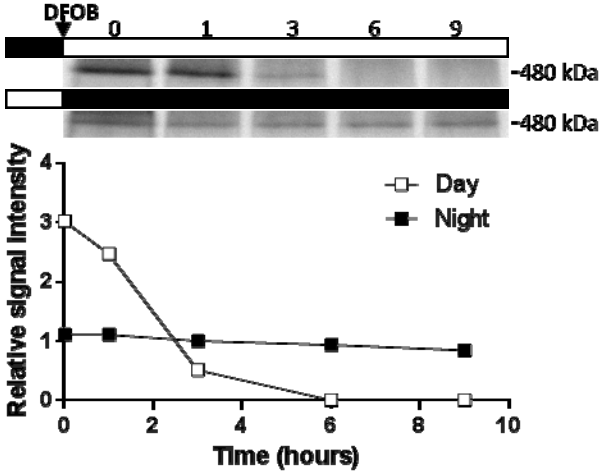


**Supplementary Figure 2: Effect of DFOB on the kinetics of ferritin iron-unloading under day/night conditions.**

Cells grown in 1µM $^{55}$Fe-citrate were washed and resuspended in Mf Medium before adding 1.5µM desferrioxamine B (DFOB). Upper part: autoradiography of $^{55}$F labelled ferritin on a blue native PAGE. Cells treated with DFOB either from dawn (Top) or dusk (bottom) and harvested every three hours.Lower part: quantization of ferritin band intensity normalised to the mean signal. During the night, DFOB had little effect on ferritin labelling.

Figure S3

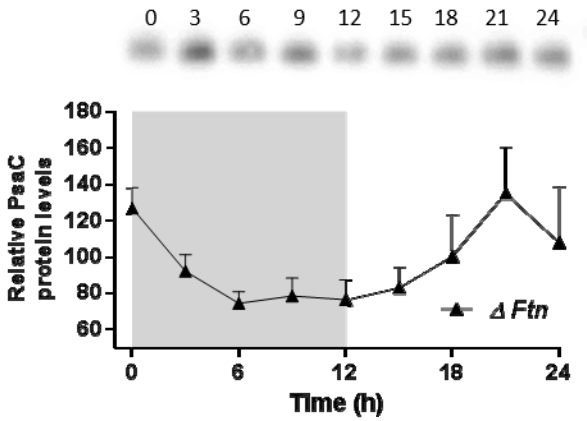


**Supplementary Figure 3: Western analysis of PsaC level under day/night conditions in in *ΔFtn* cells.**

**(A)** Upper part: western blot of analysis anti-PsaC. Cells were harvested every 3 hours during a 12:12 day/night cycle. Grey layers represent night period. Lower part: Normalised density quantization of anti-PsaC blot. Means (n=3), expressed in percent of mean signal. Means ± SD from three experiments ( n=3 ).

**Supplementary Table 1: Mass spectrometry analysis of the main iron-binding proteins presented as a** Mascot report. The main radiolabelled bands at 350, 150, 100 and 70 kDa were excised from the blue native PAGE (Figure 4) and analysed by mass spectrometry as described in Methods section.

350 kDa

| Accession | Description | Score | Coverage | # Proteins | # Unique Peptides | # Peptides | # PSMs | # AAs | MW [kDa] | calc. pI |
|---|---|---|---|---|---|---|---|---|---|---|
| 308798739 | P-type ATPase (ISS) [Ostreococcus tauri] | 1090,01 | 31,83 | 1 | 33 | 35 | 43 | 1172 | 128,2 | 6,25 |
| 308801239 | Sor-like protein (ISS) [Ostreococcus tauri] | 1006,92 | 45,24 | 1 | 15 | 16 | 52 | 347 | 37,5 | 7,39 |
| 308799545 | Glutamine synthetase, catalytic domain (ISS) [Ostreococcus tauri] | 915,59 | 45,94 | 1 | 25 | 26 | 54 | 690 | 75,4 | 5,33 |
| 308801799 | Peptide exporter, ABC superfamily (ISS) [Ostreococcus tauri] | 901,17 | 27,43 | 2 | 26 | 27 | 36 | 1079 | 119,3 | 6,49 |
| 308799207 | acetyl-CoA carboxylase (ISS) [Ostreococcus tauri] | 883,69 | 32,14 | 1 | 41 | 42 | 46 | 2123 | 233,6 | 6,24 |
| 308809732 | unnamed protein product [Ostreococcus tauri] | 877,62 | 34,49 | 1 | 26 | 26 | 38 | 864 | 95,1 | 6,32 |
| 308801004 | Pyruvate, phosphate dikinase, chloroplast [Precursor] (IC) [Ostreococcus tauri] | 818,15 | 33,51 | 2 | 26 | 27 | 43 | 931 | 100,4 | 5,25 |
| 308807779 | ACA11_ARATH Potential calcium-transporting ATPase 11, plasma membrane-type (ISS) [Ostreo | 798,95 | 33,62 | 1 | 32 | 32 | 37 | 1062 | 114,1 | 6,01 |
| 113170470 | ribulose-1,5-bisphosphate carboxylase/oxygenase large subunit [Ostreococcus tauri] | 764,94 | 48,42 | 1 | 20 | 20 | 45 | 475 | 52,5 | 6,48 |
| 308811204 | Chaperone HSP104 and related ATP-dependent Clp proteases (ISS) [Ostreococcus tauri] | 701,41 | 40,72 | 2 | 27 | 30 | 31 | 781 | 86,0 | 5,30 |
| 308808950 | NADP-glyceraldehyde-3-phosphate dehydrogenase (IC) [Ostreococcus tauri] | 629,06 | 60,32 | 2 | 16 | 21 | 29 | 378 | 40,2 | 8,25 |
| 308802856 | Magnesium chelatase H subunit (ISS) [Ostreococcus tauri] | 612,54 | 26,63 | 1 | 29 | 31 | 33 | 1397 | 153,6 | 5,59 |
| 308813361 | putative hsp70 (ISS) [Ostreococcus tauri] | 607,30 | 33,64 | 1 | 15 | 21 | 32 | 651 | 72,2 | 8,32 |
| 500000445 | chloroplast inner envelope protein-related (ISS) [Ostreococcus tauri] | 597,57 | 25,04 | 1 | 24 | 20 | 34 | 1174 | 127,6 | 6,10 |
| 113170490 | Atp1 [Ostreococcus tauri] | 568,50 | 39,76 | 1 | 18 | 18 | 20 | 508 | 55,1 | 5,76 |
| 113170421 | AtpE [Ostreococcus tauri] | 563,54 | 42,44 | 1 | 16 | 16 | 22 | 483 | 51,8 | 4,93 |
| 308800160 | Bip Luminal binding protein precursor, probable (IC) [Ostreococcus tauri] | 557,68 | 28,96 | 1 | 14 | 19 | 23 | 663 | 73,2 | 5,03 |
| 113170436 | TufA [Ostreococcus tauri] | 527,42 | 50,12 | 1 | 15 | 16 | 26 | 409 | 44,4 | 5,15 |
| 308810280 | RuBisCO subunit binding-protein alpha subunit, chloroplast [Prec (IC) [Ostreococcus tauri] | 504,09 | 35,30 | 1 | 15 | 16 | 19 | 575 | 61,2 | 5,10 |
| 308806437 | Transketolase (ISS) [Ostreococcus tauri] | 484,44 | 19,73 | 1 | 11 | 12 | 14 | 745 | 80,8 | 6,47 |
| 308809675 | Trierin protease homolog (ISS) [Ostreococcus tauri] | 473,04 | 17,04 | 1 | 20 | 22 | 26 | 1467 | 161,1 | 6,30 |
| 308808432 | Nia, nitrate reductase apoenzyme (IC) [Ostreococcus tauri] | 462,02 | 22,58 | 1 | 19 | 20 | 22 | 952 | 106,1 | 6,25 |
| 308806706 | Acetyl-CoA carboxylase (ISS) [Ostreococcus tauri] | 451,56 | 22,96 | 1 | 26 | 28 | 30 | 1272 | 137,4 | 6,38 |
| 308800570 | Ggh geranylgeranyl reductase (IC) [Ostreococcus tauri] | 444,12 | 36,58 | 1 | 14 | 14 | 17 | 462 | 51,4 | 8,03 |
| 308801769 | unnamed protein product [Ostreococcus tauri] | 443,93 | 15,82 | 1 | 17 | 20 | 21 | 1536 | 171,8 | 4,33 |
| 308812023 | Dur3 urea high-affinity symporter (IC) [Ostreococcus tauri] | 431,80 | 18,45 | 1 | 12 | 12 | 17 | 710 | 75,6 | 6,36 |
| 308799235 | vacuolar-type H+-pyrophosphatase (ISS) [Ostreococcus tauri] | 424,01 | 16,75 | 2 | 12 | 12 | 15 | 794 | 83,0 | 5,39 |
| 113170458 | AtpA [Ostreococcus tauri] | 415,91 | 31,15 | 1 | 13 | 14 | 20 | 504 | 53,9 | 5,39 |
| 308806027 | RUBISCO SUBUNIT BINDING-PROTEIN BETA-2 SUBUNIT (60 KD CHAPERONIN) (IC) [Ostreo | 414,64 | 30,60 | 1 | 15 | 18 | 21 | 621 | 65,9 | 5,19 |

150 kDa Band

| Accession | Description | Score | Coverage | # Proteins | # Unique Peptides | # Peptides | # PSMs | # AAs | MW [kDa] | calc. pI |
|---|---|---|---|---|---|---|---|---|---|---|
| 308811414 | ferredoxin-dependent glutamate synthase (ISS) [Ostreococcus tauri] | 1995,87 | 52,17 | 1 | 58 | 59 | 117 | 1382 | 148,1 | 5,33 |
| 308806437 | Transketolase (ISS) [Ostreococcus tauri] | 1852,42 | 49,53 | 1 | 23 | 25 | 95 | 745 | 80,8 | 6,47 |
| 308811328 | Mitochondrial elongation factor (ISS) [Ostreococcus tauri] | 1133,92 | 46,46 | 1 | 37 | 37 | 58 | 820 | 91,3 | 5,30 |
| 308813361 | putative hsp70 (ISS) [Ostreococcus tauri] | 1084,79 | 39,32 | 1 | 21 | 26 | 54 | 651 | 72,2 | 8,32 |
| 308800160 | Bip Luminal binding protein precursor, probable (IC) [Ostreococcus tauri] | 1034,57 | 45,55 | 1 | 26 | 30 | 46 | 663 | 73,2 | 5,03 |
| 308799607 | unnamed protein product [Ostreococcus tauri] | 907,30 | 32,43 | 1 | 11 | 11 | 48 | 441 | 46,9 | 4,49 |
| 308808950 | NADP-glyceraldehyde-3-phosphate dehydrogenase (IC) [Ostreococcus tauri] | 906,20 | 58,20 | 2 | 19 | 24 | 48 | 378 | 40,2 | 8,25 |
| 308810280 | RuBisCO subunit binding-protein alpha subunit, chloroplast [Prec (IC) [Ostreococcus tauri] | 897,85 | 40,87 | 1 | 21 | 21 | 27 | 575 | 61,2 | 5,10 |
| 308803252 | heat shock protein 70 / HSP70 (ISS) [Ostreococcus tauri] | 874,42 | 40,86 | 1 | 22 | 22 | 28 | 673 | 72,0 | 5,37 |
| 308799163 | oxidoreducta (ISS) [Ostreococcus tauri] | 863,47 | 47,97 | 1 | 32 | 32 | 41 | 790 | 86,1 | 8,22 |
| 308799545 | Glutamine synthetase, catalytic domain (ISS) [Ostreococcus tauri] | 814,61 | 38,55 | 1 | 19 | 20 | 35 | 690 | 75,4 | 5,33 |
| 308798869 | enolase (ISS) [Ostreococcus tauri] | 769,55 | 22,96 | 1 | 23 | 25 | 46 | 1228 | 134,4 | 8,36 |
| 308806027 | RUBISCO SUBUNIT BINDING-PROTEIN BETA-2 SUBUNIT (60 KD CHAPERONIN) (IC) [Ostreo | 768,16 | 39,61 | 1 | 22 | 23 | 28 | 621 | 65,9 | 5,19 |
| 308810507 | EF-1 alpha-like protein (ISS) [Ostreococcus tauri] | 752,28 | 50,00 | 3 | 24 | 24 | 39 | 490 | 54,1 | 8,16 |
| 308806473 | Elongation factor G, chloroplast precursor (ISS) [Ostreococcus tauri] | 729,53 | 30,63 | 1 | 20 | 20 | 27 | 790 | 86,5 | 5,44 |
| 113170421 | AtpE [Ostreococcus tauri] | 679,50 | 48,45 | 1 | 15 | 17 | 30 | 483 | 51,8 | 4,33 |
| 308812592 | NIPSNAP-related protein (ISS) [Ostreococcus tauri] | 660,00 | 56,79 | 1 | 16 | 16 | 23 | 280 | 31,4 | 8,29 |
| 308811204 | Chaperone HSP104 and related ATP-dependent Clp proteases (ISS) [Ostreococcus tauri] | 651,70 | 38,41 | 2 | 26 | 27 | 28 | 781 | 86,0 | 5,30 |
| 308812197 | phosphoglucomutase (ISS) [Ostreococcus tauri] | 645,00 | 42,58 | 1 | 19 | 19 | 21 | 559 | 60,4 | 5,08 |
| 308813007 | pyruvate dehydrogenase E1 component beta (ISS) [Ostreococcus tauri] | 644,73 | 29,70 | 1 | 21 | 23 | 30 | 835 | 91,1 | 6,39 |
| 308800356 | dnaK-type molecular chaperone hsp70b precursor, chloroplast-Chlamydomonas reinhardtii (ISS) | 639,12 | 31,32 | 1 | 17 | 18 | 25 | 562 | 59,8 | 7,02 |
| 500010272 | phosphoenolpyruvate carboxylase 2, LaPEPC2 (ISS) [Ostreococcus tauri] | 630,77 | 31,95 | 1 | 29 | 29 | 33 | 1014 | 114,0 | 6,20 |
| 113170436 | TufA [Ostreococcus tauri] | 633,35 | 63,57 | 1 | 18 | 19 | 33 | 409 | 44,4 | 5,15 |
| 308804786 | Hsp70 chaperone (ISS) [Ostreococcus tauri] | 619,74 | 29,43 | 1 | 14 | 14 | 26 | 581 | 62,7 | 8,34 |
| 308801004 | Pyruvate, phosphate dikinase, chloroplast [Precursor] (IC) [Ostreococcus tauri] | 606,63 | 25,78 | 2 | 22 | 22 | 25 | 931 | 100,4 | 5,25 |
| 308812558 | GMP synthetase (ISS) [Ostreococcus tauri] | 596,32 | 35,93 | 1 | 22 | 22 | 30 | 604 | 66,4 | 6,30 |
| 308801769 | unnamed protein product [Ostreococcus tauri] | 579,10 | 15,76 | 1 | 17 | 20 | 22 | 1536 | 171,8 | 4,33 |
| 308812292 | MGC53673 protein (ISS) [Ostreococcus tauri] | 575,12 | 49,31 | 1 | 25 | 27 | 37 | 651 | 71,2 | 8,02 |

100 kDa

| Accession | Description | Score | Coverage | # Proteins | # Unique Peptides | # Peptides | # PSMs | # AAs | MW [kDa] | calc. pI |
|---|---|---|---|---|---|---|---|---|---|---|
| 308798869 | enolase (ISS) [Ostreococcus tauri] | 1188,40 | 21,58 | 1 | 23 | 23 | 61 | 1228 | 134,4 | 8,36 |
| 308808950 | NADP-glyceraldehyde-3-phosphate dehydrogenase (IC) [Ostreococcus tauri] | 1078,44 | 58,47 | 2 | 18 | 21 | 48 | 378 | 40,2 | 8,25 |
| 308813361 | putative hsp70 (ISS) [Ostreococcus tauri] | 1033,80 | 36,71 | 1 | 19 | 23 | 46 | 651 | 72,2 | 8,32 |
| 308808434 | Nii, plastid-targeted nitrite reductase apoenzyme (IC) [Ostreococcus tauri] | 984,90 | 47,26 | 1 | 42 | 42 | 59 | 986 | 108,4 | 7,08 |
| 308806437 | Transketolase (ISS) [Ostreococcus tauri] | 907,82 | 29,93 | 1 | 17 | 17 | 43 | 745 | 80,8 | 6,47 |
| 308812292 | MGC53673 protein (ISS) [Ostreococcus tauri] | 862,74 | 56,84 | 1 | 30 | 31 | 55 | 651 | 71,2 | 8,02 |
| 113170121 | AtpE [Ostreococcus tauri] | 849,06 | 46,58 | 1 | 16 | 17 | 36 | 493 | 51,8 | 4,93 |
| 308813696 | predicted serine-pyruvate aminotransferase (ISS) [Ostreococcus tauri] | 814,87 | 24,19 | 1 | 14 | 14 | 38 | 868 | 93,7 | 7,18 |
| 308806027 | RUBISCO SUBUNIT BINDING-PROTEIN BETA-2 SUBUNIT (60 KD CHAPERONIN) (IC) [Ostreo | 779,72 | 47,02 | 1 | 23 | 25 | 34 | 621 | 65,9 | 5,49 |
| 308801693 | putative ketol-acid reductoisomerase (ISS) [Ostreococcus tauri] | 712,47 | 34,13 | 1 | 16 | 17 | 27 | 545 | 59,3 | 6,74 |
| 308802948 | RuBisCO activase (IC) [Ostreococcus tauri] | 692,59 | 49,39 | 1 | 15 | 15 | 30 | 407 | 44,5 | 6,44 |
| 113170436 | TufA [Ostreococcus tauri] | 689,08 | 44,99 | 1 | 14 | 15 | 28 | 409 | 44,4 | 5,15 |
| 308800160 | Bip Luminal binding protein precursor, probable (IC) [Ostreococcus tauri] | 681,88 | 33,18 | 1 | 17 | 21 | 26 | 663 | 73,2 | 5,03 |
| 308809581 | cytosolic phosphoglucose isomerase (ISS) [Ostreococcus tauri] | 671,47 | 32,37 | 2 | 19 | 19 | 34 | 590 | 65,0 | 5,36 |
| 308806473 | Elongation factor G, chloroplast precursor (ISS) [Ostreococcus tauri] | 653,82 | 33,16 | 1 | 20 | 22 | 33 | 790 | 86,5 | 5,44 |
| 300005344 | pitrilysin metalloproteinase 1 (ISS) [Ostreococcus tauri] | 644,50 | 32,45 | 1 | 25 | 26 | 30 | 903 | 100,0 | 5,70 |
| 308810280 | RuBisCO subunit binding-protein alpha subunit, chloroplast [Precursor] (IC) [Ostreococcus tauri] | 636,98 | 40,35 | 1 | 19 | 19 | 20 | 575 | 61,2 | 5,10 |
| 308808936 | putative UV-damaged DNA binding factor (ISS) [Ostreococcus tauri] | 634,55 | 20,90 | 2 | 23 | 23 | 25 | 1282 | 140,8 | 5,34 |
| 308803422 | putative lipoamide dehydrogenase (ISS) [Ostreococcus tauri] | 632,79 | 38,57 | 1 | 13 | 14 | 23 | 516 | 54,6 | 6,35 |
| 308813865 | S-adenosylmethionine synthetase (ISS) [Ostreococcus tauri] | 621,54 | 46,89 | 1 | 15 | 15 | 24 | 386 | 41,8 | 5,81 |
| 308801004 | Pyruvate, phosphate dikinase, chloroplast [Precursor] (IC) [Ostreococcus tauri] | 609,54 | 27,07 | 2 | 23 | 23 | 27 | 931 | 100,4 | 5,25 |
| 308812197 | phosphoglucomutase (ISS) [Ostreococcus tauri] | 590,51 | 35,42 | 1 | 16 | 16 | 19 | 559 | 60,4 | 5,38 |
| 113170490 | Atp1 [Ostreococcus tauri] | 571,29 | 41,54 | 1 | 20 | 20 | 25 | 508 | 55,1 | 5,76 |
| 308800794 | DPEI (ISS) [Ostreococcus tauri] | 563,71 | 33,05 | 1 | 2 | 19 | 26 | 593 | 65,5 | 6,33 |
| 308804139 | Serine racemase (ISS) [Ostreococcus tauri] | 546,52 | 39,26 | 1 | 15 | 15 | 22 | 512 | 54,3 | 7,01 |
| 308800050 | AtpE ATP synthase beta chain, mitochondrial precursor (IC) [Ostreococcus tauri] | 529,47 | 38,87 | 1 | 13 | 14 | 23 | 530 | 57,0 | 5,37 |
| 308810507 | EF-1 alpha-like protein (ISS) [Ostreococcus tauri] | 528,29 | 48,78 | 3 | 22 | 22 | 32 | 490 | 54,1 | 8,16 |
| 308809041 | starch phosphorylase (ISS) [Ostreococcus tauri] | 524,19 | 24,87 | 3 | 19 | 19 | 23 | 933 | 104,3 | 5,30 |
| 308813204 | Chaperone HSP104 and related ATP-dependent Clp proteases (ISS) [Ostreococcus tauri] | 521,47 | 36,11 | 2 | 22 | 24 | 25 | 781 | 86,0 | 5,30 |

70 kDa

| Accession | Description | Score | Coverage | # Proteins | # Unique Peptides | # Peptides | # PSMs | # AAs | MW [kDa] | calc. pI |
|---|---|---|---|---|---|---|---|---|---|---|
| 308811847 | M1 aminopeptidase (ISS) [Ostreococcus tauri] | 821,88 | 37,92 | 1 | 33 | 33 | 42 | 923 | 102,3 | 5,91 |
| 308806027 | RUBISCO SUBUNIT BINDING-PROTEIN BETA-2 SUBUNIT (60 KD CHAPERONIN) (IC) [Ostreo | 806,31 | 50,08 | 1 | 26 | 26 | 31 | 621 | 65,9 | 5,49 |
| 308810507 | EF-1 alpha-like protein (ISS) [Ostreococcus tauri] | 341,19 | 56,73 | 3 | 26 | 26 | 59 | 490 | 54,1 | 8,16 |
| 308813865 | S-adenosylmethionine synthetase (ISS) [Ostreococcus tauri] | 1229,14 | 32,12 | 1 | 25 | 25 | 48 | 386 | 41,8 | 5,81 |
| 308798869 | enolase (ISS) [Ostreococcus tauri] | 1263,15 | 23,62 | 1 | 25 | 26 | 74 | 1228 | 134,4 | 8,36 |
| 308803651 | Cyclophilin type, U box-containing peptidyl-prolyl cis-trans isomerase (ISS) [Ostreococcus tauri] | 784,30 | 67,62 | 1 | 25 | 26 | 40 | 386 | 42,3 | 4,33 |
| 308809718 | Sulfite Reductase (ISS) [Ostreococcus tauri] | 590,31 | 47,82 | 1 | 25 | 27 | 35 | 665 | 73,4 | 7,43 |
| 113170421 | AtpE [Ostreococcus tauri] | 1444,74 | 32,61 | 1 | 24 | 25 | 68 | 483 | 51,8 | 4,93 |
| 113170490 | Atp1 [Ostreococcus tauri] | 1085,24 | 52,76 | 1 | 24 | 25 | 42 | 508 | 55,1 | 5,76 |
| 308800844 | external rotenone-insensitive NADPH dehydrogenase (ISS) [Ostreococcus tauri] | 662,40 | 44,48 | 1 | 24 | 26 | 32 | 589 | 65,2 | 6,81 |
| 308801693 | putative ketol-acid reductoisomerase (ISS) [Ostreococcus tauri] | 845,55 | 55,41 | 1 | 23 | 25 | 36 | 545 | 59,3 | 6,74 |
| 308808814 | unnamed protein product [Ostreococcus tauri] | 818,00 | 52,97 | 1 | 23 | 24 | 39 | 421 | 45,7 | 8,14 |
| 113170436 | TufA [Ostreococcus tauri] | 1086,56 | 79,22 | 1 | 22 | 23 | 55 | 409 | 44,4 | 5,15 |
| 308813204 | Chaperone HSP104 and related ATP-dependent Clp proteases (ISS) [Ostreococcus tauri] | 413,74 | 32,78 | 1 | 21 | 22 | 22 | 781 | 86,0 | 5,30 |
| 308808950 | NADP-glyceraldehyde-3-phosphate dehydrogenase (IC) [Ostreococcus tauri] | 1191,62 | 60,32 | 2 | 21 | 26 | 49 | 378 | 40,2 | 8,25 |
| 308812197 | phosphoglucomutase (ISS) [Ostreococcus tauri] | 667,88 | 46,51 | 1 | 20 | 20 | 22 | 559 | 60,4 | 5,38 |
| 308802948 | RuBisCO activase (IC) [Ostreococcus tauri] | 1618,55 | 51,43 | 1 | 20 | 21 | 75 | 407 | 44,5 | 6,44 |
| 308808836 | Amine oxidase (ISS) [Ostreococcus tauri] | 547,42 | 42,19 | 1 | 20 | 22 | 27 | 602 | 66,7 | 6,30 |
| 308813696 | predicted serine-pyruvate aminotransferase (ISS) [Ostreococcus tauri] | 1215,00 | 33,87 | 1 | 19 | 20 | 66 | 868 | 93,7 | 7,18 |

# 3 Chapitre 3 : Comparaison de la réponse à la carence en fer de différents écotypes d'*Ostreococcus*

Dans l'océan mondial, le genre *Ostreococcus* est dominant dans plusieurs écosystèmes lagunaires et côtiers de picophytoplanctons eucaryotes (Rodríguez *et al.*, 2005; Demir-Hilton *et al.*, 2011; Marie *et al.*, 2006). Plusieurs écotypes d'*Ostreococcus* qui se sont adaptés à des niches écologiques variées, notamment du point de la lumière, ont été caractérisés (Cardol *et al.*, 2008; Six *et al.*, 2008). Certains de ces écotypes proviennent de milieux oligotrophes où le fer est très peu bio-disponible. Nous nous sommes intéressés à plusieurs écotypes représentatifs afin de comprendre comment ils optimisent l'utilisation et/ou l'assimilation du fer. L'objectif est de découvrir quelles sont les différentes solutions adoptées par le genre *Ostreococcus* pour gérer la disponibilité en fer. Les différents écotypes étudiés proviennent de zones côtières et lagunaires, oligotrophes ou mésotrophes. RCC789 est un écotype côtier vivant en milieu mésotrophe (Port de Barcelone) tout comme l'écotype lagunaire OTTH95 (*Ostreococcus tauri*) de l'étang de Thau. RCC802 et RCC809 sont des écotypes de profondeur, 65m et 105m respectivement. RCC802 isolé en méditerranée orientale provient d'un milieu oligotrophe. Les taux de croissances des différents écotypes ont été déterminés pour différentes concentrations de Fer-EDTA. Tandis que les écotypes côtier et lagunaire ne peuvent pas se développer en dessous de 108nM de Fe-EDTA, la souche océanique profonde RCC 809 est capable de survivre à des concentrations en Fe-EDTA plus faibles (27nM). Le résultat le plus intéressant concerne la souche RCC802 qui est capable de maintenir un taux de croissance constant quelle que soit la concentration en Fe-EDTA utilisée (>5.4 nM).

Plusieurs hypothèses peuvent expliquer la capacité à survivre à la carence en fer. (1) les cellules assimilent et/ou stockent mieux le fer. (2) les cellules réduisent leurs besoins au niveau du PSI en favorisant un cycle alternatif d'oxydation du pool de plastoquinone ce qui permet au PSII de fonctionner en circuit fermé (Cardol *et al.*, 2008). (3) Les cellules réduisent leurs besoins en fer en réduisant leur taille et/ou biomasse cellulaire.

Nous avons pu démontrer que l'assimilation du fer et la charge de la ferritine ne sont pas plus importants dans RCC802 par rapport aux autres écotypes. En revanche l'auto fluorescence rouge de la chlorophylle déjà faible par rapport à celle des autres écotypes diminue quand la souche RCC802 est carencée en fer. La mesure de la production de dioxygène diminue également de façon proportionnelle à la quantité de chlorophylle. Ces résultats indiquent donc que la production en dioxygène ne varie pas suivant les conditions de

carence. Il paraît donc plus probable que la RCC802 soit capable de faire varier sa taille/biomasse cellulaire en fonction du fer. De fait, j'ai pu mesurer une forte réduction de la biomasse cellulaire (protéines) en situation de carence contrairement à la souche de référence OTTH95. Cette hypothèse est confortée par l'analyse du mutant de taille KO de LOVHK d'*O. tauri* qui gère mieux la carence en fer que la souche sauvage.

Une étude transcriptomique par RNAseq Illumina de la réponse à la carence en fer en fonction du cycle jour/nuit est en cours chez RCC802 et OTTH95 pour identifier les acteurs potentiels impliqués dans la gestion de la carence en fer dans le cadre de l'ANR Phytoiron.

Ces résultats font l'objet d'un manuscrit en préparation.

### 1. Article 5:

Iron ecotypes in eukaryotic marine picophytoplancton: acclimation to iron limitation through cell biomass reduction.

Botebol H, Lesuisse E, Sutak R, Lozano JC, Schatt P, Vergé V, Gueunegues, A, Blain S and Bouget FY.

# Iron ecotypes in eukaryotic marine picophytoplankton: acclimation to iron limitation through cell biomass reduction.

Hugo Botebol[1,2], Emmanuel Lesuisse[3,], Robert Sutak[4], Christophe Six[5], Jean-Claude Lozano[1,2], Philippe

Schatt[1,2], Valérie Vergé[1,6], Audrey Gueunegues[1,2], Stéphane Blain[1,2,§], and François-Yves Bouget[1,2,§]

1- Sorbonne Universités, UPMC Univ Paris 06, UMR 7621, Laboratoire d'Océanographie Microbienne, Observatoire Océanologique, F-66650 Banyuls/mer, France

2- CNRS, UMR 7621, Laboratoire d'Océanographie Microbienne.
Microbienne, Observatoire Océanologique, F-66650 Banyuls/mer, France

3- Université Paris Diderot (Paris 07), Centre National de la Recherche Scientifique, Institut Jacques Monod, F–75013 Paris, France.

4- Department of Parasitology, Faculty of Science, Charles University, 12844 Prague, Czech Republic5- Unité Mixte de Service, UMS2348,F-66651, Banyuls/Mer, France.

5- CNRS, UPMC Univ Paris 06, UMR 7144, Groupe Plancton Océanique, BP 74, 29682 Roscoff Cedex,

6- Unité Mixte de Service, UMS2348,F-66651, Banyuls/Mer, France.

§ -Corresponding authors

E-mail: fy.bouget@obs-banyuls.fr; blain@obs-banyuls.fr

**Running title: Iron ecotypes in Ostreococcus**

# INTRODUCTION

Iron is essential for living organisms, in particular for photosynthetic phytoplanktonic species in which iron-sulphur centre and heme containing proteins are involved in electron transfer, during photosynthesis or nitrate reduction. The great oxidation event which occurred 2.4 billion years ago, behind the oxygenation of the atmosphere, has led to a massive oxidation of soluble reduced iron into much less soluble oxidized iron in the oceans (Falkowski, 2006). In modern oceans, the bioavailability of iron is usually low and, often this micronutrient is limiting to primary production by phytoplankton, as well illustrated in high chlorophyll low nutrient areas (Coale *et al.*, 1996; Blain *et al.*, 2007).

Phytoplanktonic species are diverse in size, shape and in phylogenetic origin, and, therefore they have evolved specific strategies to colonize ecological niches where iron is limiting (for a review see Morrissey & Bowler, 2012). Physiological and molecular responses to iron limitation have been well studied in nanophytoplankton. In oceanic diatoms, for example, reduction of iron needs can be achieved by optimizing photosynthetic architecture through reduction of the PSI and $cyt_{b6/f}$, and substitution of iron-rich proteins of photosynthetic electron transfer chain such as ferredoxin and $cyt_{c6}$, by copper or flavin - containing proteins such as plastocyanin and flavodoxin (Strzepek *et al.* 2004; Peers & Price, 2006; Lommer *et al.*, 2010). Iron storage into ferritin would constitute an alternative strategy to cope with sporadic iron supply in pennate diatoms (Marchetti *et al.*, 2009; Lommer *et al.*, 2012; Morrissey & Bowler, 2012) CB).

Pioneer studies on cultures of nanophytoplankton have revealed that the iron uptake rate depends on the cell surface so that small cells that have an optimal surface/volume ratio are favoured under iron limitation (Sunda & Huntsman, 1997). Paroxadically the acclimation and adaptation strategies are less understood in picophytoplankton than in nanophytoplankton, though small phytoplanktonic cells, such as *Prochloroccus* are dominant in oligotrophic waters (Scanlan, 2003; Martiny *et al.*, 2009). Metagenomic studies in iron-depleted regions point to the presence of Prochloroccus clades adapted to iron scarcity (Venter *et al.*, 2010).

These adaptations would rely on specific genes repertoires, such as the replacement of iron Super Oxide Dismutase (SOD) by Nickel SOD (Dufresne *et al.*, 2003; Palenik *et al.*, 2003).

Small eukaryotic picophytoplankton, has been less studied than its prokaryotic counterpart. Within picoeukaryotes, the order of *Mamelliales* has received lots of attention since the discovery of *Ostreococcus tauri* (Courties *et al.*, 1994). The order of *Mamelliales* encompasses the genera *Ostreococcus*, *Bathycoccus* and *Micromonas*. *Mamelliales* species are relatively easy to cultivate, numerous ecotypes have been isolated and several representatives have been sequenced (Derelle *et al.*, 2006; Palenik *et al.*, 2007; Worden *et al.*, 2009). *O. tauri* is one of the most advanced micro-algal genetic system, with molecular tools such as genetic transformation, including gene replacement by homologous recombination (Corellou *et al.*, 2009; Lozano *et al.*, 2014). *Ostreococcus* species have a world wide geographic distribution, but they have been found predominantly in mesotrophic costal ecosystems. *Ostreococcus* blooms have been reported in several locations including the Thau lagoon (A Vaquer *et al.*, 1996; Bec *et al.*, 2005), the West Neck bay (O' Kelly *et al.*, 2003) or the Chilean Upwelling ecosystem (Collado-Fabbri *et al.*, 2011). These picoalgae contribute significantly to primary production and carbon flow to higher trophic levels since they are subjected to intense grazing (Bec *et al.*, 2005). Ribosomal DNA clades partition Ostreococcus species into 4 phylogenetic clades (A-D) and physiological studies have shown the presence of high light and low light ecotypes (Six *et al.*, 2008; Rodríguez *et al.*, 2005; Subirana *et al.*, 2013). Partitioning based on ecological niches, however, suggest the presence of only two clades of Ostreococcus Ol and OlI which contains coastal and oceanic strains, respectively (Demir-Hilton *et al.*, 2011).

Although genomic and oceanographic studies point to the existence of iron-ecotypes in picophytoplankton, physiological evidences are lacking. We have compared the physiological responses to iron limitation of several *Ostreococcus* species from different clades and from different ecological niches. We identified a Mediterranean ecotype with low iron requirement, RCC802. Adaptation and acclimation strategies appear to rely mainly on cell biomass reduction in response to iron limitation. This was confirmed by the analysis of an *O. tauri* cell biomass mutant which has an improved survival under iron limitation.

## RESULTS

### Growth of *Ostreococcus* species under iron limitation

Several species of *Ostreococcus* representative of the different clades were selected from the Roscoff Culture Collection and their growth was determined under various iron concentrations (Figure 1). Except for the clade B low light ecotype RCC809 which is an Atlantic strain isolated at ~105m depth, all other ecotypes come from the Mediterranean sea (Figure 1A). Two coastal ecotypes were included in the study, RCC789 (clade D), from Barcelona harbour, and the lagoon ecotype OTTH595 (clade C) known as *O.tauri,* the first *Ostreococcus* species discovered in the *Thau* lagoon in 1995. Both OTTH595 and RCC789 come from eutrophic areas, where nutrient including iron bioavailability are high. RCC802 (clade A) has been isolated at a 65m depth between Sicily and Tunisia during the PROSOPE cruise (Claustre *et al.*, 2002). RCC802 (central to eastern meditarennean sea) and RCC809 (eastern tropical atlantic) comes environments where scarcity of nutrients result in low chlorophyll a concentration in surface waters. These geographic zones, however, are exposed to sporadic iron fertilization through aeolian mineral dust from the Sahara desert (Guieu *et al.*, 2002; Mills *et al.*, 2004)

*Ostreococcus* strains were acclimated in AQUIL medium containing 5.4 nM Fe-EDTA (1.7:2) during one week to remove contaminant iron before monitoring growth rates under various concentrations of Fe-EDTA ranging from 5.4 to 1080 nM. Three different types of responses were observed (Fig. 1B). The coastal strains OTTH595 and RCC789 were the more sensitive to iron limitation. Their growth rates drop dramatically for Fe-EDTA concentrations below 270nM (0.42 $d^{-1}$ ± 0.02 at 270nM to 0.16 $d^{-1}$ ± 0.04 at 54 nM Fe-EDTA for OTTH95; no growth of RCC789 at 54 nM). RCC809 displayed an intermediate response with a growth rate of 0.5 $d^{-1}$ at 54 nM Fe-EDTA and of 0.15 $d^{-1}$ at 5.4 nM Fe-EDTA. RCC802 out competed other strains, maintaining high growth rates (≈1 $d^{-1}$) for all conditions of Fe-EDTA, except at 5.4 nM concentration for which a 20% decrease in growth rate (0.8 ± 0.09 $d^{-1}$) was observed. Comparison of growth rates between iron depleted and iron full conditions indicates that RCC802 acclimates to severe iron limitation as efficiently as oceanic species such as *Emiliana huxleyi* or *Thalassiosira oceanica* (Table 1, Sunda & Huntsman, 1995).

**Iron uptake and iron content in *Ostreococcus* ecotypes**

Iron assimilation was determined in the different ecotypes. Since the coastal strains OTTH595 and RCC789 exhibit similar responses to iron limitation (Figure 1B), only OTTH595 together with RCC802 and RCC809 were studied further. Iron was provided as 1 µM $^{55}$ferric-citrate and the uptake was monitored for 30 minutes (Fig. 2A). The uptake rate was higher in RCC809 (9.47 ± 2.4 fmole/min/$10^6$ cells) and OTTH595 (7.81 ± 1.86 fmole/min/$10^6$ cells) than in RCC802 (1.23 ± 0.07 fmole/min/$10^6$ cells). The average diameter of invidual cells estimated by measuring the electrical resistance of individual cells was used to calculate cell surface assuming that coccoid cells are spherical (Figure S1). Under these conditions RCC802 cells were smaller, 1.16 ± 0.01µm, than RCC809 and 0TTH95 with diameters of respectively 1.45µm and 1.53 ± 0.01µm (Fig. S1). For direct comparison of ecotypes, the rates of iron uptake rates were normalised to the cell surface. The rates iron uptake were similar in RCC809 (1.44 ± 0.37 zmole/min/µm²) and OTTH595 (1.08 ± 0.26 zmole/min/µm²), that is 3 to 4 fold higher than in RCC802 (0.29 ± 0.02 zmole/min/µm²).

Iron binding to the iron-storage protein ferritin was determined in RCC802, RCC809 and OTTH595 strains (Fig. 2C). Cells were incubated for nine hours with $^{55}$ferric-citrate and 15 µg of proteins were resolved on blue native gels. Autoradiography revealed a 480 kDa band corresponding to ferritin in the 3 ecotypes. The quantification of the $^{55}$Fe labelling shows about 30% more labelling of ferritin RCC809 than in the two other ecotypes.

Cellular iron content was determined after one week of incubation with various concentrations of $^{55}$ferric-citrate (Fig. 3C). For the concentrations between 1 nM and 100 nM, the highest amount of radioactivity was measured in RCC809 (291 ± 19 fg $^{55}$Fe/$10^6$ cells at 10 nM). For concentrations above 1 µM $^{55}$ferric-citrate the incorporation of radioactive iron was the highest in RCC802 (4.7 ± 0.5 pg$^{55}$Fe/$10^6$ cells at 1 µM). For all iron concentrations, the lowest incorporation of $^{55}$Fe was observed in OTTH595.

**Photosynthetic activity in response to iron limitation**

The photosynthetic activity was estimated for various iron concentrations, by measuring dioxygen net production in OTTH595 and RCC802 ecotypes using Optical oxygen sensors. The dioxygen production and respiration were determined for iron conditions corresponding to iron limiting conditions for RCC802 and OTTH595 (108nM and 5,4nM,

respectively) and iron full conditions (1080nM and 108nM respectively). For both conditions, the dioxygen production resulting from photosynthesis in the light and consumption due to respiration in the dark, were lower in RCC802 than in OTTH595 (Fig. S2). Both respiration and dioxygen production were similar under iron limiting and repleted conditions in OTTH595 (Fig. S2). In RCC802 in contrast, the dioxygen production and consumption decreased at low iron concentrations.

The net dioxygen productions (production-consumption) were lower in RCC802 than in OTTH595 by three and ten-fold factors in iron limiting and iron full conditions respectively (Fig. 3A). Similarly, the chlorophyll content inferred from red fluorescence (FL3 parameter) was lower in RCC802 than in OTTH595 by two fold under iron repleted conditions and this difference was more pronounced under iron limitation with a more than 5 fold reduction in RCC802 vs OTTH595 (Fig. 3). The net production of dioxygen normalised to the FL3 parameter was lower in RCC802 than in OTTH595 and for both ecotypes it was very similar under iron repleted and iron limiting conditions (Fig. 3). Together these results indicate that RCC802 is able to reduce significantly its amount of chlorophyll per cell while maintaining its photosynthetic activity.

**Cell biomass reduction in response to iron limitation**

Together Figure 1 and Figure 3 suggest that in response to iron limitation the RCC802 ecotype reduces its amount of chlorophyll per cell and its photosynthetic activity while maintaining its growth rate. In OTTH595, in contrast, the amount of chlorophyll per cell and the dioxygen production are fairly constant between iron limiting and iron repleted conditions. The chlorophyll red fluorescence parameter (FL3) was determined in the OTTH95, RCC802 and RCC809 ecotypes exposed to various amounts of Fe-EDTA (Figure 4). Figure 4A shows that for all ecotypes the FL3 value decreases in response to iron limitation. For all Fe-EDTA concentrations, two to three fold lower values of FL3 were observed in RCC802 (between 38.5 ± 0.37 and 11.73 ±0.13) than RCC809 (between 65.17± 0.26 and 35.05± 0.31) and OTTH595 (between 83.38±0.84 and 39.24± 0.69). Furthermore, the reduction in chlorophyll red fluorescence was more pronounced between iron repleted and iron limiting condition for RCC802 (3.3 fold reduction) than for RCC809 (1.86 fold reduction) and OTTH595 (2.12 fold reduction).

The total protein content per cell was quantified under the same conditions for each ecotype (Fig 4B). In iron repleted conditions the protein content per cell was about two fold lower in RCC802 (8.31 ± 1.19 pg/cell) than in OTTH595 (17.5± 0.20 pg/cell) and RCC809 (16.47± 0.52 pg/cell). In RCC802, like for the FL3 parameter, the cellular protein content decreased in response to iron limitation, down to 4.36 ± 0.39 pg/cell) at 5.4 nM Fe-EDTA (≈50% reduction). In the other ecotypes, though the protein contents were higher in iron repleted conditions, only moderate responses to iron limitation were observed, from ≈ 16 to ≈12pg/cell in RCC809 and from ≈18 to ≈15 pg/cell in OTTH595. For Fe-EDTA below 54 nM and 270 nM for RCC802 and OTTH595 respectively, the protein content per cell were stable. It is worth noting that below these iron concentrations, cell growth was severely impacted (see Fig 1). Figure 3C shows that the highest growth rates where observed for small cell biomass both iron limiting and iron non-limiting conditions. Together these results indicate all ecotypes reduce to some extent their cellular protein content in response to iron limitation.

**Improved survival of an OTTH595 cell biomass mutant under iron limitation**

To test the hypothesis that the reduction of cell biomass is a strategy to face iron limitation, we investigated the response of a knock out mutant of OTTH595 in LOV-Histidine Kinase ($Ko_{LOV\text{-}HK}$) (Djouani Tahri et al.,in prep). This mutant has about twice less carbon, nitrogen, chlorophyll and carotenoid pigments pigment than OTTH595. The growth rates of $Ko_{LOV\text{-}HK}$ cells were determined under the same iron conditions as in Figure 1B. For all Fe-EDTA concentrations, except the lowest (5.4nM), cell growth was observed even below 54 nM Fe-EDTA, a concentration for which no cell growth was detected in OTTH595 (*WT*) cells (Fig 5 and Fig 1B).The growth rates of $Ko_{LOV\text{-}HK}$ cells range between 1.26±0.016 $d^{-1}$ at 1080 nM Fe-EDTA and 0.23 ±0.03 $d^{-1}$ at 13.5 nM Fe-EDTA.

The growth rate ratio betwen iron limiting and iron repleted condition ranged between 0.18 (13.5 nM), 0.39 (27 nM), 0.52 (54 nM) for $Ko_{LOV\text{-}HK}$ cells, compared to 0 (no cell growth) below 54 nM and 0.34 (54 nM) for OTTH595, and 0.15 (13.5 nM), 0.25 (27 nM), 0.57 (54 nM) for RCC809 (inferred from Fig. 1B). These results indicate that $KoL_{OV\text{-}HK}$ displays similar growth capacities as RCC809 under iron limitation, suggesting that a reduction in cellular biomass is sufficient to improve cell growth under iron limitation.

## DISCUSSION

### Iron ecotypes in the genus Ostreococcus

Differentiation of ecotypes based on the ability to grow in iron limiting conditions identifies three different types of response (Fig. 1). The coastal strains OTTH595 and RCC789 grow only under iron conditions above 54 to 108 nM Fe-EDTA and the oceanic RCC809 low light ecotype above 27 nM. RCC802 in contrast grows well at all concentrations of Fe-EDTA with only a 20% reduction in growth rate at 5.4 nM. Comparison of growth rate inhibition between iron repleted and iron limiting conditions suggests that RCC802 has the ability to grow under severe iron limitation like oceanic species such as the diatom *T. Oceanica* or the coccolithophore *E. huxlyei*. In contrast coastal ecotypes have much higher iron requirements. These differences in grow rates are correlated to differences in physiological responses, such as chlorophyll fluorescence, dioxygen production, protein content, iron content and iron uptake in response to iron limitation (Figures 1-4). Both RCC802 and to some extend RCC809 strains come from geographic areas where iron bioavailability is low and iron supply from the Sahara dust is sporadic. Together these results support strongly the existence of iron ecotypes in the genus *Ostreococcus*. Interestingly, growth rates are higher in RCC802 than in other strain not only under iron depleted but also under iron repleted conditions, suggesting that RCC802 may be not specific of low iron environment but instead acclimates efficiently to fluctuating environmental iron bioavailability. Similarly ecotypes such as RCC809, considered as low light ecotypes, are rather adapted to periods in the deep euphotic zone than to low light per se (Six *et al.*, 2008; Rodríguez *et al.*, 2005; Worden, 2006). Recently, two Ostreococcus clades, OI and OII were defined according to ecological niche partitioning (Demir-Hilton *et al.*, 2011). On the basis of this classification OTTH595 and RCC789 are likely to belong to high light mesotrophic 0I clade, while RCC809 and RCC802 which where both isolated in deep bloom at 60 and 105 m respectively would belong to the low light oligotrophic OII clade.

### Different capacities of iron storage and uptake for different ecotypes

Comparison of the different *Ostreoccoccus* species revealed that iron uptake and iron storage into ferritin were the lowest in RCC802, that is the best performing strain under iron limitation (Figure 2). Under low iron concentrations, iron content was also lower in RCC802 than in RCC809 but it was higher under iron repleted conditions above 1000 nM Fe-EDTA.

This raises the hypothesis that RCC802 may store iron in repleted conditions and use it under iron limiting conditions as suggested in pennate diatoms (Marchetti *et al.*, 2006, 2012, 2009). However this is unlikely to be the case since in the growth rates experiments, cells were grown without iron to deplete iron internal stores prior to monitoring cell growth under various concentrations of Fe-EDTA. Compared to OTTH595, the deep oceanic species RCC809 had the highest uptake rate, the highest loading of ferritin and the highest iron content under iron limiting conditions, suggesting that efficient mechanisms assimilation and storage may contribute to its improved survival under iron limiting conditions.

Comparison of dioxygen production and consumption between iron repleted and iron limiting conditions indicate that in the high iron ecotype OTTH595 neither the dioxygen production nor consumption resulting from photosynthetic activity and mitochondrial respiration respectively, vary between iron repleted and iron limiting conditions. In contrast in the low iron ecotype RCC802, the net dioxygen production decreased dramatically between iron depleted and iron repleted conditions while the growth rate was only slightly reduced.

Noteworthy, the dioxygen consumption resulting from respiration was proportionally more reduced than the production resulting from photosynthesis. This observation is puzzling since phytoplanktonic species usually acclimate to low iron environment by reducing their photosynthetic activity and increasing mitochondrial respiratory activity (Nunn *et al.*, 2013; Lommer *et al.*, 2012)).When normalized to the chlorophyll fluorescence, the net production of dioxygen was constant between iron depleted and iron repleted conditions. Together these results suggest that RCC802 may be constitutively adapted to low iron conditions.

**Cell biomass reduction: a strategy to cope with iron scarcity**

Acclimation to iron limitation often involves cell size reduction, so that surface to volume ratio is optimal for uptake (Sunda & Huntsman, 1997; Lommer *et al.*, 2012; Nunn *et al.*, 2013). In agreement with this hypothesis the low iron ecotype RCC802 has the smallest cell volume. However, iron uptake per unit of cell surface is smaller in RCC802 than in OTTH595 and the other ecotypes, suggesting that the cell size per se is not a critical factor in the acclimation of RCC802 to low iron conditions. In contrast, the cell biomass as estimated from the total amount of protein per cell is much lower in RCC802 than in other species and like chlorophyll red fluorescence. Protein cellular content and chlorophyll content reduces even more in response to iron limitation in RCC802, so that the dioxygen production remains

constant between iron repleted and iron limiting conditions. In the low iron ecotype *T.oceanica* a similar reduction of protein content per cell was observed. The reduction of cellular protein contents was possibly due to a smaller number of chloroplasts per cell (Lommer *et al.*, 2012). *Ostreococcus* species, unlike diatoms, contain a single chloroplast per cell which occupies about 50% of the cell. Therefore, the reduction of protein and chlorophyll content per cell in RCC802 is likely to reflect a global reduction of the photosynthetic machinery and of the chloroplast. In support of the cell biomass reduction hypothesis, the $Ko_{LOV\text{-}HK}$ mutant of OTTH595 which displays low cellular biomass in term of protein and chlorophyll content and more generally carbon and nitrogen content, exhibit an improved survival under iron limiting conditions. LOV-HK is a blue light photoreceptor that is required for circadian clock function, however its involvement in response to iron limitation, if any, is currently unknown and how LOV-HK regulates cellular biomass remains to be established. Under natural conditions, the lagoon OTTH595 strains is never exposed to iron limitation and the wild type cells acclimates poorly to iron limitation, suggesting that OTT595 has no physiological acclimation and/or dedicated genes set such as RCC802. It is therefore, amazing that a simple reduction of cellular biomass in a high iron ecotype is sufficient to improve significantly the response to iron limitation.

**CONCLUSIONS:**

Our results establish the existence of *Ostreococcus* low iron ecotypes, such as RCC802 that are constitutively adapted to low iron conditions and grow as well under iron limiting and iron repleted conditions. They confirm field studies suggesting that picoeukaryotes should not be seen only as components of mesotrophic areas (De Milton et al., 2011). The main adaptation and acclimation to low iron environment involves cell biomass reduction rather than cell volume reduction. Other response to iron limitation in RCC809 may involve higher iron uptake and storagea capacities.

## Material and Methods

### Algal Strains and cell culture

The strains Ostreococcus tauri (strain OTTH595, isolated from Thau Lagoon, France), Ostreococcus sp. RCC802 (isolated from 65 m in the Sicily channel, Italy , Ostreococcus sp. RCC809 (isolated from 105 m in the tropical Atlantic Ocean), and Ostreococcus sp. RCC789 (strain BL_82-7_clonal, isolated from surface water of Barcelona harbour, Spain) were obtained from the Roscoff Culture Collection. Cells were grown at 20°C under constant blue light (20 µmole quanta.$s^{-1}$.$m^{-2}$) in AQUIL medium (Price *et al.*, 1988; Fourquez *et al.*, 2014; Botebol *et al.*, 2014) unless otherwise stated.

For short term uptake, protein radiolabelling and iron content determination experiments, cells were grown in modified F (Mf) medium (Sutak *et al.*, 2010, 2012; Botebol, Sutak, *et al.*, 2014) and iron was provided as ferric citrate (1:20) at 0.1 µM final concentration since the uptake is much faster with ferric citrate compared to Ferric-EDTA. The chemical speciation of iron was estimated using the GEOCHEM-EZ software (http://www.plantmineralnutrition.net/Geochem/Geochem%20Download.htm) (Shaff *et al.*, 2009) and the MINEQL+4.62.2 software (http://www.mineql.com/) (Kraepiel *et al.*, 1999).

### Culture medium

Cells were grown in AQUIL medium (Price *et al.*, 1988) without $SiO_3$, all culture work and subsampling were conducted in a clean room (class 10,000) equipped with a laminar flow hood (class 100). We used 24-wells plates, polycarbonate bottles and plastic-ware soaked in 10% HCl for 24 h and subsequently soaked overnight with ultrapure water (18.2 MOhm resistivity, Elga). All the lab-ware was systematically sterilized three times by microwaving (5 min, power 750 W) and then dried under the laminar flow hood before use. Synthetic ocean water (SOW; Price et al., 1988) and solutions of inorganic nutrients ($NO_3^-$ and $PO_4^{3-}$)were separately purified by removing trace metals using a Chelex 100 ion exchange resin (Bio-Rad). All solutions were filtered through metal-free 0.2 mm syringe Acrodisc filters (Pall Corporation) before use. Vitamins (B12, thiamin, and biotin), phosphate, and nitrate were added in the same proportions as detailed in Price et al. (1989). Trace metal solutions were buffered with 0.1 mol $L^{-1}$ of EDTA to result in free-ion concentrations similar to those calculated in Granger and Price (1999). Fe-replete (+Fe) and Fe-limited (-Fe) conditions were obtained by adding 60 µL premixed solutions of Fe–EDTA (1 : 1) to 20 mL of modified Aquil, yielding final total Fe concentrations of 1.8 mmol.$L^{-1}$ and 5.4 nmol.$L^{-1}$, respectively. The premixed solution and the final medium were equilibrated for 24 h in the dark at 20 °C. (Granger & Price, 1999) demonstrated that the labile inorganic Fe concentrations in the modified Aquil were directly proportional to the total Fe

added. According to the work of (Granger & Price, 1999), the labile inorganic Fe concentrations in the resulting modified Aquil medium were 35.8 pmol.$L^{-1}$ and 11.6 nmol.$L^{-1}$ in -Fe and +Fe conditions, respectively. The concentrations of total Fe used in our study covered the range of concentrations in coastal and offshore marine environments.

## Growth rate experiment

Before experiment, the strains were acclimated during 5 days in 1.5 mL of AQUIL medium in low iron condition (5.4nM Fe-EDTA) with an inoculum of 1 x $10^9$ cells. Then iron gradient conditions (AQUIL media supplemented with 5.4, 13.5, 27, 54, 108, 270, 540 or 1080 nM Fe-EDTA (1:1)) was inoculated with 1 x $10^9$ acclimated cells before being conducted in triplicate at 20°C, under 20 µmol photons.$m^{-2}$.$s^{-1}$ continuous blue light. Samplings were made in triplicate, cells count and chlorophyll fluorescence were analysed with a flow cytometer (BD Accury C6).

## Medium for iron uptake and iron accumulation

The composition of Mf medium (standard medium used for cell growth) was the following (for 1l medium): sea salts (Sigma) 40 g (composition: $Cl^-$ 19.29 g, $Na^+$ 10.78 g, $SO_4^{2-}$ 2.66 g,$Mg^{2+}$ 1.32 g, $K^+$ 420 mg, $Ca^{2+}$ 400 mg, $CO_3^{2-}$/$HCO^{3-}$ 200 mg, $Sr^{2+}$ 8.8 mg, $BO^{2-}$ 5.6 mg, $Br^-$ 56 mg, $I^-$ 0.24 mg, $Li^+$ 0.3 mg, $F^-$ 1mg); MOPS 250 mg (pH 7.3); $NH_4NO_3$ 2.66 mg; $NaNO_3$ 75 mg; $Na_2SiO_3.5H_2O$ 22.8 mg; $NaH_2PO_4$ 15 mg; 1 ml of vitamin stock (thiamine HCl 20 mg/l, biotin 1 mg/l, B12 1 mg/l); 1 ml of trace metal stock ($MnCl_2.4H_2O$ 200 mg/l, $ZnSO_4.7H_2O$ 40 mg/l, $Na_2MoO_4.2H_2O$ 20 mg/l, $CoCl_2.6H_2O$ 14 mg/l, $Na_3VO_4.nH_2O$ 10 mg/l, $NiCl_2$ 10 mg/l,$H_2SeO_3$ 10 mg/l); and 1 ml of antibiotic stock (penicillin sodium and streptomycin sulfate 100 mg/ ml). The Mf medium was buffered with 1 g/l HEPES (pH 7.5). Iron was added in the form of ferric citrate (1:20).

## Iron uptake assays

Iron uptake by micro-algae was assayed in microtiter plates or in 2 ml micro-centrifuge tubes as previously described (Sutak *et al.*, 2012). Iron uptake assays were performed with concentrated cell suspensions (from 50 to 250 million cells/100 µl) incubated in Mf medium (synthetic seawater, the composition of which was described previously (Sutak *et al.*, 2012). $^{55}Fe$ (29,600 MBq/mg) was added as 1 µM ferric citrate (1:20), ferric ascorbate (1:100) or ferric EDTA (1:1.2) as we described previously (Botebol *et al.*, 2014). Iron uptake was stopped at chosen intervals by adding a mixture of strong iron chelators (1 mM Bathophenanthroline sulfonate (BPS), 0.15 mM desferrioxamine B (DFOB), 50 mM EDTA) to the cell suspensions. After 2 min cells were harvested and washed on filters with a cell harvester (Brandel), or harvested and washed by centrifugation. In either cases, the cells were washed three times with a washing buffer containing strong iron chelators (480 mM NaCl, 20 mM KCl, 0.1 mM $MgCl_2$, 0.1 mM $CaCl_2$, 0.1 mM BPS, 0.15 mM DFOB, 50 mM EDTA, 1 mM salicyl hydroxamic acid (SHAM) and 10 mM HEPES pH 7.5). Cell pigments were bleached with

sodium hypochlorite before scintillation counting in a Wallac 1450 Micro Beta TriLux scintillation counter.

## Intracellular iron content

For iron accumulation experiment, cells grew in Mf without iron during a week before being shifted to Mf containing 1, 10, 100, 1000 or 1000nM of $^{55}$Fe (29,600 MBq/mg) added as ferric-citrate. After one week of growth, cells were harvested and washed in the same way as for iron uptake experiment. Cell pigments were bleached with sodium hypochlorite before scintillation counting in a Wallac 1450 Micro Beta TriLux scintillation counter.

## Electrophoresis

Cells grown in the presence of 1 µM $^{55}$Fe(III)-citrate (1:20) were disrupted by sonication on ice. Proteins were solubilised with 0.7% digitonin and resolved in a blue native PAGE using the Novex Native PAGE Bis-Tris Gel 3%–12% System (Invitrogen) according to the manufacturer protocol. The gels were vacuum dried and autoradiographed for 2-10 days using a TyphoonTrio Phosphorimager (Amersham).$^{55}$Fe signals were quantified using the ImageJ software (Abràmoff *et al.*, 2004). Quantifications are relative to the mean signal.

## Dioxygen measurements

Dioxygen levels were measured using a 24-channel SensorDish oxygen Reader (Presens, regenburg Germany). Cells were grown for one week in sealed OxoDishes® 4mL vials in AQUIL media containing 5.4 and 108 nM Fe-EDTA for RCC8002, and 108 and 1080 nM Fe-EDTA concentrations for OTTH595. The SDR was placed in a thermostated box (FloraLED), at 20°C under blue LEDS (20 µmole quanta.$s^{-1}$.$m^{-2}$). Before recording, light was switch off for 12 hours, the dioxygen levels were measured during 1h with 20 µmole quanta.$m^{-2}$.$s^{-1}$ blue light irradiance. Then dioxygen consumption was monitored during 1 hour in constant darkness. Positive control was cell free medium oxygenated for 1h and the negative control (0% $O_2$) was made by dissolving 0.2g of sodium L-ascorbate in 10mL of 0.1M NaOH

## Protein quantification

The different ecotypes were grown in AQUIL medium with various concentrations of Fe-EDTA between 5.4, and 540nM, in 24-wells plates exposed to 20 µmolequanta.$s^{-1}$.$m^{-2}$of blue light. After 6 days of growth, cells were harvested in 2mL micro-tubes by centrifugation at 8,000.x g for 10 min,, resuspended and centrifuged at 10,000 x g for 15 min to remove the remaining medium. Dry pellets

were frozen in liquid nitrogen before conservation at -80°C. All manipulations were carried out on ice. Cells pellets were grinded in 50µL extraction buffer (50mM Tris-HCl pH7.4, 100mM NaCl, 5mM EDTA, 0.5% (v/v) NP40 (sigma), 10% (v/v) Glycerol ) using Tissue Lyser (Quiagen). The samples were then centrifuged at 10,000 g for 10 min to remove filter debris. The supernatant was collected, and the total protein concentration was determined using BCA (Bicinchoninic Acid) assay as describe in (Smith *et al.*, 1985).

## Cell size measurements

The different ecotypes were grown in AQUIL medium with various concentrations of Fe-EDTA between 5.4, and 270nM, in 24-wells plates exposed to 20 µmolequanta.$s^{-1}$.$m^{-2}$of continuous blue light. After 6 days of growth, cell samples were diluted in 10mL of 9‰ phosphate buffer (CASYton$^{TM}$) to a concentration below 25000 cells.$ml^{-1}$. Cell diameters and volume were determined by electronic pulse area analysis using a CASY model TTC Cell Counter & Analyser equipped with 45µm capillary pore. Cell diameters were measured using at least 800µL from the diluted cell samples, with total of events above 20 000. Coccoid cells were assumed to be spherical to calculate cellular volumes. Biological triplicates were performed.

## REFERENCES


Abràmoff MD, Magalhães PJ, Ram SJ. (2004). Image processing with ImageJ. *Biophotonics Int* **11**:36–42.

Bec B, Husseini-Ratrema, Collos Y, Souchu P, Vaquer A. (2005). Phytoplankton seasonal dynamics in a Mediterranean coastal lagoon: emphasis on the picoeukaryote community. *J Plankton Res* **27**:881–894.

Blain S, Quéguiner B, Armand L, Belviso S, Bombled B, Bopp L, *et al.* (2007). Effect of natural iron fertilization on carbon sequestration in the Southern Ocean. *Nature* **446**:1070–4.

Botebol H, Lesuisse E, Sutak R, Lozano J, Schatt P, Vergé V, *et al.* (2014). A pivotal role of ferritin in the day night regulation of iron uptake and recycling in marine phytoplankton.

Botebol H, Sutak R, Scheiber IF, Blaiseau P-L, Bouget F-Y, Camadro J-M, *et al.* (2014). Different iron sources to study the physiology and biochemistry of iron metabolism in marine micro-algae. *Biometals* **27**:75–88.

Claustre H, Morel A, Hooker SB, Babin M, Antoine D, Oubelkheir K, *et al.* (2002). Is desert dust making oligotrophic waters greener ? *Geophys Res Lett* **29**:107 1–4.

Coale K, Fitzwater S, Gordon R. (1996). Control of community growth and export production by upwelled iron in the equatorial Pacific Ocean. *Nature*.

Collado-Fabbri S, Vaulot D, Ulloa O. (2011). Structure and seasonal dynamics of the eukaryotic picophytoplankton community in a wind-driven coastal upwelling ecosystem. *Limnol Oceanogr* **56**:2334–2346.

Corellou F, Schwartz C, Motta J-P, Djouani-Tahri EB, Sanchez F, Bouget F-Y. (2009). Clocks in the green lineage: comparative functional analysis of the circadian architecture of the picoeukaryote ostreococcus. *Plant Cell* **21**:3436–49.

Courties C, Vaquer A, Troussellier M. (1994). Smallest eukaryotic organism. *Nature* **370**:255.

Demir-Hilton E, Sudek S, Cuvelier ML, Gentemann CL, Zehr JP, Worden AZ. (2011). Global distribution patterns of distinct clades of the photosynthetic picoeukaryote Ostreococcus. *ISME J* **5**:1095–107.

Derelle E, Ferraz C, Rombauts S, Rouzé P, Worden AZ, Robbens S, *et al.* (2006). Genome analysis of the smallest free-living eukaryote Ostreococcus tauri unveils many unique features. *Proc Natl Acad Sci U S A* **103**:11647–52.

Dufresne A, Salanoubat M, Partensky F, Artiguenave F, Axmann IM, Barbe V, *et al.* (2003). Genome sequence of the cyanobacterium Prochlorococcus marinus SS120, a nearly minimal oxyphototrophic genome. *Proc Natl Acad Sci U S A* **100**:10020–5.

Falkowski PG. (2006). Tracing Oxygen's Imprint on Earth's Metabolic Evolution. *Sci* **311** :1724–1725.

Fourquez M, Devez A, Schaumann A, Guéneuguès A, Jouenne T, Obernosterer I, *et al.* (2014). Effects of iron limitation on growth and carbon metabolism in oceanic and coastal heterotrophic bacteria. *Limnol Oceanogr* **59**:349–360.

Granger J, Price NM. (1999). The importance of siderophores in iron nutrition of heterotrophic marine bacteria. *Limnol Oceanogr* **44**:541–555.

Guieu C, Bozec Y, Blain S, Ridame C, Sarthou G, Leblond N. (2002). Impact of high Saharan dust inputs on dissolved iron concentrations in the Mediterranean Sea. *Geophys Res Lett* **29**:2–5.

Kraepiel A, Keiler KC, Morel FMM. (1999). A Model for Metal Adsorption on Montmorillonite. *J Colloid Interface Sci* **210**:43–54.

Lommer M, Roy A-S, Schilhabel M, Schreiber S, Rosenstiel P, LaRoche J. (2010). Recent transfer of an iron-regulated gene from the plastid to the nuclear genome in an oceanic diatom adapted to chronic iron limitation. *BMC Genomics* **11**:718.

Lommer M, Specht M, Roy A-S, Kraemer L, Andreson R, Gutowska M a, *et al.* (2012). Genome and low-iron response of an oceanic diatom adapted to chronic iron limitation. *Genome Biol* **13**:R66.

Lozano J, Schatt P, Botebol H, Vergé V, Lesuisse E, Blain S, *et al.* (2014). Efficient gene targeting and removal of foreign DNA by homologous recombination in the picoeukaryote Ostreococcus. *Plant J* **78**:1073–83.

Marchetti A, Maldonado MT, Lane ES, Harrison PJ. (2006). Comparison of oceanic of the pennate diatom Pseudo-nitzschia : Iron requirements ( high-nitrate , low-chlorophyll waters ) and coastal species external iron concentrations. *Limnol Oceanogr* **51**:2092–2101.

Marchetti A, Parker MS, Moccia LP, Lin EO, Arrieta AL, Ribalet F, *et al.* (2009). Ferritin is used for iron storage in bloom-forming marine pennate diatoms. *Nature* **457**:467–70.

Marchetti A, Schruth DM, Durkin C a, Parker MS, Kodner RB, Berthiaume CT, *et al.* (2012). Comparative metatranscriptomics identifies molecular bases for the physiological responses of phytoplankton to varying iron availability. *Proc Natl Acad Sci U S A* **109**:E317–25.

Martiny AC, Huang Y, Li W. (2009). Occurrence of phosphate acquisition genes in Prochlorococcus cells from different ocean regions. *Environ Microbiol* **11**:1340–7.

Mills MM, Ridame C, Davey M, La Roche J, Geider RJ. (2004). Iron and phosphorus co-limit nitrogen fixation in the eastern tropical North Atlantic. *Nature* **429**:292–4.

Morrissey J, Bowler C. (2012). Iron Utilization in Marine Cyanobacteria and Eukaryotic Algae. *Front Microbiol* **3**:43.

Nunn BL, Faux JF, Hippmann A a, Maldonado MT, Harvey HR, Goodlett DR, *et al.* (2013). Diatom proteomics reveals unique acclimation strategies to mitigate fe limitation. *PLoS One* **8**:e75653.

O' Kelly CJ, Sieracki ME, Thier EC, Hobson IC. (2003). A transient bloom of Ostreococcus (Chlorophyta, Prasinophyceae) in West Neck Bay, Long Island, New York. *J Phycol* **854**:850–854.

Palenik B, Brahamsha B, Land M, Hauser L, Chain P, Lamerdin J, *et al.* (2003). The genome of a motile marine Synechococcus. *Nature* **424**:1037–1042.

Palenik B, Grimwood J, Aerts A, Rouzé P, Salamov A, Putnam N, *et al.* (2007). The tiny eukaryote Ostreococcus provides genomic insights into the paradox of plankton speciation. *Proc Natl Acad Sci U S A* **104**:7705–10.

Peers G, Price NM. (2006). Copper-containing plastocyanin used for electron transport by an oceanic diatom. *Nature* **441**:341–4.

Price NM, Harrison GI, Hering JG, Hudson RJ, Nirel PM, Palenik B, *et al.* (1988). Preparation and chemistry of the artificial algal culture medium Aquil. *Biol Oceeanography* **6**:443–461.

Rodríguez F, Derelle E, Guillou L, Le Gall F, Vaulot D, Moreau H. (2005). Ecotype diversity in the marine picoeukaryote Ostreococcus (Chlorophyta, Prasinophyceae). *Environ Microbiol* **7**:853–9.

Scanlan DJ. (2003). Physiological diversity and niche adaptation in marine Synechococcus. *Adv Microb Physiol* **47**:1–64.

Shaff JE, Schultz B a., Craft EJ, Clark RT, Kochian L V. (2009). GEOCHEM-EZ: a chemical speciation program with greater power and flexibility. *Plant Soil* **330**:207–214.

Six C, Finkel Z, Rodríguez F, Marie D. (2008). Contrasting photoacclimation costs in ecotypes of the marine eukaryotic picoplankter Ostreococcus. *Limnol Oceanogr* **53**:255–265.

Smith P, Krohn R, Hermanson G. (1985). Measurement of protein using bicinchoninic acid. *Anal Biochem* **150**:76–85.

Strzepek RF, Harrison PJ. (2004). Photosynthetic architecture differs in coastal and oceanic diatoms. *Nature* **431**:689–692.

Subirana L, Péquin B, Michely S, Escande M-L, Meilland J, Derelle E, *et al.* (2013). Morphology, genome plasticity, and phylogeny in the genus ostreococcus reveal a cryptic species, O. mediterraneus sp. nov. (Mamiellales, Mamiellophyceae). *Protist* **164**:643–59.

Sunda WG, Huntsman SA. (1997). Interrelated influence of iron, light and cell size on marine phytoplankton growth. *Nature* **2051**:1193–1197.

Sunda WG, Huntsman SA. (1995). Iron uptake and growth limitation in oceanic and coastal phytoplankton. *Mar Chem* **50**:189–206.

Sutak R, Botebol H, Blaiseau P-L, Léger T, Bouget F-Y, Camadro J-M, *et al.* (2012). A comparative study of iron uptake mechanisms in marine microalgae: iron binding at the cell surface is a critical step. *Plant Physiol* **160**:2271–84.

Sutak R, Slapeta J, San Roman M, Camadro J-M, Lesuisse E. (2010). Nonreductive iron uptake mechanism in the marine alveolate Chromera velia. *Plant Physiol* **154**:991–1000.

Vaquer A, Troussellier M, Courties C, Bibent B. (1996). Standing stock and dynamics of picophytoplankton in the Thau Lagoon (northwest Mediterranean coast). *Limnol Oceanogr* **41**:1821–1828.

Venter JC, Rusch DB, Martiny AC, Dupont CL, Halpern AL. (2010). Characterization of Prochlorococcus clades from iron-depleted oceanic regions. *Proc Natl Acad Sci* **107**:16184–16189.

Worden A. (2006). Picoeukaryote diversity in coastal waters of the Pacific Ocean. *Aquat Microb Ecol* **43**:165–175.

Worden A, Lee J, Mock T, Rouzé P, Simmons MP, Aerts AL, *et al.* (2009). Green evolution and dynamic adaptations revealed by genomes of the marine picoeukaryotes Micromonas. *Science (80- )* **9375**:268–272.

Table 1: Comparative inhibition of growth rate between iron limiting and iron repleted conditions

| Organisms | Growth rate ratio ( -Fe/+Fe ) |
|---|---|
| *Pelagomonas calceolate** | 0,92 (4.3nM / 232nM) |
| *Emiliana huxleyi** | 0,88 (3.9nM / 299nM) |
| *Thalassiosira oceanica** | 0,70 (4.2nM / 303nM) |
| *Prorocentrum minimum** | 0,42 (4.3nM / 299 nM) |
| *Thalassiosira weissflogii** | 0,00 (4.3nM / 301nM) |
| *Ostreococcus‡* | |
| RCC 802 | 0,79 (5.4nM / 270nM) |
| RCC 809 | 0,14 (5.4nM / 270nM) |
| | 0.38 (27nM / 270nM) |
| OTTH 595 | 0,00 (27nM / 270nM) |
| | 0.40 (54nM / 270nM) |
| RCC 789 | 0,00 (54nM / 270nM) |

*from (Sunda & Huntsman, 1995)

‡this study

**FIGURES LEGENDS**

Figure. 1

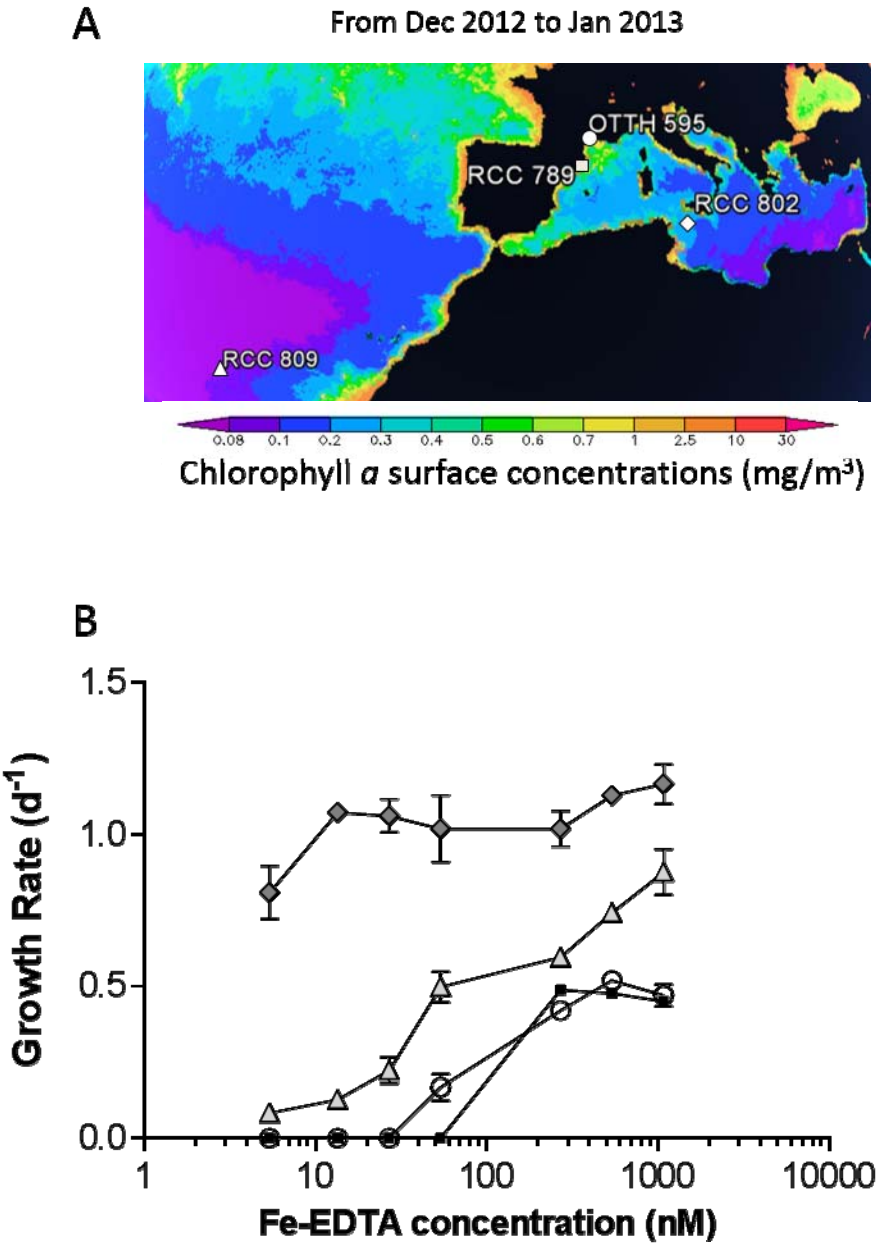


**Figure 1**: **Iron ecotypes in *Ostreococcus*. A.** Map of average surface concentrations of chlorophyll a, MODIS-Aqua 4km data collected from December 2012 to January 2013 produced with the Giovanni online data system, developed and maintained by the NASA GES DISC. **B.** Growth rate of *Ostreococcus* species under various iron concentrations (from 5.4nM to

1080nM Fe-EDTA). OTTH 595 (○), RCC789 (■), RCC 809 (Δ) and RCC802 (◊). Mean ± SD of three experiments.

Figure. 2

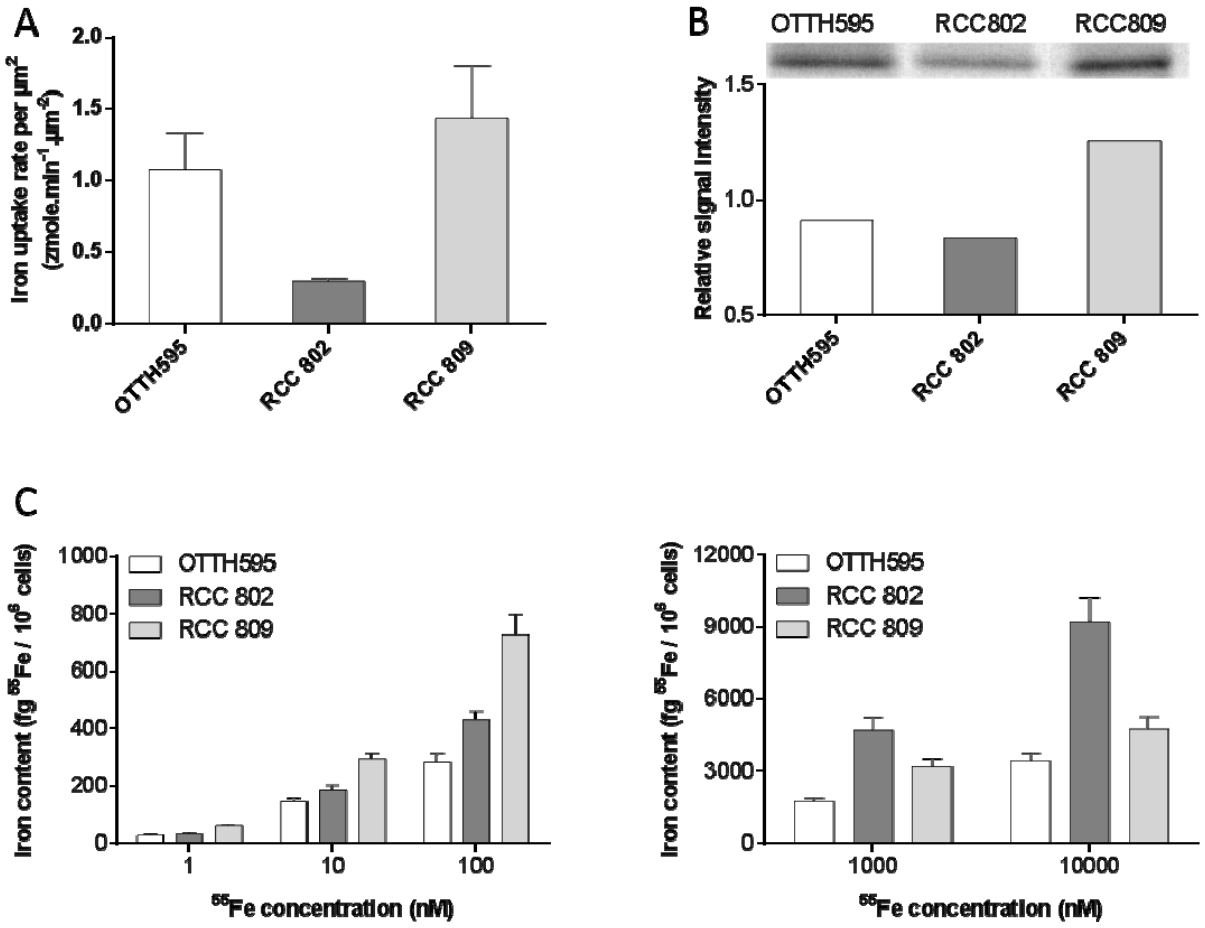


**<u>Figure 2:</u> Iron: uptake, iron content and ferritin loading in *Ostreococcus* iron ecotypes**

**A.** Uptake of iron in *Ostreococcus* ecotypes. *Ostreococcus* cells were grown during five days in 0.1µM ferric citrate before measuring the uptake of $^{55}$Fe(III)- citrate (1µM) during 30 minutes. Cellular radioactive iron content was counted by liquid scintillation. Mean ± SD from three experiments. **B.** $^{55}$Fe radiolabelling of ferritin in *Ostreococcus* ecotypes. Upper part: autoradiography of blue native PAGE loaded with 15µg of protein extracted from cells which of been growing for 9 hours in 2µM $^{55}$Fe(III)- citrate (protein per lane). Lower part: Quantization of radioactive signal intensity normalised to the mean signal. Both OTTH595 and RCC802 have less $^{55}$Fe labelling of ferritin band than RCC809. **C.** Iron content of

*Ostreococcus* ecotypes. Cells were grown for week in $^{55}$Fe(III)-citrate at low (left panel) or high concentrations (right panel). Cellular radioactive iron content was counted by liquid scintillation). Mean ± SD from three experiments.

Figure 3

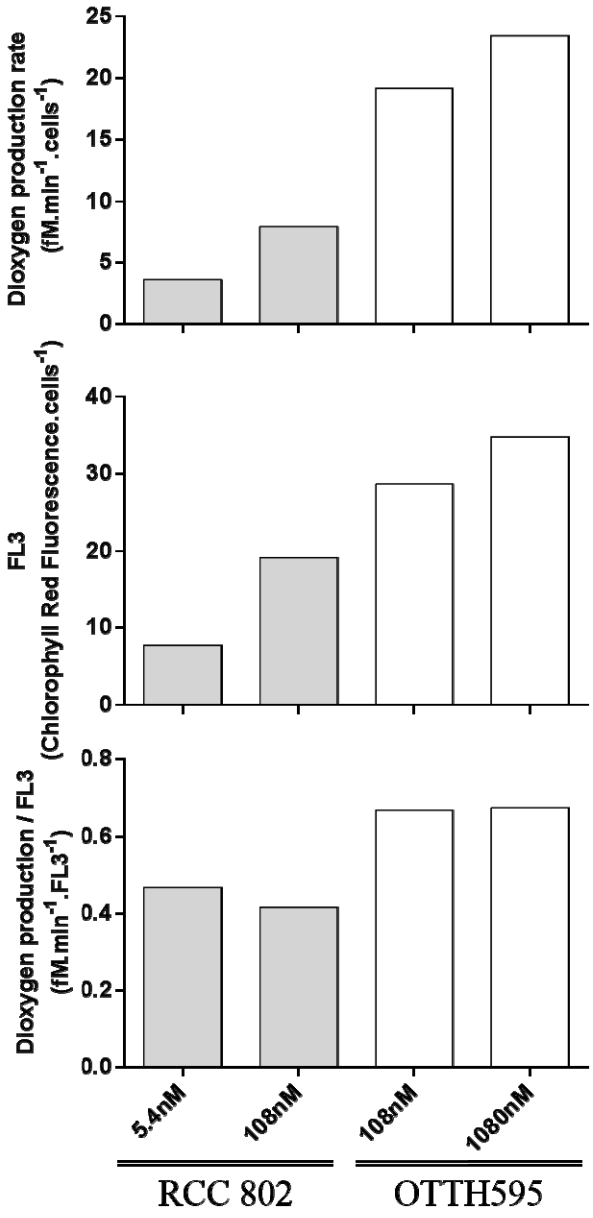


**<u>Figure 3:</u> Photosynthetic activity in response to iron imitation**

**Upper part**: Rate of Net dioxygen production in RCC802 (grey boxes) and OTTH595 (white boxes). Dioxygen production resulting from photosynthesis was measured during one hour, at 20°C under blue LED light at 20 µmole.quanta.$s^{-1}$.$m^{-2}$ using oxodish sensor. Dioxygen consumption resulting from respiration during one hour in darkness was subtracted to obtain the net production (see Figure S2). The rate of dioxygen net production is lower in RCC802 low iron ecotype than in OTTH595 high iron ecotype. Net dioxygen production decreases in response to iron limitation in both ecotypes.

**Middle part**: Red fluorescence of chlorophyll as determined by flow cytometry FL3 parameter. The FL3 parameter is higher in OTTH595 than in RCC802. A decrease in FL3 is observed in response to iron limitation in both ecotypes.

**Lower part:** Ratio of net dioxygen production normalized to chlorophyll red fluorescence. The ratios are constant between iron repleted and iron limiting conditions for both ecotypes.

Figure. 4

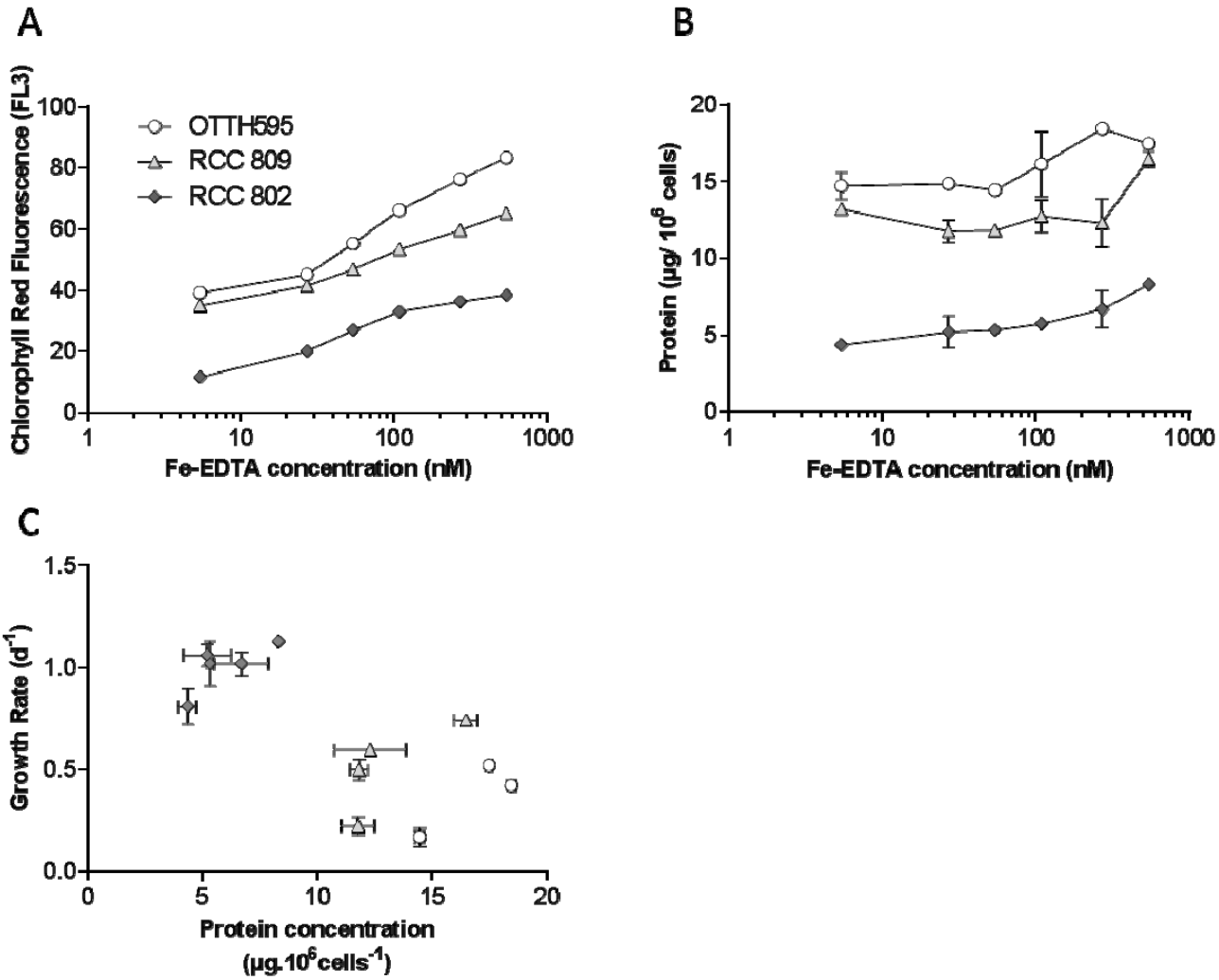


**<u>Figure 4:</u> Biomass reduction in response to iron limitation**

Ostreococcus strains were grown OTTH595 (○), RCC809 (Δ), and RCC802 (◊) were grown for a week in AQUIL medium containing various concentration of Fe-EDTA between 5.4, and 540nM. **(A)** The FL3 parameter was lower in the low iron ecotype RCC802. In all species the FL3 red fluorescence decreases in response to iron limitation **(B)** The protein content per cell was lower in RCC802 also and it decreases dramatically in response to iron limitation, unlike in the other ecotypes. (**C)** Plot of growth rates inferred from Figure 1 as a function of protein content per cell reveals that higher growth rates are found in smaller cells under iron limiting and iron repleted conditions. Species are OTTH595 (○), RCC809 (Δ), and RCC802 (◊). Mean ± SD from three experiments.

Figure. 5

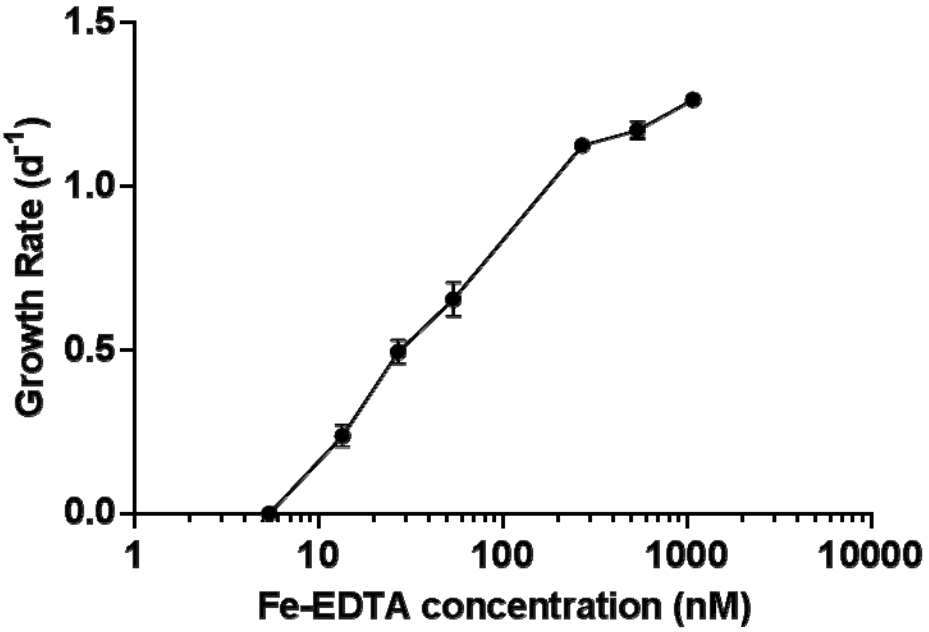


**Figure 5: Improved survival of a OTTH595 cell biomass mutant under iron limitation.** Growth rate of OTTH595 $Ko_{LOV\text{-}HK}$ cell biomass mutant (●) under various iron concentrations (between 5.4nM and 1080 nM Fe-EDTA). Compared to WT control (Fig. 1), $Ko_{LOV\text{-}HK}$ displays higher growth rates and survives at lower concentrations of Fe-EDTA. Mean ± SD from three experiments.

Figure S1:

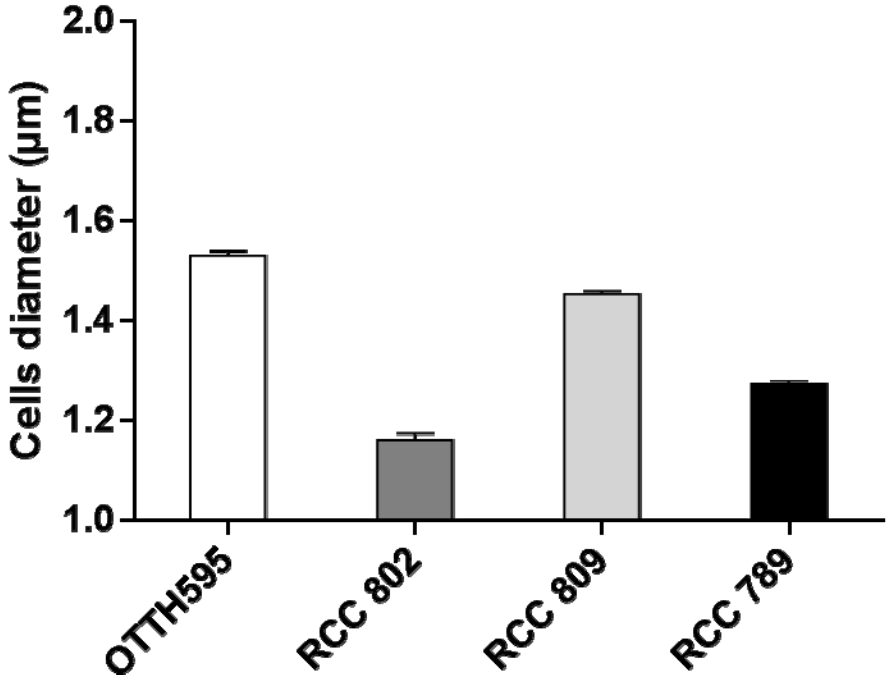


**SUPPLEMENTARY FIGURES LEGENDS**

**Figure S1: Cell diameter of *Ostreococcus* ecotypes**

Cell diameter of Ostreococcus ecotypes grown in Mf at 20°C with 20 µmole.quanta.$s^{-1}$.$m^{-2}$ of continuous blue light for a week. Cell diameter were determined with a Casy Cell Counter TTC. Mean ± SD from biological triplicates.

Figure S2

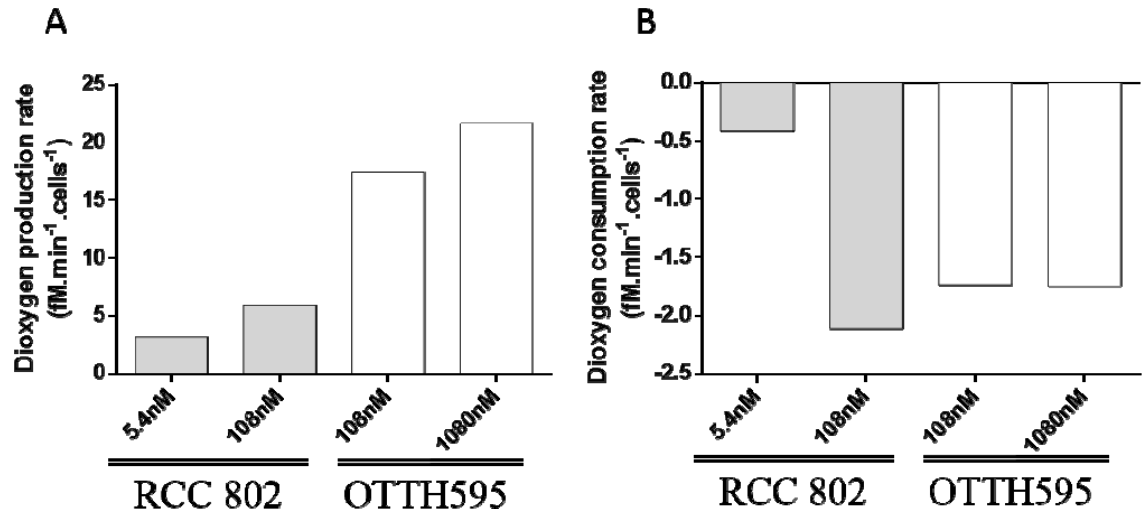


**Figure S2: Dioxygen production and consumption rates in iron limiting and iron replete conditions**

**A.** Rate of brut dioxygen production resulting from photosynthesis measured during one hour, at 20°C under blue LED light at 20 µmole.quanta.$s^{-1}$.$m^{-2}$ using oxodish sensor. The rate of dioxygen brut production is lower in RCC802 low iron ecotype than in OTTH595 high iron ecotype. Brut dioxygen production decreases in response to iron limitation in both ecotypes. **B.** Rate of net dioxygen consumption resulting from respiration determined during one hour in darkness using oxodish sensor. Rate of dioxygen consumption are similar in iron full condition for both RCC 802 (108nM) and OTTH595 (1080nM). Whereas RCC 802 consumes 4 times less dioxygen in iron limiting (5.4nM) than in iron full condition, OTTH595 iron limited cells (108nM) keep the same dioxygen consumption rate. Grey boxes (RCC802) and white boxes (OTTH595).

# III. Conclusions et Perspectives

## 1 Les systèmes d'importation du fer chez *O.tauri*

La Figure 13 est une représentation schématique qui regroupe l'ensemble des hypothèses concernant les systèmes d'importation du fer chez *O.tauri*. Les expériences de chasse réalisées chez *O.tauri* ont montré que la charge en $^{55}$Fe des cellules diminuait au cours du temps après dilution isotopique (Sutak *et al.*, 2012), ce qui suggère l'existence d'une étape de fixation du fer à la membrane avant importation dans la cellule, comme chez *Chromera velia* (Sutak *et al.*, 2010). Ainsi le fer en interaction avec la membrane serait à l'équilibre avec le fer libre dans le milieu. Cependant comme le fer n'est pas décroché par des chélateurs forts comme le DF0B, il serait sans doute fixé à des récepteurs membranaires capables de l'immobiliser très fortement (**A**).

Ces récepteurs pourraient être des protéines membranaires qui concentrent le fer à proximité des systèmes d'import, comme FEA1 chez *C. reinhardtii* (Allen *et al.*, 2007). Il est aussi possible qu'il existe un système qui séquestre le fer à la surface cellulaire avant import et/ou réduction, comme chez *Dunaliella salina* où un complexe est formé de 2 transferrine, une cupredoxine et d'une glycoprotéine (p130B) qui interagissent pour capter le fer à la surface cellulaire avant de l'importer (Paz *et al.*, 2007).

(**B**) Du fait de sa spéciation chimique et physique en milieu marin (Boyd and Ellwood, 2010), le fer libre est une espèce chimique ayant une durée de vie très courte dans l'océan. La plupart du temps, le fer est présent sous forme solide, de colloïde ou complexé à des ligands ayant des spécificités variables (Shaked *et al.*, 2005).

Plusieurs études ont montré que la présence d'exo-polysaccharides (EPS) secrétés par le phytoplancton permet d'augmenter la part de fer soluble, biologiquement accessible pour l'assimilation par le phytoplancton (Hassler, Alasonati, *et al.*, 2011; Hassler, Schoemann, *et al.*, 2011). Certains EPS diminuent le taux de ré-oxydation du Fe(II) en Fe(III) (González *et al.*, 2014; Öztürk *et al.*, 2004) et stabilisent ainsi le fer ferreux à proximité de la cellule. D'autres EPS, notamment ceux contenant des groupements catéchols, sont capables de réduire le fer ferrique en fer ferreux (Santana-Casiano *et al.*, 2014).

Le genre *Ostreococcus* qui est dépourvu de paroi cellulaire, secrète beaucoup de polysaccharides et forme des biofilms (**C**). La zone à proximité de la membrane plasmique riche en EPS pourrait contenir des sucres capables *(i)* de fixer le fer afin de le stabiliser et le concentrer à proximité de la membrane, où un récepteur membranaire le prendrait en charge.

*(ii)* de réduire le $Fe^{3+}$ avant import, une première étape habituellement indispensable à l'assimilation du $Fe^{3+}$.

La majorité des systèmes d'import du $Fe^{3+}$ font intervenir des réductases ferriques comme les NOX, NADH-CBR et $cyt_{b561}$. Ces enzymes réduisent le $Fe^{3+}$ en $Fe^{2+}$ à proximité ou au niveau de la membrane plasmique. Le fer ferreux ainsi produit est ensuite transporté vers le cytoplasme à l'aide de perméases à cations bivalents. Plusieurs gènes codant pour des réductases ferriques ont été identifiés dans le génome d*'O.tauri*, mais il n'a pas été possible au cours de cette étude de mettre en évidence ce type d'activité réductase chez *O.tauri*. Malgré l'absence d'activité réductase, *O.tauri* importe quand même du $Fe^{3+}$, ce qui suggère l'existence d'autres moyens d'import du $Fe^{3+}$ Il est possible qu'une perméase de type FTR prenne en charge le $Fe^{3+}$ après fixation à la membrane (**D**), mais ce type de perméase à $Fe^{3+}$ capable d'importer le fer indépendamment d'une ferroxydase à cuivre n'a pas encore été décrit. L'existence d'un système d'import du fer non réductif, comme chez *Chromera velia*, n'est pas à exclure.

Les EPS capables de réduire le $Fe^{3+}$ chez *O.tauri* pourraient aussi séquestrer le $Fe^{2+}$ jusqu'à assimilation par la cellule empêchant ainsi la détection de la réduction du $Fe^{3+}$ en $Fe^{2+}$. L'immobilisation des EPS d'*O.tauri* sur une colonne d'affinité, suivi de l'étude de leurs propriétés de ligands et de leurs capacités de réduction du fer, permettrat de mieux comprendre leur implication dans l'assimilation du fer chez *O.tauri*.

Le fer ferreux est une forme peu abondante du fer qui est habituellement importé dans la cellule à l'aide de perméases de type ZIP/NRAMP (**E**) ou d'un complexe cupredoxine/Fe-transporteur (**F**). Chez *O.tauri*, le KO *NRAMP* est létal et il existe un gène codant pour une cupredoxine. De plus l'assimilation du $Fe^{2+}$ diminue lorsqu'*O.tauri* est cultivé en absence de cuivre, mais l'assimilation du $Fe^{3+}$ n'est pas impacté (Botebol, Sutak, *et al.*, 2014). Il existerait donc des systèmes d'import distincts pour le $Fe^{2+}$ et le $Fe^{3+}$ chez *O.tauri*. L'importation du fer ferreux serait dépendante d'une protéine contenant du cuivre qui pourrait être une cupredoxine. Cependant la partie Fe-Transporteur qui permet le passage du fer à travers la membrane n'a pas été identifiée. L'étude de l'assimilation du fer ferreux dans une souche où l'on a supprimé cette cupredoxine permettrait de tester cette hypothèse.

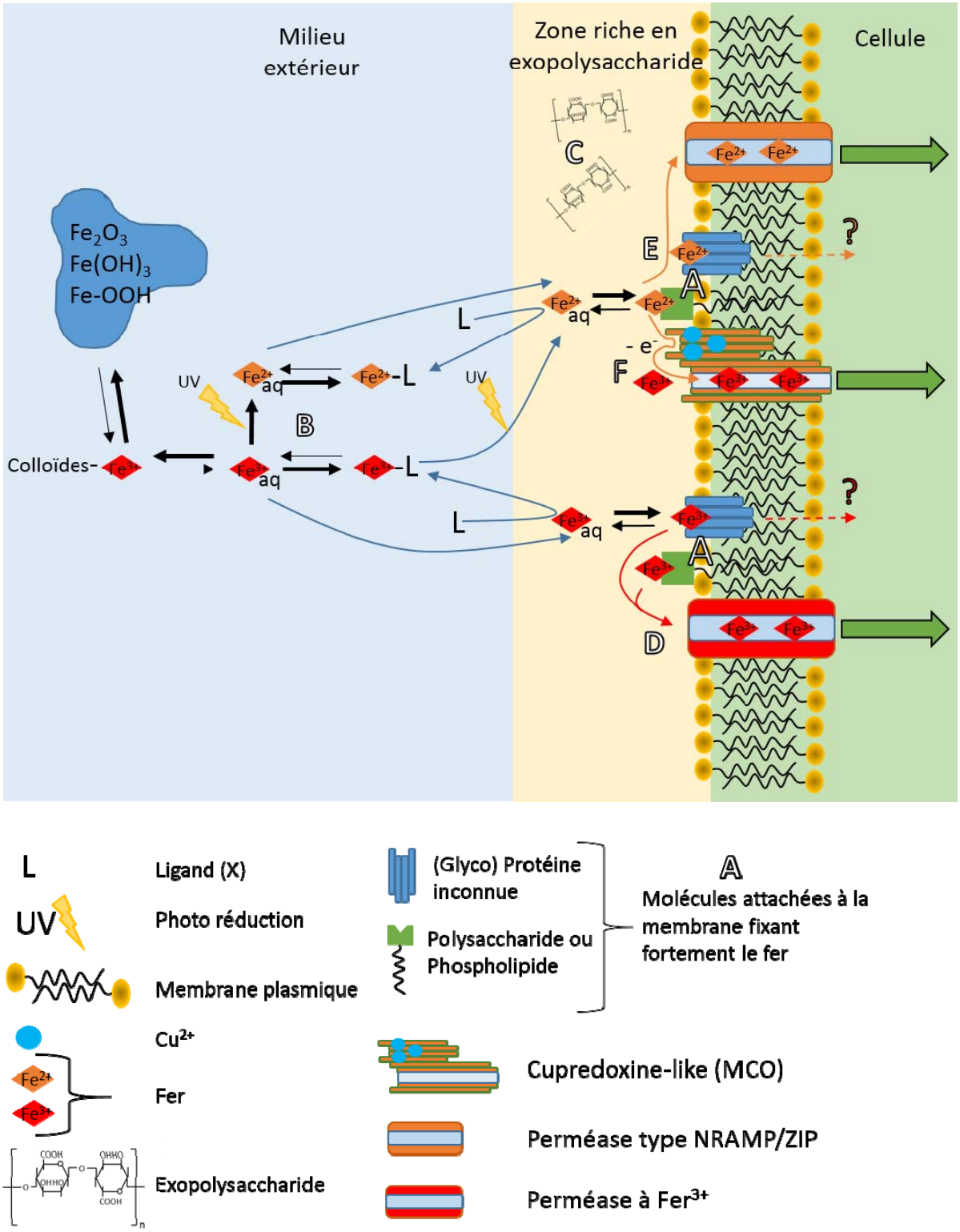


*Figure 13: Proposition de représentation des systèmes d'import du fer chez Ostreococcus tauri*

## 2 Régulation de l'importation du fer au cours du cycle jour/nuit chez *O.tauri*

Au cours de cette étude nous avons mis en évidence que les cinétiques d'assimilation du fer au cours du cycle jour/nuit chez *O.tauri* avaient des profils différents suivant la forme de fer fournie aux cellules. Le fer ferrique est importé plus rapidement en fin de journée et de nuit. En revanche l'importation du fer ferreux a principalement lieu en milieu de journée et en fin de nuit. Les différences entre les profils de ces cinétiques d'assimilation confirment la présence de systèmes d'import différents pour le $Fe^{2+}$ et le $Fe^{3+}$ (Botebol, Sutak, *et al.*, 2014). De façon surprenante, l'assimilation du fer chez les autres microalgues étudiées présente des différences par rapport à *O. tauri* au cours du cycle jour/nuit. Chez *P.tricornutum*, on observe un pic d'incorporation au début de la journée et un autre au début de la nuit. Cependant les profils des cinétiques d'assimilation sont similaires quelle que soit la forme du fer mise à disposition des cellules de *P.tricornutum*. Les systèmes d'assimilation du fer seraient donc sous le contrôle d'un même régulon chez cette diatomée. Chez *E. Huxlei*, l'assimilation du fer ne présente pas de rythme journalier (Botebol, Sutak, *et al.*, 2014) mais on observe une assimilation préférentielle du $Fe^{2+}$, cohérente avec l'absence d'activité réductase ferrique.

La Figure 14 illustre les liens possible entre le cycle de vie et l'importation du fer chez *O.tauri*. La vitesse d'assimilation du fer ferreux est élevée tout au long de la journée et maximale en milieu de journée, au moment du pic d'intensité lumineuse. On sait que la lumière facilite la réduction du $Fe^{3+}$ en $Fe^{2+}$ par la réaction de photoréduction. Les cultures n'ayant pas été soumises à des variations d'intensité lumineuse au cours de la journée, comme la lumière solaire, il est probable que ce système d'assimilation du $Fe^{2+}$ soit sous un contrôle photopériodique de type circadien qui permettrait de caler l'import du fer ferreux au moment où l'intensité lumineuse, et donc la photoréduction, est maximale (**A**).

Une étude transcriptomique a révélé que chez *O. tauri,* les gènes codant pour des protéines sécrétées présentent un pic d'expression en début de journée pendant les 3 heures précédant le pic d'assimilation du fer ferreux (**B**) (Monnier *et al.*, 2010). Il est donc possible que des EPS secrétés au cours de cette période de temps facilitent l'assimilation du fer ferreux. Cependant il est aussi possible que ce soit des (glyco)-protéines membranaires produites au cours de la même période de temps qui interviennent.

Ce pic de vitesse d'assimilation du fer ferreux a lieu au moment où de nombreux gènes associés à la photosynthèse et à la photoprotection sont exprimés, ce qui suggère que ce fer est

utilisé pour la réparation des photosystèmes endommagés et/ou pour la néosynthèse des protéines du chloroplaste avant la cytokinèse (**C**).

Trois heures avant le crépuscule, lorsque l'import du fer ferreux diminue, la vitesse d'assimilation du fer ferrique augmente, ce fer pourrait contribuer à maintenir l'apport en fer à la cellule, de façon à préparer la division cellulaire qui se déroule en fin de journée chez *O.tauri,* en constituant des stocks de fer pour les nouvelles cellules. Il est aussi possible qu'un stock en fer suffisant soit l'un des prérequis nécessaires au déclenchement de la division (**D**).

En fin de nuit, l'assimilation du fer ferrique et du fer ferreux augmente à nouveau, et il est possible que ce fer soit destiné à intégrer l'appareil photosynthétique lors de la néo synthèse des photosystèmes, qui se déroule peu avant l'aube. Cette assimilation du fer ferreux se déroule la nuit, en absence de photoréduction, ce qui suggère l'existence d'un système d'assimilation indépendant de la lumière. Il est possible qu'un transporteur de cations bivalents type NRAMP, justement transcrit à ce moment de la nuit, transporte le fer vers l'intérieur de la cellule. (**E**)

L'assimilation du fer est fortement régulée au cours du cycle jour/nuit sans doute de façon à apporter à *O.tauri* suffisamment de fer à des moments clé de son cycle cellulaire. Il est probable que les différents systèmes d'importation du fer chez *O.tauri* soient sous contrôle de l'horloge circadienne.

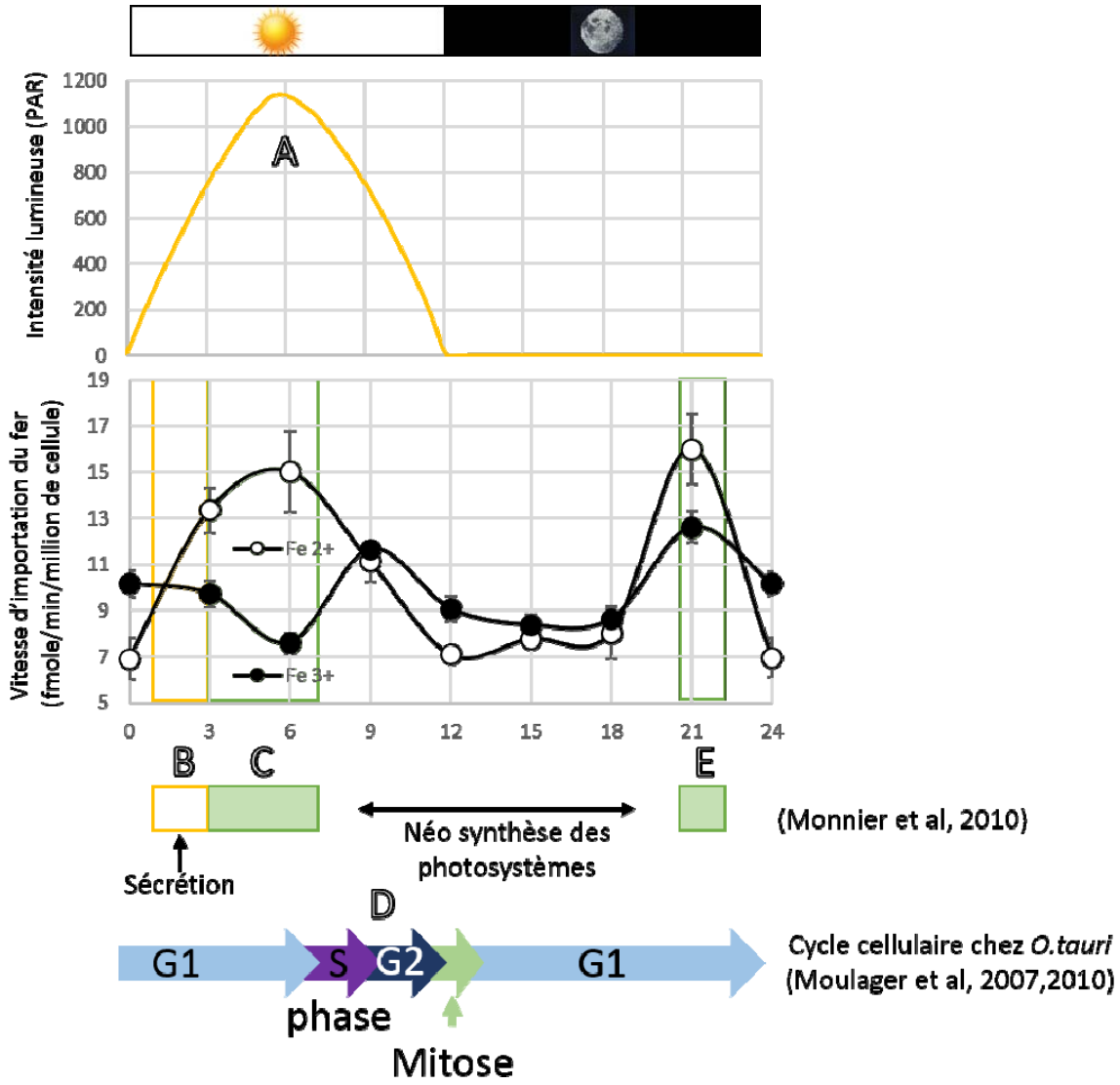


*Figure 14: Lien possible entre la régulation de l'import du fer et le cycle de vie d'Ostreococcus tauri*

## 3 Implication de la ferritine dans la régulation de l'homéostasie du fer chez *O.tauri*

Nous avons mis en évidence que la ferritine était impliquée dans la régulation de l'homéostasie du fer chez *O.tauri,* aussi bien au cours de la croissance, de par son rôle dans l'assimilation du fer, que lors de la survie lorsque les ressources en fer du milieu sont épuisées (Botebol, Lesuisse, *et al.*, 2014). La Figure 15 est un modèle représentant le rôle de la ferritine dans la régulation de l'homéostasie du fer intracellulaire.

(**1**) Nous avons pu observer dans deux expériences différentes, *in situ* (Ottesen *et al.*, 2013) et *in vitro* (Monnier *et al.*, 2010) que la transcription de la ferritine est régulée par l'alternance jour/nuit. Le pic d'expression de l'ARNm de la ferritine à lieu à la tombée de la nuit, et son minimum à l'aube. Les gènes codant pour les protéines des photosystèmes et pour certaines protéines de la voie de fixation de l'azote (Fd-GOGAT) ont un profil d'expression antiphasique par rapport à la ferritine, le pic d'expression se produisant en milieu de journée

(**2**) La synthèse de la ferritine se déroule sous contrôle de l'horloge circadienne et du cycle jour/nuit (Botebol, Lesuisse, *et al.*, 2014). Le rapporteur FTN-Luc présente un signal qui augmente à partir du crépuscule et tout au long de la nuit jusqu'à atteindre un maximum avant l'aube. A l'aube le signal diminue brutalement, suggérant qu'une dégradation de la ferritine-luc est induite par la lumière. L'utilisation d'inhibiteur du protéasome, situé dans le cytosol, le noyau et le réticulum endoplasmique, n'a pas permis d'interrompre cette dégradation, mais la ferritine présente une séquence d'adressage à la mitochondrie/chloroplaste. Il est donc fort probable que l'inhibition du protéasome n'affecte pas la dégradation de la ferritine.

(**3**) Le complexe de ferritine serait majoritairement présent la nuit, cependant le chargement direct de la ferritine lors des expériences d'assimilation du fer, quel que soit le moment de la journée, indique l'existence de complexes de ferritine fonctionnels le jour. Le *KoFer* présente des contenus en fer deux fois plus faibles que la souche sauvage, il est donc possible que lors de la croissance des cellules, les complexes de ferritine constituent un stock de fer pour soutenir la croissance.

(**4**) Les expériences d'assimilation du fer réalisées en utilisant le mutant *KoFer* montrent des vitesses d'assimilation fortement réduites, mais le profil de ces vitesses d'assimilation au cours de la journée reste similaire à celui des cellules sauvages. L'absence de ferritine réduit la vitesse mais n'affecte pas le moment de l'assimilation du fer. La ferritine serait donc plutôt

impliquée dans le transit intracellulaire du fer après assimilation, que dans la régulation du moment de l'assimilation.

(**5**) Lorsque le fer extracellulaire est en excès (augmente par rapport à la condition de pré culture), la traduction du rapporteur FTN-Luc est induite. On peut penser que les complexes de ferritine sont saturés, et que pour séquestrer le fer excédentaire, les cellules en produisent de nouveaux. Même si nous ne savons pas encore par quels mécanismes la transcription et/ou la traduction de la ferritine est induite, plusieurs hypothèses sont viables :

*i)* la saturation en fer des complexes de ferritine augmente la concentration en fer libre dans la cellule, modifiant les niveaux de fer intracellulaire. Chez *O.tauri*, comme chez les plantes angiospermes, on trouve en amont du promoteur de la ferritine un élément *cis* tel que IDRS (Iron Dependent Regulatory Sequence) (Strozycki *et al.*, 2010; Briat *et al.*, 2010) connu pour permettre la répression de la ferritine en absence de fer (Petit *et al.*, 2001; Tarantino *et al.*, 2003; Ravet *et al.*, 2009). Ainsi l'augmentation du fer libre dans la cellule conduirait à la dé-répression du gène de la ferritine. Il est aussi possible que les ROS produites lors l'incorporation massive du fer dans les complexes de ferritine servent de signal pour induire la production de ferritine. L'ajout de molécules protectrices contre le stress oxydant lorsque les cellules sont en présence d'un excès de fer permettrait de déterminer l'implication des ROS dans l'induction de la ferritine.

*ii)* les molécules/protéines responsables du transport du fer depuis la membrane vers les complexes de ferritine sont saturés. Leur accumulation pourrait servir de signal à la cellule. L'identification puis la délétion des gènes codant les protéines interagissant avec la ferritine pourrait permettre de trouver des protéines impliquées à la fois dans le chargement de la ferritine et le renseignement du statut en fer. *iii)* la saturation des récepteurs membranaires spécifiques du fer pourrait renseigner les cellules quant aux quantités disponibles dans le milieu, leur permettant d'augmenter leurs espaces de stockage en conséquence.

(**6**) Lorsque les ressources en fer du milieu sont épuisées, nous avons pu observer un déplacement du pool de fer intracellulaire. Le fer est présent la nuit au sein de la ferritine, puis il pourrait être récupéré à l'aube, soit par dégradation du complexe de ferritine, soit à l'aide de chaperonnes et d'un apport de pouvoir réducteur. L'étude de la charge en $^{55}$Fe de la ferritine, en présence d'inhibiteur de la dégradation protéique, permettrait de déterminer si la dégradation du complexe de ferritine est indispensable au recyclage du fer. Au milieu de la journée, le fer associé à la ferritine est à son niveau le plus bas, puis la charge de la ferritine

augmente à nouveau à partir de la fin de journée jusqu'à la fin de la nuit, atteignant un niveau semblable à celui observé au début de l'expérience. A l'opposé, certaines protéines impliquées dans l'assimilation de l'azote, tel que la Fd–GOGAT et la nitrite réductase, ont été identifiées dans les bandes protéiques chargées en fer la journée. Ces deux protéines catalysent les réactions chimiques dont elles sont responsables à l'aide de la ferrédoxine, en utilisant le pouvoir réducteur produit par la photosynthèse (Inokuchi and Kuma, 2002). Ainsi les ressources en fer d'*O.tauri* seraient recyclées pour faire face à la carence, le fer serait réparti entre la photosynthèse et l'assimilation d'azote la journée avant d'être stocké la nuit dans la ferritine.

(7) Au cours de cette étude, nous avons mis en évidence que la ferritine était exprimée sous contrôle du cycle jour/nuit et de l'horloge circadienne (Botebol, Lesuisse, *et al.*, 2014). Cependant, dans les lignées rapportrices où l'insert ferritine-luc a remplacé le gène sauvage (RH), l'expression de la ferritine-luc n'a plus de profil d'expression rythmique lorsque les souches sont transférées en condition lumière continue. La mutation de la ferritine semble donc influencer directement sa propre régulation, suggérant que la présence de complexes de ferritine actifs est nécessaire à la régulation circadienne de l'expression du monomère de ferritine. Nous avons aussi pu observer que le fer disponible dans le milieu de culture influait sur la période d'un gène central de l'horloge circadienne, CCA1. En effet, lorsqu'une lignée cca1-luc est placée dans des milieux avec des concentrations en fer différentes de sa condition de pré-acclimatation, sa période d'oscillation libre augmente. Ainsi il est possible que, comme chez *A.thaliana* (Salomé *et al.*, 2013), l'homéostasie du fer influe directement sur la periode de l'horloge circadienne d'*O.tauri*. Les complexes de ferritines étant au centre de la régulation de l'homéostasie du fer, leur absence ne peut avoir comme résultats que l'augmentation du pool de fer libre dans la cellule. Ainsi, en absence de signaux lumineux, l'absence de régulateur intracellulaire de l'homéostasie du fer conduirait à l'expression constitutive du promoteur ferritine. Ceci soulève des questions à propos du comportement de l'horloge circadienne quand la ferritine est absente. Est-ce que cette dérégulation de l'homéostasie du fer affecte l'expression circadienne des gènes de l'oscillateur central? La construction d'une lignée rapportrice CCA1-luc dans laquelle on muterait la ferritine permettrait de répondre à cette question.

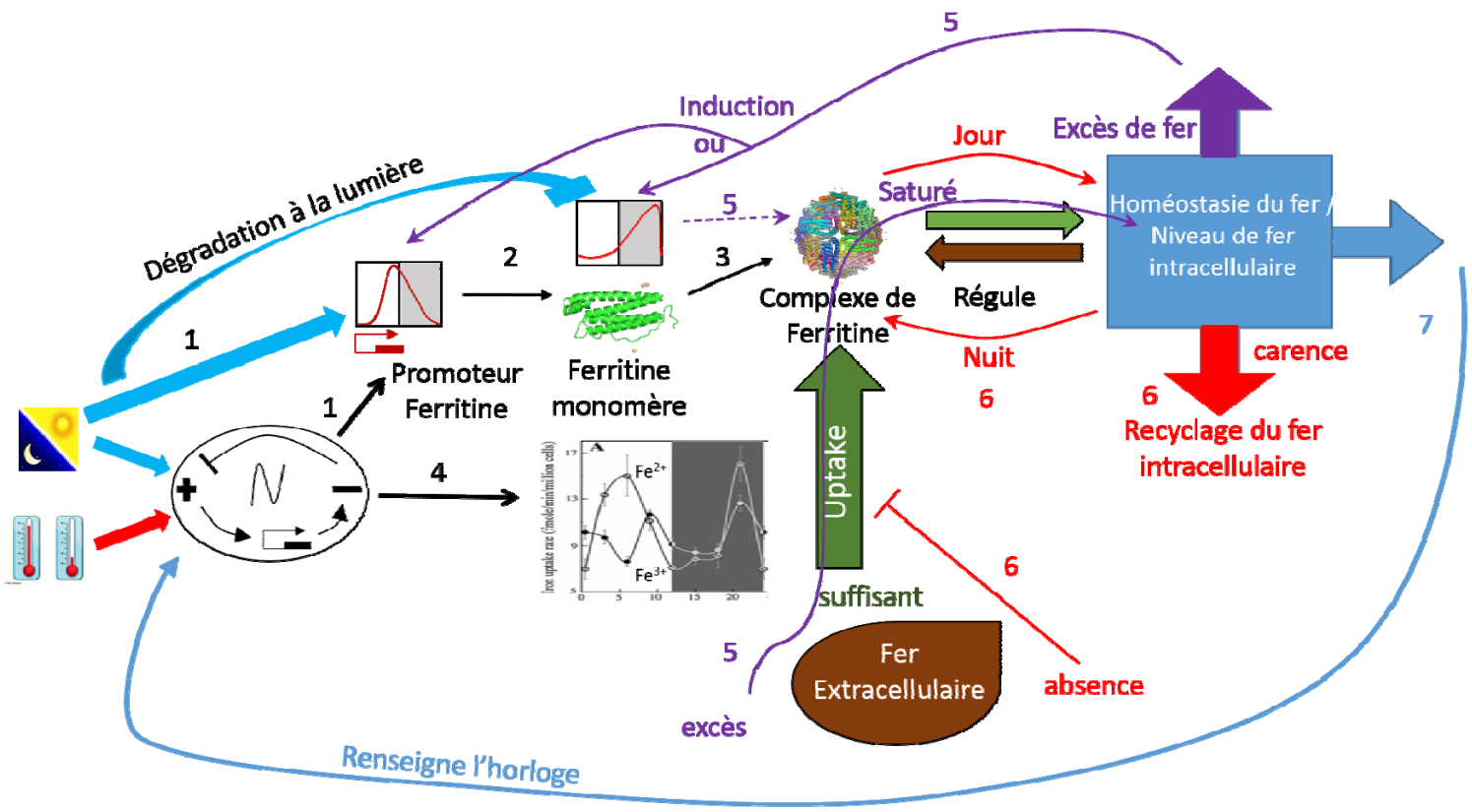


*Figure 15:Implication de la ferritine dans la régulation de l'homéostasie du fer chez Ostreococcus tauri*

# 4 Stratégies de survie des écotypes du genre *Ostreococcus* face à la carence en fer

Au cours de ma thèse je me suis également intéressé à caractériser la réponse à la carence en fer chez différents écotypes du genre *Ostreococcus*. Nous avons pu voir que le pico phytoplancton utilisait des stratégies variées et complémentaires pour s'acclimater, voire s'adapter à la carence en fer. Chez *Ostreococcus* nous avons pu observer que les écotypes RCC 789 (Clade D) et OTTH595 (Clade C) ont la même sensibilité à la carence en fer, ils ne se développent plus et meurent pour des concentrations en dessous de 108 nM de Fe-EDTA. Ces deux écotypes proviennent de zones côtières où les apports en fer depuis le littoral maintiennent des concentrations relativement élevées en fer (Demir-Hilton *et al.*, 2011). Il apparait donc qu'ayant colonisé une niche écologique où le fer est en quantité suffisante, ces écotypes n'ont pas développé de stratégies de survie à la carence en fer aussi efficaces que celles des deux autres écotypes testés, la RCC 802 (Clade A) et la RCC 809 (Clade B). Ces deux écotypes ont été isolés dans des zones profondes de l'atlantique (RCC809) et oligotrophe de la méditerranée (RCC 802). Au cours de cette étude nous avons pu voir que la RCC 809 présentait des vitesses d'assimilation plus élevées que les autres écotypes, suggérant l'existence de système d'assimilation du fer optimisé. La bande protéique située à 480kDa, contenant la ferritine, est deux fois plus chargée en $^{55}$Fe chez cet écotype, et de même, son contenu en $^{55}$Fe est deux fois plus élevé que celui des autres écotypes en condition de carence en fer. Il semblerait donc que cet écotype fait des stocks de fer de façon plus efficace pour faire face à la carence. De plus, cet écotype utilise une stratégie d'adaptation à la baisse de luminosité appelé σ-type (Strzepek *et al.*, 2011; Six *et al.*, 2008) qui consiste à multiplier ses antennes photosynthétiques plutôt que ses centres réactionnels, se faisant il optimise l'utilisation de la lumière sans augmenter ses besoin en fer. Ainsi cet écotype utilise sans doute moins de fer pour la photosynthèse et, dans nos conditions expérimentales à faible luminosité (20µE), sa stratégie d'acclimatation peut lui permettre d'avoir une activité photosynthétique beaucoup plus efficace que les écotypes de surface (Clade C, D). Toutes ces données expliquent la capacité de la RCC 809 à survivre lorsque les concentrations en fer sont faibles, inférieures à 54 nM de Fe-EDTA.

La RCC 802 (Clade A) est le seul écotype dont le taux de croissance n'est réduit que lorsque le fer disponible (Fe') atteint des concentrations de 5.4 nM Fe-EDTA. Ce maintien des

performances de croissance de la RCC 802 ne semble pas être lié à des capacités d'assimilation du fer accrues, car sa vitesse d'assimilation est la plus faible parmi les écotypes testés. De la même façon, la bande de ferritine chez la RCC 802 est peu chargée, suggérant que la ferritine n'est pas le stock principal de fer. Par contre, c'est l'écotype qui contient le plus de fer lorsqu'il est cultivé en présence d'un excès de fer, suggérant que la RCC 802 pourrait survivre en constituant de grandes réserves de fer en prévision des carences à venir. Nous avons aussi pu observer que la RCC 802 avait un niveau de fluorescence rouge de la chlorophylle (FL3), deux fois plus faible que ceux des autres souches étudiées ainsi qu'une biomasse deux fois moindre. De plus, cette souche est capable de réduire sa chlorophylle et sa biomasse de plus de 50% lorsqu'elle est en condition de carence, en diminuant légèrement son efficacité photosynthétique. Il est donc probable que cette souche ait un avantage adaptatif dû à sa faible biomasse et qu'elle ait développé une stratégie d'acclimatation à la carence en fer qui consiste à réduire sa biomasse, diminuant ainsi ses besoins en fer. Cette hypothèse est renforcée par le comportement du Ko de LOV HK dans des conditions de carence. En effet, le Ko de LOV HK, construit à partir de la souche OTTH595 (*O.tauri*, Clade C), présente une taille et une biomasse réduites par rapport à la souche sauvage. Ce mutant est capable de maintenir en situation de carence en fer un taux de croissance au moins deux fois plus élevé que la souche sauvage OTTH595 et notamment continue à croître à des concentrations en fer pour lesquelles OTTH595 survit tout juste, quand il ne meurt pas. Comme chez la RCC 802, la fluorescence rouge diminue significativement en même temps que le fer disponible. Ainsi, en mutant un seul gène de l'écotype OTTH595, nous avons pu améliorer ses capacités de survie à la carence en fer en réduisant la biomasse de la cellule.

La RCC 802 ayant une biomasse réduite, il est possible qu'elle ait un volume et une surface cellulaire réduite. Dans ce cas, la normalisation des vitesses assimilation du fer par cellule n'est plus pertinente, il serait plus intéressant de normaliser par rapport à la surface cellulaire (Sunda and Huntsman, 1997). Il faudra donc déterminer la taille et le volume cellulaire de ces écotypes pour comparer plus avant leurs capacités d'assimilation du fer.

Il est aussi possible que la RCC 802 ait un nombre réduit de métalloenzymes à fer, ce qui lui permettrait de faire face plus facilement à la carence en fer. Une étude RNAseq de la RCC 802 en condition +Fe / -Fe et associé à un assemblage de novo du génome de la RCC 802 est en cours et devrait permettre de vérifier cette hypothèse.

# IV. **Références Bibliographiques**

**Allen, A.E., Roche, J. La, Maheswari, U., Lommer, M., Schauer, N., Lopez, P.J., Finazzi, G., Fernie, A.R. and Bowler, C.** (2008) Whole-cell response of the pennate diatom Phaeodactylum tricornutum to iron starvation. *Proc. Natl. Acad. Sci. U. S. A.*, **105**, 10438–43.

**Allen, M.D., Campo, J. a del, Kropat, J. and Merchant, S.S.** (2007) FEA1, FEA2, and FRE1, encoding two homologous secreted proteins and a candidate ferrireductase, are expressed coordinately with FOX1 and FTR1 in iron-deficient Chlamydomonas reinhardtii. *Eukaryot. Cell*, **6**, 1841–52.

**Andrews, S.C., Robinson, A.K. and Rodriguez-Quiñones, F.** (2003) Bacterial iron homeostasis. *FEMS Microbiol. Rev.*, **27**, 215–237.

**Arístegui, J., Duarte, C.M., Reche, I. and Gómez-Pinchetti, J.L.** (2014) Krill excretion boosts microbial activity in the Southern Ocean. *PLoS One*, **9**, e89391.

**Armstrong, R. a.** (2008) Nutrient uptake rate as a function of cell size and surface transporter density: A Michaelis-like approximation to the model of Pasciak and Gavis. *Deep Sea Res. Part I Oceanogr. Res. Pap.*, **55**, 1311–1317.

**Arosio, P., Ingrassia, R. and Cavadini, P.** (2009) Ferritins: a family of molecules for iron storage, antioxidation and more. *Biochim. Biophys. Acta*, **1790**, 589–99.

**Aschoff, J.** (1979) Circadian Rhythms: Influences of Internal and External Factors on the Period Measured in Constant Conditions1. *Z. Tierpsychol.*, **49**, 225–249.

**Baar, H.J.W. de and Jong, J.T.M. de** (2001) Distributions, sources and sinks of iron in seawater. *IUPAC Ser. Anal. Phys. Chem. Environ. Syst.*, **7**, 123–254.

**Bagnaresi, P., Basso, B. and Pupillo, P.** (1997) The NADH-dependent Fe(3+)-chelate reductases of tomato roots. *Planta*, **202**, 427–34.

**Baldauf, S.L.** (2003) The Deep Roots of Eukaryotes. *Sci.* , **300** , 1703–1706.

**Beinert, H., Holm, R.H. and Münck, E.** (1997) Iron-Sulfur Clusters: Nature's Modular, Multipurpose Structures. *Sci.* , **277** , 653–659.

**Bennett, S. a., Achterberg, E.P., Connelly, D.P., Statham, P.J., Fones, G.R. and German, C.R.** (2008) The distribution and stabilisation of dissolved Fe in deep-sea hydrothermal plumes. *Earth Planet. Sci. Lett.*, **270**, 157–167.

**Ben-Shem, A., Frolow, F. and Nelson, N.** (2003) Crystal structure of plant photosystem I. *Nature*, **426**, 630–635.

**Bento, I., Martins, L.O., Gato Lopes, G., Armenia Carrondo, M. and Lindley, P.F.** (2005) Dioxygen reduction by multi-copper oxidases; a structural perspective. *Dalt. Trans.*, 3507–3513.

**Blaby-Haas, C.E. and Merchant, S.S.** (2012) The ins and outs of algal metal transport. *Biochim. Biophys. Acta*, **1823**, 1531–52.

**Blain, S., Sarthou, G. and Laan, P.** (2008) Distribution of dissolved iron during the natural iron-fertilization experiment KEOPS (Kerguelen Plateau, Southern Ocean). *Deep Sea Res. Part II Top. Stud. Oceanogr.*, **55**, 594–605.

**Botebol, H., Lesuisse, E., Sutak, R., et al.** (2014) A pivotal role of ferritin in the day night regulation of iron uptake and recycling in marine phytoplankton.

**Botebol, H., Sutak, R., Scheiber, I.F., Blaiseau, P.-L., Bouget, F.-Y., Camadro, J.-M. and Lesuisse, E.** (2014) Different iron sources to study the physiology and biochemistry of iron metabolism in marine micro-algae. *Biometals*, **27**, 75–88.

**Bouget, F.-Y., Lefranc, M., Thommen, Q., Pfeuty, B., Lozano, J.-C., Schatt, P., Botebol, H. and Vergé, V.** (2014) Transcriptional versus non-transcriptional clocks: A case study in Ostreococcus. *Mar. Genomics*, **14**, 17–22.

**Boyd, P.W. and Ellwood, M.J.** (2010) The biogeochemical cycle of iron in the ocean. *Nat. Geosci.*, **3**, 675–682.

**Boyle, E. a., Bergquist, B. a., Kayser, R. a. and Mahowald, N.** (2005) Iron, manganese, and lead at Hawaii Ocean Time-series station ALOHA: Temporal variability and an intermediate water hydrothermal plume. *Geochim. Cosmochim. Acta*, **69**, 933–952.

**Briat, J.-F., Duc, C., Ravet, K. and Gaymard, F.** (2010) Ferritins and iron storage in plants. *Biochim. Biophys. Acta*, **1800**, 806–14.

**Bruland, K.W., Rue, E.L. and Smith, G.J.** (2001) Iron and macronutrients in California coastal upwelling regimes: Implications for diatom blooms. *Limnol. Oceanogr.*, **46**, 1661–1674.

**Butler, A.** (1998) Acquisition and Utilization of Transition Metal Ions by Marine Organisms. *Sci.* , **281** , 207–209.

**Cardol, P., Bailleul, B., Rappaport, F., et al.** (2008) An original adaptation of photosynthesis in the marine green alga Ostreococcus. *Proc. Natl. Acad. Sci. U. S. A.*, **105**, 7881–6.

**Carmona, F., Palacios, Ò., Gálvez, N., Cuesta, R., Atrian, S., Capdevila, M. and Domínguez-Vera, J.M.** (2013) Ferritin iron uptake and release in the presence of metals and metalloproteins: Chemical implications in the brain. *Coord. Chem. Rev.*, **257**, 2752–2764.

**Carre, I. a.** (2002) MYB transcription factors in the Arabidopsis circadian clock. *J. Exp. Bot.*, **53**, 1551–1557.

**Chen, Y.-Y., Wang, Y., Shin, L.-J., et al.** (2013) Iron is involved in maintenance of circadian period length in Arabidopsis. *Plant Physiol.*, **161**, 1409–20.

**Chrétiennot-Dinet, M.-J., Courties, C., Vaquer, A., Neveux, J., Claustre, H., Lautier, J. and Machado, M.C.** (1995) A new marine picoeucaryote: Ostreococcus tauri gen. et sp. nov. (Chlorophyta, Prasinophyceae). *Phycologia*, **34**, 285–292.

**Corellou, F., Schwartz, C., Motta, J.-P., Djouani-Tahri, E.B., Sanchez, F. and Bouget, F.-Y.** (2009) Clocks in the green lineage: comparative functional analysis of the circadian architecture of the picoeukaryote ostreococcus. *Plant Cell*, **21**, 3436–49.

**Courties, C., Perasso, R., Chrétiennot-Dinnet, M., Gouy, M., Guillou, L. and Troussellier, M.** (1998) Phylogenetic analysis and genome size of Ostreococcus tauri (Chlorophyta). *J. Phycol.*, **34**, 844–849.

**Courties, C., Vaquer, A. and Troussellier, M.** (1994) Smallest eukaryotic organism. *Nature*, **370**, 255.

**Cramer, W.A. and Knaff, D.B.** (1991) Energy Transduction in Biological Membranes. A Textbook of Bioenergetics.

**Demir-Hilton, E., Sudek, S., Cuvelier, M.L., Gentemann, C.L., Zehr, J.P. and Worden, A.Z.** (2011) Global distribution patterns of distinct clades of the photosynthetic picoeukaryote Ostreococcus. *ISME J.*, **5**, 1095–107.

**Derelle, E., Ferraz, C., Lagoda, P., et al.** (2002) DNA libraries for sequencing the genome of ostreococcus tauri (chlorophyta, prasinophyceae ): the smallest free-living eukaryotic cell. *J. Phycol.*, **38**, 1150–1156.

**Derelle, E., Ferraz, C., Rombauts, S., et al.** (2006) Genome analysis of the smallest free-living eukaryote Ostreococcus tauri unveils many unique features. *Proc. Natl. Acad. Sci. U. S. A.*, **103**, 11647–52.

**Djouani-tahri, E.B., Christie, J.M., Sanchez-Ferandin, S., Sanchez, F., Bouget, F.-Y. and Corellou, F.** (2011) A eukaryotic LOV-histidine kinase with circadian clock function in the picoalga Ostreococcus. *Plant J.*, **65**, 578–88.

**Douglas, T. and Ripoll, D.R.** (1998) Calculated electrostatic gradients in recombinant human H-chain ferritin. *Protein Sci.*, **7**, 1083–91.

**Duc, C., Cellier, F., Lobréaux, S., Briat, J.-F. and Gaymard, F.** (2009) Regulation of iron homeostasis in Arabidopsis thaliana by the clock regulator time for coffee. *J. Biol. Chem.*, **284**, 36271–81.

**Edgar, R.S., Green, E.W., Zhao, Y., et al.** (2012) Peroxiredoxins are conserved markers of circadian rhythms. *Nature*, **485**, 459–64.

**Elizabeth C. Theil** (2003) Ferritin: at the crossroads of iron and oxygen metabolism. *J. Nutr.*, **133**, 1549S.

**Elrod, V. a.** (2004) The flux of iron from continental shelf sediments: A missing source for global budgets. *Geophys. Res. Lett.*, **31**, L12307.

**Falkowski, P.G.** (2006) Tracing Oxygen's Imprint on Earth's Metabolic Evolution. *Sci.* , **311** , 1724–1725.

**Fay, P.** (1992) Oxygen relations of nitrogen fixation in cyanobacteria. *Microbiol. Rev.*, **56**, 340–73.

**Fontaine, S. La, Quinn, J. and Nakamoto, S.** (2002) Copper-dependent iron assimilation pathway in the model photosynthetic eukaryote Chlamydomonas reinhardtii. *Eukaryot. Cell*, **1**, 736–757.

**Gendron, J.M., Pruneda-Paz, J.L., Doherty, C.J., Gross, A.M., Kang, S.E. and Kay, S. a** (2012) Arabidopsis circadian clock protein, TOC1, is a DNA-binding transcription factor. *Proc. Natl. Acad. Sci. U. S. A.*, **109**, 3167–72.

**González, a G., Santana-Casiano, J.M., González-Dávila, M., Pérez-Almeida, N. and Suárez de Tangil, M.** (2014) Effect of Dunaliella tertiolecta organic exudates on the Fe(II) oxidation kinetics in seawater. *Environ. Sci. Technol.*, **48**, 7933–41.

**Goswami, T., Bhattacharjee, A., Babal, P., Searle, S., Moore, E., Li, M. and Blackwell, J.M.** (2001) Natural-resistance-associated macrophage protein 1 is an H+/bivalent cation antiporter. *J. Biochem.*, **354**, 511–519.

**Guieu, C. and Martin, J.M.** (2002) The Level and Fate of Metals in the Danube River Plume. *Estuar. Coast. Shelf Sci.*, **54**, 501–512.

**Gunshin, H., Mackenzie, B., Berger, U., Gunshin, Y., Romero, M., Boron, W., Nussberger, S., Gollan, J. and Hediger, M.** (1997) Cloning and characterization of a mammalian proton-coupled metal-ion transporter. *Nature*, **388**, 6264–6268.

**Harmer, S.L.** (2009) The circadian system in higher plants. *Annu. Rev. Plant Biol.*, **60**, 357–77.

**Harrison, P. and Arosio, P.** (1996) The ferritins: molecular properties, iron storage function and cellular regulation. *Biochim. Biophys. Acta (BBA)-Bioenergetics*, **1275**, 161–203.

**Hassler, C.S., Alasonati, E., Mancuso Nichols, C. a. and Slaveykova, V.I.** (2011) Exopolysaccharides produced by bacteria isolated from the pelagic Southern Ocean — Role in Fe binding, chemical reactivity, and bioavailability. *Mar. Chem.*, **123**, 88–98.

**Hassler, C.S., Schoemann, V., Nichols, C.M., Butler, E.C. V and Boyd, P.W.** (2011) Saccharides enhance iron bioavailability to Southern Ocean phytoplankton. *Proc. Natl. Acad. Sci. U. S. A.*, **108**, 1076–81.

**Heijde, M., Zabulon, G., Corellou, F., et al.** (2010) Characterization of two members of the cryptochrome/photolyase family from Ostreococcus tauri provides insights into the origin and evolution of cryptochromes. *Plant. Cell Environ.*, **33**, 1614–26.

**Henderson, G.P., Gan, L. and Jensen, G.J.** (2007) 3-D ultrastructure of O. tauri: electron cryotomography of an entire eukaryotic cell. *PLoS One*, **2**, e749.

**Hoffmann, L.J., Breitbarth, E., Ardelan, M.V., Duggen, S., Olgun, N., Hassellöv, M. and Wängberg, S.-Å.** (2012) Influence of trace metal release from volcanic ash on growth of Thalassiosira pseudonana and Emiliania huxleyi. *Mar. Chem.*, **132-133**, 28–33.

**Hong, S., Kim, S. a, Guerinot, M. Lou and McClung, C.R.** (2013) Reciprocal interaction of the circadian clock with the iron homeostasis network in Arabidopsis. *Plant Physiol.*, **161**, 893–903.

**Huang, W., Pérez-García, P., Pokhilko, A., Millar, A.J., Antoshechkin, I., Riechmann, J.L. and Más, P.** (2012) Mapping the core of the Arabidopsis circadian clock defines the network structure of the oscillator. *Science (80-. ).*, **336**, 75–9.

**Hudson, R.J. and Morel, F.M.M.** (1990) Iron transport in marine phytoplankton: Kinetics of cellular and medium coordination reactions. *Limnol. Oceanogr.*, **35**, 1002–1020.

**Inokuchi, R. and Kuma, K.** (2002) Nitrogen-assimilating enzymes in land plants and algae: phylogenic and physiological perspectives. *Physiol. Plant.*, **116**, 1–11.

**Jensen, P.E., Gilpin, M., Knoetzel, J. and Scheller, H. V** (2000) The PSI-K subunit of photosystem I is involved in the interaction between light-harvesting complex I and the photosystem I reaction center core. *J. Biol. Chem.*, **275**, 24701–8.

**Jickells, T.D., An, Z.S., Andersen, K.K., et al.** (2005) Global Iron Connections Between Desert Dust, Ocean Biogeochemistry, and Climate. *Science (80-. ).*, **308**, 67–71.

**Johnson, C.H. and Egli, M.** (2014) Metabolic compensation and circadian resilience in prokaryotic cyanobacteria. *Annu. Rev. Biochem.*, **83**, 221–47.

**Johnson, K.S., Gordon, R.M. and Coale, K.H.** (1997) What controls dissolved iron concentrations in the world ocean? Authors' closing comments. *Mar. Chem.*, **57**, 181–186.

**Katsuyama, M.** (2012) Physiological roles of NOX/NADPH oxidase, the superoxide-generating enzyme. *J. Clin. Biochem. Nutr.*, **50**, 9–22.

**Kirchman, D.L.** (1994) The uptake of inorganic nutrients by heterotrophic bacteria. *Microb. Ecol.*, **28**, 255–71.

**Konijn, A.M., Glickstein, H., Vaisman, B., Meyron-Holtz, E.G., Slotki, I.N. and Cabantchik, Z.I.** (1999) The cellular labile iron pool and intracellular ferritin in K562 cells. *Blood*, **94**, 2128–34.

**Kühlbrandt, W., Wang, D. and Fujiyoshi, Y.** (1994) Atomic model of plant light-harvesting complex by electron crystallography. *Nature*, **367**, 614–621.

**Kustka, A.B., Allen, A.E. and Morel, F.M.M.** (2007) Sequence Analysis and Transcriptional Regulation of Iron Acquisition Genes in Two Marine Diatoms 1. *J. Phycol.*, **43**, 715–729.

**Lannuzel, D., Schoemann, V., Jong, J. de, Chou, L., Delille, B., Becquevort, S. and Tison, J.-L.** (2008) Iron study during a time series in the western Weddell pack ice. *Mar. Chem.*, **108**, 85–95.

**Lannuzel, D., Schoemann, V., Jong, J. de, Pasquer, B., Merwe, P. van der, Masson, F., Tison, J.-L. and Bowie, A.** (2010) Distribution of dissolved iron in Antarctic sea ice: Spatial, seasonal, and inter-annual variability. *J. Geophys. Res.*, **115**, G03022.

**Lavery, T.J., Roudnew, B., Gill, P., Seymour, J., Seuront, L., Johnson, G., Mitchell, J.G. and Smetacek, V.** (2010) Iron defecation by sperm whales stimulates carbon export in the Southern Ocean. *Proc. R. Soc. B Biol. Sci.*, **277**, 3527–3531.

**Liu, X. and Millero, F.J.** (2002) The solubility of iron in seawater. *Mar. Chem.*, **77**, 43–54.

**Liu, X.S., Patterson, L.D., Miller, M.J. and Theil, E.C.** (2007) Peptides selected for the protein nanocage pores change the rate of iron recovery from the ferritin mineral. *J. Biol. Chem.*, **282**, 31821–5.

**Liu, Z., Yan, H., Wang, K., Kuang, T., Zhang, J., Gui, L., An, X. and Chang, W.** (2004) Crystal structure of spinach major light-harvesting complex at 2.72 A resolution. *Nature*, **428**, 287–292.

**Lommer, M., Specht, M., Roy, A.-S., et al.** (2012) Genome and low-iron response of an oceanic diatom adapted to chronic iron limitation. *Genome Biol.*, **13**, R66.

**Lukianova, O. a and David, S.S.** (2005) A role for iron-sulfur clusters in DNA repair. *Curr. Opin. Chem. Biol.*, **9**, 145–51.

**Mahowald, N.M., Engelstaedter, S., Luo, C., et al.** (2008) Atmospheric Iron Deposition: Global Distribution, Variability, and Human Perturbations. *Ann. Rev. Mar. Sci.*, **1**, 245–278.

**Maldonado, M.T., Allen, A.E., Chong, J.S., Lin, K., Leus, D., Karpenko, N. and Harris, S.L.** (2006) Copper-dependent iron transport in coastal and oceanic diatoms. *Limnol. Oceanogr.*, **51**, 1729–1743.

**Marchetti, A., Maldonado, M.T., Lane, E.S. and Harrison, P.J.** (2006) Comparison of oceanic of the pennate diatom Pseudo-nitzschia : Iron requirements ( high-nitrate , low-chlorophyll waters ) and coastal species external iron concentrations. *Limnol. Oceanogr.*, **51**, 2092–2101.

**Marchetti, A., Parker, M.S., Moccia, L.P., Lin, E.O., Arrieta, A.L., Ribalet, F., Murphy, M.E.P., Maldonado, M.T. and Armbrust, E.V.** (2009) Ferritin is used for iron storage in bloom-forming marine pennate diatoms. *Nature*, **457**, 467–70.

**Marie, D., Zhu, F., Balagué, V., Ras, J. and Vaulot, D.** (2006) Eukaryotic picoplankton communities of the Mediterranean Sea in summer assessed by molecular approaches (DGGE, TTGE, QPCR). *FEMS Microbiol. Ecol.*, **55**, 403–15.

**McHugh, J.P., Rodríguez-Quinoñes, F., Abdul-Tehrani, H., Svistunenko, D. a, Poole, R.K., Cooper, C.E. and Andrews, S.C.** (2003) Global iron-dependent gene regulation in Escherichia coli. A new mechanism for iron homeostasis. *J. Biol. Chem.*, **278**, 29478–86.

**Millar, A.J.** (2004) Input signals to the plant circadian clock. *J. Exp. Bot.*, **55**, 277–83.

**Mittler, R.** (2002) Oxidative stress, antioxidants and stress tolerance. *Trends Plant Sci.*, **7**, 405–410.

**Mizoguchi, T., Wheatley, K., Hanzawa, Y., Wright, L., Mizoguchi, M., Song, H.R., Carré, I. a and Coupland, G.** (2002) LHY and CCA1 are partially redundant genes required to maintain circadian rhythms in Arabidopsis. *Dev. Cell*, **2**, 629–41.

**Moffett, J.W.** (2001) Transformations among different forms of iron in the ocean. In *The Biogeochemistry of Iron in Seawater*. IUPAC Series on Analytical and Physical Chemistry of Environmental Systems, pp. 343–372.

**Monnier, A., Liverani, S., Bouvet, R., Jesson, B., Smith, J.Q., Mosser, J., Corellou, F. and Bouget, F.-Y.** (2010) Orchestrated transcription of biological processes in the marine picoeukaryote Ostreococcus exposed to light/dark cycles. *BMC Genomics*, **11**, 192.

**Morant, P.-E., Thommen, Q., Pfeuty, B., Vandermoere, C., Corellou, F., Bouget, F.-Y. and Lefranc, M.** (2010) A robust two-gene oscillator at the core of Ostreococcus tauri circadian clock. *Chaos*, **20**, 045108.

**Morel, F.M.M. and Price, N.M.** (2003) The Biogeochemical Cycles of Trace Metals in the Oceans. *Science (80-. ).*, **300**, 944–947.

**Morrissey, J. and Bowler, C.** (2012) Iron Utilization in Marine Cyanobacteria and Eukaryotic Algae. *Front. Microbiol.*, **3**, 43.

**Moseley, J.L., Allinger, T., Herzog, S., Hoerth, P., Wehinger, E., Merchant, S. and Hippler, M.** (2002) Adaptation to Fe-deficiency requires remodeling of the photosynthetic apparatus. *EMBO J.*, **21**, 6709–20.

**Moulager, M., Corellou, F., Vergé, V., Escande, M.-L. and Bouget, F.-Y.** (2010) Integration of light signals by the retinoblastoma pathway in the control of S phase entry in the picophytoplanktonic cell Ostreococcus. *PLoS Genet.*, **6**, e1000957.

**Müh, F., Glöckner, C., Hellmich, J. and Zouni, A.** (2012) Light-induced quinone reduction in photosystem II. *Biochim. Biophys. Acta*, **1817**, 44–65.

**Naumann, B., Busch, A., Allmer, J., Ostendorf, E., Zeller, M., Kirchhoff, H. and Hippler, M.** (2007) Comparative quantitative proteomics to investigate the remodeling of bioenergetic pathways under iron deficiency in Chlamydomonas reinhardtii. *Proteomics*, **7**, 3964–79.

**Naumann, B., Stauber, E.J., Busch, A., Sommer, F. and Hippler, M.** (2005) N-terminal processing of Lhca3 Is a key step in remodeling of the photosystem I-light-harvesting complex under iron deficiency in Chlamydomonas reinhardtii. *J. Biol. Chem.*, **280**, 20431–41.

**Nodwell, L.M. and Price, N.M.** (2001) Direct use of inorganic colloidal iron by marine mixotrophic phytoplankton. *Limnol. Oceanogr.*, **46**, 765–777.

**O'Neill, J.S., Ooijen, G. van, Dixon, L.E., Troein, C., Corellou, F., Bouget, F.-Y., Reddy, A.B. and Millar, A.J.** (2011) Circadian rhythms persist without transcription in a eukaryote. *Nature*, **469**, 554–8.

**Oexle, H., Gnaiger, E. and Weiss, G.** (1999) Iron-dependent changes in cellular energy metabolism: influence on citric acid cycle and oxidative phosphorylation. *Biochim. Biophys. Acta*, **1413**, 99–107.

**Ottesen, E. a, Young, C.R., Eppley, J.M., Ryan, J.P., Chavez, F.P., Scholin, C. a and Delong, E.F.** (2013) Pattern and synchrony of gene expression among sympatric marine microbial populations. *Proc. Natl. Acad. Sci. U. S. A.*, **110**, E488–E497.

**Öztürk, M., Croot, P.L., Bertilsson, S., Abrahamsson, K., Karlson, B., David, R., Fransson, A. and Sakshaug, E.** (2004) Iron enrichment and photoreduction of iron under UV and PAR in the presence of hydroxycarboxylic acid: implications for phytoplankton growth in the Southern Ocean. *Deep Sea Res. Part II Top. Stud. Oceanogr.*, **51**, 2841–2856.

**Pasciak, W.J. and Gavis, J.** (1974) Transport limitation of nutrient uptake in phytoplankton. *Limnol. Oceanogr.*, **19**, 881–888.

**Pasciak, W.J. and Gavis, J.** (1975) Transport limited nutrient uptake rates in Ditylum. *Limnol. Oceanogr.*, **20**, 604–617.

**Paz, Y., Katz, A. and Pick, U.** (2007) A multicopper ferroxidase involved in iron binding to transferrins in Dunaliella salina plasma membranes. *J. Biol. Chem.*, **282**, 8658–66.

**Peers, G., Quesnel, S.-A. and Price, N.M.** (2005) Copper requirements for iron acquisition and growth of coastal and oceanic diatoms. *Limnol. Oceanogr.*, **50**, 1149–1158.

**Petit, J.M., Wuytswinkel, O. van, Briat, J.F. and Lobréaux, S.** (2001) Characterization of an iron-dependent regulatory sequence involved in the transcriptional control of AtFer1 and ZmFer1 plant ferritin genes by iron. *J. Biol. Chem.*, **276**, 5584–90.

**Pfeuty, B., Thommen, Q., Corellou, F., Djouani-Tahri, E.B., Bouget, F.-Y. and Lefranc, M.** (2012) Circadian clocks in changing weather and seasons: lessons from the picoalga Ostreococcus tauri. *Bioessays*, **34**, 781–90.

**Picard, V., Govoni, G., Jabado, N. and Gros, P.** (2000) Nramp 2 (DCT1/DMT1) expressed at the plasma membrane transports iron and other divalent cations into a calcein-accessible cytoplasmic pool. *J. Biol. Chem.*, **275**, 35738–45.

**Posey, J.E. and Gherardini, F.C.** (2000) Lack of a Role for Iron in the Lyme Disease Pathogen. *Sci.* , **288** , 1651–1653.

**Raven, J.A., Evans, M.C.W. and Korb, R.E.** (1999) The role of trace metals in photosynthetic electron transport in O2 -evolving organisms. *Photochem. Photobiol.*, **60**, 111–149.

**Ravet, K., Touraine, B., Boucherez, J., Briat, J.-F., Gaymard, F. and Cellier, F.** (2009) Ferritins control interaction between iron homeostasis and oxidative stress in Arabidopsis. *Plant J.*, **57**, 400–12.

**Reinhardt, I., Haebel, S., Herbik, A. and Buckhout, T.J.** (2006) Proteomic Studies under Iron Stress: Iron Deficiency-Induced Regulation of Protein Synthesis in the Green Alga Chlamydomonas reinhardtii. In L. Barton and J. Abadia, eds. *Iron Nutrition in Plants and Rhizospheric Microorganisms SE - 19*. Springer Netherlands, pp. 371–393.

**Robbens, S., Derelle, E., Ferraz, C., Wuyts, J., Moreau, H. and Peer, Y. Van de** (2007) The complete chloroplast and mitochondrial DNA sequence of Ostreococcus tauri: organelle genomes of the smallest eukaryote are examples of compaction. *Mol. Biol. Evol.*, **24**, 956–68.

**Robinson, N.J., Procter, C.M., Connolly, E.L. and Guerinot, M.L.** (1999) A ferric-chelate reductase for iron uptake from soils. *Nature*, **397**, 694–7.

**Roche, J. La, Boyd, P.W., McKay, R. and Geider, R.J.** (1996) Flavodoxin as an in situ marker for iron stress in phytoplankton. *Nature*, **382**, 802–805.

**Rodríguez, F., Derelle, E., Guillou, L., Gall, F. Le, Vaulot, D. and Moreau, H.** (2005) Ecotype diversity in the marine picoeukaryote Ostreococcus (Chlorophyta, Prasinophyceae). *Environ. Microbiol.*, **7**, 853–9.

**Rue, E. and Bruland, K.** (2001) Domoic acid binds iron and copper: a possible role for the toxin produced by the marine diatom Pseudo-nitzschia. *Mar. Chem.*, **76**, 127–134.

**Rueter, J.G. and Ades., D.R.** (1987) The role of iron nutrition in photosynthesis and nitrogen assimilation in Scenedesmus quadricauda (Chlorophyceae). *J. Phycol.*, **23**, 452–457.

**Saito, M. a, Bertrand, E.M., Dutkiewicz, S., Bulygin, V. V, Moran, D.M., Monteiro, F.M., Follows, M.J., Valois, F.W. and Waterbury, J.B.** (2011) Iron conservation by reduction of metalloenzyme inventories in the marine diazotroph Crocosphaera watsonii. *Proc. Natl. Acad. Sci. U. S. A.*, **108**, 2184–9.

**Saito, M. a, Noble, A.E., Tagliabue, A., Goepfert, T.J., Lamborg, C.H. and Jenkins, W.J.** (2013) Slow-spreading submarine ridges in the South Atlantic as a significant oceanic iron source. *Nat. Geosci.*, **6**, 775–779.

**Salomé, P.A., Oliva, M., Weigel, D. and Krämer, U.** (2013) Circadian clock adjustment to plant iron status depends on chloroplast and phytochrome function. *EMBO J.*, **32**, 511–23.

**Santana-Casiano, J.M., González-Dávila, M., González, A.G., Rico, M., López, A. and Martel, A.** (2014) Characterization of phenolic exudates from Phaeodactylum tricornutum and their effects on the chemistry of Fe(II)–Fe(III). *Mar. Chem.*, **158**, 10–16.

**Sarthou, G., Vincent, D., Christaki, U., Obernosterer, I., Timmermans, K.R. and Brussaard, C.P.D.** (2008) The fate of biogenic iron during a phytoplankton bloom induced by natural fertilisation: Impact of copepod grazing. *Deep Sea Res. Part II Top. Stud. Oceanogr.*, **55**, 734–751.

**Schaffer, R., Ramsay, N., Samach, a, Corden, S., Putterill, J., Carré, I. a and Coupland, G.** (1998) The late elongated hypocotyl mutation of Arabidopsis disrupts circadian rhythms and the photoperiodic control of flowering. *Cell*, **93**, 1219–29.

**Shaked, Y., Kustka, A. and Morel, F.** (2005) A general kinetic model for iron acquisition by eukaryotic phytoplankton. *Limnol. Oceanogr.*, **50**, 872–882.

**Shi, H., Bencze, K.Z., Stemmler, T.L. and Philpott, C.C.** (2008) A cytosolic iron chaperone that delivers iron to ferritin. *Science (80-. ).*, **320**, 1207–10.

**Shi, T., Ilikchyan, I., Rabouille, S. and Zehr, J.P.** (2010) Genome-wide analysis of diel gene expression in the unicellular N(2)-fixing cyanobacterium Crocosphaera watsonii WH 8501. *ISME J.*, **4**, 621–32.

**Shi, T., Sun, Y. and Falkowski, P.G.** (2007) Effects of iron limitation on the expression of metabolic genes in the marine cyanobacterium Trichodesmium erythraeum IMS101. *Environ. Microbiol.*, **9**, 2945–56.

**Six, C., Finkel, Z., Rodríguez, F. and Marie, D.** (2008) Contrasting photoacclimation costs in ecotypes of the marine eukaryotic picoplankter Ostreococcus. *Limnol. Oceanogr.*, **53**, 255–265.

**Somerville, G., Mikoryak, C. and Reitzer, L.** (1999) Physiological characterization of Pseudomonas aeruginosa during exotoxin A synthesis: glutamate, iron limitation, and aconitase activity. *J. Bacteriol.*, **181**, 1072–1078.

**Sparla, F., Bagnaresi, P., Scagliarini, S. and Trost, P.** (1997) NADH:Fe(III)-chelate reductase of maize roots is an active cytochrome b5 reductase. *FEBS Lett.*, **414**, 571–575.

**Strayer, C., Oyama, T., Schultz, T.F., Raman, R., Somers, D.E., Más, P., Panda, S., Kreps, J.A. and Kay, S.A.** (2000) Cloning of the Arabidopsis Clock Gene TOC1, an Autoregulatory Response Regulator Homolog. *Sci.* , **289** , 768–771.

**Strozycki, P.M., Szymanski, M., Szczurek, A., Barciszewski, J. and Figlerowicz, M.** (2010) A new family of ferritin genes from Lupinus luteus--comparative analysis of plant ferritins, their gene structure, and evolution. *Mol. Biol. Evol.*, **27**, 91–101.

**Strzepek, R.F. and Harrison, P.J.** (2004) Photosynthetic architecture differs in coastal and oceanic diatoms. *Nature*, **431**, 689–692.

**Strzepek, R.F., Hunter, K. a., Frew, R.D., Harrison, P.J. and Boyd, P.W.** (2012) Iron-light interactions differ in Southern Ocean phytoplankton. *Limnol. Oceanogr.*, **57**, 1182–1200.

**Strzepek, R.F., Maldonado, M.T., Hunter, K. a., Frew, R.D. and Boyd, P.W.** (2011) Adaptive strategies by Southern Ocean phytoplankton to lessen iron limitation: Uptake of organically complexed iron and reduced cellular iron requirements. *Limnol. Oceanogr.*, **56**, 1983–2002.

**Sunda, W.G. and Huntsman, S.A.** (1997) Interrelated influence of iron, light and cell size on marine phytoplankton growth. *Nature*, **2051**, 1193–1197.

**Sunda, W.G. and Huntsman, S.A.** (1995) Iron uptake and growth limitation in oceanic and coastal phytoplankton. *Mar. Chem.*, **50**, 189–206.

**Sutak, R., Botebol, H., Blaiseau, P.-L., Léger, T., Bouget, F.-Y., Camadro, J.-M. and Lesuisse, E.** (2012) A comparative study of iron uptake mechanisms in marine microalgae: iron binding at the cell surface is a critical step. *Plant Physiol.*, **160**, 2271–84.

**Sutak, R., Slapeta, J., San Roman, M., Camadro, J.-M. and Lesuisse, E.** (2010) Nonreductive iron uptake mechanism in the marine alveolate Chromera velia. *Plant Physiol.*, **154**, 991–1000.

**Tagliabue, A., Sallée, J.-B., Bowie, A.R., Lévy, M., Swart, S. and Boyd, P.W.** (2014) Surface-water iron supplies in the Southern Ocean sustained by deep winter mixing. *Nat. Geosci.*, **7**, 314–320.

**Tarantino, D., Petit, J.-M., Lobreaux, S., Briat, J.-F., Soave, C. and Murgia, I.** (2003) Differential involvement of the IDRS cis-element in the developmental and environmental regulation of the AtFer1 ferritin gene from Arabidopsis. *Planta*, **217**, 709–16.

**Tardy, F.** (1997) Localisation et fonctions du cycle des xanthophylles dans les chloroplastes des plantes supérieures.

**Terzulli, A. and Kosman, D.J.** (2010) Analysis of the high-affinity iron uptake system at the Chlamydomonas reinhardtii plasma membrane. *Eukaryot. Cell*, **9**, 815–26.

**Thingstad, T.F.** (2000) Elements of a theory for the mechanisms controlling abundance, diversity, and biogeochemical role of lytic bacterial viruses in aquatic systems. *Limnol. Oceanogr.*, **45**, 1320–1328.

**Thommen, Q., Pfeuty, B., Morant, P.-E., Corellou, F., Bouget, F.-Y. and Lefranc, M.** (2010) Robustness of circadian clocks to daylight fluctuations: hints from the picoeucaryote Ostreococcus tauri. *PLoS Comput. Biol.*, **6**, e1000990.

**Thompson, A.W., Huang, K., Saito, M. a and Chisholm, S.W.** (2011) Transcriptome response of high- and low-light-adapted Prochlorococcus strains to changing iron availability. *ISME J.*, **5**, 1580–94.

**Torres, M.A. and Dangl, J.L.** (2005) Functions of the respiratory burst oxidase in biotic interactions, abiotic stress and development. *Curr. Opin. Plant Biol.*, **8**, 397–403.

**Tortell, P.D., Maldonado, M.T., Granger, J. and Price, N.M.** (1999) Marine bacteria and biogeochemical cycling of iron in the oceans. *FEMS Microbiol. Ecol.*, **29**, 1–11.

**Toulza, E., Tagliabue, A., Blain, S. and Piganeau, G.** (2012) Analysis of the global ocean sampling (GOS) project for trends in iron uptake by surface ocean microbes. *PLoS One*, **7**, e30931.

**Vert, G., Barberon, M., Zelazny, E., Séguéla, M., Briat, J.-F. and Curie, C.** (2009) Arabidopsis IRT2 cooperates with the high-affinity iron uptake system to maintain iron homeostasis in root epidermal cells. *Planta*, **229**, 1171–9.

**Vert, G. and Grotz, N.** (2002) IRT1, an Arabidopsis transporter essential for iron uptake from the soil and for plant growth. *Plant Cell*, **14**, 1223–1233.

**Wade, V., Treffry, A., Laulhère, J., Bauminger, E.R., Cleton, M.I., Mann, S., Briat, J.-F. and Harrison, P.M.** (1993) Structure and composition of ferritin cores from pea seed(Pisum sativum). *Biochim. Biophys. Acta-Protein Struct.*, **1161**, 91–96.

**Waldo, G.S., Wright, E., Whang, Z.H., Briat, J.F., Theil, E.C. and Sayers, D.E.** (1995) Formation of the ferritin iron mineral occurs in plastids. *Plant Physiol.*, **109**, 797–802.

**Wang, Z.Y. and Tobin, E.M.** (1998) Constitutive expression of the CIRCADIAN CLOCK ASSOCIATED 1 (CCA1) gene disrupts circadian rhythms and suppresses its own expression. *Cell*, **93**, 1207–17.

**Waters, E.** (2003) Molecular adaptation and the origin of land plants. *Mol. Phylogenet. Evol.*, **29**, 456–463.

**Williams, R.G. and Follows, M.J.** (2011) *Ocean dynamics and the carbon cycle: Principles and mechanisms*, Cambridge University Press.

**Woolum, J.C.** (1991) A Re-Examination of the Role of the Nucleus in Generating the Circadian Rhythm in Acetabularia. *J. Biol. Rhythm.* , **6** , 129–136.

**Wu, H., Roy, S., Alami, M., Green, B.R. and Campbell, D. a** (2012) Photosystem II Photoinactivation, Repair and Protection in Marine Centric Diatoms. *Plant Physiol.*, **160**, 464–476.

**Wu, J., Boyle, E., Sunda, W.G. and Wen, L.-S.** (2001) Soluble and Colloidal Iron in the Oligotrophic North Atlantic and North Pacific. *Science (80-. ).*, **293**, 847–849.

**Xoconostle-Cázares, B., Ruiz-Medrano, R. and Lucas, W.J.** (2000) Proteolytic processing of CmPP36, a protein from the cytochrome b(5) reductase family, is required for entry into the phloem translocation pathway. *Plant J.*, **24**, 735–47.

**Yi, Y. and Guerinot, M.L.** (1996) Genetic evidence that induction of root Fe (III) chelate reductase activity is necessary for iron uptake under iron deficiency†. *Plant J.*, **10**, 835–844.

**Yruela, I.** (2013) Transition metals in plant photosynthesis. *Metallomics*.

**Yun, C.-W., Bauler, M., Moore, R.E., Klebba, P.E. and Philpott, C.C.** (2001) The Role of the FRE Family of Plasma Membrane Reductases in the Uptake of Siderophore-Iron in Saccharomyces cerevisiae . *J. Biol. Chem.* , **276** , 10218–10223.

**Zhang, Y., Liu, G. and Shen, J.** (2005) Hydrogen production in batch culture of mixed bacteria with sucrose under different iron concentrations. *Int. J. Hydrogen Energy*, **30**, 855–860.

**Zhu, S.-H. and Green, B.R.** (2010) Photoprotection in the diatom Thalassiosira pseudonana: role of LI818-like proteins in response to high light stress. *Biochim. Biophys. Acta*, **1797**, 1449–57.

# V.**Annexe**

# 1 REVIEW: Transcriptional versus non-transcriptional clocks: A case study in *Ostreococcus*

François-Yves Bouget, Marc Lefranc, Quentin Thommen , Benjamin Pfeuty , Jean-Claude Lozano, Philippe Schatt, Hugo Botebol, Valérie Vergé

Marine Genomics 14 (2014) 17–22

Marine Genomics

Volume 14, April 2014, Pages 17-22

Marine Rhythms

Review

# Transcriptional versus non-transcriptional clocks: A case study in *Ostreococcus*

François-Yves Bouget [a,b,*], Marc Lefranc [c], Quentin Thommen [c], Benjamin Pfeuty [c], Jean-Claude Lozano [a,b], Philippe Schatt [a,b], Hugo Botebol [a,b], Valérie Vergé [a,d]

[a] Sorbonne Universités, Université Pierre et Marie Curie (Paris 06), Observatoire Océanologique, F-66651 Banyuls/Mer, France
[b] Centre National de la Recherche Scientifique, Unité Mixte de Recherche, UMR7621, LOMIC, Laboratoire d'Océanographie Microbienne, F-66651 Banyuls/Mer, France
[c] Laboratoire de Physique des Lasers, Atomes et Molécules, Université Lille 1, CNRS, Unité Mixte de Recherche 8523, Unité de Formation et de Recherche de Physique, Villeneuve d'Ascq, France
[d] Centre National de la Recherche Scientifique Unité Mixte de Service, UMS2348, F-66651 Banyuls/Mer, France

ARTICLE INFO

*Article history:*
Received 21 October 2013
Received in revised form 6 January 2014
Accepted 23 January 2014
Available online 7 February 2014

*Keywords:*
Circadian clock
*Ostreococcus*
Photoreceptor
Marine phytoplankton
Systems biology

ABSTRACT

Circadian rhythms are ubiquitous on earth from cyanobacteria to land plants and animals. Circadian clocks are synchronized to the day/night cycle by environmental factors such as light and temperature. In eukaryotes, clocks rely on complex gene regulatory networks involving transcriptional regulation but also post-transcriptional and post-translational regulations. In multicellular organisms clocks are found at multiple levels from cells to organs and whole organisms, making the study of clock mechanisms more complex. In recent years the picoalga *Ostreococcus* has emerged as a new circadian model organism thanks to its reduced gene redundancy and its minimalist cellular organization. A simplified version of the "green" plant clock, involving the master clock genes *TOC1* and *CCA1*, has been revealed when the functional genomics and mathematical model approaches were combined.
Specific photoreceptors such as a blue light sensing LOV histidine kinase mediate light input to the *Ostreococcus* clock. Non-transcriptional redox rhythms have also been identified recently in *Ostreococcus* and human red blood cells. This review highlights the progress made recently in the understanding of circadian clock architecture and function in *Ostreococcus* in the context of the marine environment.



**Contents**



## 1. Introduction

Most living organisms are exposed to changes in light and temperature in a 24 hour period due to the rotation of the earth around its axis. Light is the main source of energy for photosynthetic organisms which

* Corresponding author at: Centre National de la Recherche Scientifique, Unité Mixte de Recherche, UMR7621, LOMIC, Laboratoire d'Océanographie Microbienne, F-66651, Banyuls/Mer, France.
*E-mail address:* fy.bouget@obs-banyuls.fr (F.-Y. Bouget).

1874-7787/$ – see front matter © 2014 Elsevier B.V. All rights reserved.
http://dx.doi.org/10.1016/j.margen.2014.01.004

constitute the basis of food chains in terrestrial and oceanic environments. Light, however, can be detrimental to cells as UV radiation damages genetic material. Living organisms have evolved endogenous clocks, called circadian clocks, which allow them to best benefit from the 24 hour day/night cycle. In photosynthetic organisms, for example, the transcription of photosynthesis proteins is under circadian control and begins before dawn so that photosynthesis can start as soon as light appears (Harmer and Kay, 2000; Monnier et al., 2010). As well as anticipating periodic environmental changes the circadian clock orchestrates biological processes during the day/night cycle thus avoiding incompatible processes occurring at the same time. During the cell division cycle DNA should not be exposed to reactive oxygen species or damaging UV light both of which can induce mutations. Circadian regulation of cell division has been evidenced in several microalgae including *Ostreococcus* and *Chlamydomonas* (Moulager et al., 2007; Goto and Johnson, 1995). Furthermore, circadian rhythms of survival to UV radiation have been observed in *Chlamydomonas*, the cells being most vulnerable at the time of nuclear division (Nikaido and Johnson, 2000). This suggests that light-sensitive processes are phased along the day/night cycle to avoid sunlight induced damage.

Although the earth rotation period is constant from day to day, the relative day to night length, the photoperiod, varies during the year, the winter/summer differences being more pronounced at high latitudes. A key feature of circadian clocks is their ability to be entrained to a wide range of photoperiods. This feature is called flexibility. The clock, however, must also be resistant (or robust) to noisy light input not linked to earth rotation. These light fluctuations usually arise from weather conditions (e.g. clouds in the sky) or factors that alter the water column mixing for phytoplanktonic microorganisms. The circadian clock can also be entrained by temperature cycles, but its free-running period is less sensitive to temperature variations so that seasonal changes in temperature have little effect on circadian rhythms. Last but not the least, persistence under free running conditions with a period of ~24 h is the main property of circadian rhythms.

Circadian rhythms have been observed at the cellular level in animals, plants and bacteria. The emergence of genetic approaches in model organisms has enabled scientists to identify first clock mutants (e.g. long-period, short-period of even arrhythmic), then clock genes. Twenty years after the initial genetic studies in model organisms, the molecular clock architecture of the circadian clock is well established in several organisms including *Drosophila* (insects), mice (mammals), *Neurospora* (fungi) and *Arabidopsis* (plants). The nature of circadian rhythms, however, is complex in multicellular organisms, since rhythms and underlying clocks are observed not only at the cellular level but also at the organ and whole organism levels. Furthermore these clocks can be uncoupled, for example during jetlag. This adds an additional level of complexity when studying the circadian clock at the molecular level.

## 2. *Ostreococcus* a new circadian model organism

In recent years the green picoalga *Ostreococcus tauri* has emerged as a new model organism for functional genomics and systems biology approaches. This minimalist cell of only 1 μm in diameter has only one chloroplast and a single mitochondrion in addition to the nucleus. The genome of only 12.6 Mb (the size of *Saccharomyces cerevisiae* genome) is the most compact of known eukaryotic genomes with intergenic regions smaller than 200 bp (Derelle et al., 2006). The gene families are extremely reduced with very little gene redundancy facilitating the use of reverse genetic approaches. Molecular tools based on genetic transformation, such as gene functional analysis by overexpression/knockdown or luciferase reporter fusions have been used to monitor circadian rhythms and analyze the function.

Besides the molecular tools described above, *Ostreococcus* has many advantages for circadian studies. Cells can be easily synchronized with the day/night cycle. Under 12:12 light/dark cycles, most biological processes are temporally orchestrated. In *Ostreococcus*, Bayesian Fourier clustering analysis has revealed clusters of co-regulated genes involved in specific biological processes expressed rhythmic of candidate genes (Corellou et al., 2009; Moulager et al., 2010; Djouani-Tahri et al., 2011a; Heijde et al., 2010) along the day/night cycle. The extent of this is unprecedented when compared to other eukaryotes. (Monnier et al., 2010). This genome-wide transcriptomic study of gene expression indicates that transcriptional regulations play a key role in the diurnal/circadian regulation of gene expression. During the night genes involved in general transcription, ribosome synthesis and translation are successively transcribed. From dawn to dusk, clusters are enriched in genes involved in photosynthesis, response to UV stress (midday), DNA replication and finally, cell division at the end of the day (Moulager et al., 2007; Monnier et al., 2010). Rhythms of cell division and the transcription of key cell cycle regulators persist under constant light, consistent with a circadian control of cell division (Corellou et al., 2009; Djouani-Tahri et al., 2011a; Moulager et al., 2007; Heijde et al., 2010). Cell cycle related proteins such as dynamin and kinesin were also found to be upregulated during the daylight-to-darkness transition in shotgun proteomic analysis (Le Bihan et al., 2011).

## 3. A simple transcriptional clock

### 3.1. A two-gene oscillator

The overall architecture of transcriptional circadian clocks is conserved between kingdoms although the main molecular players are different. The ~24 hour rhythm results from transcriptional translational feedback loops in which clock components activate the synthesis of their own repressors. Synthetic biology is able to reproduce rhythms based on simple genetic circuits such as the represillator in bacteria (Elowitz and Leibler, 2000). The resulting oscillations, however, are noisy and the periods much shorter than 24 h. Delays resulting from translational regulation, protein degradation, post-translational modifications and subcellular localization of clock components allow the circadian period to extend to ~24 h in mathematical models. Although a simple oscillator should be sufficient to generate a rhythm, the clocks of model organisms such as *Drosophila* or *Arabidopsis* have been shown to rely on multiple coupled loops (e.g. morning and evening loops) which allow more flexibility (Troein et al., 2009).

Extensive searches have been performed in silico to identify putative conserved clock components in *Ostreococcus*, taking advantage of the sequenced genome. Only two putative candidates with homology to Time of CAB expression1 (TOC1) and Circadian Clock associated1 (CCA1) transcription factors have been identified. These were also the first two clock components identified in plants (Strayer et al., 2000; Green and Tobin, 1999). It was proposed initially that TOC1 and CCA1 interact in a simple negative feedback loop in which CCA1 represses the transcription of *TOC1*,TOC1 TOC1 activates the synthesis of *CCA1* (Alabadí et al., 2001). However *TOC1* transcription is thought to begin once CCA1 has been degraded. This model has been challenged further by genetic analysis and modeling approaches (reviewed in Carré and Veflingstad, 2013). The current outline of the *Arabidopsis* clock relies on three coupled loops, and unlike the above model, TOC1 is a repressor of *CCA1* transcription (Huang et al., 2012; Gendron et al., 2012). In *Ostreococcus* CCA1 has been shown to bind in vitro a perfectly conserved AAAATATCT evening element motif, found in the promoter of *TOC1*, which is required for circadian expression of *TOC1* (Corellou et al., 2009). Overexpression of CCA1 leads to a downregulation of *TOC1* consistent with a repressing activity of CCA1. CCA1 repression by antisense had no effect on circadian rhythms of TOC1 in constant light. However, it caused aberrant patterns of rhythmic expression under 6:6 cycles, suggesting altered circadian regulation of TOC1 responses to light. This suggests that either CCA1 repression was not sufficient to destabilize the TOC1/CCA1 loop in the antisense lines studied or that

another component compensated for the reduced levels of CCA1. In *Ostreococcus* either downregulation or overexpression of TOC1 results in strong arrhythmic phenotypes. Such phenotypes must be carefully interpreted as arrhythmic phenotypes due to abnormal light responses masking the function of the central circadian clock. A phosphate inducible expression system was used to drive ectopic expression of *TOC1*. Phosphate addition to the medium caused downregulation of TOC1 overexpression and allow circadian clock function to resume (Djouani-Tahri et al., 2011b). The CCA1-luc luminescence peak occurred at fixed times after phosphate addition in all conditions. This result showing that phosphate sensitivity is not gated by the circadian system, suggests that reducing the level of TOC1 overexpression has an immediate effect to restart the function of the clock, confirming the central role of TOC1 in the circadian clock of *Ostreococcus*.

In summary, TOC1 and CCA1 expression profiles and functional analysis are compatible with TOC1 being an activator of *CCA1* transcription around dusk, CCA1 repressing the transcription of *TOC1* (Fig. 1A). However biochemical evidence for a direct activation of *CCA1* transcription by TOC1 is still lacking. The patterns of expression of *TOC1* and *CCA1* are clearly different between *Ostreococcus* and *Arabidopsis* and the clock circuit is likely to be much simpler is *Ostreococcus*, however one cannot completely rule out that in *Ostreococcus*, like in *Arabidopsis*, TOC1 is a repressor of *CCA1* transcription.

### 3.2. A flexible and robust TOC1/CCA1 transcriptional clock

TOC1 belongs to the family of pseudo-response regulators (PRR). In *Arabidopsis*, several PRRs related to TOC1 participate in morning and evening oscillators (Fujiwara et al., 2008; Para et al., 2007). CCA1 is a MYB transcription factor of the REVEILLE family of which there are 9 members including Long Hypocotyl (LHY) (Kim and Carre, 2002). Only the two functional plant-like clock genes *TOC1* and *CCA1* have been identified in *Ostreococcus*. This raises the question: can a simple CCA1/TOC1 transcriptional translational feedback loop form a functional circadian clock in this organism? Mathematical modeling proved to be helpful in addressing this question as it was found that a minimalist mathematical model of the CCA1/TOC1 transcriptional translation feedback loop could accurately reproduce the expression profile of *TOC1* and *CCA1* transcripts and proteins under light/dark cycles (Thommen et al., 2010; Morant et al., 2010).

An unexpected but far-reaching conclusion of these works was that the data could be matched without incorporating any light-sensing mechanism in the model, exactly as if the clock was free-running. However, it is well known that such a mechanism is required to entrain the clock to the day/night cycle and ensure a precise phase relationship between them. The paradox was resolved by a mathematical analysis, which showed that the entrainment mechanism can be effective yet remain "invisible" if the clock is sensitive to light only in specific time intervals (e.g. at dusk and dawn), and unresponsive to it during most of the daylight period (Thommen et al., 2010; Pfeuty et al., 2012). This most likely reflects a strategy to protect the clock from daylight fluctuations (Thommen et al., 2010), which seems to be at work in many organisms (Pfeuty et al., 2012). This clock is not only robust but also highly flexible as the expression patterns of TOC1 and CCA1 vary markedly with daylight duration (photoperiod) so as to adjust clock signals according to season. Remarkably, the minimal free-running clock model can also accurately reproduce TOC1 and CCA1 time profiles within a wide range of photoperiods provided that certain kinetic constants are allowed to take different values for different photoperiods in the adjustment (Thommen et al., 2012). This result suggests that the clock is under control of slow feedback loops serving as photoperiod sensors, which is consistent with the observation that experimental expression patterns depend on photoperiod. For example, a simple way to implement such a mechanism is when a protein is expressed only during daylight and is relatively stable. Its level will then reflect photoperiod and may be used to affect some kinetic constants of

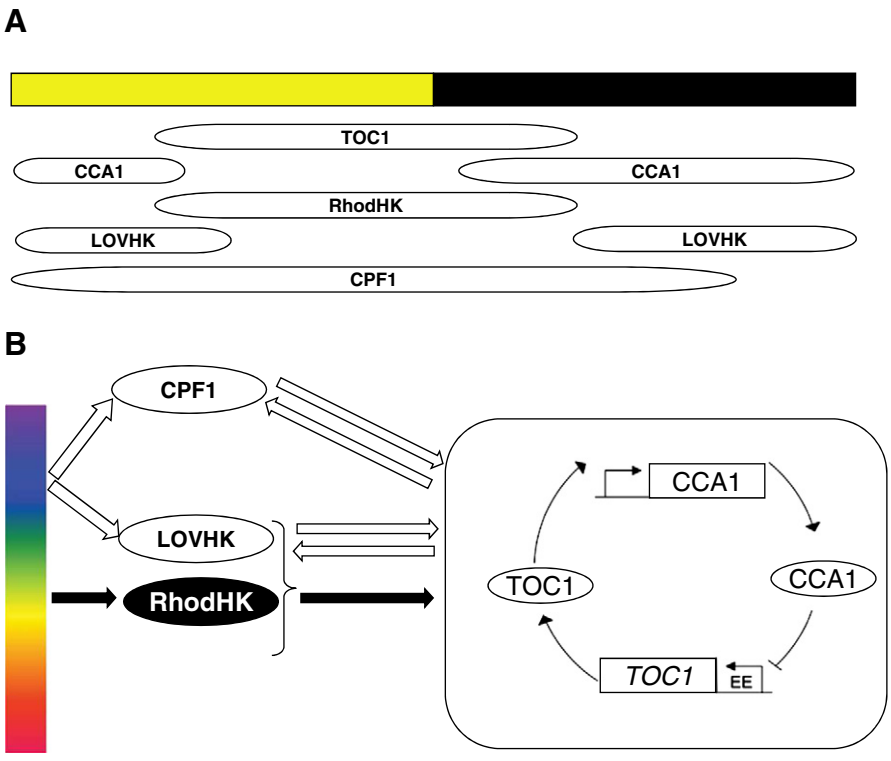


**Fig. 1.** The circadian clock of *Ostreococcus*. (A) Windows of expression of clock genes under 12:12 day/night cycles inferred from microarray expression data (Monnier et al., 2010). (B) Schematic representation of the TOC1/CCA1 transcriptional translational feedback loop and light input pathways to the clock. CCA1 represses *TOC1* transcription by binding to a conserved EE motif in the *TOC1* promoter. TOC1 would activate the transcription of *CCA1*. CPF1 and LOVK are blue light photoreceptors required for clock function. RhodHK is a putative rhodopsin photoreceptor which may also, like LOVHK, sense and transduce light signal to the clock, in a TCS signaling pathway.

the core TOC1-CCA1 loop. More elaborate mechanisms measuring coincidence between expression patterns and daylight period can also be imagined (Imaizumi and Kay, 2006). Taken together, these findings indicate that the clock machinery is able to enforce robustness to daylight fluctuations throughout the year in spite of the flexibility observed. Interestingly, the above conclusions could be reached without having to identify the actual light-sensing mechanisms.

A fully detailed model of the TOC1/CCA1 loop was also produced by fitting multiple transcriptional and translational luciferase patterns of expression for *TOC1* and *CCA1* (Troein et al., 2011). In addition to reproducing the complex profiles of expression under a wide range of photoperiods, this model was also able to predict the transient behavior of the clock when complicated light regimes were applied. Despite its apparent simplicity, this model requires multiple assumptions to reproduce and predict experimental patterns of expression. These include: (i) a light accumulator which regulates the accumulation of TOC1 from dawn, (ii) a light dependent degradation of CCA1 both in the cytosol and the nucleus, (iii) a light-dependent degradation and activation of TOC1 which restricts the profile of active TOC1 at the light/dark transition. This dark dependent proteasomal-degradation of TOC1 was demonstrated experimentally using the proteasome inhibitor MG132 (Djouani-tahri et al., 2010). Furthermore the degradation of CCA1 appears to be under circadian clock-control. However, whether this mathematical model satisfies the properties unveiled by the other modeling approaches has not yet been tested.

In summary, both reduced and developed models indicate that a simple TOC1/CCA1 transcriptional translational feedback loop accounts for the main clock properties including robustness to light fluctuations and flexibility. They also imply that clock components are sensitive to light directly and indirectly and that coupling to light must be restricted in time over the day/night cycle. Gating of light entry to the transcriptional translational feedback loops could be achieved by a clock-dependent regulation at specific times of the day.

## 4. Light input to the transcriptional clock

Light is the main environmental cue that synchronizes the circadian clock to the day/night cycle. Several classes of specific photoreceptors mediate light input to the clock in animals, fungi and plants. These include the cryptochromes, which are blue light specific, the phytochromes, which are red light sensing in plants and the rhodopsins, which can sense a wide range of wavelength from blue to green in animals.

### 4.1. Cryptochromes

The cryptochrome photoreceptors (CRY) share a common origin with DNA photolyases which are involved in DNA repair (Ahmad and Cashmore, 1993). The *Ostreococcus* genome has four putative cryptochromes (OtCPF) and a cyanobacteria type of Cryptochrome DASH named OtCPF2 (Heijde et al., 2010). OtCPF1 and OtCPF2 have been further characterized. Both proteins bind the flavin cofactor FAD and display a fluorescence emission spectrum characteristic of cryptochromes (absorption at 450 nm, maximum emission at 532 nm). OtCPF1 has 6-4 photolyase activity whereas OtCPF2 is a CPD photolyase. OtCPF1 was shown to be under circadian control and knockdown of OtCPF1 leads to period lengthening of the CCA1-luc circadian reporter, suggesting that OtCPF1 is required for circadian function in *Ostreococcus* (Heijde et al., 2010).

In mammals the CRY protein is a central clock protein complex that acts as an inhibitor of the CLOCK:BMAL transcription factor. It is interesting that OtCPF1 also inhibits the CLOCK/BMAL mediated transcriptional activity of an E box containing promoter in vitro, as previously observed in the diatom *Phaeodactylum* (Coesel et al., 2009). The relevance of these observations to circadian clock regulation is not, however, clear in microalgae since CLOCK and BMAL components are neither present in *Ostreococcus* nor in *Phaeodactylum*. CLOCK/BMAL are BHLH-type transcription factors widely distributed in eukaryotes and play a role in animal and plant circadian clocks. Since *Ostreococcus* contains a single BHLH transcription factor, it would be interesting to determine if OtCPF1 inhibits its transcriptional activity.

### 4.2. LOV-histidine kinase

The LOV (Light, Oxygen, or Voltage sensing) domain binds a flavin as cofactor (Christie et al., 1999). In response to blue light a blue-shifted cysteine (C4-a)-thiol photoadduct is formed in proteins such as phototropins (Salomon et al., 2000). This process is fully reversible in darkness. The rate of adduct reversion in the dark defines the photocycle. The LOV domain is found in a number of circadian clock proteins. In *Neurospora*, the LOV-containing proteins WC1 and WC2 (White Collar 1 and White Collar 2) are blue-light receptors which mediate light input to the circadian clock through direct binding to the *frequency* (*frq*) promoter (Froehlich et al., 2002). In *Arabidopsis*, ZTL (Zeitlupe), LKP2 (LOV Kelch repeat Protein 2) and FKF1 (Flavin-binding, Kelch repeat, F-box) are involved in clock regulation and photoperiod-dependent flowering (Demarsy and Fankhauser, 2009).

LOV containing histidine kinase (LOVHK) has been discovered in a wide range of bacteria (Krauss et al., 2009). Recently LOVHKs were identified in silico in green algae including *Ostreococcus* and *Chlamydomonas* (Djouani-Tahri et al., 2011a). Functional analysis of a LOVHK from *O. tauri* indicates that it operates as a new class of eukaryotic blue-light receptor with a fast photocycle. LOVHK is required for sustaining circadian rhythms under blue light since knockdown or overexpression of *LOVHK* results in arrhythmia of the circadian reporter CCA1-Luc under constant blue light. In contrast circadian function in blue light is not affected by overexpression of a photochemically inactive form of LOVHK. Under red light, however, *LOVHK* knockdown lines also displayed circadian defects, suggesting that either LOVHK serves to integrate different light qualities or that it plays a role in the clock independently of its blue light photoreceptor activity. In *Caulobacter*, LOVHK appears to be a redox sensor (Purcell et al., 2010). In *Ostreococcus*, such a redox sensor may be used to sense the metabolic status like the ldpA protein in cyanobacteria (Ivleva et al., 2005).

### 4.3. Different photoreceptors for different depths?

Besides cryptochromes and LOVHK, *O. tauri* contains another putative blue light photoreceptor of the phototropin family, a LOV serine/threonine kinase. Its circadian function remains to be determined (Heijde et al., 2010; Djouani-Tahri et al., 2011a). No red light phytochrome-like photoreceptor has been identified in silico in *O. tauri*. A rhodopsin-histidine kinase (RhodHK), is the only candidate for longer wavelength sensing. In *Drosophila*, rhodopsins are circadian photoreceptors which sense light qualities from blue to green and yellow (Klarsfeld et al., 2011).

Notably, *Ostreococcus* TOC1 may be a functional Response Regulator (RR), unlike its *Arabidopsis* homologue which lacks an essential Aspartate residue involved in Hisp-Asp two component systems (TCS) signaling pathways. In TCS, in response to specific environmental cues, HKs autophosphorylate on a conserved histidine residue. The phosphoryl group is then transferred to a conserved aspartate residue in downstream RR, either directly or via a histidine phospho-transfer protein (HPT). The number of putative TCS players is low in *O. tauri*. LOVHK and RhodHK are the only two histidine kinases present in the genome. In addition 5 putative RRs including TOC1 and a single HPT have been identified (Pfeuty et al., 2012). LOVHK and RhodHK may mediate distinct light qualities (e.g. blue and green to yellow) to the RR TOC1 in a light sensing TCS. Longer wavelengths could be sensed by the clock in the upper part of the water column predominantly by RhodHK. LOVHK, in contrast, would sense light at all depths of the euphotic zone, since blue light penetrates deeper in the sea. This light

sensing TCS could be used to track light intensity variations which occur normally over the day/night cycle while ignoring those which arise during water column mixing. Such a depth sensor would confer both robustness and flexibility to the circadian clock.

These two histidine kinases could, alternatively, be used to sense quantitative changes in light intensity at different times of the day/night cycle since LOVHK and RhodHK have distinct patterns of expression, the first peaking at dawn and the second at dusk. A hypothesis on how light input pathways may be connected to the TOC1/CCA1 oscillator is presented in Fig. 1.

LOVHK and CPF1 are blue light photoreceptors which are required for the circadian clock function (Fig. 1B). Their circadian regulation defines their phase of expression at specific times of the day. Conversely, the light input to the clock is likely to be gated by the photoreceptor pattern of expression. In response to specific wavelengths, such as blue light, LOVHK would become phosphorylated on a conserved histidine (his) residue. The phosphoresidue would be transferred to the conserved aspartate residue of the TOC1 receiver domain. RhodHK may similarly regulate TOC1 by phosphorylation in response to specific wavelengths sensed by the rhodopsin domain.

## 5. Non-transcriptional clocks

Until recently it was largely assumed that eukaryotic circadian clocks rely almost exclusively on transcriptional translational feedback loops and transcription factors were identified as central clock components in all model organisms. In the cyanobacteria *Synechococcus*, however, circadian rhythms of the KaiC protein phosphorylation are observed when transcription is inhibited. Remarkably the three purified KaiA, KaiB and KaiC proteins are able to resume circadian rhythms of KaiC in a test tube, demonstrating the existence of non-transcriptional clocks in this microorganism (Nakajima et al., 2005). A report in the 1980s about the polynucleated giant cell *Acetabularia* has indicated that non-transcriptional rhythms can exist in eukaryotes. It was observed that these cells maintain circadian rhythms of photosynthesis and chloroplast movement for several weeks after enucleation (Woolum, 1991). The relevance of this observation to other eukaryotes was questioned until recently.

As in *Synechococcus*, transcription ceases in *Ostreococcus* soon after transfer to constant darkness (O'Neill et al., 2011). When the cells were placed back under constant light, the rhythmicity of the *CCA1-Luc* was recovered. The phase of CCA1-Luc, however, was not reset by light ON but instead was dependent on the time of transfer to light, suggesting that an invisible non-transcriptional clock gated the response of CCA1-luc to the light ON signal.

Peroxiredoxins (PRX) are ubiquitous antioxidant enzymes found in eukaryotes that scavenge reactive oxygen species. In *Ostreococcus* the only PRX is localized in the chloroplast. Monitoring of PRX sulphonylation by Western blot analysis revealed circadian rhythms under constant darkness, i.e. in the absence of transcription (O'Neill et al., 2011). Such circadian rhythms have also been detected in human red blood cells which constitute naturally enucleated cells. Oxidation–reduction circadian cycles of PRX of this type are widely distributed among eukaryotes and prokaryotes (Edgar et al., 2012). In *Ostreococcus*, rhythms of PRX oxidation were also observed under constant light in WT cells and in a *CCA1-luc* reporter line (Edgar et al., 2012; O'Neill et al., 2011). Analysis of PRX levels under constant light revealed altered PRX rhythms in the long period *TOC1-luc* line relative to the *CCA1-luc* control line (O'Neill et al., 2011) and in the *TOC1oxCCA1:luc* arrhythmic mutant *TOC1oxCCA1-luc* relative to the Wild type cells (Wt) control (Edgar et al., 2012). Little differences, however, were observed between the free running period of *TOC1oxCCA1-luc* (18.8 h) and the Wt control (19.2 h). In these experiments, equal loading of proteins was checked by eye using the Rubisco small subunit as a loading control. We, therefore, performed a replicate experiment in which proteins of Wt cells grown under circadian conditions of constant light or constant darkness, were quantified and loaded on SDS-PAGE denaturing gels at the exact same concentration (Fig. 2). PRX levels of sulphonylation were quantified by Western blot analysis as previously described (O'Neill et al., 2011). Rhythmic patterns of PRX sulphonylations were observed under constant darkness (Fig. 2A) but not under constant light (Fig. 2B). On the basis of these results, reinvestigation of the patterns of PRX oxidation in clock mutants is indicated to assess the hierarchy between transcriptional and non-transcriptional clocks. Unfortunately knockdown/overexpression strategies cannot be used in constant darkness where robust circadian rhythms of PRX are observed since transcription ceases in this condition.

## 6. Future challenges and opportunities in *Ostreococcus* circadian research

Experimental results and modeling approaches both demonstrate that a two gene TOC1–CCA1 loop would be sufficient to account for the robustness and flexibility of the circadian clock in *Ostreococcus*. Mathematical models, however, require either a differential light input to the TOC1/CCA1 oscillator or even multiple light-dependent regulations of TOC1 and CCA1 (Thommen et al., 2010; Troein et al., 2011) suggesting that the clock may gate light input to its photoreceptors over the day/night cycle. The blue light photoreceptor LOVHK could play such a role since it is under circadian control and it required for

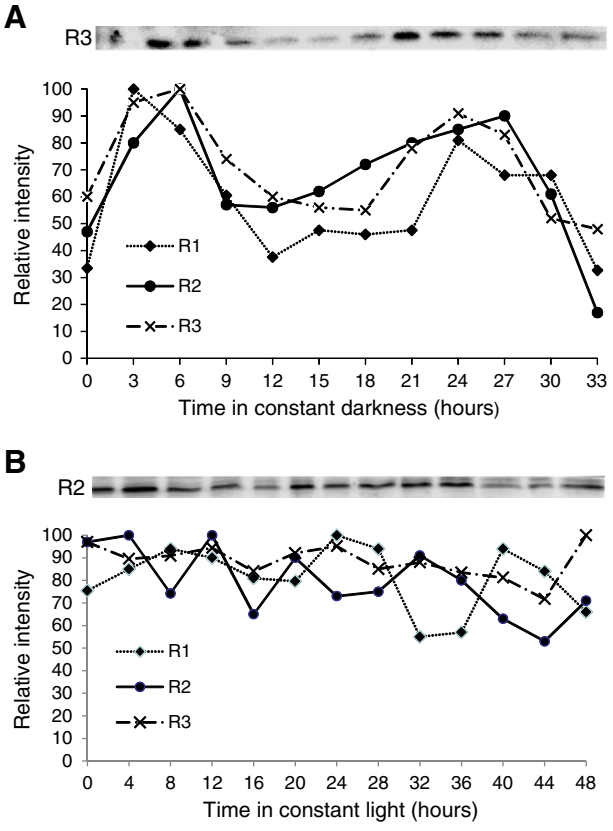


**Fig. 2.** Non-transcriptional rhythms of PRX sulphonylation in *Ostreococcus*. Cells were entrained under 12:12 day/night cycles before being released under constant darkness (A) or constant light (B). Proteins were extracted from 15 ml cultures sampled from 12 h after transfer to constant conditions, as previously described (O'Neill et al., 2011). Protein extracts were quantified in triplicate using BCA protein assay (Moulager et al., 2010). Five micrograms of proteins were loaded per lane. Gel migration and Western blot analysis were performed as previously described (O'Neill et al., 2011) using a polyclonal anti Peroxiredoxin-SO3 rabbit antibody (AB16830, Abcam) at 1/2000 dilution combined with a HRP-conjugated goat anti rabbit antibody at a 1/5000 dilution. ECL-prime (Life Technologies) was used for immuno-detection and the signals were quantified using the Bioprofile Software (Vilber Lourmat). Three independent replicates (R1 to R3) are shown.

clock function. The role of RhodHK also needs further investigation. LOVHK and RhodHK have distinct phases of expression, LOVHK peaking in the morning and RhodHK at dusk. They could be involved in coupled morning and evening oscillators, mediating light to TOC1 or other response regulators through a TCS.

Transcription factors (TFs) are central players of circadian transcriptional clocks. The *O. tauri* genome contains only a limited set (120 putative DNA binding TFs compared with ~2000 in the land plant *Arabidopsis*) and the gene families are small, limiting gene redundancy. This provides a unique opportunity for genome-wide investigation of TFs in this minimalist clock system using reverse genetic approaches. Hierarchical transcription of genes involved in specific biological processes occurs over the day/night cycle and transcriptional patterns of genes involved in starch biosynthesis can accurately predict daily patterns of starch content based on a quasi-steady-state, constraint modeling approach (Sorokina et al., 2011). In *Ostreococcus*, therefore, by combining modeling, bioinformatics and genetic approaches, it may be possible to unravel the complex gene regulatory networks sustaining the circadian regulation of metabolic pathways.

Circadian clocks have been studied almost exclusively in terrestrial organisms and very little is known about clock function in the oceans. How do clocks of free-floating organisms manage to tell the time of day in a fluctuating light environment? The sea temperature, unlike the land temperature is fairly constant over the day night cycle. Can marine clocks be entrained by temperature cycles and are they temperature-compensated? Finally and more importantly, what is the adaptive value of the circadian clock for marine phytoplankton?

## Acknowledgments

We are grateful to Joan and Eamonn Groves for proofreading and editing the manuscript.

## References

Ahmad, M., Cashmore, A., 1993. HY4 gene of *A. thaliana* encodes a protein with characteristics of a blue-light photoreceptor. Nature 8, 653–658.
Alabadí, D., Oyama, T., Yanovsky, M.J., Harmon, F.G., Más, P., Kay, S.A., 2001. Reciprocal regulation between TOC1 and LHY/CCA1 within the *Arabidopsis* circadian clock. Science 293, 880–883.
Carré, I., Veflingstad, S.R., 2013. Seminars in cell & developmental biology emerging design principles in the *Arabidopsis* circadian clock. Semin. Cell Dev. Biol. 24, 393–398.
Christie, J.M., Salomon, M., Nozue, K., Wada, M., Briggs, W.R., 1999. LOV (light, oxygen, or voltage) domains of the blue-light photoreceptor phototropin (nph1): binding sites for the chromophore flavin mononucleotide. Proc. Natl. Acad. Sci. U. S. A. 96, 8779–8783.
Coesel, S., Mangogna, M., Ishikawa, T., Heijde, M., Rogato, A., Finazzi, G., Todo, T., Bowler, C., Falciatore, A., 2009. Diatom PtCPF1 is a new cryptochrome/photolyase family member with DNA repair and transcription regulation activity. EMBO Rep. 10, 655–661.
Corellou, F., Schwartz, C., Motta, J.-P., Djouani-Tahri, E.B., Sanchez, F., Bouget, F.-Y., 2009. Clocks in the green lineage: comparative functional analysis of the circadian architecture of the picoeukaryote ostreococcus. Plant Cell 21, 3436–3449.
Demarsy, E., Fankhauser, C., 2009. Higher plants use LOV to perceive blue light. Curr. Opin. Plant Biol. 12, 69–74.
Derelle, E., Ferraz, C., Rombauts, S., Rouzé, P., Worden, A.Z., Robbens, S., Partensky, F., Degroeve, S., Echeynié, S., Cooke, R., Saeys, Y., Wuyts, J., Jabbari, K., Bowler, C., Panaud, O., Piégu, B., Ball, S.G., Ral, J.-P., Bouget, F.-Y., Piganeau, G., et al., 2006. Genome analysis of the smallest free-living eukaryote *Ostreococcus tauri* unveils many unique features. Proc. Natl. Acad. Sci. U. S. A. 103, 11647–11652.
Djouani-Tahri, E.-B., Christie, J.M., Sanchez-Ferandin, S., Sanchez, F., Bouget, F.-Y., Corellou, F., 2011a. A eukaryotic LOV-histidine kinase with circadian clock function in the picoalga *Ostreococcus*. Plant J. 65, 578–588.
Djouani-tahri, E.B., Motta, J.P., Bouget, F.-Y., Corellou, F., 2010. Insights into the regulation of the core clock component TOC1. Plant Signal. Behav. 5, 332–335.
Djouani-Tahri, E.B., Sanchez, F., Lozano, J.-C., Bouget, F.-Y., 2011b. A phosphate-regulated promoter for fine-tuned and reversible overexpression in *Ostreococcus*: application to circadian clock functional analysis. PLoS ONE 6, e28471.
Edgar, R.S., Green, E.W., Zhao, Y., Van Ooijen, G., Olmedo, M., Qin, X., Xu, Y., Pan, M., Valekunja, U.K., Feeney, K.A., Maywood, E.S., Hastings, M.H., Baliga, N.S., Merrow, M., Millar, A.J., Johnson, C.H., Kyriacou, C.P., O'Neill, J.S., Reddy, A.B., 2012. Peroxiredoxins are conserved markers of circadian rhythms. Nature 485, 459–464.
Elowitz, M.B., Leibler, S., 2000. A synthetic oscillatory network of transcriptional regulators. Nature 403, 335–338.
Froehlich, A.C., Liu, Y., Loros, J.J., Dunlap, J.C., 2002. White Collar-1, a circadian blue light photoreceptor, binding to the frequency promoter. Science 297, 815–819.
Fujiwara, S., Wang, L., Han, L., Suh, S.-S., Salomé, P. a, McClung, C.R., Somers, D.E., 2008. Post-translational regulation of the *Arabidopsis* circadian clock through selective proteolysis and phosphorylation of pseudo-response regulator proteins. J. Biol. Chem. 283, 23073–23083.
Gendron, J.M., Pruneda-Paz, J.L., Doherty, C.J., Gross, A.M., Kang, S.E., Kay, S.A., 2012. *Arabidopsis* circadian clock protein, TOC1, is a DNA-binding transcription factor. Proc. Natl. Acad. Sci. U. S. A. 109, 3167–3172.
Goto, K., Johnson, C.H., 1995. Is the cell division cycle gated by a circadian clock? The case of *Chlamydomonas reinhardtii*. J. Cell Biol. 129, 1061–1069.
Green, R.M., Tobin, E.M., 1999. Loss of the circadian clock-associated protein 1 in *Arabidopsis* results in altered clock-regulated gene expression. Proc. Natl. Acad. Sci. U. S. A. 96, 4176–4179.
Harmer, S.L., Kay, S.A., 2000. Orchestrated transcription of key pathways in *Arabidopsis* by the circadian clock. Science 290, 2110–2113.
Heijde, M., Zabulon, G., Corellou, F., Ishikawa, T., Brazard, J., Usman, A., Sanchez, F., Plaza, P., Martin, M., Falciatore, A., Todo, T., Bouget, F.-Y., Bowler, C., 2010. Characterization of two members of the cryptochrome/photolyase family from *Ostreococcus tauri* provides insights into the origin and evolution of cryptochromes. Plant Cell Environ. 33, 1614–1626.
Huang, W., Perez-Garcia, P., Pokhilko, A., Millar, A.J., Antoshechkin, I., Riechmann, J.L., Mas, P., 2012. Mapping the core of the *Arabidopsis* circadian clock defines the network structure of the oscillator. Science 336, 75–79.
Imaizumi, T., Kay, S.A., 2006. Photoperiodic control of flowering: not only by coincidence. Trends Plant Sci. 11, 550–558.
Ivleva, N.B., Bramlett, M.R., Lindahl, P.A., Golden, S.S., 2005. LdpA: a component of the circadian clock senses redox state of the cell. EMBO J. 24, 1202–1210.
Kim, Y., Carre, I.A., 2002. MYB transcription factors in the *Arabidopsis* circadian clock. J. Exp. Bot. 53, 1551–1557.
Klarsfeld, A., Picot, M., Vias, C., Chélot, E., Rouyer, F., 2011. Identifying specific light inputs for each subgroup of brain clock neurons in *Drosophila* larvae. J. Neurosci. 31, 17406–17415.
Krauss, U., Minh, B.Q., Losi, A., Gärtner, W., Eggert, T., Von Haeseler, A., Jaeger, K.-E., 2009. Distribution and phylogeny of light-oxygen-voltage-blue-light-signaling proteins in the three kingdoms of life. J. Bacteriol. 191, 7234–7242.
Le Bihan, T., Martin, S.F., Chirnside, E.S., Van Ooijen, G., Barrios-Llerena, M.E., O'Neill, J.S., Shliaha, P.V., Kerr, L.E., Millar, A.J., 2011. Shotgun proteomic analysis of the unicellular alga *Ostreococcus tauri*. J. Proteome 74, 2060–2070.
Monnier, A., Liverani, S., Bouvet, R., Jesson, B., Smith, J.Q., Mosser, J., Corellou, F., Bouget, F.-Y., 2010. Orchestrated transcription of biological processes in the marine picoeukaryote *Ostreococcus* exposed to light/dark cycles. BMC Genomics 11, 192.
Morant, P.-E., Thommen, Q., Pfeuty, B., Vandermoere, C., Corellou, F., Bouget, F.-Y., Lefranc, M., 2010. A robust two-gene oscillator at the core of *Ostreococcus tauri* circadian clock. Chaos 20, 045108.
Moulager, M., Corellou, F., Vergé, V., Escande, M.-L., Bouget, F.-Y., 2010. Integration of light signals by the retinoblastoma pathway in the control of S phase entry in the picophytoplanktonic cell *Ostreococcus*. PLoS Genet. 6, e1000957.
Moulager, M., Monnier, A., Jesson, B., Bouvet, R., Mosser, J., Schwartz, C., Garnier, L., Corellou, F., Bouget, F.-Y., 2007. Light-dependent regulation of cell division in *Ostreococcus*: evidence for a major transcriptional input. Plant Physiol. 144, 1360–1369.
Nakajima, M., Imai, K., Ito, H., Nishiwaki, T., Murayama, Y., Iwasaki, H., Oyama, T., Kondo, T., 2005. Reconstitution of circadian oscillation of cyanobacterial KaiC phosphorylation in vitro. Science 308, 414–415.
Nikaido, S.S., Johnson, C.H., 2000. Daily and circadian variation in survival from ultraviolet radiation in *Chlamydomonas reinhardtii*. Photochem. Photobiol. 71, 758–765.
O'Neill, J.S., Van Ooijen, G., Dixon, L.E., Troein, C., Corellou, F., Bouget, F.-Y., Reddy, A.B., Millar, A.J., 2011. Circadian rhythms persist without transcription in a eukaryote. Nature 469, 554–558.
Para, A., Farré, E.M., Imaizumi, T., Pruneda-Paz, J.L., Harmon, F.G., Kay, S.A., 2007. PRR3 Is a vascular regulator of TOC1 stability in the *Arabidopsis* circadian clock. Plant Cell 19, 3462–3473.
Pfeuty, B., Thommen, Q., Corellou, F., Djouani-Tahri, E.B., Bouget, F.-Y., Lefranc, M., 2012. Circadian clocks in changing weather and seasons: lessons from the picoalga *Ostreococcus tauri*. BioEssays 34, 781–790.
Purcell, E., McDonald, C., Palfey, B., Crosson, S., 2010. An analysis of the solution structure and signaling mechanism of LovK, a sensor histidine kinase integrating light and redox signals. Biochemistry 49, 6761–6770.
Salomon, M., Christie, J.M., Knieb, E., Lempert, U., Briggs, W.R., 2000. Photochemical and Mutational Analysis of the FMN-binding Domains of the Plant. 9401–9410.
Sorokina, O., Corellou, F., Dauvillée, D., Sorokin, A., Goryanin, I., Ball, S., Bouget, F.-Y., Millar, A.J., 2011. Microarray data can predict diurnal changes of starch content in the picoalga *Ostreococcus*. BMC Syst. Biol. 5, 36.
Strayer, C., Oyama, T., Schultz, T.F., Raman, R., Somers, D.E., Más, P., Panda, S., Kreps, J.A., Kay, S.A., 2000. Cloning of the *Arabidopsis* clock gene TOC1, an autoregulatory response regulator homolog. Science 289, 768–771.
Thommen, Q., Pfeuty, B., Morant, P.-E., Corellou, F., Bouget, F.-Y., Lefranc, M., 2010. Robustness of circadian clocks to daylight fluctuations: hints from the picoeucaryote *Ostreococcus tauri*. PLoS Comput. Biol. 6, e1000990.
Thommen, Q., Pfeuty, B., Corellou, F., Bouget, F.Y., Lefranc, M., 2012. Robust and flexible response of Ostreococcus tauri circadian clock to light/dark cycles of varying photoperiod. FEBS J 279, 3432–3448.
Troein, C., Corellou, F., Dixon, L.E., Van Ooijen, G., O'Neill, J.S., Bouget, F.-Y., Millar, A.J., 2011. Multiple light inputs to a simple clock circuit allow complex biological rhythms. Plant J. 66, 375–385.
Troein, C., Locke, J.C.W., Turner, M.S., Millar, A.J., 2009. Weather and seasons together demand complex biological clocks. Curr. Biol. 19, 1961–1964.
Woolum, J., 1991. A re-examination of the role of the nucleus in generating the circadian rhythm in *Acetabularia*. J. Biol. Rhythm. 129–136.

Résumé

Le fer est un élément présent en abondance dans la croûte terrestre, indispensable à la quasi-totalité des êtres vivants. Cependant, en milieu marin la biodisponibilité du fer est souvent faible et sporadique. Les micro-algues du phytoplancton ont développé des stratégies pour faire face à cette limitation en fer et s'adapter à des niches écologiques variables. Les micro-algues vertes du genre *Ostreococcus* (Prasinophyceae) présentent une large distribution géographique dans l'océan mondial, et de nombreux écotypes venant de milieux contrastés ont été isolés. L'objectif principal de ma thèse était d'étudier les différentes stratégies mises en place par le genre *Ostreococcus*, et notamment l'influence de la lumière et de l'horloge circadienne, dans la gestion de la carence en fer. Mon travail s'est focalisé sur l'étude d'*Ostreococcus tauri,* écotype lagunaire (Clade C), que de récentes techniques de transformation par insertion et recombinaison homologue ont promu comme un organisme modèle pour des approches de génétique fonctionnelle. J'ai étudié la ferritine, une protéine impliquée dans la gestion de la réserve en fer chez de nombreux organismes, et mis en évidence sa régulation par l'alternance jour/nuit et l'horloge circadienne. J'ai montré son rôle dans l'assimilation du fer, la régulation de l'homéostasie du fer et le recyclage du fer intracellulaire lors d'une carence. Enfin, j'ai caractérisé les stratégies d'acclimatation et d'adaptation à la carence en fer chez plusieurs écotypes d'Ostreococcus, dont *O. tauri*, RCC 802 (Clade A), RCC 809 (Clade B) et un mutant de taille/biomasse. Une stratégie d'acclimatation par réduction de la biomasse cellulaire a été mise en évidence.

Mots-clés : micro-algues, ferritine, *Ostreococcus*, fer, écotypes, régulation de l'homéostasie du fer

Summary

Iron is an abundant element in the earth crust and is essential for almost organisms. In the marine environment, however, its bioavailability is often low and the iron supplies sporadic. Phytoplanktonic species have developed various strategies to face iron limitation and adapt to different ecological niches. Green picoalgae from the genus *Ostreococcus* (Prasinophyceae) are widespread in the global ocean and numerous ecotypes have been isolated from contrasted environments. The main objective of my thesis was to identify the strategie(s) used by the genus *Ostreococcus* in response to iron starvation and in particular the influence of the day/night cycle and the circadian clock in the regulation of iron homeostasis. I focused my work on the lagoon ecotype, *Ostreococcus tauri* (Clade C), which has emerged as a model organism for functional genomics approaches thanks to the development of genetic transformation by random insertion and homologous recombination. I have studied ferritin, a protein involved in iron storage which is present throughout the tree of life. I showed that ferritin is regulated by the light/dark cycle and the circadian clock and that it is a key player in the regulation of iron uptake and the recycling. Finally, I characterized the acclimation and adaptation strategies to iron limitations of several *Ostreococcus* ecotypes including *O.tauri*, RCC802 (Clade A), RCC809 (Clade B) and a cell biomass mutant of *O.tauri*. The reduction of cell biomass appears to be a main mechanism of acclimation in response to iron limitation.

Key-word: microalgae, ferritin, Ostreococcus, iron, ecotypes, regulation of iron homeostasis